MARCO TARASCO

How microplastics and adsorbed pollutants affect zebrafish development?

UAlg FCT
UNIVERSIDADE DO ALGARVE
FACULDADE DE CIÊNCIAS E TECNOLOGIA

2022

MARCO TARASCO

How microplastics and adsorbed pollutants affect zebrafish development?

Doutoramento em Ciências do Mar,
da Terra e do Ambiente

Trabalho efetuado sob a orientação de:
Prof. M. Leonor Cancela
Prof. Maria João Bebianno
Prof. Didier Y. R. Stainier

UAlg FCT
UNIVERSIDADE DO ALGARVE
FACULDADE DE CIÊNCIAS E TECNOLOGIA
2022

How microplastics and adsorbed pollutants affect zebrafish development?

Declaro ser o autor deste trabalho, que é original e inédito. Autores e trabalhos consultados estão devidamente citados no texto e constam da listagem de referências incluída.

Think positive, be dynamic.

ACKNOWLEDGEMENTS

This work is the “final product” of a great journey where many people have contributed every day from the beginning to the end!! I don’t know where I would be without your support!

I would like to start by thanking my supervisors who never doubt and always supported my decisions, and most importantly never complained about me travelling around to learn new techniques and expand my scientific network.

To Prof. Leonor Cancela, who welcome me in BIOSKEL Lab from 2015 and gave me the possibility not only to accomplish my Master but also this PhD. She always supported my ideas and was always available to help me with any problem.

To Prof. Maria João Bebianno, that kindly accepted to supervise my work, and was always available to help me and share valuable suggestions.

To Prof. Didier Stainier, who always welcomed me in his lab whenever I needed, giving me the opportunity to develop many experimental parts of this work. Most importantly joining his lab was very stimulating and gave me the opportunity to expand my knowledge, learn new techniques and get valuable experiences.

A special THANKS goes to Vincent, that although was not my official supervisor, accompanied me during this work, every day. The best mentor every student dreams to have! Always available for discussions, suggestions, corrections, and everything you can think off. You taught me how to be an independent scientist, and most importantly how to write and be perfectionist in my work. I guess you also have unlimited patience for not getting tired of hearing my daily complains. ;)

To Gavaia, that spent many hours with me looking at fish bones and off course was always available for scientific advises. Most importantly, I will never forget all the time we shared fishing together in the wildest places of Algarve, which always ended up with amazing barbecues!

To Fabrice, who I occasionally met during a microscopy course and not only became an important reference in my scientific career but also a good friend, always open to discuss everything. You really put a lot of effort in teaching me everything about ImageJ and macros. Thanks to you my morphometric analysis was always fast and smooth ;). I assure you, that all the shared knowledge, will always be a part of me and will help me in my next scientific challenges.

I would like to thank all friends and lab colleagues from BIOSKEL, MPI and other CCMAR labs for their help and the nice time we spent together, making my work easier and enjoyable. A special thanks to Joana (or Calimera), for being always there every time I needed some help, but most importantly for being a good friend and share with me many laughs, beers, and good times. To João for being on my side as a good friend (and of course as lab mate) from when I started my master until today, but especially for all the good times we spent in front of a beer, talking about science, life, and future perspectives. Thank you also for always telling me I could reach this day and for providing me a sofa to sleep whenever I needed it. To Anabela, that welcome me in Bad Nauheim with a positive vibe and shared with me many precious scientific advises and many nice moments. A big hug and thanks to Vânia, Iris, Catia, Helena and Mike for all the time we spent together in and outside the lab, especially during parties and dinners. To also my friends in Bad Nauheim, Srinath, Leoni and Vahan

that from the very beginning welcome me in the lab with open arms and helped me a lot during this time and we shared many funny moments.

To Fran, the first friend I met when I arrived in Faro, always trustworthy and kind, sharing with me many moments of laughs, kayak, and outdoor trips!

To Jo, who started the master with me and was always by my side in many different occasions. We really had great university time and although we were not close during my PhD, I know that we will always be proud of what we will accomplish in life. To Giacomo, my surf buddy and good friend, who not only shared with me many hours in the water during our surf trips but also nice memories.

To Alessio and Katia, lab colleagues, neighbors, and good friends, but most importantly, two people you know you can count on! Always happy to help or share any experience with me. We practically shared everything, nice moments, laughs and sometimes even problems (mostly complaining about not working experiments). I will never forget our fishing trips, coffee breaks, lunches, dinners, Friday's pasta parties and entire afternoons playing together.

To my girlfriend Adriana, who in the last two years of my PhD, was always there by my side, in good days to celebrate or in bad days to comfort me. She has been a really good listener and I bet, now she knows more than me about zebrafish! (You don't want to know how much time she spent listening to my infinite talks). Thank you for sharing this path with me, and for reminding me, to give my best in everything I do. I really enjoyed sharing everything with you, from our scientific discussions to planning our holidays or simply preparing a pizza together, and I look forward for many more of these moments.

A special hug goes to my parents, that always supported my crazy dreams and never doubt about my life choices. Thank you for always being there for me! You supported me every day and provided me with all the right "ingredients" to make me become the man I am today!

To my brother Enzo, who never doubt about my choices and was always available to talk about anything, especially for sharing spearfishing tips.

To my brother Adriano, that always pushed me to be a better version of myself, to do the right experiences and supported me all the time. You have always been there for me, opening my mind and giving me the strength to challenge my life. There is no price for everything you taught me and shared with me! Thanks bro! It's time to daremore ;)

To Maria (Cogny), that although the first day I met you, I hit you with a snowboard, you never stopped being supportive and open to talk about anything. I really enjoyed all the amazing moments, travels, laughs, and experiences we shared together.

I guess I should also thank the ocean, the place where I go every time I'm free, to clear my mind and enjoy my hobbies. A special thanks goes to the 5 kg gilthead seabream, a trophy I will never forget ;)

Thank you all for sharing this path with me!

FUNDINGS

Marco Tarasco was supported by the Portuguese Foundation for Science and Technology (FCT) through the PhD grant SFRH/BD/128634/2017 and COVID/BD/151848/2021 and by NEUBIAS-COST STSM program as part of action CA15124. This work was funded by FCT through projects UID/Multi/04326/2019, UID/00350/2020, UIDB/04326/2020, UID/MAR/00350/2013 and from the operational programs MAR2020 and COMPETE 2020 through projects OSTEOMAR MAR-02.01.01-FEAMP-0057 and EMBRC.PT ALG-01-0145-FEDER-022121.

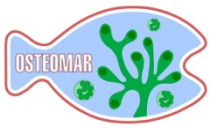

ABSTRACT

The presence of microplastics in the aquatic ecosystem represents a major issue for the environment and human health. The capacity of organic pollutants such as benzo[α]pyrene (BaP) to adsorb onto microplastic particles raises additional concerns, as it creates a new route for toxic compounds to enter the food web. Current knowledge on the impact of pristine and/or contaminated microplastics on aquatic organisms remains insufficient, and this work aims at providing new insights by evaluating their biological effects in zebrafish (*Danio rerio*). The ZEB316, a stand-alone housing system built with inert materials, and a comprehensive set of ImageJ semi-automatic tools were first developed and optimized to perform state-of-the-art toxicological studies and obtain meaningful data from morphometric analysis of bright-field/fluorescence images. Zebrafish larvae were exposed throughout their development to polyethylene microplastics, pristine or spiked with BaP, supplemented in the fish diet. While exposure up to 30 days post-fertilization only increased the incidence of skeletal deformities, long-term exposure to pristine/contaminated microplastics not only jeopardized fish growth, reproduction performance, and skeletal health, but it also caused an intergenerational effect. To further study the mechanisms underlying BaP osteotoxicity, several bone-related *in vivo* assays were used to evaluate the effects of waterborne exposure to BaP during bone development and regeneration. BaP inhibited osteoblast maturation and ECM mineralization and stimulated osteoclast activity, thus affecting bone remodeling. Transgenic and transcriptomic approaches suggested that besides the activation of xenobiotic and metabolic pathways, which may negatively impact extracellular matrix formation and organization, BaP activates inflammatory mechanisms that recruit neutrophils, which affect both osteoblast and osteoclast activity, possibly through a direct interaction of the neutrophils with the bone matrix. This work provides novel data on the effects of microplastics exposure during zebrafish development, in particular its osteotoxic effects, and gives new insights into the cellular and molecular players involved in BaP osteotoxicity.

Keywords: Microplastics; Benzo[α]pyrene; Zebrafish *Danio rerio*; Osteotoxicity; Fish development; ImageJ.

RESUMO

A presença de microplásticos no ecossistema aquático é, nos dias de hoje, uma realidade extremamente preocupante que acarreta sérios riscos para o meio ambiente e para a saúde pública. A capacidade dos microplásticos de adsorverem poluentes orgânicos, como é o caso do benzo[α]pireno (BaP), levanta preocupações adicionais, pois cria uma nova rota de entrada de compostos tóxicos na cadeia alimentar. No entanto, o conhecimento atual sobre o impacto dos microplásticos, inalterados e/ou contaminados, nos organismos aquáticos é ainda insuficiente e requer estudos adicionais. O trabalho desenvolvido no âmbito desta tese pretende assim fornecer novos dados sobre os efeitos biológicos dos microplásticos utilizando como modelo o peixe-zebra (*Danio rerio*). Pequenos teleósteos, como é o caso do peixe-zebra, oferecem vantagens significativas relativamente aos modelos animais clássicos e são atualmente utilizados como organismos de primeira linha para avaliar os riscos ambientais associados aos compostos tóxicos presentes nos meios aquáticos.

Estudos toxicológicos requerem o uso de materiais inertes e condições controladas, todavia, nenhum dos sistemas atualmente comercializados é adequado para avaliar o efeito tóxico dos microplásticos. Estes sistemas contêm componentes feitos de polímeros plásticos que podem libertar partículas plásticas micrométricas, lixiviar os constituintes químicos ou adsorver os compostos químicos em estudo. O sistema de aquários autônomo ZEB316 foi desenvolvido no âmbito deste trabalho com o objetivo de suprimir esta necessidade e de facultar uma solução económica e fácil de implementar que permita a realização de estudos toxicológicos de última geração. Este sistema é construído com materiais inertes e resistentes à corrosão e proporciona boas condições de alojamento através de um sistema eficiente de recirculação e filtragem da água. A avaliação dos parâmetros da água e do desempenho do crescimento dos peixes mostrou que o sistema ZEB316 oferece condições de alojamento comparáveis à dos sistemas comercialmente disponíveis.

A maioria dos resultados obtidos no âmbito desta dissertação provêm da análise de imagens de microscopia de campo claro e/ou fluorescência. Embora o uso de imagens de microscopia seja comum na maioria dos laboratórios e permita obter uma

quantidade considerável de informação, a análise destas imagens é geralmente um processo moroso, em parte devido à falta de ferramentas automáticas/semiautomáticas dedicadas que permitam a sua análise. Nesse sentido, desenvolvemos diversas macros para o software ImageJ, com o objetivo de reduzir o erro associado à análise pelo usuário, aumentando assim a reprodutibilidade dos dados e a padronização das metodologias experimentais. Uma vez que o foco deste trabalho está centrado no estudo da osteotoxicidade, é de salientar o desenvolvimento de um conjunto de macros específicas para esse fim e denominadas ZFBONE. Este conjunto de ferramentas permite aos usuários avaliar, a partir de imagens 2D, parâmetros morfométricos de várias estruturas ósseas (por exemplo, opérculo, raios e escamas da barbatana caudal), mas também a extensão e a intensidade das colorações específicas do osso. Além disso, outras macros foram desenvolvidas para outros fins, por exemplo, para analisar os vários parâmetros morfométricos relativos aos embriões de peixe ou para avaliar cortes histológicos. Uma vez desenvolvidos os meios e técnicas necessários para a execução dos ensaios toxicológicos, e subsequente análise dos resultados, procedeu-se à realização das várias experiências que visam compreender efeito biológico dos microplásticos e contaminates no peixe-zebra. Assim, larvas de peixe-zebra foram produzidas e mantidas no sistema previamente descrito, ZEB316, e expostas cronicamente, durante o seu desenvolvimento, a partículas de polietileno de 20-27 μm, inalteradas (MP) ou contaminadas com benzo[α]pireno (MP-BaP). Estas partículas foram adicionadas à dieta dos peixes através de uma suplementação a 1% m/m. Apesar de não se ter registado qualquer alteração ao nível dos parâmetros morfológicos aos 30 dias pós-fertilização (dpf), a presença de MP e MP-BaP acabou por ter um efeito negativo no crescimento dos espécimes aos 90 e 360 dpf. A fecundidade relativa, a morfologia do ovo/embrião e a área do vitelo também sofreram um impacto negativo em peixes-zebra alimentados com MP-BaP. No que respeita ao estado geral do esqueleto, os peixes expostos a dietas experimentais contendo MP e MP-BaP sofreram um aumento significativo na incidência de deformações esqueléticas aos 30 dpf quando comparados com peixes alimentados com a dieta controlo, bem como um desenvolvimento anómalo da barbatana caudal e escamas, e uma diminuição da qualidade do osso aos 90 dpf. Um comprometimento da formação óssea intergeracional foi também observado na prole de espécimes expostos a MP ou MP-BaP, que se refletiu numa redução do osso opercular dos

descendentes aos 6 dpf. Além de um claro efeito no desenvolvimento ósseo, a análise histológica do intestino revelou ainda um número reduzido de células caliciformes em peixes alimentados com dieta MP-BaP, um claro sinal de inflamação intestinal. Finalmente, a exposição das larvas a MP-BaP levou a um aumento da expressão de genes associados à via de resposta do BaP, ao mesmo tempo que impactou negativamente na expressão de genes envolvidos no estresse oxidativo.

Os resultados obtidos indicaram um maior comprometimento do desenvolvimento ósseo no peixe-zebra quando sujeito a uma dieta contendo microplásticos contaminados com BaP (MP-BaP), por comparação com a dieta contendo microplásticos não contaminados (MP). Outros autores demostraram também que a presença de BaP afeta a formação das vértebras e o desenvolvimento generalizado do esqueleto, no entanto os mecanismos envolvidos nestes fenómenos permanecem pouco estudados. Desta forma, realizámos ensaios adicionais *in vivo* com o objetivo de avaliar os efeitos osteotóxicos do BaP durante o desenvolvimento e regeneração óssea em peixe-zebra. A exposição aguda de larvas de peixe-zebra entre os 3 e os 6 dpf ao BaP levou a uma redução do tamanho do osso opercular e uma diminuição quantitativa de células positivas para osteocalcina, indicando um efeito composto na maturação dos osteoblastos. Por sua vez, quando se trata de uma exposição crônica das larvas de peixe-zebra ao BaP, entre os 3 e os 30 dpf, verificou-se que o desenvolvimento do esqueleto axial é afetado, aumentando a incidência e gravidade das deformações esqueléticas. Em peixes jovens adultos, observou-se ainda que a exposição ao BaP afetou não só a mineralização dos raios da barbatana caudal e escamas recém-formados, como prejudicou também o seu padrão morfológico, fenómenos que têm por base uma remodelação óssea desequilibrada. Relativamente às análises de expressão genética de vários marcadores verificou-se que o BaP induziu a ativação das vias xenobióticas e metabólicas e impactou negativamente na formação e organização da matriz extracelular. Curiosamente, a exposição ao BaP regulou positivamente os marcadores de inflamação nas larvas e aumentou o recrutamento de neutrófilos. Uma interação direta entre neutrófilos e a matriz extracelular óssea, ou células responsáveis pela formação do osso, foi observada *in vivo*, o que sugere um papel dos neutrófilos nos mecanismos subjacentes à osteotoxicidade do BaP.

Globalmente, os resultados obtidos no âmbito deste trabalho sugerem que a exposição crónica a microplásticos inalterados e/ou contaminados não prejudica apenas o crescimento dos peixes, mas também o seu desempenho a nível reprodutivo, saúde geral do seu esqueleto, e compromete a descendência por meio de efeitos intergeracionais. Além disso, este trabalho fornece novos dados sobre os principais mecanismos celulares e moleculares envolvidos na osteotoxicidade do BaP e aborda o possível papel dos neutrófilos na redução da resposta óssea inflamatória.

Palavras-chave: Microplásticos; Benzo[α]pireno; Peixe-zebra *Danio rerio*; Osteotoxicidade; Desenvolvimento do peixe; ImageJ.

TABLE OF CONTENTS

LIST OF ABBREVIATIONS AND ACRONYMS

3-MC	3-methylcholanthrene
Acp5a	Acid phosphatase 5a, tartrate resistant
Ahr	Aryl hydrocarbon receptor
Alpl	Alkaline phosphatase, biomineralization associated
ANOVA	Analysis of variance
AR-S	Alizarin red S
BaP	Benzo[α]pyrene
BIF	Bifurcation point
Bmp2b	Bone morphogenetic protein 2b
BP3	Benzophenone-3
BPA	Bisphenol A
Calcitriol	1α,25-dihydroxyvitamin D_3
CASA	Computer-assisted sperm analysis
CAT	Catalase
Col10a1a	Collagen, type X, alpha 1a
Col1a1a	collagen, type I, alpha 1a
Col2a1a	Collagen, type II, alpha 1a
Ctsk	Cathepsin K
Cyp1a	Cytochrome P450, family 1, subfamily A
DEMIN	Demineralized area
DMSO	Dimethyl sulfoxide
dpa	Days post-amputation
dpf	Days post-fertilization
dpp	Days post-plucking
ECM	Extracellular matrix
Eef1a1l1	Eukaryotic translation elongation factor 1 alpha 1, like 1
EFSA	European Food Safety Authority
EtOH	Ethanol
FAO	Food and Agriculture Organization
FDR	False discovery rate
Fosab	v-fos FBJ murine osteosarcoma viral oncogene homolog Ab

GESAMP	Group of experts on the scientific aspects of marine environmental protection
GFP	Green fluorescent protein
GPx	Glutathione peroxidase
GST	Glutathione-S-transferase
HBSS	Hank's balanced salt solution
Hd	Head area
HDPE	High-density polyethylene
hpf	Hours post-fertilization
Hsp70	Heat shock cognate 70-kd protein, tandem duplicate 1
Hsp90	Heat shock protein 90, alpha (cytosolic), class A member 1, tandem duplicate 1
IJ	Intersegment joint
IJL	Intersegment joint in the left branch of the bifurcated ray
IJR	Intersegment joint in the right branch of the bifurcated ray
Il1β	Interleukin 1, beta
Il6	Interleukin 6 (interferon, beta 2)
LDPE	Low-density polyethylene
Lyz	Lysozyme
M-CSF	Macrophage colony stimulating factor
MAX Thr	Maximum threshold value
MIN Thr	Minimum threshold value
Mmp13a	Matrix metallopeptidase 13a
Mmp9	Matrix metallopeptidase 9
MP-BaP	Microplastic diet spiked with BaP
MP	Pristine microplastics diet
MPs	Microplastics
Mpx	Myeloid-specific peroxidase
MS222	Tricaine methanesulfonate
MSC	Mesenchymal stem cell
Nr1i2	Nuclear receptor subfamily 1, group I, member 2
Oc / Bglap	Osteocalcin / bone gamma-carboxyglutamate (gla) protein
Op	Operculum area
PAH	Polycyclic aromatic hydrocarbon

PANTHER	Protein Analysis THrough Evolutionary Relationships
PBS	Phosphate buffered saline
PCB	Polychlorinated biphenyl
PE	Polyethylene
PET / PETE	Polyethylene terephthalate
PFA	Paraformaldehyde
PFOS	Perfluorooctanesulfonic acid
POP	Persistent organic pollutant
PP	Polypropylene
PS	Polystyrene
PVC	Polyvinyl chloride
Pxr	Pregnane X receptor
qPCR	Quantitative real time PCR
Rank	Receptor activator of nuclear factor kappa-B
Rankl	Receptor activator of nuclear factor kappa-B ligand
RAY	Ray width
REG	Regenerated area
RMA	*de novo* mineralized area
RNA-seq	RNA sequencing
ROI	Region of interest
ROS	Reactive oxygen species
Rps18	Ribosomal protein S18
Runx2b	RUNX family transcription factor 2b
Scale AR	Scale aspect ratio
Sod	Superoxide dismutase
Sp7	Sp7 transcription factor
Spp1	Secreted phosphoprotein 1
STU	Stump width
Tnfα	Tumor necrosis factor alpha
TRAP	Tartrate-resistant acid phosphatase
TSH	Thyroid stimulating hormone
UNEP	United Nations Environment Programme
Vdr	Vitamin D receptor
µCT	Micro-computed tomography

PREAMBLE

This dissertation is divided into seven chapters. **Chapter 1** (*General introduction*) addresses current knowledge on microplastic pollution, microplastic toxicity, zebrafish as animal model, focusing at the end on bone homeostasis and osteotoxicity. **Chapter 2** (*ZEB316: a small stand-alone housing system to study microplastics and organic pollutants in small teleosts*) illustrates the design and development of a stand-alone housing system, which was used to expose zebrafish to microplastics through supplemented diets. **Chapter 3** (*ImageJ macro development*) describes the development of macro-instructions for ImageJ to perform morphometric analysis of different bone structures. **Chapter 4** (*Screening of mineralogenic and osteogenic compounds in zebrafish – tools to improve assay throughput and data accuracy*) reviews the available zebrafish *in vivo* assays to assess osteotoxic/osteogenic activities. **Chapter 5** (*Effects of pristine or contaminated polyethylene microplastics on zebrafish development*) explores the effects of microplastic dietary exposure on zebrafish throughout development. **Chapter 6** (*New insights into benzo[α]pyrene osteotoxicity in zebrafish*) focus on gaining insights into waterborne BaP osteotoxicity. **Chapter 7** (*Conclusions and perspectives*) summarizes the interpretation of the results collected within the scope of this work and discusses future directions that could be followed to further assess the impact of microplastics and adsorbed pollutants on fish homeostasis.

Statement: The author conceived, designed, performed the experiments and analytical procedures, and wrote or participated in the writing of the manuscripts included in this dissertation.

Ethical statement: People involved in animal handling and experimentation received proper training (category B courses accredited by the Federation of Laboratory Animal Science Associations). Fish facilities were accredited by the Portuguese National Authority for Animal Health (DGAV). Procedures involving animals were performed following the EU and Portuguese legislation for animal experimentation and welfare (Directives 86/609/CEE and 2010/63/EU; Portaria 1005/92, 466/95 and 1131/97; Decreto-Lei 113/2013) and under authorization no. 012769/2021. All efforts were made to minimize pain, distress, and discomfort.

Chapter 1

General introduction

1.1. THE PLASTIC ERA

Plastic pollution has greatly increased in the last decades and became a major concern for the environment and human health. The extensive use of plastic products in every aspect of our daily life, has driven the annual plastic worldwide production from 1.7 million tons in 1950 to 368 million tons in 2019[1] (Fig. 1.1A). Plastic products are usually preferred over other materials due to their excellent properties such as lightweight, flexibility and plasticity, corrosion resistance, electrical and thermal insulation and, most importantly, their low-cost production. In the past decades, due to the increase of anthropogenic activities and to the fact that society has become addicted to single use or disposable plastic, enormous quantity of plastic has been produced. It was estimated that from 1950 to 2017, 9.2 billion metric tons of plastic have been produced and of that, only around 10% has been recycled or incinerated (12%), while the rest is either currently in use (30%) or accumulating in landfills or in our environments as litter (48%)[2–5] (Fig. 1.1B).

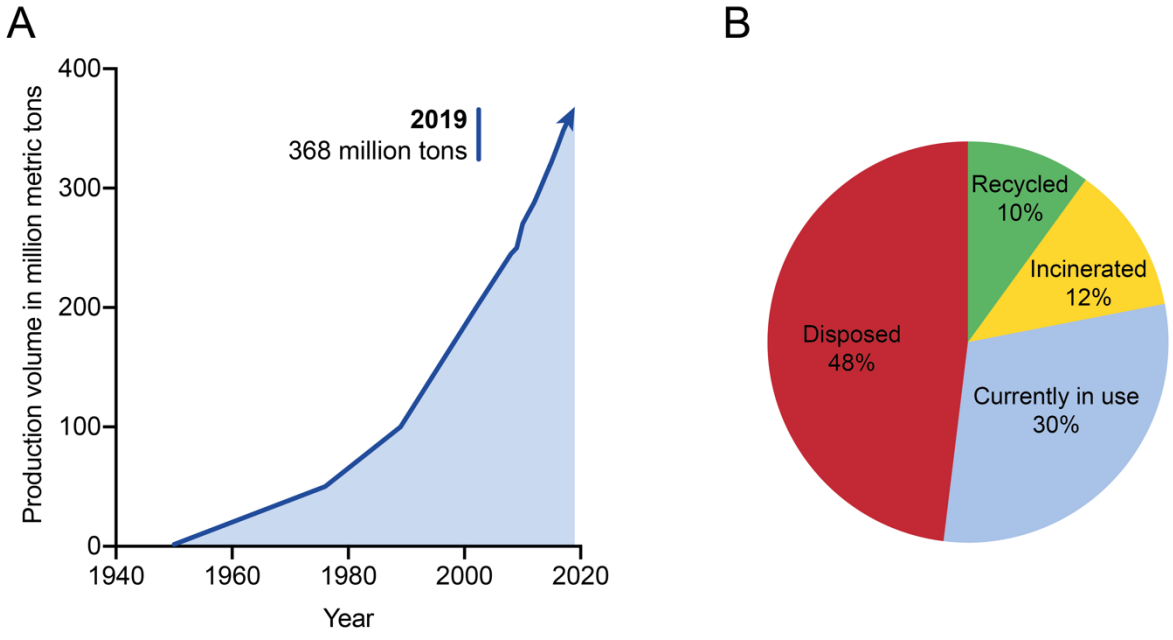

Figure 1.1. (**A**) Global plastic production from 1950 to 2019 and (**B**) fate of produced plastic. Based on data from Plastics Europe 2020, Geyer et al. (2017) and Wayman et al. (2021)[1,5,6].

1.1.1. Types of plastic polymers

Plastics are man-made organic polymers derived from the polymerization of monomers which are normally extracted from fossil-based resources such as oil or gas[7]. Plastic physicochemical properties (i.e., strength, melting point, etc.) can be customized by changing the type of monomer, which results in a different type of plastic. Plastic is not all the same; in fact, a large variety of polymers exists[8], that are used depending on their properties, for a myriad of end-use markets such as packaging, household and personal goods, building, constructions, automobile and electronic industries, and for this reason are identified with different numbers (Fig. 1.2).

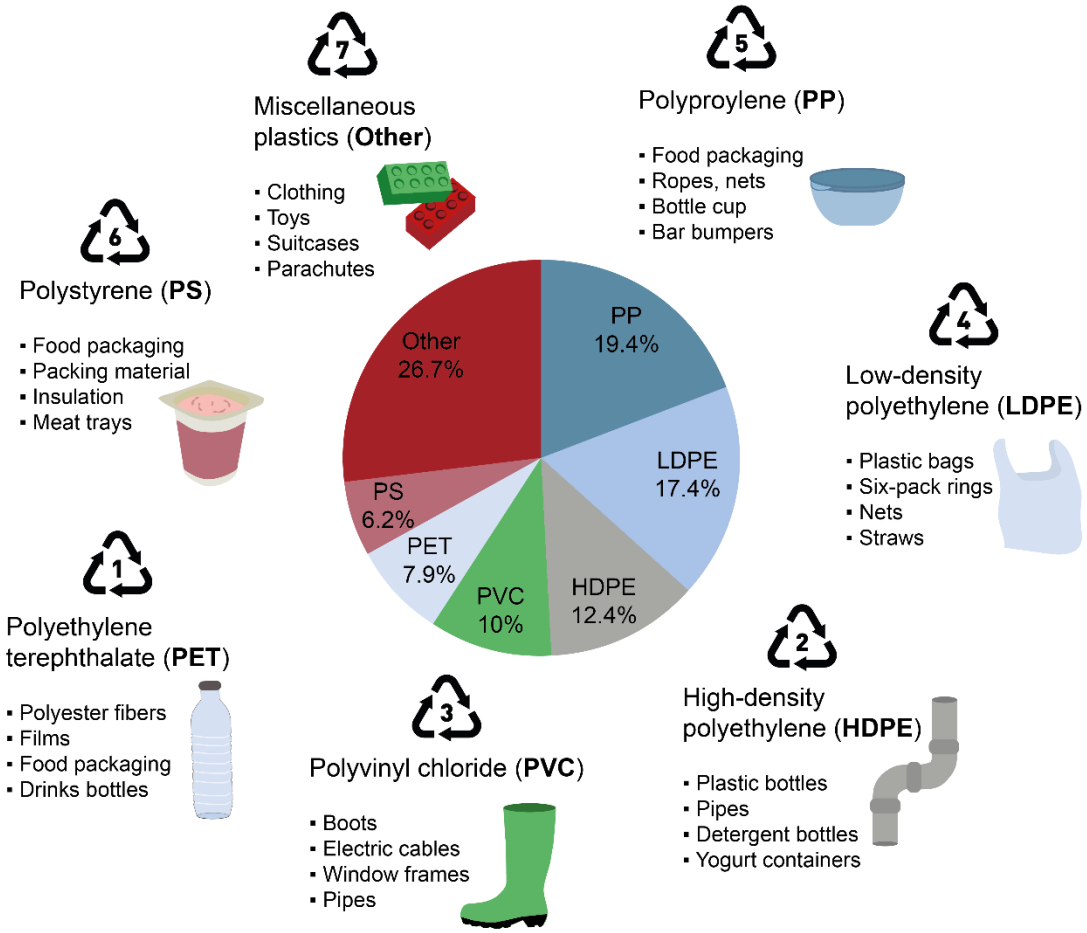

Figure 1.2. Common plastic polymers and their manufacturing demand in 2019. Based on data from Plastics Europe 2020[1].

Polyethylene (PE) is made by the polymerization of ethylene monomers and although it has the simplest basic structure in comparison to any other plastic polymer, it is today the most common plastic in use. Polyethylene has in fact many attractive

features such as low price, electrical insulation, chemical resistance, good processability, toughness, flexibility, and transparency[9]. Although polyethylene is available in a variety of grades and formulations to suit different needs (there are around 10 different types of polyethylene), high-density polyethylene (HDPE) and low-density polyethylene (LDPE) are the most common types. While HDPE is strong and resistant to moisture/chemical, typically used for cartons, containers and building materials (i.e., milk cartons, buckets, pipes, and toys), LDPE is softer, clearer, and more flexible, normally used for beverage cartons and other products (i.e., sandwiches bags, garbage or grocery bags and beverage cups). Because it has many applications, polyethylene accounts for 30% of the total plastics market[1] and, since it is commonly used for single use products (plastic bags, films, etc.), it rapidly ends up in the waste stream. Polyethylene is ubiquitous and the most abundant plastic type polluting aquatic ecosystems[10–13]. Finally, compared to other plastics, polyethylene has the highest sorption and diffusion capacity for hydrophobic, organic contaminants, due to its high permeability, greater free volume, flexibility, and mobility, that allows organic compounds, especially PAHs, to diffuse quickly through its molecular structure[9,14–16].

Besides PE, other plastic polymers are manufactured. Polyethylene terephthalate (PET or PETE) is transparent, lightweight, strong, heat resistant, typically used in food packaging or other products (i.e., beer bottles, jelly jars, clothing, ropes). Polyvinyl chloride (PVC) is resistant to weathering and chemicals, is impermeable to germs and does not conduct electricity, which makes this material perfect to be used for building, healthcare, and high-tech applications (i.e., floor covering, pipes, hoses, medical tubing). Polypropylene (PP) is more heat resistant than other polymers, hard but flexible and translucent, thus normally used to produce drinking straws, bottle caps, hot food containers, packaging tape and disposable diapers. Polystyrene (PS) is low-cost, rigid and insulates very well, thus widely used in the food packaging and construction market (i.e., styrofoam, take-out food containers, shipping and product packaging, egg cartons, cutlery and building insulation). Finally, other types of polymers or a mix of the ones described above are classified as OTHER kinds of plastic, and normally are not recyclable products (i.e., baby bottles, eyeglasses, medical storage containers).

1.1.2. Chemical additives improve plastic properties

In order to improve the performance, functionality and aging of plastic polymers, chemical additives such as stabilizers, antioxidants, flame retardants, antistatic agents, lubricants, colorants, reinforcements (e.g., glass fibers) are commonly added during the manufacturing process to enhance plastic properties[17]. For instance, plasticizers such as chlorinated paraffins, butyl benzyl phthalate (BBP) and Bis(2-ethylhexyl)phthalate (DEHP) are used to improve polymer flexibility, durability and stretchability[18]; Antioxidants and UV stabilizers such as nonylphenol (NP) and bisphenol A (BPA) delay plastic degradation when exposed to light[19]; Heat stabilizers such as cadmium and lead prevent thermal degradation[20]; Slip agents such as fatty acid amides reduce the friction surface coefficient[21]; Flame retardant such as chlorinated paraffins prevent the start or slowdown fire[22]; Biocides such as arsenic compounds are used as antimicrobials[23].

1.1.3. Plastic pollution in aquatic ecosystems

Aquatic environment (lakes, rivers, and oceans) is downstream from nearly every terrestrial location, and thus receives most of the plastic waste generated on land. Annual input of plastic from land to ocean is estimated between 4.8 and 12.7 million metric tons and is likely to drastically increase[24]. Plastic waste either come from land-based sources (human littering, agricultural and industrial facilities, natural storms, etc.) or ocean-based sources (illegal waste disposal in open sea, fishing activities, lost cargo, shipping, offshore platforms, etc.)[25]. Plastic is then spread around the world by the action of wind, currents, rivers, and waves. Plastic pollution is ubiquitous and massive with more than 5.25 trillion particles, such as microplastics, weighing 268,940 tons floating in the world's oceans[26]. Besides ethical and esthetical issues, plastic waste can negatively impact terrestrial/aquatic ecosystems, e.g., injure mammals, birds, reptiles, and fish by entanglement or cause their death by ingestion[27,28]. Plastic can also participate in the transport of non-native species[29] or smothering of the seabed and corals[30]. Over prolonged periods, exposure to different abiotic factors (i.e., light, temperature, wind, water, freezing and thawing, frictional stress) and/or biotic factors (i.e., biting, chewing, digestive fragmentation and other biochemical processes) can affect the structural integrity of plastic polymers that are

degraded into smaller fragments (see review by Zhang et al. (2021)[31] and references therein). Plastic fragments have been classified by the scientific community into five groups, based on their size: megaplastics (>1 m); macroplastics (<1 m), mesoplastics (<2.5 cm), microplastics (<5 mm); and nanoplastics (<1 µm). Plastic debris can also be classified according to their shape (i.e., spheres, films, fragments, or fibers). Because they are persistent, invisible to human eye and a threat to human health and the environment, microplastics have become in the last decade an issue of global concern[32–36].

1.2. MICROPLASTICS

Microplastics (MPs) are massively present in aquatic ecosystems and in the food web, representing a major concern for environment and human health. Thus, many international environmental and food agencies (e.g., UNEP, EFSA, GESAMP) have placed microplastics as one of the top priority research topics[37–39]. Small plastic debris can be classified as primary or secondary microplastics. Primary microplastics are manufactured intentionally at microscopic scale for industrial applications[40], e.g., in personal care products (cosmetics, deodorants, facial scrubs, shower gels, toothpaste, etc.), in industrial manufacturing (nurdles) and in synthetic textiles (plastic fibers). They are released into the aquatic environment through the runoff of urban/industrial effluents. Secondary microplastics originate from the breakdown of larger plastic particles already present into the environment[7,31].

Nowadays, microplastic are found almost everywhere on earth. Their presence has been reported at the ocean's surface but also in deep oceans at 10,890 meters[41], sediments and atmosphere, drifting in the air or falling with rain over mountains and cities. Plastic debris have reached even the most remote places on earth such as in Alps and Arctic snow[42], Antarctic ice[43], and even on the top of Mount Everest[44]. Beside the damage that they may cause to the aquatic life, microplastics also pose a threat to human health. In fact, microplastics can be ingested by any animal living on earth, then accumulated and transferred into the food chain, reaching humans as final consumers. In this regard, microplastics have also been found in goods of our daily life such as table salt, drinking water, beer, meat, and fish[45–48].

1.2.1. Chemical absorption or additives leaching microplastics

There are two main routes in which microplastics can be associated with chemicals, either during their manufacturing processes or by absorption of chemicals present into the environment. Chemicals leaching from microplastic and chemical absorption onto microplastics are complicated processes. In fact, the absorption/desorption chemical kinetics depends on several dynamic factors such as microplastic characteristic (i.e., polymer type, structure, size, shape and surface properties), water media parameters (i.e., temperature, pH, salinity) and chemical properties (i.e., solubility, stability, and redox state)[15,17] (Fig. 1.3). During plastic production, different additives are used to enhance plastic properties which may leach into the aquatic media or animal tissues upon ingestion of microplastics.

Recent studies have examined the chemical additive leaching out of the microplastics (see review by Bridson et al. (2021)[49]) upon abiotic/biotic weathering factors to determine the rate of release and their bioaccessibility. PE garbage bags and PVC electric cables incubated in seawater for one month leached out different types of phthalates (i.e., chemicals used as plasticizers)[50]. Degradation for 56 days of synthetic microfibers made of PET and PA released into the seawater benzophenone and bisphenol A among other additives[51]. A recent survey on PS debris collected on beaches revealed the presence in high concentrations of hexabromocyclododecanes (a common flame retardant) in all plastic debris, while some also leached out bisphenol A[52].

On the other hand, anthropogenic chemicals that end up into the aquatic ecosystems may absorb and accumulate[53] onto microplastics because of their hydrophobic nature, small size and large surface area. Polycyclic aromatic hydrocarbons (PAHs)[15,54], poly-chlorinated biphenyls (PCBs)[15,55], dichlorodiphenyltrichloroethane (DDTs)[15], metals[56,57] and pharmaceuticals[58] are persistent organic pollutants (POPs) that have been detected on plastic particles at concentrations higher than in the surrounding environment[59]. In this regard, PAHs were found to adsorb onto PP, PVC, PET, and LDPE microplastics[60]. In particular, PAHs, such as benzo[α]pyrene, have the ability to adsorb at high rates onto polyethylene[16,60,61].

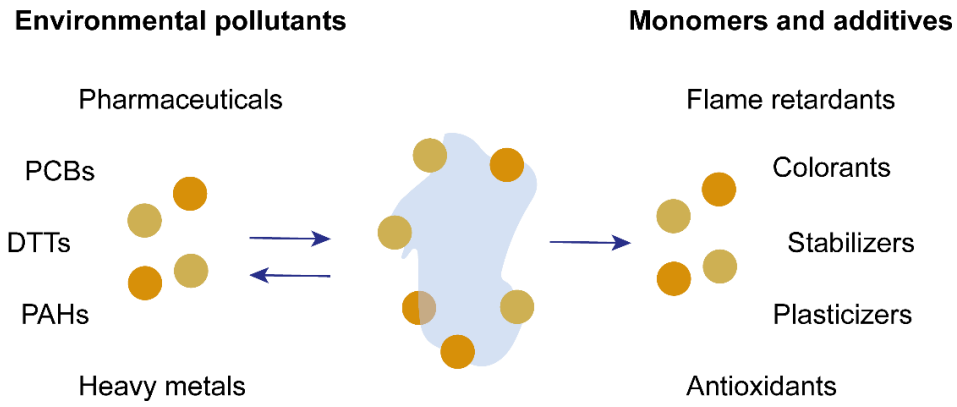

Chemical properties	Polymer properties	Environmental factors
Solubility	Surface area	pH
Stability	Surface charge	Salinity
Redox state	Density	Ionic strength
Surface charge	Weathering	Temperature
Hydrophobicity	Porosity	
	Molecular weigth	
	Crystallinity	

Figure 1.3. Factors that govern the adsorption of environmental pollutants or leaching of plastic additives. Based on information retrieved from Joo et al. (2021), Hahladakis et al. (2018), Agboola et al. (2021)[15,17,62].

1.2.2. Benzo[α]pyrene: a model PAH compound

Benzo[α]pyrene (BaP) is a member of the PAH family produced by incomplete combustion of organic matter at temperatures between 300-600 ºC. BaP presence in the environment typically results from natural events (i.e., volcanic activity and forest fires) and anthropogenic activities, such as smoking, car exhaust, petroleum exploration, residential waste burning and manufacturing of carbon, coal tar pitch and asphalt[63,64]. Because BaP and other PAHs are hydrophobic and chemically stable compounds, they are ubiquitous in the environment and have been detected in the atmosphere[65,66], aquatic ecosystems[67,68], and sediments[69]. Their lipophilic nature facilitates PAHs' accumulation in the fatty tissues of aquatic organisms thus their entry in the food web, raising environmental concerns[70,71]. Several studies have revealed the adverse effects of BaP and other PAHs on developmental, reproductive, hepatic, endocrine and immunological processes in exposed vertebrates[72,73]. Recent studies have shown that once adsorbed onto microplastics, BaP can enter the food web and accumulate into tissues upon ingestion of the contaminated microplastics[74–77].

1.2.3. Microplastic toxicity in fish

In aquatic ecosystems, microplastics are accessible to a wide array of organisms occupying different habitats, thus they have the capacity to induce adverse effects at several biological levels and possibly disrupt the entire ecosystem (Fig. 1.4). Aquatic organisms can ingest microplastics directly from the natural environment due to their inability to distinguish microplastics from natural prey or indirectly by ingestion of a organism already contaminated with microplastics. Microplastic toxicity can be physical – by blocking feeding appendages, impairing food transit through the intestine or causing false satiation thus resulting in a decrease in food intake[78,79] – or chemical – by leaching out additives or adsorbed contaminants that eventually accumulate into the animal tissues[80]. In this regard, additives such as bisphenol A, phthalates, and chlorinated paraffins are highly hazardous, and have already been identified as carcinogenic, mutagenic, endocrine disrupting and toxic to reproduction[81].

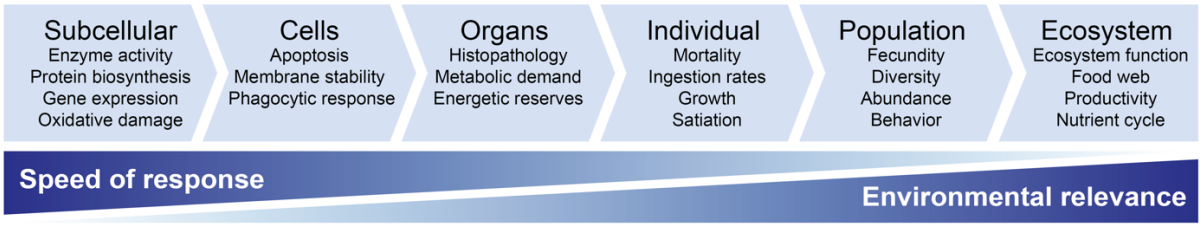

Figure 1.4. Potential impacts of exposure to microplastic among different levels of biological organization. Adapted from Galloway et al. (2017)[82].

The adverse effects of microplastic ingestion have been reported in all the different levels of the aquatic food web, from primary producers to top predators. For example, exposure to microplastic reduced feeding rates, growth, oxygen consumption and altered the development of tunicates[83,84]. Mussels exposed to microplastic showed alterations in oxidative stress enzymes, immune response, increased DNA damage and disorders in amino acids metabolism[85–89] as also reported for bottom feeders such as crabs[90,91]. Zooplankton ingestion of microplastic particles resulted in intestinal damage, delayed growth, impaired feeding, and affected their behavior, reproduction, and offspring[92,93].

Fish are central to the ocean food web and to human nutrition, and presence of several type of microplastics – mainly PE, PS and PP – have been reported in wild fish from several marine and freshwater environments (Table 1.1), including in species

marketed for human consumption such as the European sea bass (*Dicentrarchus labrax*)[94,95], gilthead seabream (*Sparus aurata*)[96], Atlantic horse mackerel (*Trachurus trachurus*)[48,94,97], Atlantic chub mackerel (*Scomber colias*)[94], common pandora (*Pagellus erythrinus*)[98], blackspot seabream (*Pagellus bogaraveo*)[98] and many other commercial species[48,99]. A recent study also showed that many of the species used in fishmeal production, contain in average 0.72 microplastics per individual, and analysis of commercial samples of fishmeal revealed the presence of 123.9 ± 16.5 microplastics/kg (mainly PE). In this regard, microplastic-containing fishmeals have the capacity to contaminate aquaculture fishes marketed for human consumption[97].

Table 1.1. Occurrence of microplastics in fish sampled in natural aquatic environments. For each case, fish species and ingested microplastic characteristics (size, color, shape, type, and concentration) are indicated. PE: polyethylene; HDPE: high-density polyethylene; LDPE: low-density polyethylene PP: polypropylene; PA: polyamide; PET: polyethylene terephthalate; PS: polystyrene; PU: polyurethane. N.A.: not available. Adapted from Wang et al. (2020)[100].

Location	Species	Size (mm)	Color	Shape	Type	Concentration	Reference
Marine							
North Pacific Central Gyre	Indian Pacific starfish (*Astronesthes indopacifica*), Pacific saury (*Cololabis saira*), lanternfish (*Hygophum reinhardtii*), Chardonnay fish (*Loweina interrupta*), Golden lanternfish (*Myctophum aurolanternatum*), Bigfin lanternfish (*Symbolophorus californiensis*)	1–2.79	White, clear, blue, green, black, yellow, etc.	Fragments, film, line, rope, foam, etc.	N.A.	35% contained microplastics (2.1 ± 5.78 items/fish)	(101)
Portuguese coast	26 species of benthic and pelagic fish	0.217-4.81	N.A.	Fibers, fragments	PP, PE, alkyd resin, rayon, PS, nylon, and acrylic	19.8% contained microplastics (1.40 ± 0.66 items/fish)	(48)
North Atlantic	10 species of mesopelagic fish	0.5–11.7	Black, blue, gray, orange, green, red	Fibers, fragments	N.A.	1.2 ± 0.54 items/individual	(102)
North Sea and Baltic Sea	Common dab (*Limanda limanda*), European flounder (*Platichthys flesus*), Atlantic cod (*Gadus morhua*), Atlantic herring (*Clupea harengus*), Atlantic mackerel (*Scomber scombrus*)	< 5	White, clear, black, blue, yellow, green, red, brown	Fragments, film, spherule, fibers	PE, PA, PP, PS, PET, PU, rubber	5.5% contained microplastics	(103)
Tokyo Bay, Japan	Japanese anchovy (*Engraulis japonicas*)	0.15–6.83	White, transparent, green, yellow, black, brown, pink	Fragments, bead, filament, foam	PE, PP, PS, others	2.3 ± 2.5 items/individual	(104)

Location	Species	Size (mm)	Color	Shape	Type	Concentration	Reference
South Africa urban harbor	Mullet (*Mugil cephalus*)	0.2–15	White, clear, red, etc.	Fibers, fragments, foam, film, line	N.A.	3.8 ± 4.7 items/individual	(105)
Western Mediterranean Sea	Blackmouth catshark (*Galeus melastomus*)	< 5	Transparent, blue, black, red, white	Fibers, fragments, film	Cellophane, PET, PP, PA, others.	0.34 ± 0.07 items/individual	(106)
Tuticorin coast, India	Indian mackerel (*Rastrilliger kanagurta*), Honeycomb grouper (*Epinephalus merra*),	0.5–1	Transparent, black, blue, red, etc.	Fiber, fragments	PE, PP	30% contained microplastics	(107)
Musa Estuary and Persian Gulf	Bartail flathead (*Platycephalus indicus*), Greater lizardfish (*Saurida tumbil*), northern whiting (*Sillago sihama*), Tongue sole (*Cynoglossus abbreviatus*)	< 0.1– > 1	Black or gray, blue, green, red, white, transparent, etc.	Fibers, fragments	N.A.	0.16–1.5 items/g	(108)
East coast of Vancouver Island, British Columbia	Juvenile Chinook salmon (*Oncorhynchus tshawytscha*)	0.1-5	Transparent, blue	Fibers	N.A.	59% contained microplastics (1.2 ± 1.4 items/fish)	(109)
Tyrrhenian Sea, Italy	Common pandora (*Pagellus erythrinus*), blackspot seabream (*Pagellus bogaraveo*)	<5	Black	Fibers	Polyamide	9.1% contained microplastics	(98)
Portuguese Northwest coast, Northeast Atlantic Ocean	European seabass (*Dicentrarchus labrax*), Atlantic horse mackerel (*Trachurus trachurus*), Atlantic chub mackerel (*Scomber colias*)	<5	*D. labrax*: blue, whitish, black, red/pink, yellow. *T. trachurus*: blue and whitish. *S. colias*: blue, whitish, black, red/pink	Fibers, fragments, pellets	PE, PS, rayon	*D. labrax*:1.2 ± 2.0 items/individual, *T. trachurus*: 0.7 ± 1.2 items/ individual, *S. colias*: 0.054 ± 0.099 items/g of tissue	(94)
Mar Menor lagoon, Spain	Gilthead seabream (*Sparus aurata*)	0.091-5, average of 0.83 ± 0.04	White, blue, red, black, brown, yellow	Fibers, fragments, film, microbeads	HDPE, LDPE, PE, PEP, PVC	20.11 ± 2.94 items/kg of fish	(96)

Location	Species	Size (mm)	Color	Shape	Type	Concentration	Reference
Coastal water of Tenerife, Canary Island, Spain	European seabass *(Dicentrarchus labrax)*	< 5	Blue, yellow, black, transparent, others	Fibers, fragments, film, lines	Cellulose, nylon, PE, PP	65% contained microplastics (1.43 ± 1.75 items/fish)	(95)
Freshwater							
Brazos River Basin, USA	Bluegill (*Lepomis macrochirus*), Longear (*Lepomis megalotis*)	0.5–5	Gray, blue, red, black, green, others	Thread, foam, line, sphere, others	N.A.	45% contained microplastics	(110)
River Thames, UK	European flounder (*Platichthys flesus*), European smelt (*Osmerus eperlanus*)	< 5	Black, clear, blue, red	Fibers, fragments	PE, PET, PA, acrylic, others	*P. flesus*: 75% contained microplastics; *O. eperlanus*: 20% contained microplastics	(111)
Eleven French rivers	Gudgeon (*Gobio gobio*)	< 5	Colored, transparent	Fibers, pellet	N.A.	12% contained microplastics	(112)
Xiangxi Bay of Three Gorges Reservoir, China	13 fish species	0.3–1.8	White, transparent, blue, red	Line, fragments, sheet	PE, PA	25.7% contained microplastics	(113)
Rio de la Plata estuary, Argentina	11 fish species	0.6–4.7	Red, green, yellow, white, black, blue	Fibers, others	N.A.	19.2 items/individual	(114)
Amazon River estuary	46 fish species	0.38–4.16	Clear, yellow, orange, blue	Pellet, sheet, fragments	PA, PE	1.2 ± 5.0 items/individual	(115)

1.3. ZEBRAFISH AS A VERTEBRATE ANIMAL MODEL

Although the occurrence and detection of microplastic in fish can be assessed in wild populations, studying the effects of microplastic at the biological level requires the use of animal models in laboratory conditions. In fact, it is extremely difficult, if not impossible, to evaluate the effect of microplastics on fish survival, development, reproduction, or offspring through environmental sampling. In this regard, most of the recent studies on the effect of microplastics in fish have been performed using zebrafish as animal model.

1.3.1. The advantages of using zebrafish

Zebrafish (*Danio rerio*) is a small freshwater fish belonging to the Cyprinidae family from the tropical regions of South and Southeast Asia. Due to numerous technical advantages (see below), zebrafish is nowadays a well-established model organism in multiple research fields, particularly in aquatic toxicology. Zebrafish has many compelling advantages such as inexpensive maintenance, small size, high fecundity, rapid/external development, and translucent body during embryogenesis. For instance, 200-300 eggs can be produced every week by a single spawning, larvae can be easily accommodated in 96-well plates, and they are able to absorb chemicals directly from the water. Larvae can also live for seven days relying on yolk sac contents providing a robust experimental approach, not affected by feeding conditions. Rapid development offers the opportunity to perform transgenerational studies. In addition, the zebrafish genome has been totally sequenced and annotated and 70% of human genes have a zebrafish ortholog[116]. In this regard, the ease in genetic manipulation/editing tools allows the development of mutant/transgenic lines which excellent proxy to get insights into specific molecular mechanisms[117,118]. Finally, the translucid nature of embryos and larvae coupled with transgenic lines or specific staining provide huge advantages in live imaging such as visualization of ingested fluorescent microplastic[74,75], bone structures and other specific cells/tissues[119,120].

1.3.2. Effects of microplastics on zebrafish

Most of the recent studies on zebrafish have evaluated the effects of microplastic exposure (pristine or contaminated with environmental pollutants) on development, neurotoxicity, behavior, immunotoxicity, intestinal damage, microbiome changes, and oxidative stress (experimental conditions and biological effects are summarized in Table 1.2). The results are somehow contradictory with several studies reporting a clear toxicity of the microplastics (normally higher in combination with pollutants), while others showed limited or no effect. Variability in biological responses may be due to the different type and size of plastic tested, different exposure duration, concentration, and route. Due to laboratory limitations (i.e., static conditions, absence of recirculating housing systems to study microplastic), most of the studies have performed short term trials, reaching a maximum of 21 days of exposure. Although short-term exposure brings new insights into the acute effects of microplastic ingestion, they do not really mimic what may happen in nature i.e., a long-term exposure throughout the complete developmental process. A single study, Cormier et al. (2021)[121], evaluated the effects of PE exposure throughout zebrafish development from 5 to 120 days post-fertilization (dpf) and PVC from 60 to 120 dpf, pristine or spiked with BaP, PFOS or BP3. After 2 months of exposure, a decreased in growth and reproduction performance was reported in all tested conditions. While reduction in larval growth did not differ between type of plastic and spiked pollutants, PVC affected reproductive output more than PE, as microplastic spiked with PFOS and BP3 affected more than those spiked with BaP.

Table 1.2. Effects of microplastics on different life stages of zebrafish. PE: polyethylene; PS: polystyrene; PVC: polyvinyl chloride. BP3: oxybenzone; BaP: benzo[a]pyrene; PFOS: perfluorooctane sulfonate; Cu: copper; BHA: butylated hydroxyanisole; Cd: cadmium; 9-NAnt: 9-nitroanthracene; Phe: phenanthrene; h: hours; d: days; m: months; N.A.: not available. Adapted from Bhagat et al. (2020)[122].

Development stage	MP size (µm)	MP type	MP and contaminant concentration	Sites of accumulation	Administration	Days of exposure	Biological effects	Reference
Embryo	11–13	PE	10 and 100 mg/L spiked with BP3 (20 µg/L), BaP (2.5 mg/L), PFOS (20 mg/L)	N.A.	Water	4	EROD activity and *cyp1a* expression increased upon exposure to MPs spiked with BP3 or BaP	(123)
Embryo	140.6 ± 80.0	PE	100 mg/L	N.A.	Water	4	No effects	(124)
Embryo	1–4	PE	10, 100, and 1000 mg/L	N.A.	Water	7	Changes in microbiome populations and in levels of triglyceride, total cholesterol, nonesterified fatty acid, total bile acid, glucose and pyruvic acid; Down-regulation of glucose and lipid metabolism-related genes	(125)
Embryo, larvae	1	PS	100 and 1000 µg/L	Embryo: chorion; Larvae: mouth, stomach, and intestinal tract	Water	5	Decrease in swimming performances	(126)
Embryo, larvae	1–5	N.A.	2 mg/L spiked with Cu (60 or 125 µg/L)	Gastrointestinal tract	Water	14	Neurotoxicity, oxidative stress and lipid damage in larvae, leading to activation of the antioxidant system and detoxification mechanisms	(127)

Development stage	MP size (μm)	MP type	MP and contaminant concentration	Sites of accumulation	Administration	Days of exposure	Biological effects	Reference
Embryo, larvae	38.26± 15.64	PE	6.2, 12.5, 25, 50 and 100 mg/L	N.A.	Water	6	Early hatching of embryos; Low survival rate of larvae; Significant morphological changes	(128)
Embryo, larvae	0.065 and 20	PS	2 mg/L spiked with BHA (1 mg/L)	Gastrointestinal tract	Water	7	Accumulation of BHA; Reduced hatching rates, increased malformation rates, and decreased number of calcified vertebrae; Disturbed metabolism of arachidonic acid, glycerophospholipid and lipids	(129)
Larvae	5–50	PS	100 and 1000 mg/L	Intestinal tract	Water	7	Altered microbiome; Decreased CAT and GSH content; Disturbed glycolipid and energy metabolism	(130)
Larvae	10–45	PE	5 and 20 mg/L	Intestinal tract	Water	14	No effects on development and growth; Transient effect on gene expression within 48 h exposure	(131)
Adult, larvae, embryo	1–5, 10–20	PE	3 mg/L spiked with BaP (10 μM)	Adult: gills; Larvae: intestinal tract; Embryo: chorion	Water	1	BaP transfer via attachment to epithelia; *cyp1a* up-regulation	(75)
Larvae	< 17.6	LDPE	5, 50 and 500 mg/L	Intestinal tract	Water	20	No effects	(132)

Development stage	MP size (μm)	MP type	MP and contaminant concentration	Sites of accumulation	Administration	Days of exposure	Biological effects	Reference
Larvae, adult	PE (11–13); PVC (125–250)	PE, PVC	PE spiked as in Cormier et al. (2019). PVC spiked with BP3 (20 μg/L), BaP (5000 μg/L), and PFOS (200 mg/L) in diet 1% w/w	N.A.	Dietary	120	Decreased growth after 2 months of exposure; Decreased reproductive performance (PVC > PE; MP+PFOS/BP3 > MP+BaP); Disrupted behavior in larvae by PVC+BP3	(121)
Adult	0.1, 5, 200	PS	500 μg/L	Intestine	Water	21	Dysfunctional intestinal immune cells	(133)
Adult	0.1, 20	PS	200 μg/L spiked with Cu (50 μg/L)	Gut, liver, and gills	Water	3	Aggravated Cu accumulation in liver and gut by MPs and natural organic matter; Increased levels of malonaldehyde, metallothionein and SOD activity	(134)
Adult	1–5, 10–20	PE	*Artemia* (10000 nauplii fed MPs)	Intestine	Dietary	14	Tropic transfer of MPs and BaP from *Artemia* to zebrafish; *cyp1a* upregulation	(74)
Adult	5	PS	20 and 100 μg/L	N.A.	Water	21	Decreased body weight; Decreased levels of glucose, pyruvic acid, α-ketoglutaric acid, and isocitrate dehydrogenase	(135)
Adult	5	PS	20 and 200 μg/L, co-exposed with Cd (10 mg/L)	N.A.	Water	21	Combined exposure cause oxidative damage and inflammation	(136)

Development stage	MP size (μm)	MP type	MP and contaminant concentration	Sites of accumulation	Administration	Days of exposure	Biological effects	Reference
Adult	125–250	PE	4% pristine MPs; 2% contaminated MP	N.A.	Dietary	21	Upregulated *prdx1*, *gstp1*, *cyp1a1* in liver; Upregulated *chrna1*, *ngn1*, *cyp1a1* in brain	(137)
Adult	4-6, 125–500	PE	*Artemia* (10000 nauplii fed 1 mg of MPs spiked with BaP) or included in diet (1% w/w)	N.A.	Dietary	21	No adverse effects detected; No BaP accumulation/transfer	(138)
Adult	100-150	PE	10 and 40 mg/L spiked with 9-NAnt (500 mg/L)	N.A.	Water	4, 7	Altered oxidative stress enzymatic activity. Inhibited markers (AChE and LDH activity) of neurotoxicity and energy metabolism disorders; Altered intestinal microbiota populations; Bioaccomulation of 9-nitroanthracene	(139)
Adult	150	PS	3 mg/L spiked with Phe (0.2 mg/L)	Intestine	Water	12, 21	Bioaccomulated phenanthrene (higher when spiked); Altered SOD, GST and CYP1A activities; Altered expression of immune (*tnfα*, *il-6*, *il-10*) and antioxidant (*sod1*, *gstr*, *cyp1a*) related genes in liver and gills	(140)

1.3.3. Microplastic effects on bone

Although ingested microplastics can impair many biological endpoints in fish (Fig. 1.5), only scarce data are available on whether they may trigger skeletal defects. Abnormal bone homeostasis in fish can result from factors such as temperature, ocean acidification, water flow, genetic background, nutrition, and exposure to environmental pollutants[141–145] and such defects may affect swimming performance and impair feeding activity, affecting fish welfare and increasing their mortality.

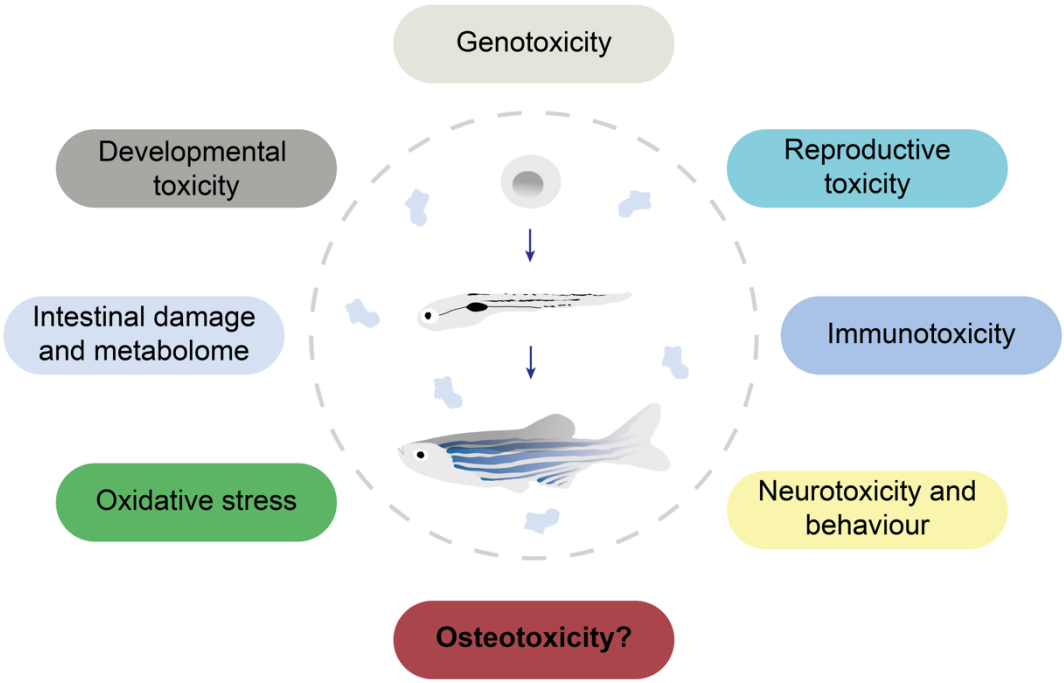

Figure 1.5. Research biological endpoints on the effects of microplastics in zebrafish. Adapted from Bhagat et al. (2020)[122].

The only study available to date was recently published by Zhao et al. (2020)[129]. They assessed the effect of two different sizes of PS microparticles (i.e., 0.065 and 20 μm) pristine or contaminated with butylated hydroxyanisole (BHA) – a synthetic antioxidant widely used to prevent aging of plastics – on skeletal development. MPs spiked with BHA increased the rate of morphological deformities upon 7 days of exposure (i.e. pericardial edema, yolk sac edema, hyperemia and spinal deformity), while pristine particles did not trigger any defects. Exposure to the smaller size of contaminated MPs (0.065 μm) for 12 days decreased the number of calcified vertebrae, while MP alone did not show any difference. In both trials, the authors showed that the effects of

MPs+BHA was always stronger when compared to waterborne exposure to BHA, suggesting that MPs may enhance contaminants toxicity. Although pristine MPs may not affect skeletal development, plastic additives but also environmental pollutants with the capacity to adsorb onto microplastics, are known to be endocrine disruptors, induce inflammation and oxidative stress and may affect bone homeostasis[146,147]. For example, bisphenol A has the ability to impair the development of cartilage and craniofacial structures in zebrafish larvae[148], while exposure to 4-nonylphenol from 4 hpf to 4 dpf impaired vertebral column development in 21 dpf zebrafish juveniles. Cadmium, commonly used during plastic production as heat stabilizer is also a disruptor of skeletal development in mammals and fish[145].

There is a lack of experimental data on the effects of pristine and contaminated microplastics on fish skeletal development, and future studies should aim at assessing the osteotoxic effects upon microplastic ingestion.

1.3.4. What is osteotoxicity?

Osteotoxicity (or bone toxicity) is generally defined as any damage to bone during its development or maintenance by acute or chronic exposure to exogenous compounds, resulting in an impaired skeletal mineralization, remodeling and morphogenesis[147]. Mechanisms underlying compound osteotoxicity have already been described, e.g., altered activity of membrane or nuclear receptors controlling the transcription of bone related genes, altered cellular redox status or altered composition of the extracellular matrix[147], but much remains to be done to understand how osteotoxicants impair cellular processes (i.e., proliferation, differentiation, apoptosis and activity) which lead to changes in physical-chemical properties of the bone (e.g., fragility, stiffness, porosity, density).

1.3.5. The importance of the skeleton

Although teleosts (such as zebrafish) and tetrapods diverged approximately 420 million years ago, skeletal functions, processes of bone formation and mineralization, skeletal tissues (cartilage and bone) and bone cell types resemble in many aspects those found in mammals[120]. The fish skeleton maintained the same mechanical functions found in other vertebrates. It provides structural support for

some tissues and organs (i.e., gill tissues and pharyngeal teeth), and protects internal organs. It facilitates movements (i.e., locomotion, articulation of the jaw and operculum movements during respiration) by providing muscles a rigid structure to generate forces[149,150]. In fish, skeleton is also central to the maintenance of mineral homeostasis by serving as a mineral reservoir of calcium and phosphorus[151,152]. It is worth to mention that while mammalian skeleton hosts the hematopoietic niche and it has endocrine functions, teleost skeleton did not conserve these non-structural functions throughout evolution[153,154].

1.3.6. Bone, the main connective tissue

Among the different tissues forming the skeleton, bone is a dense and specialized connective tissue composed of a mineralized and vascularized collagen matrix and hosting four different types of cells: osteoblasts, bone lining cells, osteocytes and osteoclasts.[155] The bone matrix is mainly composed by inorganic molecules (60%) such as hydroxyapatite ($Ca_{10}(PO_4)_6(OH)_2$), which gives hardness/ rigidity to bone, and organic molecules (40%), which provide a scaffold on which hydroxyapatite crystals can arranged. Organic molecules consist mainly of type I collagen (90%) and non-collagenous proteins (10%) such as osteocalcin, osteopontin and osteonectin. Osteocalcin has the ability to bind to calcium, mediating its association with hydroxyapatite[156]. Osteopontin is involved in biological activities such as proliferation, migration, and adhesion of several bone-related cells (i.e., osteoclast)[157]. Osteonectin links collagen to hydroxyapatite, serves as a nucleus for mineralization and regulates the formation and growth of hydroxyapatite crystals[158].

1.3.7. Bone forming cells: the osteoblasts

Bone matrix is produced by the osteoblast (4-6% of the total resident cells), which secrete both collagen and other specialized proteins. At the onset of bone formation, osteoblast secrete collagen fibers that polymerize and form an immature and unmineralized scaffold called osteoid[149]. Calcium ions then bind to matrix proteins and osteoblasts produce alkaline phosphatase to increase levels of inorganic phosphate necessary to the formation of hydroxyapatite, but also to reduce extracellular pyrophosphate concentration, an inhibitor of mineral formation[159]. In cellular bone[154], osteoblasts get buried in the mineralized bone matrix and

differentiate into osteocytes (90-95% of the total cell content), which coordinate bone response to mechanical loading (i.e., they participate in the mechanosensing system) and transduce biological signals through their cytoplasmic extensions[160]. Some osteoblasts also differentiate into bone lining cells characterized by a flat and elongated shape. These cells are quiescent and rest on the bone surface; they prevent the direct interaction of osteoclasts with bone matrix at sites where bone resorption must not occur[161] and, if necessary, are activated to become mature osteoblast[162].

Bone is formed through different processes of ossification, the two most common being endochondral and intramembranous ossification. In the course of endochondral ossification, bone forms through the replacement of a cartilaginous anlage by an osteoid and subsequent mineral deposition, while intramembranous ossification occurs directly from mesenchymal cell condensations without the formation of a cartilage matrix[149].

Osteoblasts derive from pluripotent mesenchymal stem cells (as adipocytes, chondrocytes and fibroblasts) that undergo a maturation process where transcription factors such as Runx2 and Sp7 play an important role. Runx2 is a critical determinant of osteoblast commitment that drives the differentiation of mesenchymal stem cells to pre-osteoblast[163]. During osteoblast maturation, Sp7 promotes cell proliferation and differentiation by activating the expression of essential downstream genes such as *collagen 1*/*col1a1*, *osteocalcin/bglap*, *osteonectin/sparc* and *osteopontin/spp1*, which are central to matrix mineralization[164] (Fig. 1.6). Because of their critical role during osteoblastogenesis, *osterix* (*sp7*) and *osteocalcin 2* (*bglapl*/*oc2*) are commonly used as markers of immature and mature osteoblast, respectively, and zebrafish transgenic reporter line are readily available[165,166].

1.3.8. Bone resorbing cells: the osteoclasts

Bone matrix is resorbed by osteoclasts, which are large motile multinucleated cells responsible for the dissolution of the extracellular mineralized matrix and release of minerals. Upon specific signals (e.g., from the mechanosensing system), osteoclasts are recruited to target sites at the bone surface, where they attach and create a sealed compartment. Bone resorption occurs by the acidification of this compartment and the release of proteases which breakdown the mineralized

matrix[167]. To acidify the compartment, osteoclast release protons and passively transport chloride into the compartment, which form hydrochloric acid, a potent acid responsible for the dissolution of the crystalline hydroxyapatite[168]. At the same time, lysosomal proteolytic enzymes such as cathepsin K (Ctsk) and matrix metalloproteinases (Mmp) degrade the organic components of the extracellular mineralized matrix[169,170]. During bone resorption, osteoclast secrete also tartrate-resistant acid phosphatase (TRAP, coded by *acp5* gene) into the resorption lacuna, where it de-phosphorylates the bone matrix protein osteopontin, thus promoting osteoclast detachment and migration[171]. When the breakdown of the matrix is completed, osteoclasts undergo apoptosis to avoid excessive resorption[172].

Osteoclast derive from hematopoietic precursors of the myeloid lineage which have the ability to differentiate into monocytes or macrophages[173]. Osteoclastogenesis is mainly controlled by osteoblasts through the production of several factors such as the macrophage colony stimulating factor (M-CSF; that stimulates the proliferation and fusion of osteoclast precursors), the receptor activator of NF-κB ligand (RANKL; that induces cell fusion and differentiation towards mature and activated osteoclasts by binding to RANK, a receptor present in osteoclast precursor) and osteoprotegerin (OPG) (an antagonist of RANKL), which inhibits osteoclast differentiation[173,174] (Fig. 1.6). Markers of differentiated and active osteoclasts are Ctsk, Mmp9 and Acp5.

1.3.9. Bone remodeling

Bone is a dynamic tissue that is constantly remodeled to: (1) reshape in order to adapt to mechanical loading, (2) heal after fractures or (3) participate in calcium homeostasis[179]. Bone remodeling is a physiological process in which old or damaged bone is removed by osteoclasts and replaced by new bone formed by osteoblasts. An imbalance between bone resorption and bone formation may occur under certain pathological conditions, which leads to abnormal bone structure and the development of skeletal disorders that can alter animal welfare[180]. Bone remodeling is carried out by an anatomical structure (the basic multicellular unit), which requires the coordination of the major bone cell types and occurs in four distinct phases. When osteocytes detect a micro damage or sense a deformation in bone, they emit signals to recruit osteoclast precursors at the specific site. Osteoclast precursors get attached

to the bone matrix, differentiate into active osteoclasts (multinucleated giant cells) in response to elevated concentrations of the macrophage colony-stimulating factor and RANK ligand and initiate the resorption process[175,181]. During this phase, pre-osteoblasts are also recruited from the bone marrow or from nearby capillaries, and progressively differentiate and start to produce the osteoid, contributing to bone formation and ensuring the equilibrium between bone removal and formation. At a final stage, the osteoid becomes mineralized, concluding the bone remodeling cycle[182].

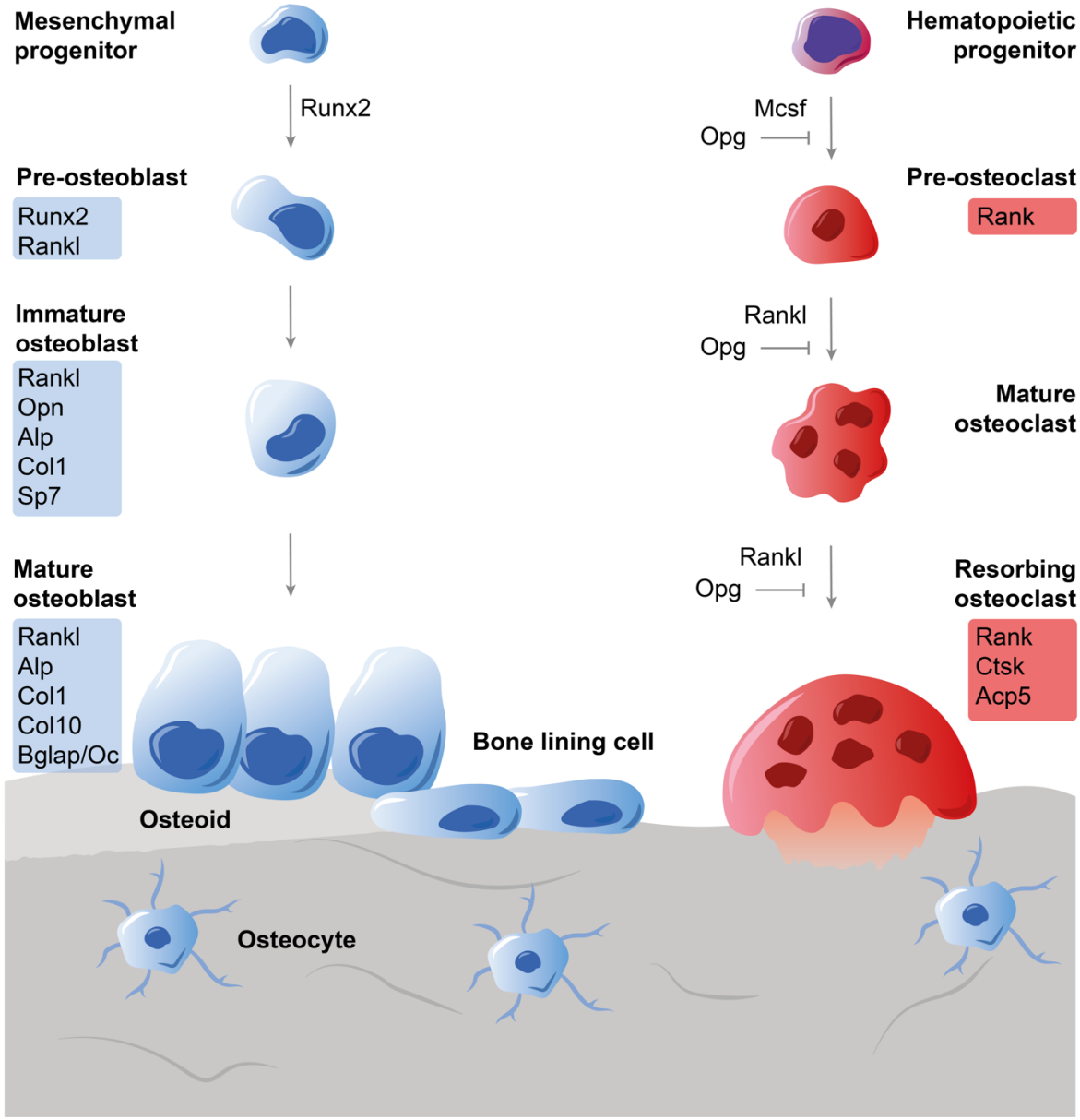

Figure 1.6. Schematic representation of the marker genes involved in osteoblastogenesis (left) and osteoclastogenesis (right). Based on data from Boyle et al. (2003), Al-Bari et al. (2020), Kim et al. (2020) and Rutkovskiy et al. (2016)[175–178]

1.3.10. Zebrafish systems to evaluate osteotoxicity

Various *in vivo* tools are available in zebrafish to study the osteotoxic effects of pollutants during bone development and regeneration. In this regard, changes in operculum growth have been extensively used to study osteotoxic compounds[144,145,183,184] during bone development. Incidence, typology, and number of deformities are normally used to evaluate the osteotoxic effects during skeletal development[144,145]. Caudal fin regeneration upon amputation and scale regeneration upon removal have been used to study osteotoxic effects on *de novo* bone formation/resorption and patterning[185–187]. In these different *in vivo* systems, osteotoxic effects are commonly detected through the morphometric analysis of bone structures that have been previously stained with bone specific dyes – which bind to mineral components of the extracellular matrix – such as alizarin red S or calcein for calcium (cation) and von Kossa for phosphate (anion). Zebrafish systems available to evaluate the effects of compounds on bone formation and regeneration will not be further detailed here as they are thoroughly reviewed in Chapter 4.

1.4. AIM AND OBJECTIVES

Although there is a large consensus on the need to collect additional data on the impact of microplastics on living organisms, the information currently available on the biological effects of pristine or contaminated microplastics is scarce or controversial. Thus, much remains to be done to uncover the mechanisms underlying microplastic toxicity, in particular in aquatic animals, which are first-in-line organisms experimenting their adverse effects. Such information is essential to improve the current knowledge on issues related to microplastic pollution but also to support the establishment of environmental management policies.

This work aims at gaining insights into the toxic effect of microplastics on bone homeostasis using zebrafish as laboratory model. Because polyethylene (PE) is it the most abundant plastic polymer polluting aquatic environments, PE microparticles ranging 20-27 µm in size were chosen as study material. Similarly, because PAHs are ubiquitous pollutants in the aquatic environment and because they have a high affinity for PE (i.e., they easily adsorb on PE particles), benzo[a]pyrene (BaP) – a model compound of the PAHs family – was chosen to contaminate microparticles and assess whether the combination microplastic and environmental pollutant could present an additional threat to aquatic life.

The specific objectives of this thesis were:

- Design and build a housing system for zebrafish to perform state-of-the-art experiments with microplastics, in particular long-term exposure, while maintaining optimal water quality for fish culture and reducing interferences from plastic particles and chemicals that could originate and leach out from the plastic parts of the commercial housing systems currently available (Chapter 2);

- Develop morphometric tools to automate and standardize data acquisition from images of bone structures that may be affected in fish exposed to pristine and contaminated microplastics and gain quality information on their osteotoxicity (Chapter 3);

- Characterize the adverse effects of a long-term exposure of zebrafish to

pristine/contaminated MPs on growth, reproductive performance and skeleton/bone formation throughout development. Because ingestion probably represents the most likely way of fish exposure to microplastics, pristine and contaminated microplastics will be supplement to fish diets. Because information on MP osteotoxicity is scarce, a particular focus will be given to adverse effects on bone growth, mineralization and regeneration but also on the incidence of skeletal deformities (Chapter 5);

- Gain insights into the mechanisms of PAH osteotoxicity through the waterborne exposure of zebrafish to benzo[a]pyrene. Because microplastics contaminated with BaP triggered a stronger osteotoxic effect, relevant information on bone-related cellular and molecular mechanisms affected by this organic pollutant are of utmost interest (Chapter 6).

Scientific data on microplastic pollution in the aquatic environment and adverse effects on aquatic life, but also arguments to validate the zebrafish as a suitable model to assess mechanisms of osteotoxicity will be presented in a general introduction (Chapter 1). Zebrafish *in vivo* systems available to assess chemical osteotoxicity and tools to collect data in a more automatized and standardized manner will also be presented briefly (Chapter 4). Finally, a general conclusion (Chapter 7) will summarize the several findings uncovered throughout this work and will present perspectives for future works on this subject to gain critical knowledge on adverse effects generated by microplastic pollution.

Chapter 2

ZEB316: a small stand-alone housing system to study microplastics and organic pollutants in small teleosts

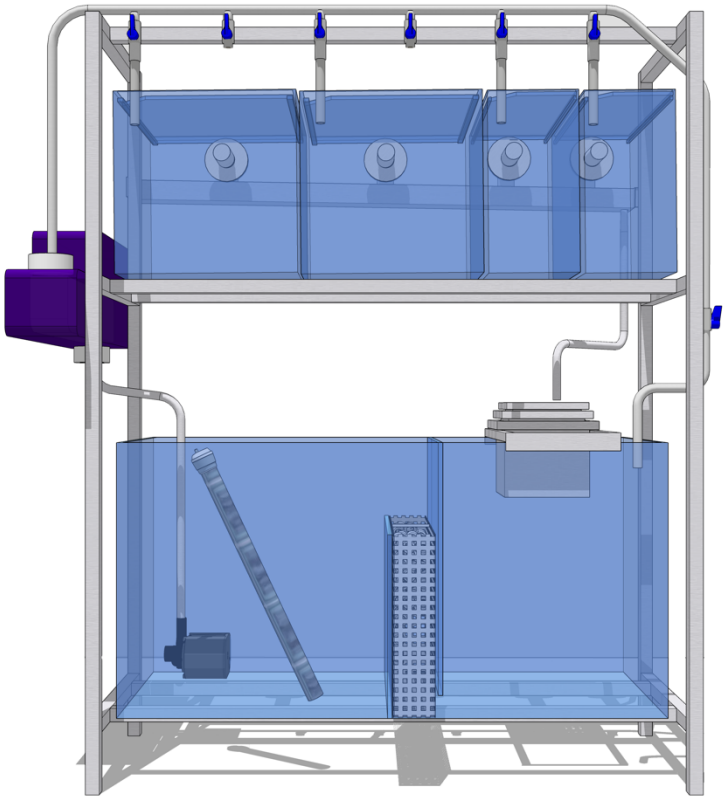

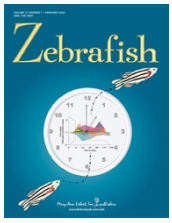

Published chapter:

Tarasco M, Gavaia PJ, Bebianno MJ, Cancela ML, Laizé V (2020). ZEB316, a small stand-alone housing system to study microplastics in small teleosts, Zebrafish, 17(1), 18-26

PREAMBLE

The growing interest of the scientific community for zebrafish as animal model has stimulated the development of commercial housing systems with water recirculation that provide a stable and optimal environment for the growth and reproduction of zebrafish. Housing systems are normally composed by several components (i.e., racks, tanks, tubing) connected to an automatized filtration unit which monitors and keeps water parameters at the desired conditions. Systems can be designed to meet specific requirements of any research lab and generally used for the maintenance of zebrafish breeders and transgenic lines. For specific research fields, such as toxicology and drug discovery, companies commercialize small stand-alone flow-through systems, that are designed specifically to evaluate the exposure of zebrafish to specific compounds. However, none of these available systems are really designed to perform studies aiming at assessing the toxic effect of microplastics. In fact, available commercial solutions are made with plastic polymer components (e.g., aquariums, valves, tubing, filtration unit) that may interfere with the experiments. Plastic components may leach manufacturing additives or even release micrometric plastic particles throughout time. Thus, research on microplastics using (zebra)fish requires the development of housing systems with no or less plastic parts.

This chapter describes the design and the building of the ZEB316, a stand-alone housing system built with inert materials to perform state-of-the-art toxicological studies. The ZEB316 was used to performed experimental exposures to microplastics within the scope of this work.

2.1. ABSTRACT

Many anthropogenic chemicals and plastic debris end up in the aquatic ecosystem worldwide, representing a major concern for the environment and human health. Small teleosts, such as zebrafish (*Danio rerio*) and Japanese medaka (*Oryzias latipes*), offer significant advantages over classical animal models and are currently used as first-line organisms to assess environmental risks associated with many aquatic toxicants. Toxicological studies require the use of inert materials and controlled conditions. Yet, none of the available commercialized systems is adequate to assess the toxic effect of microplastics because they contain components made of plastic polymers that may release micrometric plastic particles, leach manufacturing compounds, or adsorb chemicals. The ZEB316 stand-alone housing system presented here is meant to be a cost-effective and easy-to-built solution to perform state-of-the-art toxicological studies. It is built with inert and corrosion-resistant materials and provides good housing conditions through an efficient recirculation and filtration systems. Assessment of water parameters and fish growth performance showed that the ZEB316 provides housing conditions comparable to those available from commercial housing systems.

2.2. INTRODUCTION

The rapid growth of the world population and manufacturing industry has resulted in the production of numerous hazardous compounds including chemicals (e.g., metals, persistent organic pollutants, etc.) and microplastics (MPs), which eventually end up in the aquatic environment (surface and ground waters) and may combine (chemical adsorption on MPs)[7,64,188–191]. The consumption of MPs and adsorbed chemicals by aquatic organisms can induce lethal and sub-lethal toxicity, disrupt endocrine systems, impair growth and affect behavior[61,76,137,192–195]. Once they enter the aquatic food web, MPs and adsorbed chemicals may reach various organisms – including humans – and cause health disorders by impacting key biological processes[14–17]. The current knowledge associated with the effect of these hazardous compounds on human health and animal welfare is not enough to fully assess the risk associated with their presence in the aquatic environment. Many international environmental agencies (United Nations Environment Programme,

UNEP; European Food Safety Authority, EFSA; Food and Agriculture Organization, FAO) have placed pollution by chemicals and MPs as one of the top priority research topics[18,19].

Fish are central to the aquatic food web and their contamination by hazardous substances have been widely reported, including species marketed for human consumption, which may trigger severe health issues[98,199–204]. Small teleosts, such as the zebrafish (*Danio rerio*) and Japanese medaka (*Oryzias latipes*), offer significant advantages over classical animal models[205–207] and have become relevant models in various fields of science, including environmental toxicology[147,208–210]. These species are commonly used as first-line organisms to assess risks associated with many aquatic toxicants, to gain insights into the mechanisms underlying their effects and to serve also as sentinels for the presence of toxicants in the aquatic environment[211–214]. Studies aiming at collecting toxicological data in fish require the use of specific materials and controlled conditions. In this regard, contaminated effluents and organisms should be contained to avoid environmental hazards and the volume of contaminated material should be limited in order to reduce the cost associated to its disposal. The usage of plastic material should also be eliminated or greatly reduced to avoid chemical adsorption or leaching and the release of micrometric plastic particles. Toxicological studies using fish can be performed in static water conditions, although this is not optimal for long-term exposures (e.g., trans-generational experiments) due to the rapid deterioration of water quality and the large volumes that need to be renewed and disposed. Water recirculation and filtration is preferable to maintain good water quality but requires the use of a specific housing system, and therefore the duplication of several pieces of equipment related to water treatment (e.g., ultraviolet and filtration units), water recirculation (e.g., submersible pump) and temperature control (e.g., heater).

While several housing systems dedicated to toxicological studies are already commercialized, none of them are really designed to perform studies aiming at assessing the toxic effect of MPs and adsorbed chemicals. Indeed, these commercial solutions use components made of plastic polymers (e.g., pump, aquariums, valves, tubing) that can leach compounds used in the production of those plastic components. One example is bisphenol-A, an estrogen disrupter that affects invertebrate and

vertebrate development and reproduction (reviewed by Rubin, 2011[215]) and previously shown to be released from plastic tanks made of polycarbonate or polysulfone[216,217]. If reused, plastic components of the housing system could also leach out some chemicals that became adsorbed onto their surface in previous experiments. Although this has not been yet reported in the literature, plastic polymers used in commercial housing systems may also release micrometric plastic particles that could interfere with the experiments. In this regard, physical degradation by abrasive forces and wetting/drying (e.g., as a result of the water circulation or the cleaning of the plastic components), chemical degradation by oxidation and hydrolysis (e.g., as a result of the action of cleaning agents or chemicals present in fish water) and bio-degradation by microorganisms (e.g., bacteria and algae that are commonly found in fish housing systems) can lead to the release of microplastic[218–223]. Since plastic material may interfere with toxicological experiments, it should be reduced to the strict minimum or banished from the composition of fish housing systems when the impact of microplastics or chemicals adsorbed on the microplastics are assessed. Ideally, all the components should be replaced with inert materials such as glass or type 316 stainless steel. Some of the commercial systems are also flow-through and will therefore generate a large volume of contaminated water that needs to be collected and disposed accordingly, increasing the running costs of each experiment. There is also the need for economic solutions for small research facilities that cannot afford these costly commercial systems. The ZEB316 stand-alone housing system presented here is meant to be a cost-effective and easy-to-built solution to perform state-of-the-art toxicological studies. It is built with inert and corrosion-resistant material – 316 stainless steel and soda-lime float glass – and provides good housing conditions through an efficient water recirculation and filtration.

2.3. MATERIALS AND METHODS

2.3.1. Zebrafish maintenance and water parameters monitoring

Sexually mature zebrafish (AB wild-type strain) were crossed following an in-house breeding program. Fertilized eggs (N = 300) were placed into a 1-L breeding tank containing system water and 0.0002% (w/v) methylene blue to prevent fungal growth. System water was produced in glass containers using reverse osmosis treated

water supplemented with a salt mixture (Tropic Marin Pro Reef Sea Salt, Tropic Marine Center, UK) to reach a conductivity of 700 μS/cm and sodium bicarbonate (Sigma-Aldrich, Spain) to achieve a pH of 7.5. At 3 days post-fertilization (dpf), hatched larvae were transferred into a 3.5-L ZEB316 glass tank (Scalare, Portugal) or a 3.5-L ZebTEC plastic tank (Tecniplast, Italy) at a density of 100 larvae/L and maintained under static water conditions (90% of the water renewed every 2 days). At 15 dpf, post-larvae were distributed into new tanks to achieve a density of 26 post-larvae/L and maintained under recirculating water conditions (water flow of 8.4 L/h). At 30 dpf, density was adjusted to 5 fish/L. All fish were subjected to a 14–10 h light-dark photoperiod throughout the duration of the experimental work. Water parameters were measured daily (temperature, conductivity, and pH) or weekly (NH3, NO3, NO2, KH, GH and O2) to monitor water quality in both the ZEB316 and ZebTEC housing systems. It is worth to note that (1) 20% of the water was renewed once a week in the ZEB316 system, while it was done daily in the ZebTEC system, and (2) the UV sterilizer worked under a 2:4 on-off period in the ZEB316 system, while it worked continuously in the ZebTEC system. From 5 to 8 dpf, larvae were fed thrice daily: two meals of a microdiet (ZEBRAFEED, SPAROS Lda., Portugal) and one meal of rotifers (Brachionus plicatilis; 230 rotifers/mL)[224,225]. After 8 dpf onwards, larvae were fed thrice daily in a microdiet-based regime only.

2.3.2. Metallic components

Marine grade (type AISI 316L) stainless steel was used for the pipes, drainpipe and valves canalizing the water but also for the tubular structure holding the aquaria (rack) and filters. Metallic components and structures were designed at the CCMAR-BIOSKEL laboratory, while construction, welding and assembly of the different components was sub-contracted to Carlos B. França (Conceição de Faro, Portugal). Cylindrical metallic sieves were designed at the CCMAR-BIOSKEL laboratory, while construction and welding were sub-contracted to P. Duarte (Leiria, Portugal).

2.3.3. Glass components

Soda-lime float glass was used for the aquaria and sump. Glass components were designed at the CCMAR-BIOSKEL laboratory, while construction and assembly with aquatic grade silicone was sub-contracted to Scalare (Setúbal, Portugal).

2.3.4. Commercial components

Commercial components that were not designed or constructed are listed in Table 2.1. Those containing plastic pieces (and that should be replaced for each new trials) are the submersible pump (mostly in plastic) and the submersible heater (plastic head). Plastic connectors of the ultraviolet water sterilizer were replaced with custom-made 316 stainless steel connectors; still water is guided by plastic part inside the sterilizer.

2.3.5. Detection of fluorescent microplastics

In order to assess the efficacy of the ZEB316 filtration unit in retaining microplastic particles, fish were fed with ZEBRAFEED microdiet supplemented with 1% of 20-27 µm polyethylene fluorescent particles (Cospheric, Santa Barbara, CA). Paper filters piled up in the filtration unit were collected after 24 h to assess the presence of MPs. Fluorescent images were acquired using a MZ 7.5 fluorescence stereomicroscope (Leica, Germany) equipped with a GFP filter (λ_{ex} = 470–440 nm; λ_{em} = 525–550 nm) and a black-and-white F-View II camera (Olympus, Germany) with the following parameters: exposure time 100 ms, gamma 1.00, image format 1376 × 1032 pixels, binning 1×1. The number of microplastic particles trapped on the successive filter papers was determined from fluorescence images using ImageJ/Fiji 2.0v software built-in tools.

2.3.6. Statistical analysis

Statistical differences were determined through Student *t*-tests ($p < 0.05$) using Prism version 7.00 (GraphPad Software, Inc. La Jolla, CA).

2.4. RESULTS AND DISCUSSION

2.4.1. General concept

In order to design and build an aquarium system suitable for toxicological studies – e.g., to study the effects of MPs and adsorbed organic pollutants on aquatic organisms – the choice of the materials is a key parameter to be considered. In the absence of a suitable commercial system, we designed and constructed a small size recirculating system for small scale experiments – the ZEB316 system – with glass tanks, stainless steel piping and reduced plastic component to drastically decrease chemical leaching or adsorption and the generation of MPs that could interfere with toxicological experiments. The ZEB316 system is easy to build, to clean and to maintain. It is designed for bench-top applications with overall dimensions – when fully equipped – of 670-mm wide, 270-mm deep and 850-mm high (see the 3D view of the system in Fig. 2.1). Importantly, the ZEB316 system is cost-effective and therefore affordable for those laboratories with a limited budget.

Because of its remarkable resistance to chemicals and corrosion and excellent mechanical performance,[226,227] austenitic stainless steel (AISI 316L) was selected to build the metallic components of the system, insuring robustness and longevity. These components are (1) a tubular welded rack (Fig. 2.2A), which gives support to all the structure and components, and (2) a piping system for water delivery and drainage (Fig. 2.2B), which includes 6 valves to control the water flow in each tank and avoid water splashing (see magnified view in Fig. 2.2B). The piping system is fixed to the rack using threads and screws (see asterisks in Fig. 2.2B) and can be easily disassembled for cleaning, maintenance or moving. An overflow valve is installed at the end of the piping system to regulate the flow of water in excess before it returns to the sump and avoid an overload of the pump. The drainpipe fixed on the rear of the rack (Fig. 2.2C) collects the outflow of the tanks and canalizes it to the filtration unit.

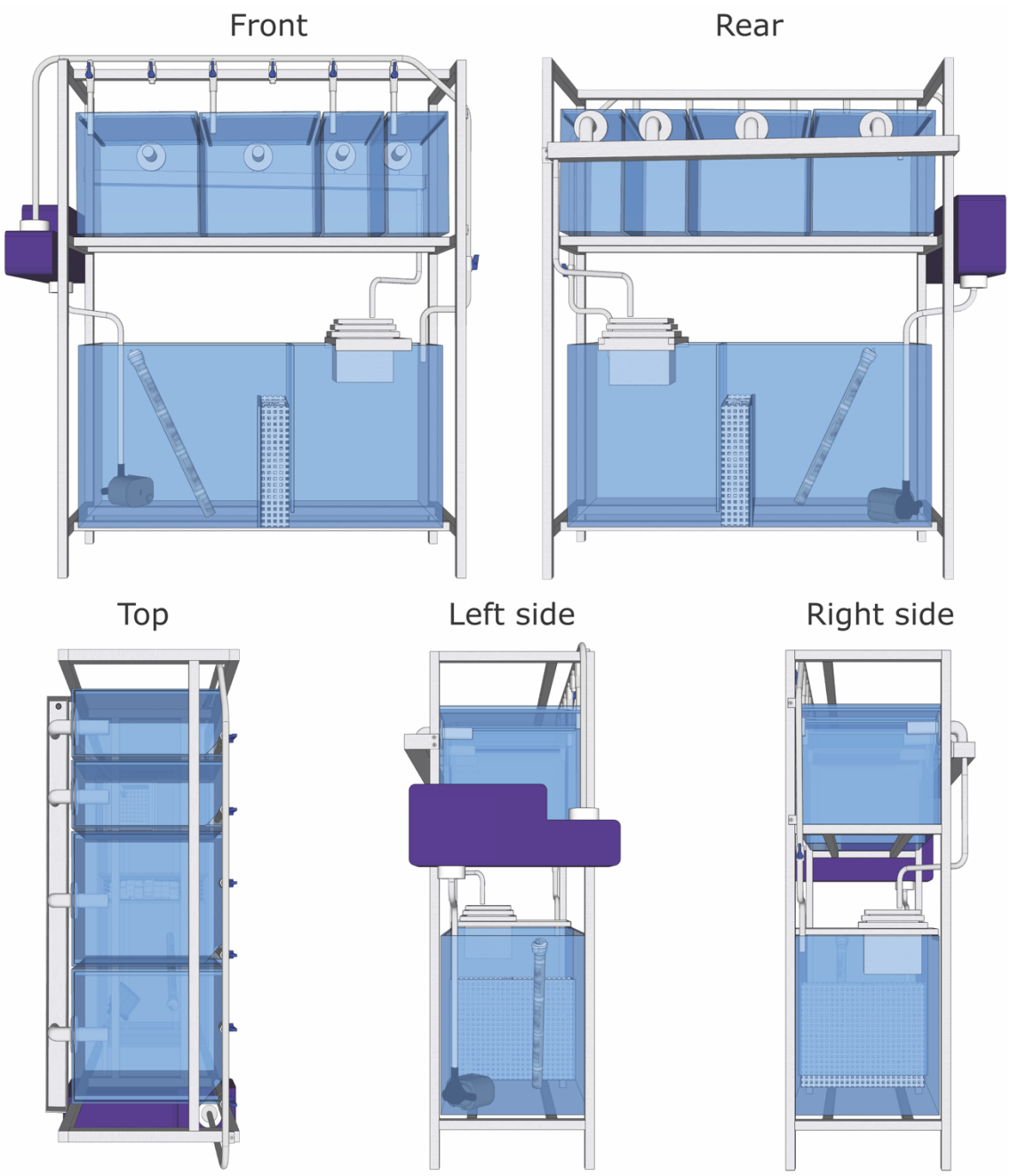

Figure 2.1. Schematic representation of the stainless steel components of the ZEB316 system, in particular the tubular rack to hold system equipment (**A**), the pipe system to distribute clean water to the aquaria (**B**), and the drainpipe to collect polluted/contaminated water (**C**). All measurements are in mm. Tubes of the rack have a 25-mm square section with a thickness of 2 mm, while pipes have a 9-mm diameter with a thickness of 1.5 mm.

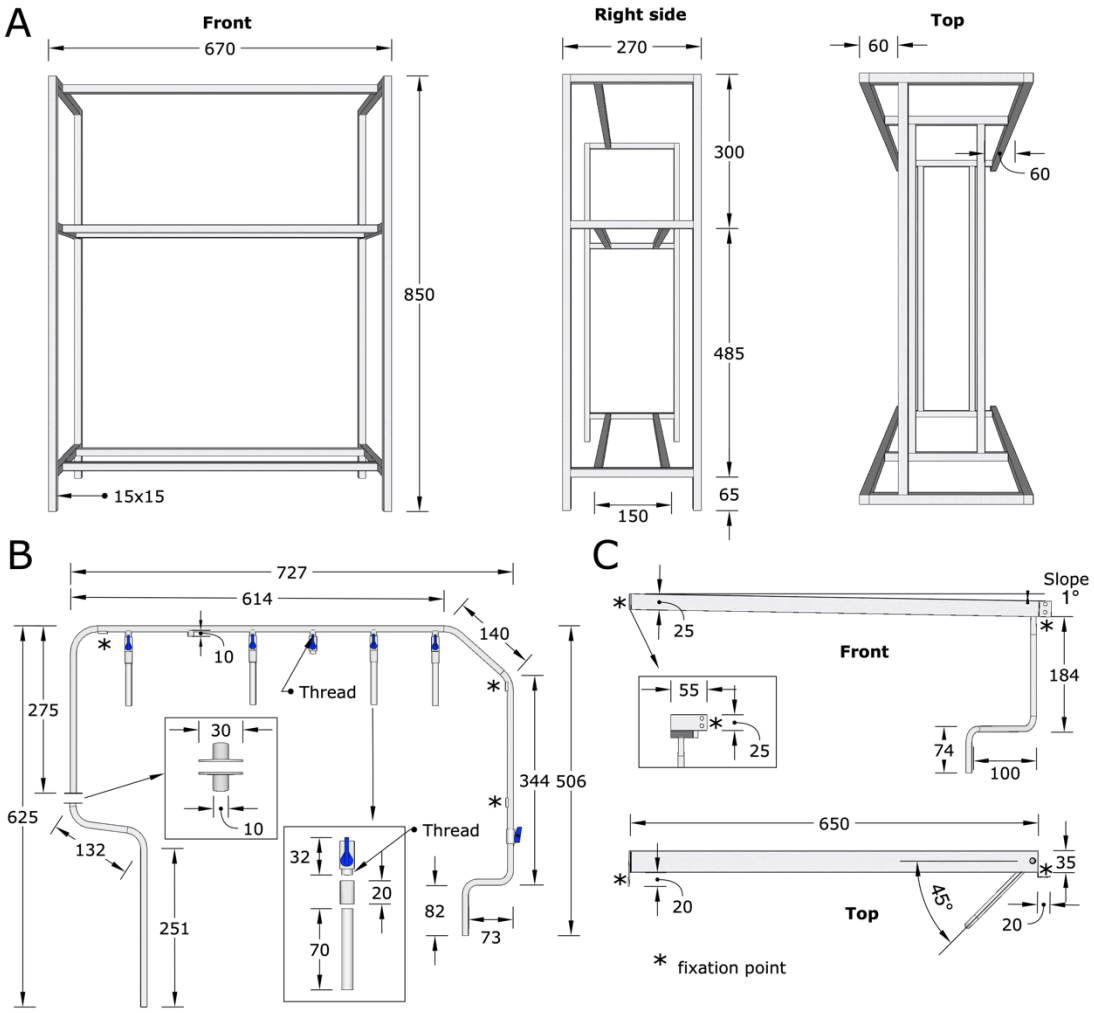

Figure 2.2. 3D overviews of the fully equipped ZEB316 system showing custom made components (e.g., stainless steel tubular rack, water pipes and filtration cassettes, glass aquaria and sump) and commercial accessories (e.g., ultraviolet water sterilizer, submersible pump and heater).

The ZEB316 rack is designed to hold the sump (Fig. 2.3A) on the bottom-shelf and the fish aquaria (Fig. 2.3B) on the top-shelf. Two different sizes of aquaria (i.e., 3.5 and 7.5 L) are available to allow variations in the experimental design; shelf can hold three 7.5-L aquaria, six 3.5-L aquaria or a combination of both. To maintain the water level and canalize the water outflow to the drainpipe, a water collector pipe was placed at the back of each aquarium (Fig. 2.3C). It is composed of 2 parts: a straight steel pipe holding a cylindrical metallic sieve (mesh sizes 0.25 mm for larvae and 1 mm for adult fish) that prevents the fish from escaping aquaria and entering the water recirculation system, and a curved pipe that directs the water into the drainpipe. Both parts are threaded to facilitate their assembly from either side of the tank and removal for cleaning. The filtration system of the ZEB316 is composed of a mechanical, a chemical and a biological filter. Mechanical and chemical filters are held in a

removable filtration unit (Fig. 2.3D) placed on the top of the sump and receiving the drained water. Three separated cassettes made in 316 stainless steel and assembled to fit one into the other (*Matryoshka*-like) hold a washable stainless steel net (250 µm mesh) to trap large debris of food and/or fish excrements and homogenize the water flow (cassette #1); a disposable 4-layers paper filter to remove particles larger than 12-14 µm (cassette #2); and a disposable activated charcoal filter to bind and remove organic compounds (cassette #3) (see Table 2.1 for commercial components). A stainless-steel box placed in-between the 2 chambers of the sump contains the biological filter, which is composed of ceramic rings (Table 2.1) that host the nitrifying bacteria (*Nitrosomonas* sp. and *Nitrobacter* sp.) necessary to the conversion of toxic nitrogenous waste products such as ammonia and nitrite into nitrate, and therefore the maintenance of a good water quality (Fig. 2.3E). An in-line ultraviolet sterilizer (Table 2.1), mounted on the left side of the rack (8-W UV lamp) at the inlet of the water distribution line, is turned on every 4h for a 2h period to sterilize the water supplied to the aquaria (Fig. 2.1). To reduce their usage, plastic components to connect the sterilizer to the pipe network were replaced by stainless-steel custom-made pieces. A 200-W submersible heater and a 8-W submersible pump (Table 2.1), placed in the sump after the biological filter, were used to maintain a constant water temperature and a constant water flow throughout the entire system (Fig. 1). These two pieces of apparatus are the only components of the ZEB316 system that contain plastic parts in contact with the fish water. Given their low price, these components can be discarded and replaced at the beginning of each new trial to avoid cross-experiment contamination with organic pollutant and microplastics.

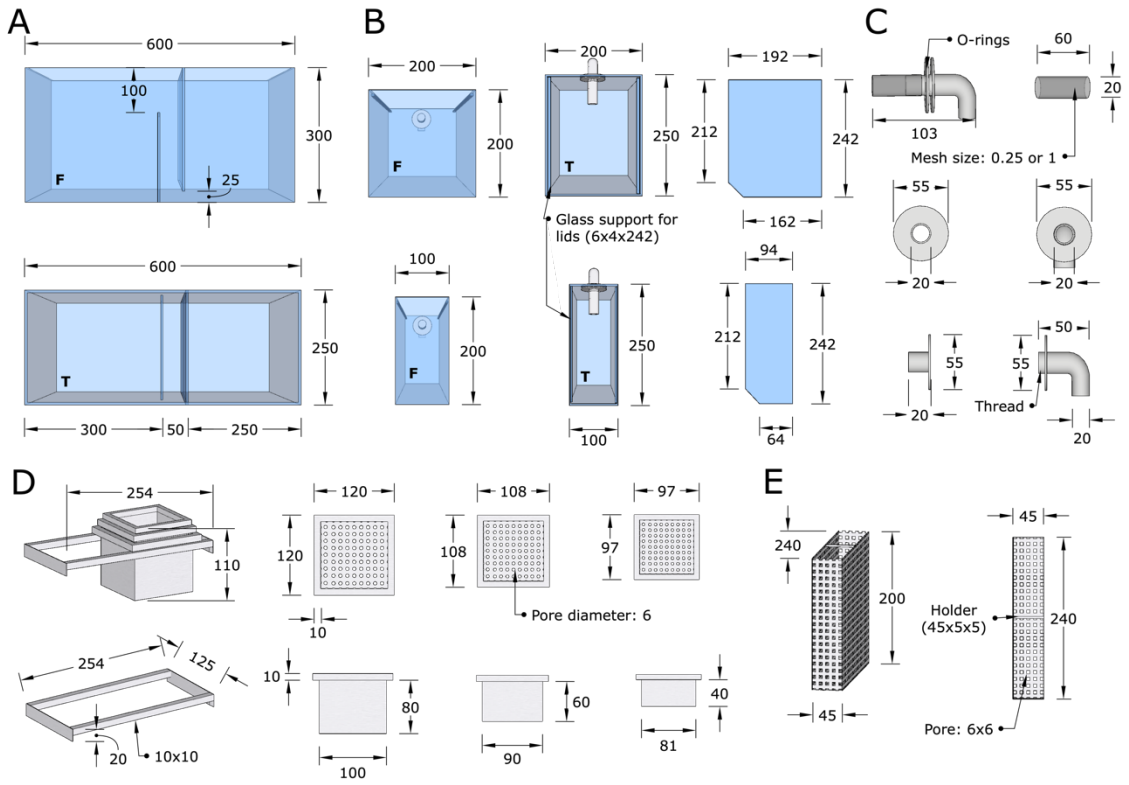

Figure 2.3. Schematic representation of the glass components (front (F) and top (T) views) and filtration system of the ZEB316 system, in particular the 30-L glass sump (**A**), the 7.5-L (top) and 3.5-L (bottom) glass aquaria including respective lids (**B**), the aquarium water outlet including the metallic net used to keep fish inside the tank (**C**), the stainless steel cassettes holding the mechanical and chemical filters (**D**) and the canister for the ceramics hosting the biological filter (**E**). Glass thickness for the sump is 5 mm while glass thickness for the aquaria is 4 mm. Stainless steel cassettes and canister have a thickness of 1 mm.

Because of its compact design and reduced pipe network, only 50 L of fish water are needed to run the ZEB316 system described in Fig. 2.1, a volume compatible with small scale toxicological studies that require an appropriate – and sometime costly – water disposable at the end of each trial. The water flow at the entrance of each aquarium is regulated by a 316 stainless steel valve and can go up to 120 L/h; it can also be interrupted for tank maintenance or when static water conditions are required (e.g., during exposure of early stage larvae or during reproduction of breeder exposed to MPs and/or organic pollutants). Depending on room temperature and heater capacity, the water temperature can be typically set between 20-34 °C, which allows the ZEB316 system to host different small teleost species – e.g., zebrafish, medaka, cavefish, mosquitofish, swordtail and guppy – that require different water temperature, and to operate different experimental set up (e.g., regeneration of zebrafish caudal fin is commonly done at 33 °C, while optimal housing is at 28 °C).

Finally, the ZEB316 system can be upgraded with components such as probes and electronic devices to control water parameters or sump water level, an automatic sump refill system in order to compensate for water evaporation or renewal, a module for room-independent illumination and a refrigerating system if water at temperature below room temperature is needed (e.g., for cavefish). Although they are more expensive, stainless steel pumps, titanium / fully-glass heaters and stainless steel UV sterilizers are commercially available to build a (almost) plastic-free housing system. Stainless steel filters of micrometric mesh can also replace paper filters in the mechanical filtration unit. They are more resistant and would last longer but they are also more expensive and will not contribute to a decrease in the use of plastic parts in the ZEB316 housing system.

Table 2.1. Commercial components installed in the ZEB316 system

Material	**Model or reference**	**Supplier**
Ultraviolet water sterilizer (8 W)	V^{2}Therm 200	Tropical Marine Center (Herts, UK)
Submersible pump (8 W)	V^{2}PowerPump 800	Tropical Marine Center
Heater (200 W)	V^{2}ecton	Tropical Marine Center
Ceramic bead rings	BLURINGS	Ferplast (Vicenza, Italy)
O-rings	25.5X3 & 16X4	Vedrol (Faro, Portugal)
Paper filter (filtration unit)	grade 603/N; 12-14 μm	Ahlstrom-Munksjö (Helsinki, Finland)
Activated charcoal (filtration unit)	HJS-21	SUNSUN (Ma'aozhen, China)
Metallic net (filtration unit)	250 μm mesh	MLGINOX (Faro, Portugal)
Metallic valves	M/F AISI316 ¼"	Metalofarense (Faro, Portugal)

2.4.2. Set up and maintenance of the ZEB316 system

Before the first usage or after the cleaning of the ZEB316 system, the biological filter needs to be inoculated with the nitrifying bacteria (e.g., *Nitrosomonas* sp. and *Nitrobacter* sp.). For this, the system was running for two weeks with 10 mL of 1 M ammonium nitrate (Sigma-Aldrich) added to the water for promoting bacterial growth, then 5 adult zebrafish were placed into each aquarium and fed daily with ZEBRAFEED microdiet. Fish density was slowly increased (up to 15 adults per 7.5-L tanks) until maturation of the biological filter was achieved (1-2 month). During this period, temperature was set at 28 °C and water flow at 8.4 L/h. The procedure for the regular maintenance of the ZEB316 system is outlined in Table 2.2. It is important to mention that glass and stainless steel components of the ZEB316 system need to be washed/decontaminated properly between experiments and plastic parts replaced. In this regard, the silicone used to assemble glass aquarium and the ceramic rings used to host the biological filter should also be replaced as it could adsorb chemicals or bind microplastics.

Table 2.2. Maintenance of the ZEB316 system

Procedure	Frequency
Check / adjust sump water level	Every week / as needed
Clean metallic net (mechanical filter)	Every day
Replace paper filter (mechanical filter)	Every day
Replace activated charcoal (chemical filter)	Every 6 months
Clean aquaria	Every week / as needed
Clean aquaria outflow nets	Every week / as needed
Sump water renewal (20%)	Every week
Check water parameters	Every day/week*

* See Table 2.3 for assays and frequency

2.4.3. Proof of concept

In order to assess its suitability to provide fish with optimal growth conditions, the ZEB316 system was compared for 1 month to the ZebTEC commercial housing system. Water parameters were measured daily (temperature, conductivity, and pH) or weekly (NH_3, NO_3, NO_2, KH, GH and O_2), and growth was assessed at 30 days post-fertilization by measuring standard and total length, abdominal width, and dry

weight. Fulton´s K factor (g/mm^3 × 10^5) was used to compare fish condition. Water parameters of the ZEB316 system remained constant throughout the proof-of-concept experiment and fell within the range of the “optimal” water parameters recommended for zebrafish housing condition[228–232]. The comparison with the ZebTEC system revealed no significant variation of the parameters, validating the design of the ZEB316 system and proving the efficacy of biological filter (Table 2.3). The survival of the fish hosted in the ZEB316 system was close to 74%, a value similar to the survival rates described in the literature[233,234] and not statistically different from the value measured in the ZebTEC system (Table 2.4). Similarly, growth performance in the two housing systems was identical and in agreement with a normal zebrafish development as previously reported[233,234] (Table 2.4).

Table 2.3. Water parameters measured daily (n=30) or weekly (n=6) in the ZEB316 and ZebTEC systems. Values are presented as the mean ± SD.

	Water parameters	ZEB316	ZebTEC
Daily	Temperature (°C)	27.54 ± 0.34	28.27 ± 0.21
	Conductivity (mS)	729.10 ± 79.85	711.90 ± 38.46
	pH	7.64 ± 0.10	7.66 ± 0.11
Weekly	Carbonate hardness (KH) (mg/L)	43.33 ± 5.16	50.00 ± 8.94
	Total hardness (GH) (mg/L)	83.33 ± 8.17	90.00 ± 10.95
	Dissolved oxygen (%)	99.67 ± 5.00	102.50 ± 1.76
	Dissolved oxygen (mg/L)	8.00 ± 0.50	8.28 ± 0.23
	Nitrite (NO_2) (mg/L)	< 0.1	< 0.1
	Nitrate (NO_3) (mg/L)	8.33 ± 2.58	12.50 ± 6.89
	Ammonia (NH_3) (mg/L)	< 0.1	< 0.1

Table 2.4 Survival rate and growth performance of fish maintained for 1 month in the ZEB316 and ZebTEC systems. Values are presented as mean ± SD (n=3).

Parameters	ZEB316	ZebTEC
Survival rate (%)	74.00 ± 3.04	76.83 ± 7.91
Standard length (mm)	5.87 ± 0.73	6.05 ± 0.90
Total length (mm)	6.59 ± 0.84	6.75 ± 1.05
Abdominal width (mm)	0.98 ± 0.20	0.99 ± 0.24
Dry weight (mg)	0.33 ± 0.05	0.39 ± 0.02
Fulton´s K factor	0.11 ± 0.01	0.12 ± 0.02

Finally, fish were exposed to ZEBRAFEED microdiet supplemented with 20-27 μm fluorescent microplastics and the retention by the mechanical filter of the MP particles excreted after ingestion or leaching out of the food pellets was determined to evaluate the potential of the ZEB316 system for toxicological studies involving microplastics. Paper filters (12-14 μm pore size) piled up in the filtration unit were collected after 24 h and imaged under fluorescence light. Images analysis revealed that the mechanical filter efficiently retained the microplastic particles (>95% of the total particles fed in the system) and that the first paper filter retained most of the particles trapped by the mechanical filter (98.8%), while the filters placed below retained the remaining particles (Fig. 2.4). Additional testing confirmed that 3-4 paper filters piled up in the filtration unit are enough to retain most of the particles but also indicated that paper filters should be renewed every 24 h. Indeed, depending on the feeding protocol and the fish density, paper filters used for periods superior to 24 h may suffer some alterations that could altered their integrity and therefore their efficacy in filtrating MP particles. Using more than 5 paper filters significantly decreased the water flow in the filtration unit and resulted in some cases in an overflow of water. As these values highly depend on the filter pore size and on the particle size, they should be re-tested for different experimental setups.

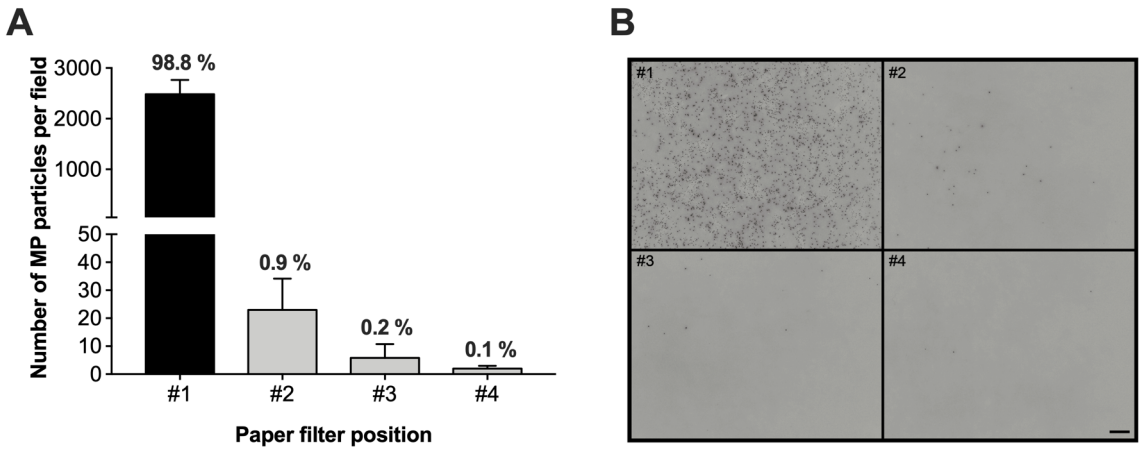

Figure 2.4. Number of microplastic particles retained by consecutive paper filters after 24 h of filtration in the ZEB316 system (**A**). Representative microscopic field used to determine the number of fluorescent microplastic particles on each paper filter (**B**). In A, positions of the paper filter in the filtration unit are indicated from top to bottom. Percentages indicated on top of each column refer to total number of MP particles detected on the filters. Values are presented as mean ± SD. Scale bar in B is 1.5 mm.

2.5. CONCLUSIONS

The ZEB316 system is not only a cost-effective, easy-to-build and easy-to-maintain alternative to commercial housing systems – estimated construction and running costs are 900 € and 100 €/year, respectively – it is also an effective solution to perform state-of-the-art toxicological experiments aiming at studying the environmental pollution by microplastics and their effect on aquatic organisms. Since it provides optimal water parameters and promotes adequate fish growth, the ZEB316 system can also be used as an affordable solution to host model teleosts in small laboratories.

Chapter 3

Development of ImageJ macros

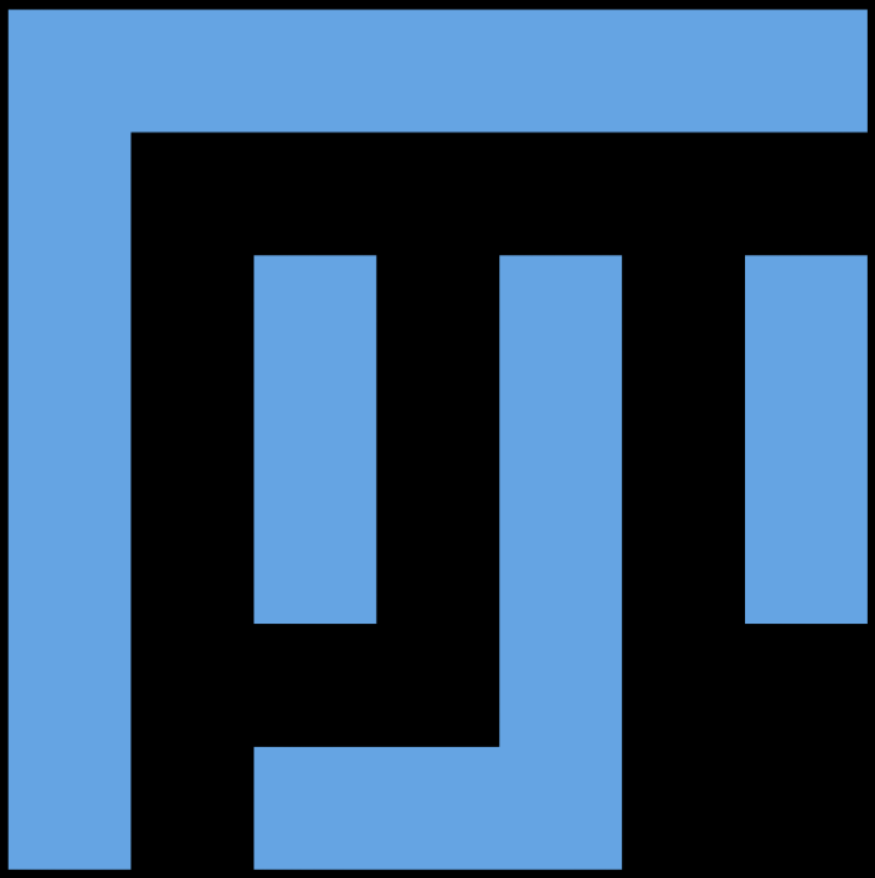

PREAMBLE

Among the technical advantages of the zebrafish over classical animal models, transparency is a dominant feature. Today, it is common practice to couple zebrafish with advance microscopy to answer scientific questions related to development, organ function, toxicology, and other fields of research. The availability of specific dyes and transgenic lines allows scientists to observe in detail the number, morphology and activity of specific cells, tissues, or organs. While imaging is now a common technique in most research laboratories and can generate a large amount of data, image analysis is often a bottleneck due to the lack of dedicated automatic/semi-automatic tools to speed up the process of data acquisition. Among the image analysis software currently available, FIJI (and ImageJ) have recently gained momentum in the scientific community. FIJI is an open source and freely available software that runs in most computer environment (Windows, macOS and Linux). FIJI works with any file format and provides tools and plugins that ease image analysis in specific workflows. It also provides the possibility to automatize image analysis through macros that allows the development of customized workflows for specific user requirements.

In the scope of this dissertation, several macros were developed to acquire meaningful data in different type of experimental procedures. This chapter illustrates ZFBONE toolset (Chapter 3.1), a set of macros dedicated to morphometric analysis of several bone structures and additional macros created for other purposes (Chapter 3.2).

Chapter 3.1

ZFBONE: an ImageJ toolset for semi-automatic analysis of zebrafish bone structures

ZFBONE

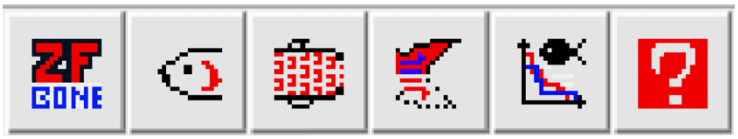

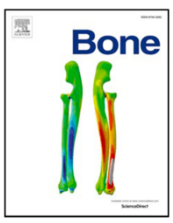

Published chapter:

Tarasco M, Cordelières F, Cancela ML, Laizé V (2020). ZFBONE: an ImageJ toolset for semi-automatic analysis of zebrafish bone structures, Bone, 138, 115480

3.1.1. ABSTRACT

The last decade has seen an increased interest in the discovery of compounds with bone anabolic activity to treat skeletal disorders such as osteoporosis and increase the well-being of patients. Due to the many technical advantages over classical rodent systems, zebrafish (*Danio rerio*) has been increasingly used in screening pipelines, in particular those aiming at identifying osteoactive compounds with pharmacological potential. Because compound osteoactivity is mostly determined in zebrafish through the morphometric analysis of bone structures, image analysis, rather than screening assay implementation, molecule availability and image acquisition, represents a bottleneck to the screening throughput. The absence of auto/semi-automatic tools for image analysis of fish bone structures is also a limitation to a broader usage of zebrafish screening pipelines. We present here ZFBONE (for ZEbrafish BONE), an open-source, freely available, user-friendly, rapid, and reliable toolset, aiming at accelerating image analysis by automating the morphometric assessment of zebrafish bone structures, but also at increasing data accuracy by reducing operator bias. Tools included in ZFBONE allow users to assess, from 2D images, morphometric parameters of several bone structures (e.g., operculum, caudal fin rays and scales) but also the extent and the intensity of bone-specific colorations. ZFBONE has been developed using the open-source ImageJ software, to make it available to the whole zebrafish research community, but also to have it easily modifiable according to user demands. ZFBONE can also be used toward the standardization of zebrafish screening protocols in academia and industry.

3.1.2. INTRODUCTION

Osteoporosis, a skeletal disorder characterized by reduced bone mineral density, affects millions of people worldwide and represents a major socio-economic burden that increases every year[235–238]. Although several drugs are already marketed to prevent or limit disease progression, they still have limited efficacy or undesirable side effects[239,240]. Thus, the discovery of bone anabolic compounds that could become the next generation of therapeutics for osteoporosis has gained momentum in the last decade, and large-scale screening of molecule libraries and natural extracts has been progressively implemented[241–245]. In this regard, zebrafish (*Danio rerio*) has

been increasingly used for compound screening as it brings technical advantages over classical animal models such as rodents, allowing quick, inexpensive, large-scale and high-throughput screening assays[120,246,247]. Zebrafish opercular bone[184], scales[187] and caudal fin rays[185] have been successfully used to assess the effects of pro/anti-osteogenic molecules during zebrafish bone development and regeneration[144,145,147,183,242,245,248]. Compound osteoactivity is mostly determined in these systems through the morphometric analysis of bone structures, and image analysis, rather than screening assay implementation, molecule availability and image acquisition, represents a bottleneck to screening throughput. Although several tools have been already developed to assess bone quality (e.g., trabecular/cortical mineral density, bone morphology and volume and osteocytes lacunae), they are not suitable for large-scale screening and for zebrafish, since they were originally developed for mammalian (essentially human and mouse) models and are fed with radiographic images that require long acquisition times (i.e. micro-computed tomography and X-ray)[249–253].

Therefore, there is a need to develop zebrafish-specific tools to accelerate image analysis by not only automating the morphometric assessment of bone structures but also increasing data accuracy by reducing operator input. These tools should also be easy to modify, user-friendly and freely available to the zebrafish research community. They should be robust and reliable in an attempt to standardize the morphometric analysis of bone structures from images in academia and industry. Here we present ZFBONE, an open-source toolset gathering different macros that can be used to assess the effects of osteogenic/osteotoxic compounds from 2D images of several zebrafish bone structures, namely the developing operculum and regenerating caudal fin rays and scales. This toolset was developed in ImageJ software and is therefore freely distributed, easy to integrate into an analysis workflow[254] and can be modified according to user demands and suggestions.

3.1.3. ZFBONE TOOLSET DESCRIPTION

3.1.3.1. Principles and approach

The idea behind the development of ZFBONE was to provide the zebrafish community with a set of semi-automatic tools to analyze the effects of bioactive

compounds on several bone structures (e.g., operculum, caudal fin ray and scale). These tools should be easily implementable in any laboratory and therefore should (1) accept standard image formats (i.e. TIFF/BMP), (2) work with simple operations through a user-friendly interface, (3) be developed using an open-source and freely available platform (i.e. ImageJ/FIJI), (4) deliver final data in a simple format that can be processed by widely distributed spreadsheet software (e.g., Excel, Prism and R), (5) report the analysis results through a simple graphical output for *a posteriori* confirmation of the data, and (6) be modifiable to fit any specific requirements. Most importantly, ZFBONE was developed to provide novice operators (such as students or young scientists) a set of simple but robust tools to get in a timely manner meaningful and accurate data.

3.1.3.2. ZFBONE toolset

ZFBONE toolbar can be easily installed in the Java-based image processing software ImageJ (https://imagej.net) or FIJI (http://fiji.sc) by saving the file "ZFBONE.ijm", provided as Supplementary Material or available online on the software versioning platform GitHub (https://github.com/MarcoTarasco/ZFBONE), in the software application folder (e.g., Applications\Fiji\macros\toolsets\ZFBONE.ijm). Once installed, ZFBONE toolbar is activated by clicking on the "More tools" menu (">>") and will appear on the main toolbar as showed in Fig. 3.1. Abbreviations of all the measurements and/or identifiers used by the different macros are described in Table 3.1.

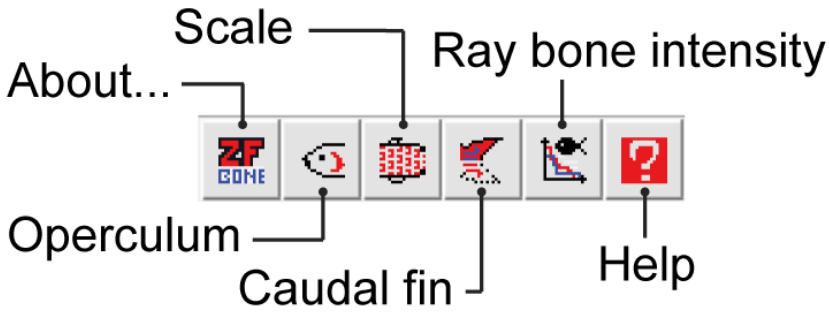

Figure 3.1. ZFBONE toolbar gathering the buttons to launch the different bone related macros (i.e., operculum assay, scale assay, caudal fin assay and ray bone intensity). The about button links to credits, while the help button links to the online manual on GitHub.

Table 3.1. Description of measurements and identifiers available in ZFBONE toolset.

Abbreviation	Measurements and identifiers	Description
Operculum macro		
Hd area	Head area	Area of the head determined by outer limits defined by the user
Op area Ch1	Operculum area in channel 1	Area of the operculum in channel 1 determined by outer limits defined by the user
Op/Hd Ch1	Ratio operculum area ch1/head area	Corrected operculum area in channel 1
Signal area Ch1	Area of signal in channel 1	Area of the signal in channel 1 given by the sum of all pixel (selected accordingly to MIN and Max Thr) in Op area Ch1
Signal area Ch2	Area of signal in channel 2	Area of the signal in channel 2 given by the sum of all pixel (selected accordingly to MIN and Max Thr) in Op area Ch1
Signal intensity Ch1	Pixel intensity in channel 1	Total pixel values in channel 1 (RawIntden) given by the sum of all pixel in Op area Ch1
Signal intensity Ch2	Pixel intensity in channel 2	Total pixel values in channel 2 (RawIntden) given by the sum of all pixel in Op area Ch1
MIN Thr Ch1 / Ch2	Minimum threshold value used in channel 1 / 2	Threshold minimum pixel value used to select signal in channel 1 / 2
MAX Thr Ch1 / Ch2	Maximum threshold value used in channel 1 / 2	Threshold maximum pixel value used to select signal in channel 1 / 2
Scale macro		
Scale area	Scale area	Area of the scale determined by outer limits defined by the user
Scale circ	Scale circularity	Circularity of the scale calculated automatically following the formula 4π × [area/(perimeter^2)]. Circularity of 1.0 indicates a perfect circle
Scale AR	Scale aspect ratio	Aspect ratio of the scale calculated automatically by fitting an ellipse on the scale area and extracting the major and minor axis

Abbreviation	Measurements and identifiers	Description
TRAP area	Area of TRAP signal	Area of TRAP signal determined by the threshold in Scale area and given by the sum of all pixel (selected accordingly to MIN and MAX Thr)
TRAP/scale area	Ratio TRAP area/Scale area	Corrected TRAP signal
DEMIN area	Demineralized area	Area of demineralized signal determined by the threshold in Scale area and given by the sum of all pixel (selected accordingly to MIN and MAX Thr)
DEMIN/scale area	Ratio Demineralized area/Scale area	Corrected demineralized signal
MIN Thr	Minimum threshold value	Threshold minimum pixel value used to select signal (TRAP or DEMIN)
MAX Thr	Maximum threshold value	Threshold maximum pixel value used to select signal (TRAP or DEMIN)
Caudal fin macro		
STU	Stump width	Width of the stump determined by the user selection
REG	Regenerated area	Area of the regenerated tissue determined by outer limits defined by the user
RMA	*de novo* mineralized area	Area of the mineralized bone determined by the threshold in REG and given by the sum of all pixel (selected accordingly to MIN and Max Thr)
RAY	Ray width	Width of the ray determined by the user selection of the first intersegment joint before STU
RAYs	Ray width average	Average of all Ray width
RMA/RAYs	Ratio *de novo* mineralized area/ray width average	Corrected *de novo* mineralized area
REG/STU	Ratio Regenerated area/Stump width	Corrected regenerated area

Abbreviation	Measurements and identifiers	Description
(RMA/RAYs)/(REG/STU)	Ratio corrected de novo mineralized area/Regenerated area	Corrected *de novo* mineralized area within corrected regenerated area
MIN Thr	Minimum threshold value	Threshold minimum pixel value used to select RMA signal
MAX Thr	Maximum threshold value	Threshold maximum pixel value used to select RMA signal
S	Segment	Identify segment number in each ray region
IJ	Intersegment joint	Landmarks identifying intersegment joints
BIF	Bifurcation point	Landmarks identifying bifurcation points
IJL	Intersegment joint in the left branch of the bifurcated ray	Landmarks identifying intersegment joints in the left branch of the bifurcated ray
IJR	Intersegment joint in the right branch of the bifurcated ray	Landmarks identifying intersegment joints in the right branch of the bifurcated ray
Ray_1-IJ-SW (IJL, IJR)	Segment width in ray #1	Width of the individual segments in each ray calculated at the middle point between 2 landmarks and by measuring pixel distances in the distance map
Ray_1-IJ-SL (IJL, IJR)	Segment length in ray #1	Length of the individual segments in each ray calculated by measuring pixel distance between 2 landmarks
STU-BIF	Distance from the stump to the bifurcation point	Distance from the stump to the bifurcation point calculated by summing all SL in each ray
BIF-IR	Distance from the bifurcation point to the inter-ray tip	Distance from the bifurcation point to the inter-ray tip calculated by averaging IJL-SL and IJR-SL
STU-IR	Distance from the stump to the inter-ray tip	Distance from the stump to the inter-ray tip calculated by summing STU-BIF and BIF-IR
Tot S-IJ (IJL, IJR)	Total number of segments	Total number of segments in each ray region
Avg SW-IJ (IJL, IJR)	Average of the segment width	Average of the segments width in each ray region
Avg SL-IJ (IJL, IJR)	Average of the segment length	Average of the segments length in each ray region

Abbreviation	Measurements and identifiers	Description
TRAP area	Area of trap signal within the regenerated area	Area of TRAP signal determined by threshold in Regenerated area and given by the sum of all pixel (selected accordingly to MIN and MAX Thr)
TRAP area/(REG/STU)	Ratio TRAP area/corrected regenerated area	Corrected TRAP signal
MIN Thr	Minimum threshold value	Threshold minimum pixel value used to select TRAP signal
MAX Thr	Maximum threshold value	Threshold maximum pixel value used to select TRAP signal
Ray intensity		
Y_Ray1	Pixel intensity value along ray #1	Pixel intensity values measured along the ray
Y_Ray1_shifted	Shifted pixel intensity value along ray #1	Pixel of highest intensity is identified in each ray and used as a reference point to align all the rays. Missing values are set to 0
Y_Ray1_shifted_normalized	Normalized pixel intensity value along ray #1	Pixel of highest intensity is set to 1 and other pixel values are corrected proportionally

3.1.3.3. Image requirements

For an optimal analysis, ZFBONE requires images saved in TIFF or BMP formats. Although natively supported by ImageJ, lossy compressed file formats such as JPEG should be avoided since compression alters both intensities and object shapes and may results in data corruption. Depending on the assay, the macros can operate with different color channels. While operculum and caudal fin MIN and MORP macros work with fluorescence images, caudal fin TRAP and scale macros require bright-field color images as staining signal is assessed using color thresholds. It is recommended that the images of an individual experiment or that need to be processed together (e.g., batch mode processing) are placed in the same folder. The folder can contain files that are not image files, since the macro will only process files ending with .tiff, .bmp and .jpg. The ray bone intensity macro requires radiographic black and white images for the analysis and tabulation separated values files (.xls or .csv extension) containing intensity data for the data pooling.

3.1.3.4. Operculum assay

The operculum macro allows the user to assess the effect of selected compounds on the growth of the opercular bone by measuring the mineralized area of the operculum stained with mineral-specific dyes, e.g., alizarin red S (AR-S) or calcein. Operculum area is normalized with the head area to correct for inter-specimen variability, as described in Tarasco et al. (2017)[184]. The operculum macro can also be used to get insights into the cellular mechanism of selected compounds, assessing their effects on bone cells by measuring fluorescence signal area and/or intensity within the operculum area in zebrafish reporter lines, e.g., *Tg*(*runx2*:GFP)[165], *Tg*(*col10a1*:EGFP)[255], *Tg*(*Ola.sp7*:mCherry)[166] and *Tg*(*Ola.oc*:EGFP)[165], where *runx2*, *col10*, *sp7* and *oc* are markers of osteoblast differentiation. To make use of the 2 channels available, the user can combine mineral staining with a cell reporter marker, e.g., AR-S fluorescence signal in channel 1 (Ch1) and osteocalcin:GFP fluorescence signal in channel 2 (Ch2).

The initial menu of the operculum macro is intended to collect information from the user to define the degree of automatization and the complexity of the analysis.

Briefly, the user first indicates whether a single image (manually opened into ImageJ/FIJI) or several images (placed in the same folder) will be analyzed. Then the user indicates his intention to either adjust the image brightness/contrast to better visualize bone structures, or not. Contrast value is set by default to 2 but can be modified by the user according to image quality. This function adjusts brightness/contrast by setting the min and max pixels intensity to (mean - contrast value × std) and (mean + contrast value × std), respectively. Briefly, image intensity distribution follows a gaussian distribution, and this function excludes pixels that are too dark/bright depending on the contrast value chosen. In batch mode, the contrast will be automatically and identically adjusted in all images. Our recommendation for inexperienced users is to first determine, in a representative image and using the single mode, whether contrast needs to be adjusted and, if yes, which value gives the best contrast. Next request is to select the number of channels to be analyzed (1 or 2) and whether to apply, or not, a threshold. If channels are from 2 different images, they need to be merged in a composite image, as a single image has to be fed to the macro. Threshold to be used by the macro can be set by the user (not interactive mode) in the user menu (set threshold Ch1/Ch2) or determined automatically (IsoData dark method [256] for Ch1/ Triangle dark method for Ch2 [257]) by the macro and later confirmed or adjusted by the user (interactive mode). Finally, the user indicates whether the head area should be measured and whether the result table should display measurements such as area and/or intensity. A diagram of the operculum macro workflow and case studies are presented in Fig. 3.2.

Analysis of operculum growth in AR-S or calcein-stained larvae (Fig. 3.2B) is probably the simplest case. It requires a single channel image and the selection of the head and operculum outer limits by the user. Output table will contain the raw measurements, the ratio operculum/head area, and the staining intensity. Analysis is more complex when AR-S signal is combined with a fluorescent reporter signal, e.g., from the *Tg*(*Ola.oc*:EGFP) transgenic line (Fig. 3.2C). In this case, the user will select a two-channel procedure and apply a threshold in Ch2. In the output table, the information for Ch1 is the same as the one described above, while the information for Ch2 includes the signal area and intensity and the threshold applied. For two reporter signals, e.g., from the *Tg*(*Ola.sp7*:mCherry; *Ola.oc*:EGFP) double transgenic line (Fig. 3.2D), the user will still select a two-channel procedure but has the possibility to apply

a threshold in Ch1 and/or Ch2. Information retrieved in output table includes the signal area and intensity and the threshold in both channels. In this latter example, measuring the head area is not needed since signal will be assessed inside the operculum area. There is therefore an option to skip this measurement. It is worth to mention that while in 1 hour an experienced user will analyze manually and get data for 59 images (operculum AR-S case with one channel), any user using the macro will be able to process 250 images (Supplementary Fig. 3.1A).

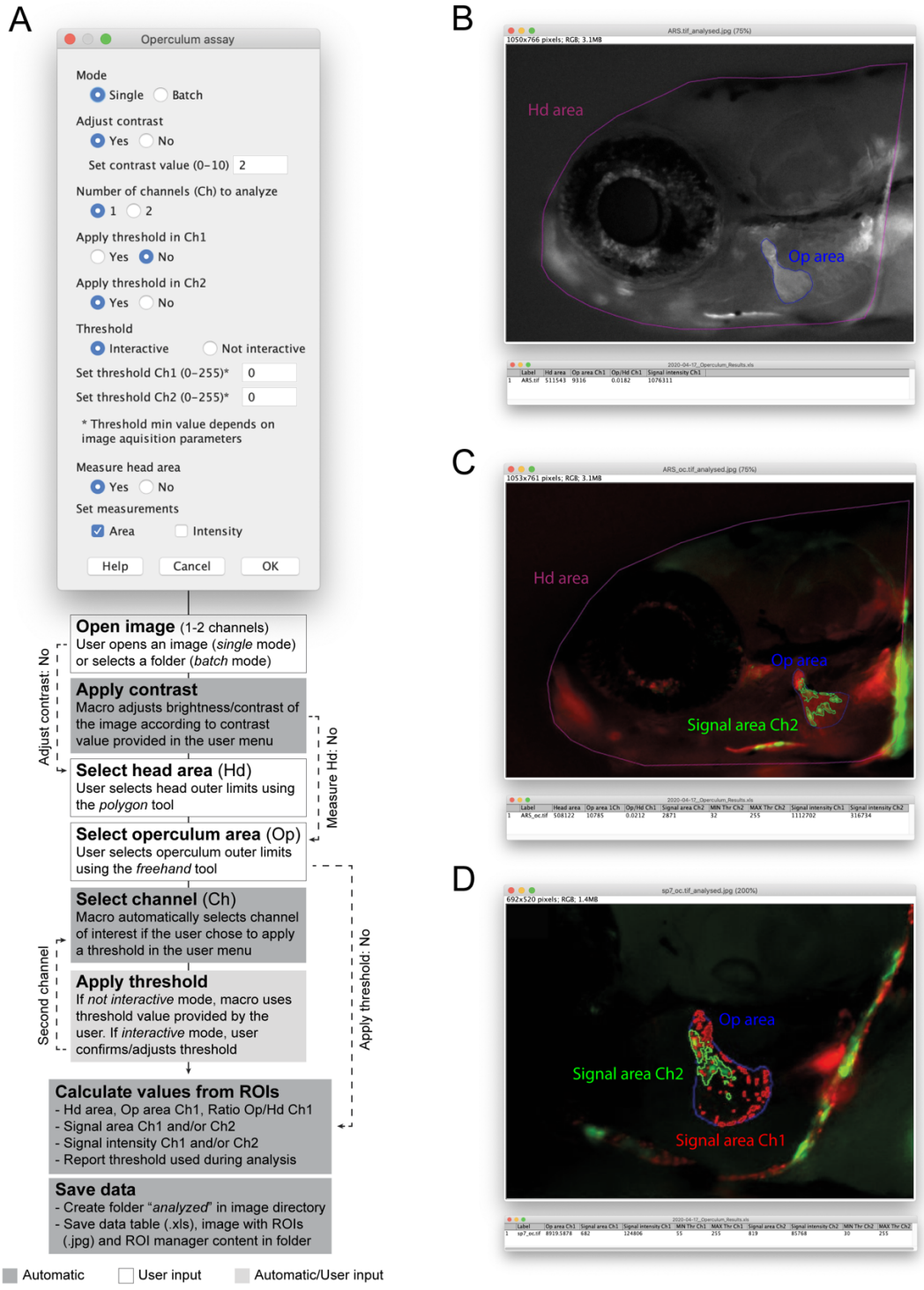

Figure 3.2. Workflow of the macro used to assess the operculum mineralized area in wild-type larvae stained with bone-specific dye (i.e., alizarin red S (AR-S) or calcein) or the operculum bone cell content in transgenic larvae expressing fluorescent proteins. **(A)** Upon selection of the macro options (initial menu) several parameters will be calculated from the region of interest (ROIs; head and operculum area) defined by the user. Operculum images can be analyzed individually or in batch. The user can adjust the image brightness/contrast selecting "yes" in adjust-contrast. The contrast value parameter is set by default at 2 but may be adjusted depending on the image acquisition. This function adjusts brightness/contrast by setting the min and max pixels intensity to (mean-n*std) and (mean+n*std), respectively. In the user menu, the user can choose to analyze 1-channel or 2-channel images. The threshold used for signal detection can be set to interactive (the macro will apply an automatic threshold and stop for the user to confirm or adjust) or to not interactive (the user defines the threshold pixel min value in set threshold Ch1/Ch2 depending on the number of channels to be analyzed; the macro will not stop for manual adjustments). The user can then select if wants to measure the head area for later normalization or not. Finally, the user can set which kind of measurements will be shown in the result table (i.e., area and/or intensity). The macro will calculate all the parameters (shown in the macro schematic in values from ROIs), then it will create a new folder in the image directory, where it will be saved: a result table, and image showing the selections and the ROI manager content. All selection tools are selected automatically during the analysis. Dark grey boxes indicate functions that are automatically computed by the macro, while white boxes indicate functions that require the user input (e.g., manual selection of bone structures) and light grey boxes indicate functions that can be manual or automatic depending on the user choices in the initial menu. **(B)** Example of macro output set to analyze wild-type larvae stained with bone specific staining (AR-S or calcein, in this example was used AR-S). In this case, contrast was adjusted to better visualize bone structures. Only the area of the head and the area of the operculum were assessed. Pixel intensity was also assessed in the operculum area. **(C)** Example of macro output set to analyze transgenic larvae labeling oc (osteocalcin; committed osteoblast) positive cells combined with bone specific staining (i.e., AR-S). In this case, no contrast was adjusted. Ch1 is AR-S signal while Ch2 is oc+ signal. **(D)** Example of macro output set to analyze double transgenic larvae labeling sp7 (osterix; pre-osteoblast) and oc (osteocalcin; committed osteoblast) positive cells. No contrast was applied, and area of the head was not measured since in this specific case the user is interested only in the 2 different reporter line signal within the operculum. AR-S, Alizarin Red S; Hd area, head area; Op area Ch1, operculum area in Ch1; Op/Hd Ch1, ration between operculum area in Ch1 and head area; Op signal Ch1, operculum signal area in Ch1; Op signal Ch2, operculum signal area in Ch2; Signal intensity Ch1, operculum pixel intensity in Ch1; Signal intensity Ch2, operculum pixel intensity in Ch2; MIN Thr Ch1/Ch2, min threshold value; MAX Thr Ch1/Ch2, max threshold value.

3.1.3.5. Scale assay

The scale macro allows the user to assess the effect of selected compounds on matrix mineralization in scales stained with von Kossa or on osteoclast activity in scales stained for tartrate-resistant acid phosphatase (TRAP), as described by De Vrieze et al. (2014)[187]. Both ontogenetic and regenerating scales can be used, and best results are achieved with images of well-individualized scales. In addition to mineralization rate and TRAP activity, the scale macro will also determine morphological parameters such as area, circularity, and aspect ratio to evaluate compound effects on bone remodeling and homeostasis.

The initial menu of the scale macro is intended to collect information from the user to define the type of analysis to be performed. Briefly, the user first indicates whether a single image (opened by the user in ImageJ/FIJI) or several images (placed in the

same folder) will be analyzed, then the type of staining that was performed on the scales (von Kossa or TRAP). The threshold that the macro will use to determine signal area can be set by the user (not interactive mode) in the user menu (set threshold) or determined automatically (MaxEntropy dark method [258]) and later confirmed or adjusted by the user (interactive mode). A diagram of scale macro action flow and case studies are presented in Fig. 3.3.

Once the options are set in the user menu, the macro will ask the user to manually outline the outer limits of each scale and add selected region to the ROI manager. Multiple scale analysis requires the user to press down the key 'T' after each selection. According to the staining indicated in the user menu, the macro will apply directly a color threshold using the YUV color space (TRAP staining; Fig. 3.3B) or transform the original image(s) in 8-bit image(s), enhance the contrast and then apply a threshold (von Kossa; Fig. 3.3C). The macro will then determine all the regions with staining within each scale using the built-in ImageJ function *analyze particles*. This function will outline each individual stained area within the scale area. Since clear/white areas in von Kossa stained scales will be associated with demineralization, the macro will exclude the clear/white areas in contact with the scale border as they are most probably false demineralized areas resulting from the threshold application (the efficient removal of these false demineralized areas largely depends on image quality). On the contrary, the strong red-violet color observed in TRAP stained scales is less prone to generate false stained areas (if threshold min value is correctly adjusted). Output table will contain the raw measurements, the ratio TRAP/scale area (or DEMIN/scale) and the threshold minimum and maximum value used for detecting the staining. It is worth to mention that while in 1 hour, an experienced user will analyze manually and get data for 40 images (one scale per image stained with TRAP), any user using the macro will be able to process 200 images (Supplementary Fig. 3.1B).

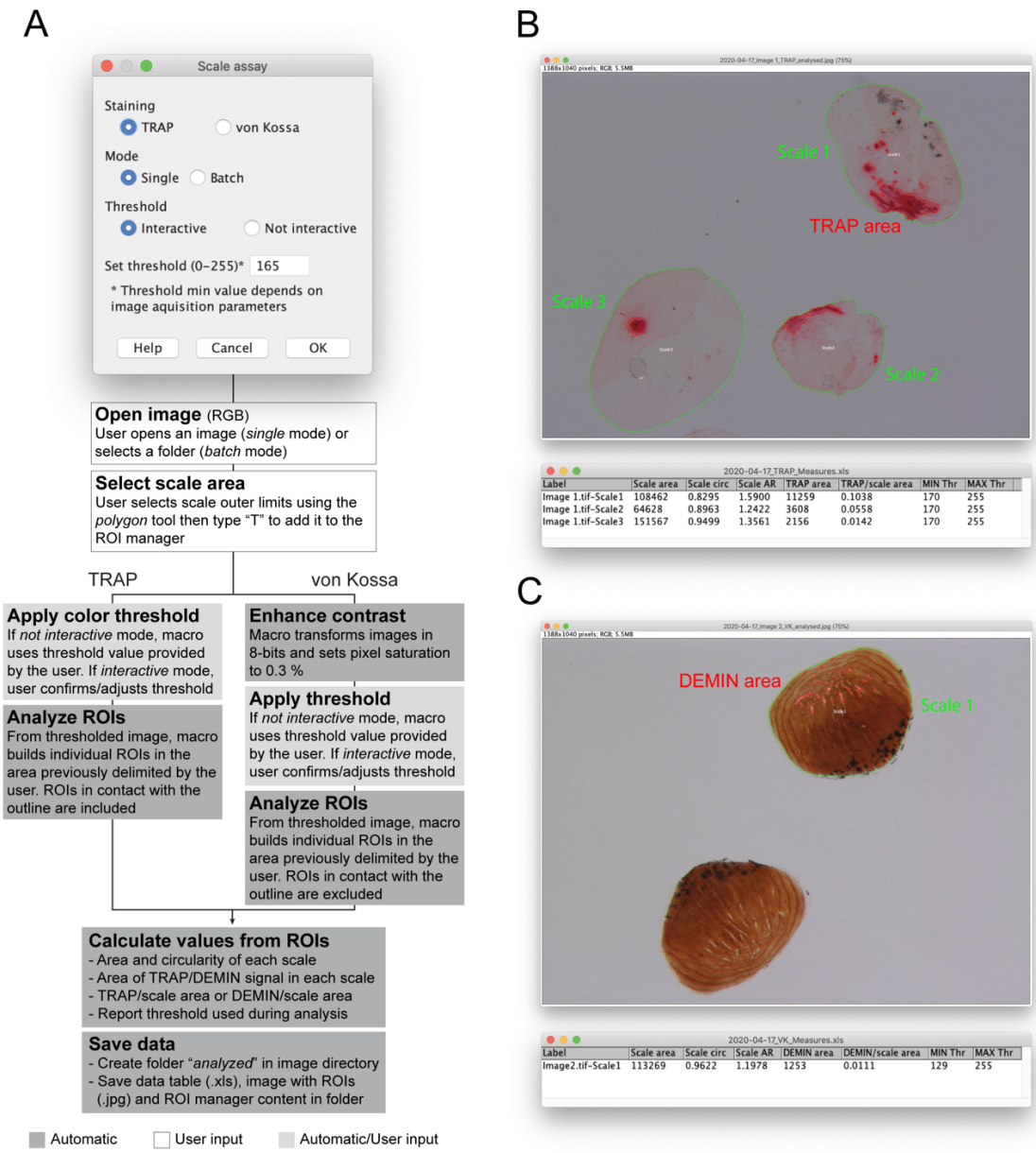

Figure 3.3. Workflow of the macro used to assess mineral content in ontogenetic/regenerated scales stained with von Kossa or osteoclast function in scales stained for tartrate-resistant acid phosphates (TRAP) activity. **(A)** Scale images can be analyzed individually or in batch. The user can select all scales present in the image (as shown in panel B) or only analyze a single scale (as shown in panel C). The threshold used for signal detection (TRAP or von Kossa) can be set to *interactive* (the macro will apply an automatic threshold and stop for the user to confirm or adjust) or to *not interactive* (the user defines the threshold pixel min value in *set threshold*; the macro will not stop for manual adjustments). The macro will calculate all the parameters (shown in the macro schematic in values from ROIs), then it will create a new folder in the image directory, where it will be saved: a result table, and image showing the selections and the ROI manager content. All tools are selected automatically during the analysis. Dark grey boxes indicate functions that are automatically computed by the macro, white boxes indicate functions that require the user input (e.g., manual selection of bone structures) and light grey boxes indicate functions that can be manual or automatic depending on the user choices in the initial menu. **(B)** Example of macro output for TRAP analysis. In this case the user wanted to select all scales present in the image and all different measurements are reported in the result table per scale. Scale circ, scale circularity; Scale AR, scale aspect ratio; TRAP area, area of TRAP detected; DEMIN area, demineralized area detected; TRAP/Scale area, ratio TRAP signa within scale area; DEMIN/Scale area, ratio demineralized area within scale area; MIN Thr, min threshold value; MAX Thr, max threshold value.

3.1.3.6. Caudal fin assay

The caudal fin macro allows the user to assess tissue regeneration and *de novo* bone formation (MIN), but also the morphometry of the rays (MORP) in ontogenetic/regenerated caudal fins stained with bone specific markers (AR-S, calcein) and osteoclast activity in TRAP stained caudal fins. The initial menu of the caudal fin macro is intended to collect information from the user to define the type of analysis to be performed. First the user indicates the type of analysis to be performed, i.e., MIN, MORP, MIN & MORP or TRAP signal. The threshold that the macro will use to determine signal area can be set by the user (not interactive mode) in the user menu (set threshold for TRAP) or determined automatically (Li dark method[259] for MIN; MaxEntropy dark method[258] for TRAP) by the macro and later confirmed or adjusted by the user (interactive mode). A diagram of caudal fin workflow and case studies are presented in Fig. 3.4.

For MIN analysis, the macro will ask the user to open two individual images of the caudal fin, first the bright-field image and then the respective fluorescence image. While the bright-field image is used to get measurements of the stump width (STU), regenerated fin area (REG) and ray width (RAY), the fluorescence image is used to determine the mineralized area (RMA) labelled by bone specific fluorochromes such as AR-S and calcein. More information about the caudal fin system can be retrieved from Cardeira et al. (2016)[185]. The macro will ask the user to select the several regions of interest, i.e., STU, REG, RAY and RMA, for the morphometric analysis of the caudal fin. Raw and normalized measurements are presented in the result table.

For MORP analysis, the macro will ask the user to open a fluorescence image and then to define the number of rays to be analyzed and identify them using landmarks. The user will also set landmarks at each intersegment joint (IJ), at the bifurcation point (BIF), and at each intersegment joint in the left branch (IJL) and in the right branch (IJR) of the bifurcated ray (see scheme in Fig. 3.4C). It is important to mention that landmarks cannot be deleted once set due to macro language limitation, and that duplication of landmarks may trigger errors. Once all landmarks are set in each of the rays previously defined, the macro automatically measures the segment length (SL) and calculates the middle point of each segment to estimate the segment width (SW). For this, the macro will create the Euclidian distance map from the

mask[260], where each pixel is replaced with a gray value equal to its distance to the nearest background pixel, that will be used to determine outer limits of the segment. The macro will generate two output tables, one containing all the raw measurements (i.e., number, width and length of each individual segment) and another presenting not only the average width and length of the segments within each ray region but also the distance between the stump and the bifurcation point (STU-BIF), the distance between the bifurcation point and the inter-ray tip (BIF-IR), where the IR is the average length of IJL and IJR, and the total distance between the stump and the inter-ray tip (STU-IR). Although MIN and MORP can be performed individually, the user can select MIN & MORP to chain the analyses and get both types of results from the same fluorescence image.

For TRAP signal assessment, the macro will ask the user to open a bright-field image and select STU and REG. The macro will apply a color threshold (automatically defined or input by the user in the user menu) and measure the TRAP signal within REG. Output table will contain the raw measurements, the ratio TRAP/REG and the threshold minimum and maximum value used for detecting TRAP staining. It is worth to mention that while in 1 hour, an experienced user will analyze manually and get data for 15 images (MIN macro), 20 images (analyzing one single ray per image, MORP macro) and 50 images (TRAP macro), any user using the macro will be able to process 50, 171, 200 images, respectively (Supplementary Fig. 3.1C-D-E).

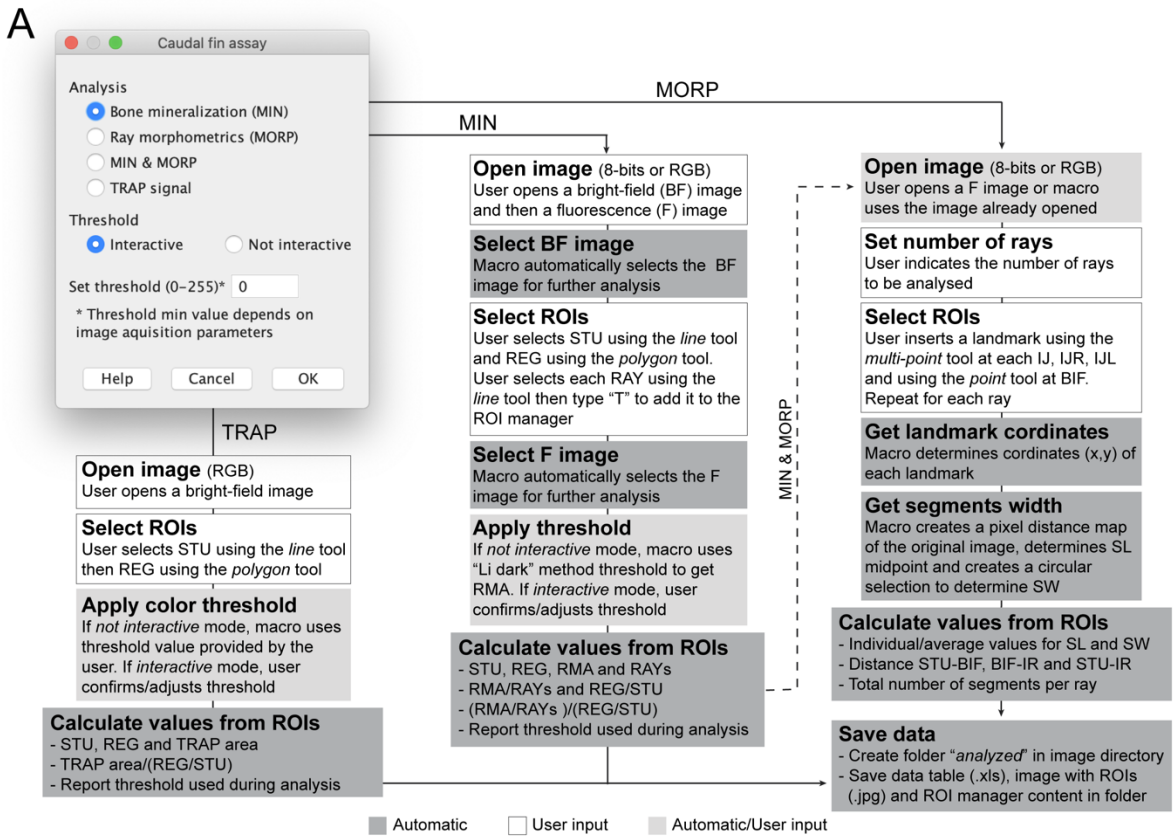
A
Caudal fin assay
Analysis
Bone mineralization (MIN)
Ray morphometrics (MORP)
MIN & MORP
TRAP signal
Threshold
Interactive
Not interactive
Set threshold (0–255)* 0
* Threshold min value depends on image aquisition parameters
Help
Cancel
OK
MORP
MIN
TRAP
Open image (RGB)
User opens a bright-field image
Select ROIs
User selects STU using the line tool then REG using the polygon tool
Apply color threshold
If not interactive mode, macro uses threshold value provided by the user. If interactive mode, user confirms/adjusts threshold
Calculate values from ROIs
- STU, REG and TRAP area
- TRAP area/(REG/STU)
- Report threshold used during analysis
Open image (8-bits or RGB)
User opens a bright-field (BF) image and then a fluorescence (F) image
Select BF image
Macro automatically selects the BF image for further analysis
Select ROIs
User selects STU using the line tool and REG using the polygon tool. User selects each RAY using the line tool then type "T" to add it to the ROI manager
Select F image
Macro automatically selects the F image for further analysis
Apply threshold
If not interactive mode, macro uses "Li dark" method threshold to get RMA. If interactive mode, user confirms/adjusts threshold
Calculate values from ROIs
- STU, REG, RMA and RAYs
- RMA/RAYs and REG/STU
- (RMA/RAYs)/(REG/STU)
- Report threshold used during analysis
MIN & MORP
Open image (8-bits or RGB)
User opens a F image or macro uses the image already opened
Set number of rays
User indicates the number of rays to be analysed
Select ROIs
User inserts a landmark using the multi-point tool at each IJ, IJR, IJL and using the point tool at BIF. Repeat for each ray
Get landmark cordinates
Macro determines cordinates (x,y) of each landmark
Get segments width
Macro creates a pixel distance map of the original image, determines SL midpoint and creates a circular selection to determine SW
Calculate values from ROIs
- Individual/average values for SL and SW
- Distance STU-BIF, BIF-IR and STU-IR
- Total number of segments per ray
Save data
- Create folder "analyzed" in image directory
- Save data table (.xls), image with ROIs (.jpg) and ROI manager content in folder
Automatic
User input
Automatic/User input

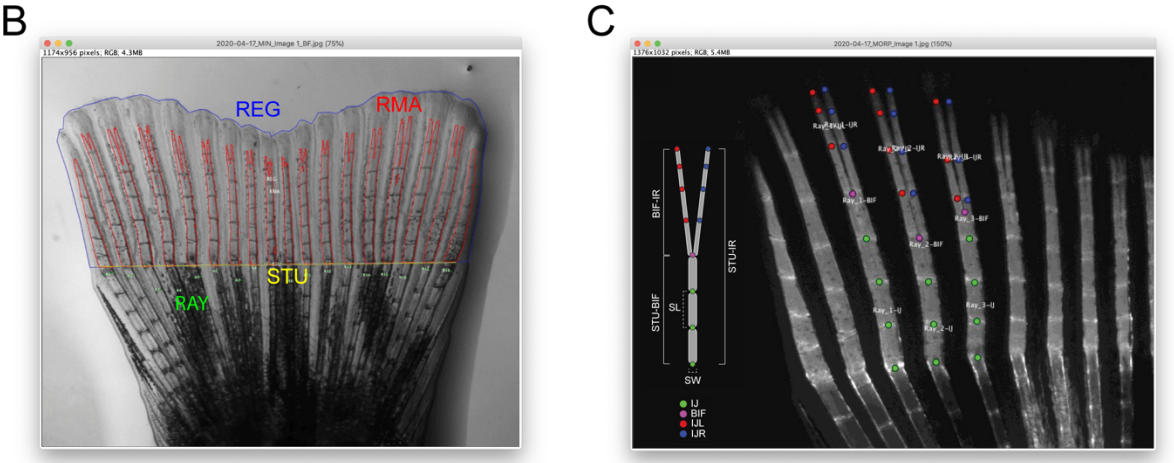
B
REG
RMA
STU
RAY
C
BIF-IR
STU-IR
STU-BIF
SL
SW
IJ
BIF
IJL
IJR

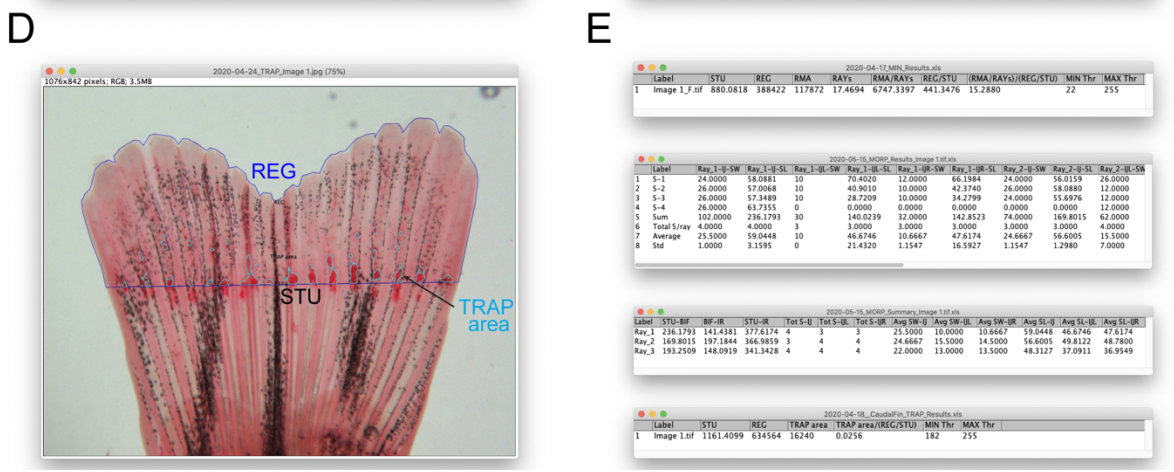
D
REG
STU
TRAP area
E

Figure 3.4. Workflow of the macro used to assess mineral content (MIN), ray morphometry (MORP) or TRAP activity in regenerated caudal fin stained with bone specific staining (AR-S or calcein) or TRAP. **(A)** After selection of the analysis to be performed, the user can set the threshold to *interactive* (the macro will apply an automatic threshold and stop for the user to confirm or adjust) or to *not interactive* (the user defines the threshold pixel min value in *set threshold*; the macro will not stop for manual adjustments). In the case the user selects in the menu options *MIN & MORP* the macro will merge both analyses. All tools are selected automatically during the analysis. Dark grey boxes indicate functions that are automatically computed by the macro, white boxes indicate functions that require the user input (e.g., manual selection of bone structures) and light grey boxes indicate functions that can be manually or automatic depending on the user choices in the initial menu. **(B)** Macro MIN analysis output. **(C)** Macro MORP analysis output. **(D)** Macro TRAP signal analysis output. **(E)** Representative result table for each macro, i.e., MIN, MORP raw data, MORP summary, TRAP signal. BF, bright-field image; F*,* fluorescence image; STU*,* stump width; REG*,* regenerated area; RMA*,* mineralized area; RAY*,* ray width; RAYs*,* average width of all rays; IJ*,* intersegment joint; BIF*,* bifurcation point; IJR*,* intersegment joint in the right branch of the bifurcated ray; IJL*,* intersegment joint in the left branch of the bifurcated ray; SL*,* segment length; SW*,* segment width; S, segment; Ray_1-IJ-SW (IJL, IJR), Segment width in ray #1; Ray_1-IJ-SL (IJL, IJR), Segment length in ray #1 ; STU-BIF, Distance from the stump to the bifurcation point; BIF-IR, Distance from the bifurcation point to the inter-ray tip; STU-IR, Distance from the stump to the inter-ray tip; Tot S-IJ (IJL, IJR), Total number of segments; Avg SW-IJ (IJL, IJR), Average of the segments width; Avg SL-IJ (IJL, IJR), Average of the segments length.

3.1.3.7. Ray bone intensity

The ray bone intensity macro allows the user to assess the effect of selected compounds on the density of regenerated caudal fin rays. The macro was developed to evaluate maximum intensity projections derived from stacked images previously acquired through micro-computed tomography (microCT). The initial menu of the macro is intended to collect information from the user to define the type of analysis to be performed, i.e., image analysis or data pooling. For image analysis, the macro will ask the user to open an image and select the rays to be analyzed (after each selection the user needs to type T to add the ray in the ROI manager). It is important to mention that, when selecting the ray, the user must include part of the callus (a thickened part of the regenerated bone that forms at the amputation plane, thus a region of higher intensity), which will serve as a reference point to align ray intensities. Once all the rays of interest are selected, the macro will automatically determine the pixel intensity along each ray, then align intensity data using the pixel of highest intensity (i.e., callus), set to 1, as reference in each ray. A graph presenting normalized pixel intensity and a table containing raw, shifted, and normalized measurements are automatically created and saved in the folder “analyzed”. For the data pooling, the macro will ask the user to select the folder containing the data tables created from image analysis and will automatically align ray intensity values using the pixel of highest intensity, set to 1, allowing the user to compare ray bone density of different fins in the same intensity plot (for example, control versus treated fins as shown in Fig. 3.5B). It is worth to

mention that while in 1 hour an experienced user will analyze manually and get data for 17 images (comparing the intensity of only 2 rays per image) any user using the macro will be able to process 333 images (Supplementary Fig. 3.1F).

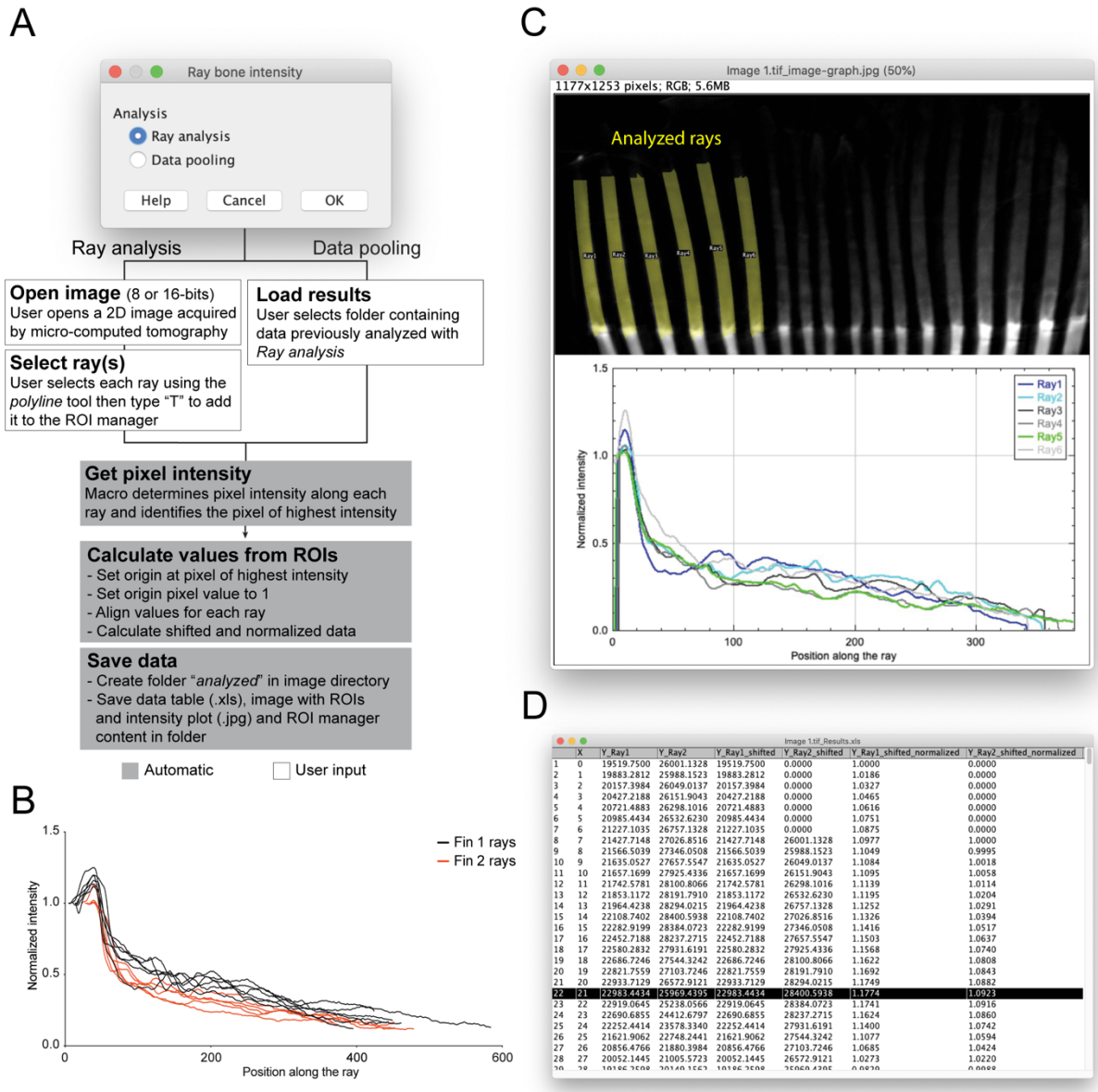

	X	Y_Ray1	Y_Ray2	Y_Ray1_shifted	Y_Ray2_shifted	Y_Ray1_shifted_normalized	Y_Ray2_shifted_normalized
1	0	19519.7500	26001.1328	19519.7500	0.0000	1.0000	0.0000
2	1	19883.2812	25988.1523	19883.2812	0.0000	1.0186	0.0000
3	2	20157.3984	26049.0137	20157.3984	0.0000	1.0327	0.0000
4	3	20427.2188	26151.9043	20427.2188	0.0000	1.0465	0.0000
5	4	20721.4883	26298.1016	20721.4883	0.0000	1.0616	0.0000
6	5	20985.4434	26532.6230	20985.4434	0.0000	1.0751	0.0000
7	6	21227.1035	26757.1328	21227.1035	0.0000	1.0875	0.0000
8	7	21427.7148	27026.8516	21427.7148	26001.1328	1.0977	1.0000
9	8	21566.5039	27346.0508	21566.5039	25988.1523	1.1049	0.9995
10	9	21635.0527	27657.5547	21635.0527	26049.0137	1.1084	1.0018
11	10	21657.1699	27925.4336	21657.1699	26151.9043	1.1095	1.0058
12	11	21742.5781	28100.8066	21742.5781	26298.1016	1.1139	1.0114
13	12	21853.1172	28191.7910	21853.1172	26532.6230	1.1195	1.0204
14	13	21964.4238	28294.0215	21964.4238	26757.1328	1.1252	1.0291
15	14	22108.7402	28400.5938	22108.7402	27026.8516	1.1326	1.0394
16	15	22282.9199	28384.0723	22282.9199	27346.0508	1.1416	1.0517
17	16	22452.7188	28237.2715	22452.7188	27657.5547	1.1503	1.0637
18	17	22580.2832	27931.6191	22580.2832	27925.4336	1.1568	1.0740
19	18	22686.7246	27544.3242	22686.7246	28100.8066	1.1622	1.0808
20	19	22821.7559	27103.7246	22821.7559	28191.7910	1.1692	1.0843
21	20	22933.7129	26572.9121	22933.7129	28294.0215	1.1749	1.0882
22	21	22983.4434	25969.4395	22983.4434	28400.5938	1.1774	1.0923
23	22	22919.0645	25238.0566	22919.0645	28384.0723	1.1741	1.0916
24	23	22690.6855	24412.6797	22690.6855	28237.2715	1.1624	1.0860
25	24	22252.4414	23578.3340	22252.4414	27931.6191	1.1400	1.0742
26	25	21621.9062	22748.2441	21621.9062	27544.3242	1.1077	1.0594
27	26	20856.4766	21880.3984	20856.4766	27103.7246	1.0685	1.0424
28	27	20052.1445	21005.5723	20052.1445	26572.9121	1.0273	1.0220

Figure 3.5. Workflow of the macro used to assess caudal fin ray intensity from imaged previously acquired through micro-computed tomography (microCT). **(A)** The Ray analysis allows the user to collect pixel intensity data from each ray (upon manual selection), while Data pooling option open the results previously collected (with Ray analysis) and allow the user to compare different caudal fins in the same intensity plot (for example control vs treated fins). All tools are selected automatically during the analysis. The user only needs to manually select the rays of interest and the macro will compute all the analysis. Dark grey boxes indicate functions that are automatically computed by the macro, white boxes indicate functions that require the user input (e.g., manual selection of bone structures) and light grey boxes indicate functions that can be manually or automatic depending on the user choices in the initial menu. **(B)** Representative example of ray's intensities calculated from 6 rays in 2 different fins. It is important to notice that all the points of max intensity of each ray are aligned and allow the comparison between different samples. After data collections with Ray analysis, the 2 different fins were aligned using the function Data pooling **(C)** Macro output from Ray analysis macro. The macro automatically saves a single image showing on top the selection made and on the bottom the intensity profile of each single ray. **(D)** Result table example from Ray analysis. X represent the pixel position along the rays,

Y_ Ray “x” represent the intensity of the pixel in each different ray, Y_Ray”x”_shifted represent the pixel values shifted to the point of max intensity (raw highlighted in the table). Values = 0 are added in order to align the intensities. Y_Ray”x”_shifted_normalized represent the pixel value normalized to 1.

3.1.3.8. Data saving

At the end of the analysis, each macro will automatically create a folder named “analyzed*”* in the image directory and save a table containing the data (.xls), an image highlighting the ROIs (.jpg) and the ROI manager content (.zip). Post-analysis access to the content of the ROI manager allow the user to confirm ROI selection or perform additional measurements. In batch mode, the macro will check in the folder “analyzed” which images were already processed and open only the images that are still to be analyzed. Data tables are named according to the macro and contain the date of the analysis (see examples in each macro figure) while ROI-presenting images are named after the original image name followed by “_analyzed”. These images allow the user to record parameters of a morphometric analysis for *a posteriori* check or re-analysis.

3.1.4. CONCLUSIONS

ZFBONE was developed to provide the zebrafish community a set of simple and robust tools to acquire, in a timely manner, meaningful and accurate data. Macros have been developed aiming at reducing user bias to increase data reproducibility toward the standardization of the screening methodology for osteoactive compounds. This toolset is easily implementable in any laboratory, presents a user-friendly interface and was developed using an open-source and freely available software, that allows the users to adapt it to any particular case. Although ZFBONE has been developed and validated using images from zebrafish, it can be used with images from other small teleost models, such as medaka. This toolset is user-friendly and, most importantly, freely available on GitHub repository. ZFBONE is only a starting point for the development of more sophisticated tools, thus we encourage users to adapt the code for their specific requirements or send us feedbacks to improve the toolset.

Chapter 3.2

Additional ImageJ macros developed within the scope of this work

Macros developed in the scope of Chapter 5

3.2.1. EGG COUNTER MACRO

The *Egg counter* macro allows the user to determine the total number of zebrafish eggs and whether they are alive or dead. Egg area and shape descriptors (circularity, aspect ratio, roundness, and solidity) are subsequently measured in selected eggs. To allow the macro to work properly, egg(s) should be imaged using a microscope with transmitted light. The initial menu of the *egg counter* macro is intended to collect information from the user to define the type of analysis to be performed (i.e., mode *All eggs* or mode *Dead-Alive*) and the threshold that will be used to determine signal area (Huang method for alive eggs/*All eggs* and Minimum method for dead eggs). This threshold can be applied automatically (not interactive mode) or later confirmed / adjusted by the user (interactive mode). A diagram of *egg counter* action flow and case studies are illustrated in Fig. 3.6 and a brief description of the 2 modes is presented below.

For the *Dead-Alive* analysis, the macro first asks the user to indicate the folder containing the images to be analyzed, then images are sequentially opened and analyzed. For each image, the macro first enhances the contrast (pixel saturation set to 0.3%) and creates a copy. Duplicated images are renamed as *All eggs* and *Dead eggs*. The macro opens the *Dead eggs* image and identifies the dead eggs using the threshold function (Fig. 3.6B). At 24 hpf, dead eggs are opaque and appear black in images taken with transmitted light (while they appear white in images taken with reflected light), making them easy to identify. The macro will add all the selected regions (i.e., dead eggs) to the Roi Manager using the built-in ImageJ function *analyze particles*. Then the macro opens the *All eggs* images and identifies the remaining eggs (supposedly alive) present in the image using the threshold function. In the binary image created by the threshold, holes are filled, and watershed is applied. Watershed function separates eggs that may be in contact with each other. The macro will add all the selected regions to the Roi Manager (i.e., all eggs) using the built-in ImageJ function *analyze particles* (Fig. 3.6C). Macro creates a new 8-bit image (based on original images info) and draws and fills in black colour all the eggs (selected by threshold in image *All eggs*) then each Roi from the *Dead eggs* image is selected, and its content is erased to the current background color (i.e., white). The intensity of each ROI (all the eggs in the image) from the *All egg* image is measured. If maximum grey

value (Max) is different from 0, egg is considered dead while if Max is equal to 0 egg is considered alive. In fact, while alive eggs are drawn completely black thus the maximum intensity is equal to zero, dead eggs have a white internal region (i.e., the selected area in *Dead eggs* image) thus maximum intensity is different from zero (Fig. 3.6D). At the end of the analysis, the macro automatically creates a folder named "*analyzed"* in the image directory where it saves (1) a table containing the data (.xls), (2) an image highlighting the ROIs (.jpg) and (3) the ROI manager content (.zip). Post-analysis access to the content of the ROI manager allows the user to confirm ROI selection or perform additional measurements. ROI-presenting images will be created and named after the original image name followed by "*_analyzed*". These images allow the user to record parameters of a morphometric analysis for *a posteriori* check or re-analysis (Fig. 3.6E).

For the *All eggs* analysis, image processing is similar to the one described above with the only difference that dead eggs will not be identified and therefore be counted together with alive eggs. This analysis is useful when users only want to count the number of eggs and get their measurements, independently of them being alive or dead.

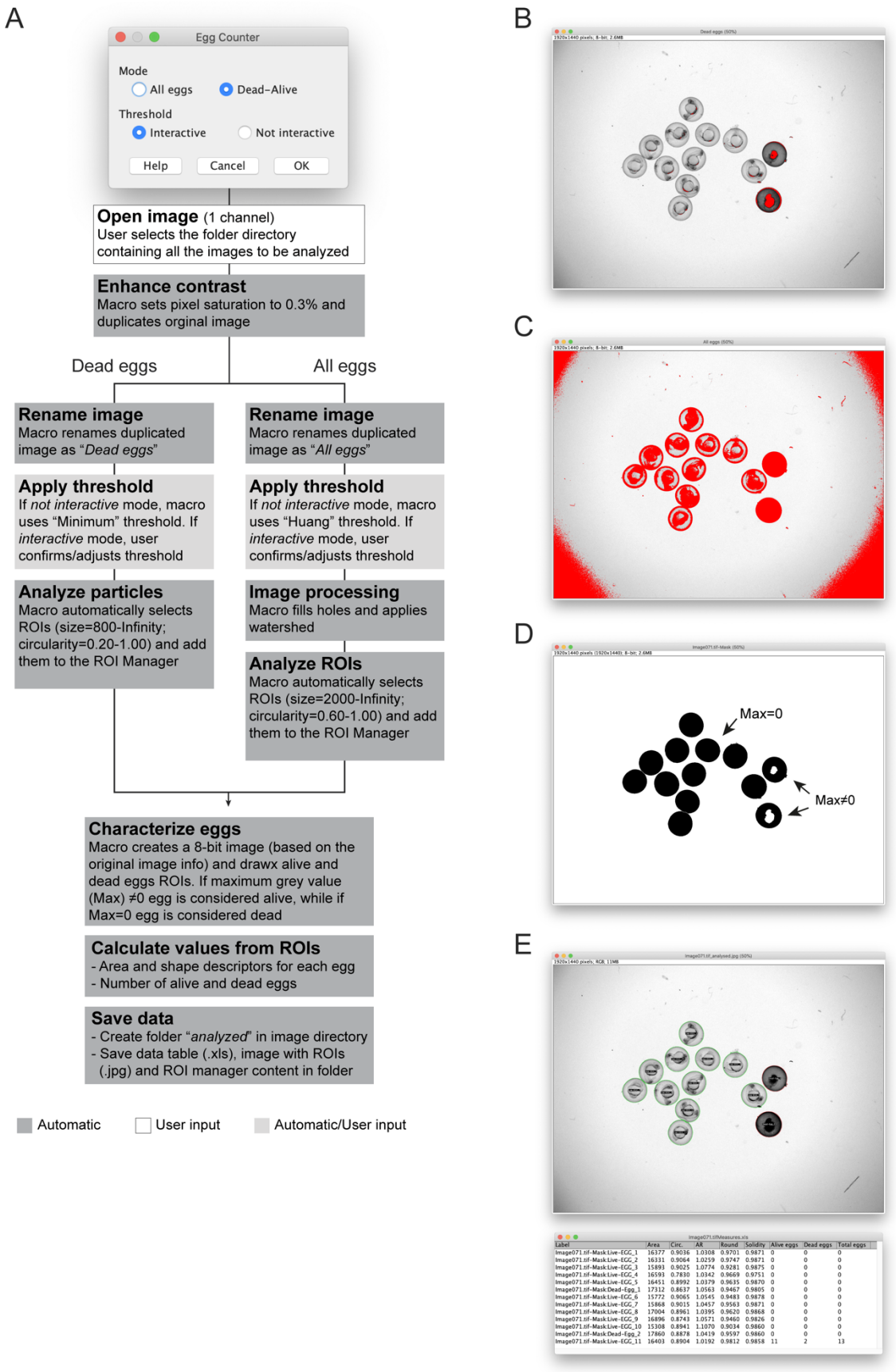

Figure 3.6. Workflow of the macro used to assess egg number (alive/dead/total) and shape parameters. **(A)** The user selects one of the two analysis modes: *All eggs* or *Dead-Alive*. While *All eggs* identify the total number of eggs and retrieves shape parameters (tested at 0 hours post-fertilization - hpf), *Dead-*

Alive identify the total number of dead and alive eggs (tested at 24 hpf). The threshold used for signal detection can be set to *interactive* (the macro applies an automatic threshold and stops for the user to confirm or adjust) or *not interactive* (the macro will not stop for manual adjustments). The macro will create a new image where selected ROIs will be drawn and based on their intensity used to identify dead or alive eggs. The macro calculates shape parameters (shown in the macro schematic in values from ROIs), then it creates a new folder in the image directory, where it saves (1) a result table, (2) an image showing the selected regions and (3) the ROI manager content. All ImageJ built-in tools are selected automatically during the analysis. Dark grey boxes indicate functions that are automatically computed by the macro, white boxes indicate functions that require the user input and light grey boxes indicate functions that can be manual or automatic depending on the user choices in the initial menu. **(B)** Example of threshold used to determine dead eggs. In this case the user can select dead eggs that appear black. **(C)** Example of threshold used to determine all the eggs. In this case the user can select all the eggs present in the image by adjusting the threshold value. **(D)** Image binary mask created by the macro to individualize alive and dead eggs according to their maximum intensity. **(E)** Example of macro output. Top image shows images automatically saved after analysis, where eggs have been selected and characterized (alive eggs are in green, dead eggs are in red). Bottom image illustrates macro result table.

3.2.2. GOBLET CELL MACRO

The *Goblet cell* macro allows the user to count the number of goblet cells present in intestinal villus. Although developed specifically for the purpose of counting goblet cells, this macro can be adapted and used for other histological analysis (i.e., count cells in a selected area). A diagram of *Goblet cell* action flow and case studies are presented in Fig. 3.7A. Briefly, the user first indicates whether a single image (opened by the user in ImageJ/FIJI) or several images (placed in the same folder) will be analyzed, then defines the maxima parameter, which identifies the goblet cells to be considered for the analysis by selecting ROIs based on their intensity compared to their surroundings (by default, maxima parameter is set to 15). For each image, the macro first enhances the image contrast (set pixel saturation to 0.3%), applies a gaussian blur filter (sigma=2) and runs the built-in ImageJ function *Find Maxima*. All the cells present in the image are selected, but the macro only counts the cells (based on their coordinates) that are present within the area of interest (i.e., a villus), which is manually selected by the user. At the end of the analysis, the macro automatically creates a folder named "analyzed*"* in the image directory and saves a table containing the data (.xls), an image highlighting the ROIs (.jpg) and the ROI manager content (.zip). Output table contains the area and the number of cells within each villus. Post-analysis access to the content of the ROI manager allows the user to confirm ROI selection or perform additional measurements. ROI-presenting images will be created and named after the original image name followed by "_analyzed". These images allow the user to record parameters of a morphometric analysis for *a posteriori* check or re-analysis (Fig. 3.7B).

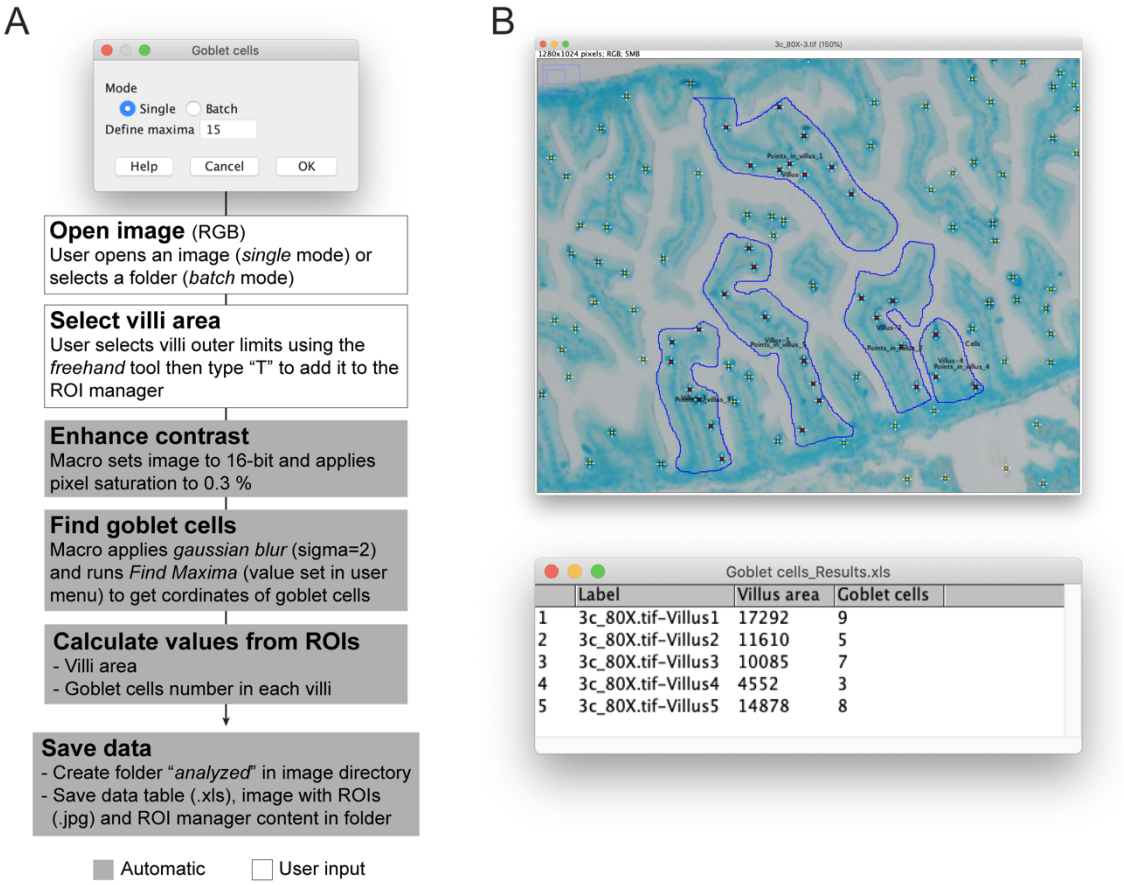

Figure 3.7. (A) Workflow of the macro used to count the number of goblet cells in selected villi. Intestine images can be analyzed individually or in batch. The user first defines the limits of the villus/villi to be analyzed using the *freehand* tool and add them to the ROI manager. The macro applies a gaussian blur filter and detect goblet cells using the *Find Maxima* tool. Depending on the quality of the images to be analyzed, the sensitivity of this tool has to be adjusted in the user menu (set by default to 15). The macro calculates the area of each villus and the number of cells in each villus, then creates a new folder in the image directory, where it saves: a result table, and image showing the selections and the ROI manager content. All tools are selected automatically during the analysis. Dark grey boxes indicate functions that are automatically computed by the macro, white boxes indicate functions that require the user input (e.g., manual selection of villi) and light grey boxes indicate functions that can be manual or automatic depending on the user choices in the initial menu. **(B)** Example of an output image and a result table. In this case, the user selected five villi in the intestine image (regions delineated with a blue line) and goblet cells identified within the selected areas are marked in red. Goblet cells present in the image but not in selected areas are marked in yellow.

Chapter 4

Screening of mineralogenic and osteogenic compounds in zebrafish: tools to improve assay throughput and data accuracy

pharmaceuticals

Chapter to be submitted:

Rosa JT, Tarasco M, Gavaia PJ, Cancela ML, Laizé V (2022). Screening of mineralogenic and osteogenic compounds in zebrafish: tools to improve assay throughput and data accuracy. To be submitted in Pharmaceuticals.

PREAMBLE

This chapter presents the several *in vivo* zebrafish assays currently available to evaluate the effect of osteogenic and osteotoxic compounds (in the scope of this dissertation) during bone development or regeneration.

Note: this chapter originated from a collaborative work and is presented here to give an overview on the zebrafish assays that have been used in the dissertation. I was involved in the writing of the paragraphs presenting the zebrafish operculum, caudal fin, and scale assays, and in the design of the illustrations.

4.1. ABSTRACT

Bone disorders affect millions of people worldwide and treatments currently available often produce undesirable secondary effects or have limited efficacy. It is therefore of utmost interest for patients' health to develop more efficient drugs with reduced off-target activity. In the long process of drug development, screening and preclinical validation, traditionally done using rodents, have recently gained momentum with the emergence of zebrafish as a suitable model organism to study pathological processes related to human bone disorders but also as a source of high-throughput screening assays to identify bone anabolic compounds. In this review, we provide a comprehensive overview of the literature related to zebrafish bone related assays and evaluate their performance toward their integration in screening pipelines for the discovery of mineralogenic/osteogenic compounds. A survey on the tools available to standardize fish housing and feeding, synchronize embryos production, and automatize specimen sorting and image acquisition/analysis toward faster and more accurate screening outputs are also presented.

4.2. INTRODUCTION

Human disorders characterized by a progressive loss of bone mineral density (e.g., osteopenia and osteoporosis) or a gradual deterioration of bone architecture and deformation of bone shape (e.g., Paget's disease of bone) affect a large part of the population worldwide and result in reduced well-being for diseased persons but also in a large financial burden on the society[261–263]. Several drugs are available to treat these bone disorders – through an action of bone resorption or formation – and minimize their impact but most of them have issues related to efficacy and/or secondary effects[261–263]. There is therefore the need to develop more efficient drugs with reduced off-target activity.

In the long process of drug development, screening and preclinical validation are commonly done using rodents (mostly mouse) as they are evolutionary close to human and many genetic/molecular tools are available. However, because of several bottlenecks related to rodents being an expensive and time-consuming animal model but also to the relative low throughput of the *in vivo* systems[264,265], alternative systems were sought to reduce the number of compounds to be tested in rodents. *In vitro*

assays using mammalian osteoblast, osteoclast and bone marrow-derived mesenchymal stem cell cultures have been established for high-throughput screening assays toward the discovery of osteogenic compounds[266–270], but they lack the cellular complexity of the *in vivo* models. The quest for systems that could bridge the gap between simple high-throughput cell-based assays and complex low-throughput whole-animal assays identified small aquatic vertebrates as promising tools for the screening of compounds, in particular those that may have an effect on bone metabolism. Because it brings many advantages over the mammalian models – e.g., a short life cycle, a large progeny and translucent larvae – but also because it shares with mammals a remarkable homology of the mechanisms regulating bone development and homeostasis, the zebrafish, a small teleost endogenous to the streams of the Southern Asia, has rapidly gained momentum as a vertebrate model organism to study pathological processes related to human bone disorders[120] but also to screen for bone anabolic compounds[120,271–274]. Because of its small size and a cost-effective husbandry, the zebrafish has also the capacity to down-scale whole-organism screening platforms and reduce associated costs, thus increase the throughput of the screening pipeline, and accelerate the identification of compounds with therapeutic applications. CRISPR/Cas9 gene editing technology has also been successfully applied to zebrafish[275,276], opening the door to the development of gene-specific mutant lines exhibiting phenotypes/traits of bone disorders (e.g., osteoporosis, osteopenia, osteoarthritis) that will allow more efficient and better targeted drug screening effort. However, despite clear advantages, translational validation and the availability of robust zebrafish models, the skepticism of the pharmaceutical industry has hindered a larger use of zebrafish in screening pipelines for drug discovery.

First approaches to screen for osteoactive compounds were largely empirical but several *in vitro* (e.g., mineralogenic cell lines), *ex vivo* (e.g., scale cultures) and *in vivo* (e.g., embryonic, and larval bone structures) systems have been developed since and recently optimized (see description below). The assessment of the mineralogenic/osteogenic potential of selected compounds is based, for most of them, on the morphometric analysis of bone structures stained with bone-specific dyes (e.g., alizarin red S and calcein) or marked with reporter proteins (e.g., GFP and mCherry) expressed by transgenic zebrafish lines (see description below). The *modus operandi* – including turnaround time, system throughput, operating skills, and requirements in

compounds – and the cellular complexity greatly varies among the different systems available but a major bottleneck common to all systems is probably the extensive time required to image the bone structures and assess their morphometry (e.g., size and shape) and density (e.g., pixel intensity) based on image analysis. Key processes have been optimized and automated, procedures in animal production have been standardized and sophisticated tools have been developed to increase the throughput and the accuracy of the zebrafish screening systems. This review presents the different zebrafish systems that can be used to screen for mineralogenic/osteogenic compounds and highlights the tools that are available to increase the throughput of these functional screenings for faster and more accurate preclinical studies.

4.3. ZEBRAFISH *IN VITRO* AND *IN VIVO* SCREENING SYSTEMS

4.3.1. *In vitro* cell systems capable of biomineralization

Many cell lines of fish origin are available (657 in the Cellosaurus version 38 of May 2021[277]) to study intracellular signaling pathways, gene transcription regulation and metabolic functions with application in biomedical, aquaculture and environmental studies. However, only 11 of these fish cell lines are suitable to assess compound mineralogenic potential, i.e., the capacity to enhance (pro-mineralogenic) or reduce (anti-mineralogenic) extracellular matrix (ECM) mineralization[278]. ZFB1 (Cellosaurus accession no. CVCL_6E12) is the only zebrafish cell line capable of *in vitro* mineralization[279]. While it has been used in studies investigating the expression of several bone-related genes throughout *in vitro* mineralization[279,280], it has not been used yet in screenings for osteogenic compounds. On the contrary, gilthead seabream VSa13 cell line[281] (Cellosaurus accession no. CVCL_S952) was successfully used in small-scale screening of extracts from marine green algae[245], halophytes[282], or environmental pollutants[144,283]. Typically, compounds are dissolved in the culture medium and exposed to the mineralizing cells in multiwell plates (Figure 1A). Culture medium supplemented with both the compounds and the mineralogenic cocktail – ascorbic acid, calcium chloride and β-glycerophosphate[284] – is renewed twice a week for 14 days, then extent of *in vitro* mineralization is assessed through alizarin red S staining and quantified by spectrophotometry[285]. Beside the low quantity of compounds needed and the cost-effective method to induce ECM mineralization, fish

mineralogenic cell lines are also advantageous as an *in vitro* cell system for drug screening because of their robustness and high mineralogenic capacity. A rather long exposure is currently the major bottlenecks in the use of cell lines to screen for mineralogenic compounds. But there is room for optimization: a stable cell clone expressing a fluorescent protein under the control of a mineralization-specific gene promoter[286] for genes up-regulated during ECM mineralization) could be used as a proxy for cell mineralogenic capacity and a reporter for compound mineralogenic activity. Such system would reduce the exposure time and remove the staining step, thus enhance screening throughput.

4.3.2. Bone formation in larval systems

The use of zebrafish embryos and larvae for compound screening and drug discovery brings several advantages in relation to throughput and ethics. Zebrafish embryo and larvae are small in size (approximately 0.7 mm for a fertilized egg and 4.2 mm for a larva at 6 days post-fertilization (dpf); Zfin) and can be easily handle using a wide bore transfer pipette or a robotic handling system (see section 4.4). They can be arrayed in multiwell plates (commonly 96-well plates) in a small volume of water thus small amounts of compounds are needed for screening assays. Because zebrafish larvae can feed on their yolk for several days, external feeding is not required until 6 dpf, which is also the maximum time to host zebrafish larvae in 96-well plates. For all these reasons, the use of zebrafish embryos and larvae for high-throughput screening should be limited to a developmental window that ranges from fertilized eggs to 6-dpf larvae. Assays using zebrafish larvae older than 120 hours post-fertilization (5 dpf) may need to get approval from an ethical committee[287], a limitation that may reduce the developmental window for the screening of some compounds. Anyhow, the exposure of zebrafish embryo/larvae to compounds is likely to be short thus enhancing screening throughput and reducing the quantity of compounds needed. In the context of this review, several dermal bone structures are being formed at 3 dpf and sufficiently mineralized at 6 dpf to be used in the screening for osteogenic compounds, e.g., parasphenoid, branchiostegal rays and operculum. Using older larvae, e.g., to assess bone structures that are formed and/or mineralized later (for example vertebral centra) will require feeding, transfer to larger wells, use of more compounds and thus will decrease the throughput of the screening pipeline.

4.3.2.1. Opercular bone growth

A flat morphology and a superficial localization on the side of the head combined with an early and rapid ossification in larval zebrafish[184] are key features that accelerated the use of zebrafish operculum to study osteoactive[241,243,245] and osteotoxic compounds[144,183,184,288], and spot it as a promising system for large-scale compound screenings. Briefly, 3-dpf larvae are exposed to compounds of interest for 3 days in multiwell plates, then bone structures are stained with alizarin red S or calcein and imaged for morphometric analysis of the operculum area (Fig. 4.1A). To correct for inter-specimen size variability, the area of larval head is used to normalize the area of the operculum. Increase or decrease in corrected operculum area indicates compounds with pro- or anti-osteogenic (or osteotoxic) properties, respectively[184]. The operculum assay is fast (4 days from exposure to data acquisition) and requires a low quantity of molecules (exposure is short and done in a reduced volume of fish water), but also few resources that are commonly found in most research institutes or easily implemented (mainly a thermostated chamber, a fluorescence stereomicroscope, and an image analysis software). It is also adaptable to different experimental conditions (specimen number, well plates, number of conditions and treatment volume) and is performed with early-stage larvae that can be produced in large quantities. ImageJ macros have been developed to speed up the rather laborious morphometric analysis[289] and tools are available to automatize larvae and liquid handling but also operculum imaging (see section 4.4). Note that the larval operculum is a simple bone structure containing mostly osteoblasts at this stage. This could be seen as an advantage to discover bone anabolic compounds, but the absence of osteoclasts is a clear drawback if screening aims at anti-resorptive molecules.

4.3.2.2. Craniofacial skeleton

Zebrafish craniofacial bones are ossified following mechanisms that have been conserved throughout vertebrate evolution and are therefore commonly used as models for mammalian cranium development[290]. Fleming et al. (2005) investigated the osteogenic potential of several molecules by assessing the mineralization of several craniofacial bones in zebrafish larvae[271]. At 3 dpf, larvae were exposed for 6 days in multiwell plates to osteoactive compounds, then stained with AR-S and area

and staining intensity of ventral bone structures was evaluated through morphometric analysis (Fig. 4.1A). The overall procedure is similar to that used in the operculum assay although exposure is a bit longer, thus requiring more compounds, and mineralization data is not normalized for inter-specimen variability, thus necessitating a higher number of specimens to reach significance. The morphometric analysis of multiple bone structures may provide more robust data but will also increase the time of data analysis, which is an issue for large scale screenings. As for the operculum assay, laborious steps such as image acquisition and analysis but also specimen handling can be automated to provide a higher throughput for drug discovery pipelines.

4.3.2.3. Vertebrae mineralization

Zebrafish vertebral centrum is formed throughout intramembranous ossification that can be detected as early as 7 dpf, when part of the notochord sheath began to mineralize[291]. Quantification of vertebrae mineralization – the number of mineralized vertebral centra or the extent of centrum mineralization – can be used as a tool to evaluate the mineralogenic or osteogenic activity of selected compounds/molecule libraries, as reported by Chen and colleagues for dorsomorphin, pentamidine, fenvalerate and alendronate, among others[272]. Zebrafish larvae are typically exposed to selected compounds/libraries for 4-9 days then stained with AR-S or calcein at 7-10 dpf and imaged for analysis (Fig. 4.1A). As for the other larval systems, advantages of this system are the low amount of material needed and the fast read out, while image analysis remains the major bottleneck. Automation of specimen handling and image acquisition/analysis is possible to reduce procedure time and increase screening throughput.

4.3.2.4. *Ex vivo* culture of elasmoid scales

Zebrafish elasmoid scales are small bone-like units of easy access that can be easily and rapidly plucked out of zebrafish skin. They are available in rather large quantities – around 200 elasmoid scales in a single adult zebrafish[292,293] – and can be cultured *ex vivo* for several days[186,294]. Thus they have been successfully used to study and discover osteogenic drug[187,295]. Scales are usually removed from the flank of the adult zebrafish in the region from behind the head to the anterior margin of the anal fin [296]. If the fish has to survive, a limited number of scales should be plucked

out. Although this has not been tested thoroughly, approximately 50 scales can be plucked out without a significant increase of the mortality[296,297]. Upon removal, scales have the ability to regenerate and can be used to assess the potential of test compounds to affect *de novo* bone formation (see next section). Simple staining procedures – e.g., TRAP (tartrate resistant acid phosphatase) staining to assess osteoclast bone resorbing activity and ALP (alkaline phosphatase) staining to assess osteoblast bone forming activity, but also von Kossa's staining to assess scale mineralization and patterning – have boosted the interest of this system for high-throughput screening. The availability of transgenic lines for bone marker genes, e.g., *Tg(sp7:mCherry)* or *Tg(Ola.Sp7:Luciferase)*, where a reporter signal easily quantifiable is used as a proxy for bone formation, has accelerated the screening procedure by shortening *ex vivo* culture, limiting scale handling and simplifying image acquisition[295]. The small size of adult zebrafish scales, less than 1 mm, is also a clear advantage for screening pipelines as they can be individualized in 384-well plates, therefore decreasing the quantity of compounds needed and enhancing throughput. While most steps of the screening pipeline using *ex vivo* cultures of elasmoid scales – including scale sorting in multiwell plates – can be automatized to further enhance throughput, the plucking of the scales has still to be done manually as it requires precision and care to avoid scale damages or animal injuries. It is also worth to mention that not all scales have the same size or the same morphology[296], thus the need to normalize data (e.g., fluorescence signal or bone-specific staining) to correct for inter-scale variability.

4.3.3. Bone structures capable of repair and regeneration

The ability of the zebrafish to fully restore damaged/amputated bone structures – e.g., fin rays, skull, jaw and scales – has been used to study molecular and cellular mechanisms underlying *de novo* bone formation[185,298–303]. Upon surgical amputation of the caudal fin, plucking of scales, craniectomy or injuries to fin rays or the lower jaw, a regenerative program initiates and missing or damaged tissues, including bone and bone-like structures, are rapidly and faithfully restored, or repaired.

4.3.3.1. Regenerating caudal fin

Zebrafish caudal fin is a simple structure composed of bony rays spaced with vascularized and innervated connective tissue and covered with a pigmented epidermis[304]. Upon amputation of the fin (i.e., finectomy), tissues are restored through epimorphic regeneration in less than two weeks[305]. The simple structure and the remarkable regenerative properties of zebrafish caudal fin have stimulated its use in screening assays aiming at identifying compounds, or extracts, with bone anabolic or mineralogenic effects[144,145,185,243] (Fig. 4.1B). Cardeira et al. (2016)[185] and Tarasco et al. (2020)[289] have recently optimized the experimental procedure toward a reduction of the assay duration: tissue restoration is accelerated by placing finectomized zebrafish at 33ºC (instead of 28ºC), regenerative and osteogenic potential of selected compounds are assessed at 5 days post-amputation (dpa), and morphometric analysis of the regenerated fin has been semi-automatized using an ImageJ macro. Advantages of the caudal fin regeneration assay are related to its capacity to provide data at multiple levels i.e., bone regeneration by determining the extent *de novo* bone formation, bone mineralization by quantifying bone mineral density, and bone patterning by assessing ray bifurcation. The late developmental stage required for this assay is clearly a limitation to screening throughput as the production and the housing of large quantities of young adults of 3-4 months is more laborious and more costly. Commercial solutions to automatically handle adult zebrafish and acquire high resolution images of the regenerated fin (see section 4.4.) combined with ImageJ macros recently developed[289] are adequate tools to enhance screening pipeline efficiency. Other limitations of the regenerating caudal fin system that can affect screening throughput are related to the finectomy – a surgery necessitating fish manipulation and anesthesia, and performed under a stereomicroscope thus a rather laborious procedure – and the high amount of compounds needed for waterborne exposure (each adult zebrafish is kept in 250 mL of fish water). While finectomy can hardly be automatized, a lower quantity of compounds could be used if fish are exposed through intraperitoneal injection, a process that is not yet automatized and should be therefore limited to compounds available in very low quantity or insoluble in water. For all these reasons, it is probably safe to say that the regenerating caudal fin system should be limited to secondary screening, where the osteogenic potential of promising compounds identified in

primary high-throughput screenings are further confirmed and characterized for underlying mechanisms.

4.3.3.2. Regenerating elasmoid scales

When they are lost or removed experimentally, zebrafish elasmoid scales can fully regenerate within 2-3 weeks following a process comparable to intramembranous ossification[303]. As for the regenerating caudal fin rays, regenerating scales can be used to assess or study compound regenerative and osteogenic potential. In this experimental setup, fish has to survive scale removal and regeneration process should also not be affected by an excessive loss of scales. Thus, a limited number of scales should be plucked out in a single adult zebrafish (see section 4.3.2.4). Normally 20-30 scales are extracted from the fish flank, afterwards fish are exposed to compounds for 5 days until regenerated scale are collected and analyzed (Fig. 4.1B). Morphometric analysis of regenerated scales can give as information on scale area, morphology, osteoclast activity and mineral deposition that can bring highlights on the bone remodeling process. As for the regeneration of the caudal fin, increasing water temperature to 33ºC will accelerate the regeneration of the elasmoid scales, which can then be used at 5 days post-plucking (dpp) to screen for molecules with osteogenic potential.

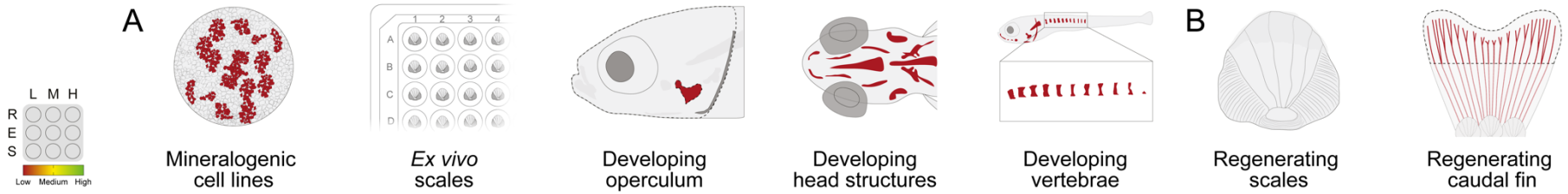

	Mineralogenic cell lines	*Ex vivo* scales	Developing operculum	Developing head structures	Developing vertebrae	Regenerating scales	Regenerating caudal fin
Assay throughput (see legend above)							
Developmental stage	*	6 months	3 dpf	3 dpf	3 dpf	3/4 months	3/4 months
Exposure duration	15 days	3 days	3 days	6 days	4-9 days	4-21 days	5 days
Exposure	Culture medium	Culture medium	Embryo medium	Embryo medium	Embryo medium	Waterborne/IP	Waterborne/IP
Set-up	24/48-well plate	96/384-well plate	6-well plate	96-well plate	12-well plate	Cup	Cup
Density	13000 cells/cm^2	1 scale/well	1.5 larvae/mL (in 10 mL)	3 larvae/mL (in 330 µL)	2 larvae/mL (in 4 mL)	5 fish/L	5 fish/L
Cellular complexity	Single cell type	Osteoblast/osteoclast	Mostly osteoblast	Mostly osteoblast	Mostly osteoblast	Osteoblast/osteoclast	Osteoblast/osteoclast
Temperature (°C)	28	28	28	28	28	28/33	28/33
Based on	Vijayakumar et al., 2013	Pasqualetti et al., 2012	Tarasco et al., 2017	Fleming et al., 2005	Chen et al., 2017	de Vrieze et al., 2014	Cardeira et al., 2016

Figure 4.1. Overview on the zebrafish assays available for the screening of osteoactive extracts or compounds. (**A**) Zebrafish models of bone development. (**B**) Zebrafish models of bone repair and regeneration. R, number of experimental units; E, exposure duration; S, set-up; L, low; M, medium; H, high; dpf, days post-fertilization; IP, intraperitoneal injection; * Cell line developed from a mixture of calcified tissues from juvenile zebrafish and composed of osteoprogenitor cells.

4.3.4. Mutant and transgenic lines for phenotypic screening of bone anabolic compounds

Skeletal genetic disorders represent a large heterogeneous group of rare hereditary diseases that appear during development, growth, or adulthood[306] and are characterized by a variety of skeletal phenotypes, clinical symptoms and molecular mechanisms. Patients' whole genome sequencing (WGS) and genome wide association studies (GWAS) have improved our understanding of the genetic basis of skeletal diseases and unveiled important data on genotype to phenotype correlation[307–311]. Nevertheless, the characterization of gene contribution to specific skeletal traits and diseases requires functional testing and appropriate screening systems. *In vitro* cell systems, despite useful to study cell signalling pathways, evaluated the role of specific knockouts and knock-ins on cell survival, proliferation, and mineralization, and to perform high throughput screening assays, are rather limited to mimic the complex nature of genetic skeletal disorders, thus *in vivo* systems would often come across as being more suitable. Rodents are traditionally well-established model animals to study the physiology and pathology of the mammalian skeleton, however the process of generating *in vivo* systems (e.g., mutant and transgenic lines) to access disease-related gene function is costly and time-consuming. Also, the low throughput of these *in vivo* systems often hampers the execution of large screening assays, a crucial step in the timely development of therapeutics. In contrast, zebrafish is an emerging – though well-established – model animal that brings technical and economic benefits to large scale screening and is often seen as a species that could bridge the gap between basic high-throughput *in vitro* cell screening assays and complex low-throughput *in vivo* mammalian systems; thus, it holds a great deal of promise for the screening and the identification of bone anabolic compounds for developing next-generation drugs. Although zebrafish and humans are separated by more than 400 myr of evolution, they are very similar on what concerns bone homeostasis and skeletogenesis. In this regard, molecular mechanisms and cell types associated to skeleton development and mineralization have been remarkably conserved throughout evolution[120,312–315] and 80% of human disease-related proteins have well-conserved orthologs in the zebrafish genome[316]. This, together with the amenability of zebrafish genome to genetic manipulation,

prompted the development of genetic and transgenic variants to study human skeletal genetic disorders in basic and pre-clinical research. Gene editing techniques used to generate zebrafish skeletal disease models have evolved rapidly. At first, random point mutations induced by chemicals mutagens (e.g., 1-ethyl-1-nitrosourea (ENU)[317] were used to generate mutant lines with bone phenotypes that resemble human disorders. Morpholinos – oligonucleotide analogs with the ability to bind genes and transiently knock-down their function – were used in zebrafish embryos to develop morphants targeting genes central to zebrafish early skeletal development[318]. However, due to the transient nature of morphants phenotype, the study of bone mineralization and remodelling is limited as it happens later during development. The development of zebrafish mutant lines recently gained momentum with major advances in genome sequencing[316] and genome editing tools, e.g., TALEN[319] and CRISPR)/Cas9 systems[275,320]. These breakthroughs enabled the tailoring of gene-specific mutations (e.g., point mutations or deletion of specific gene regions) and the replication of the mutations found in GWAS and patients' genomes. Zebrafish is also a unique model to study the function of genes whose mutations in rodent orthologs are lethal. Indeed, teleost-specific whole genome duplication[321] resulted in the presence of two gene copies in zebrafish genome. In many cases, the two copies were maintained so that a viable loss of function can be obtained and studied due to a partitioning gene function[322].

Several reviews addressing the use of zebrafish mutant lines to study skeletal disorders have been recently published[120,246,312–314,323–325], whose content will not be repeated here. According to the most recent review, more than 80 different zebrafish mutant lines are available to study 78 human skeletal disorders (reviewed in Marí-Beffa et al. (2021)[324]), out of the 461 classified by the Nosology Committee of the International Skeletal Dysplasia Society[306]. Also, approximately 50 transgenic reporter lines have been developed and used to investigate zebrafish skeleton[246,314]. Many of these mutant and transgenic lines are accessible through repositories such as the Zebrafish International Resource Center (ZIRC) and the European Zebrafish Resource Center (EZRC), while important data – e.g., genes, alleles, transgenic lines, gene expression profiles, phenotypes and orthology - are available at the Zebrafish Information Network (ZFIN). Moreover, the external development and translucent body at embryonic and larval stages, or in alternative the use of *casper*[326] or

crystal[327] mutants which possess ghost-like phenotype inclusively at juvenile or adult stages, associated with the many fluorescent markers (e.g., GFP, CFP and mCherry) or fluorescent stains for mineralized bone (e.g., alizarin red S, calcein) available, allow real time live imaging that can be used to follow the progression of skeletal developmental pathologies in the different mutant lines. This type of approach combined with the facility to obtain embryos in quantity for large screening assays, holds great opportunities to screen for molecules capable of rescuing pathologic phenotypes, study their mechanisms of action and possible toxic and side effects in the different organs. It is worth to mention that many drugs that are active in humans are known to trigger similar effects in zebrafish, which is also true for known osteogenic compounds such as calcitriol, parathyroid hormone (PTH), bisphosphonates and several natural compounds (reviewed in Rosa et al. (2021)[274]). In fact, and as a proof of the conservation of important metabolic pathways between zebrafish and humans, bone metabolic disorders as it can be osteoporosis, can also be mimic in wild type zebrafish with resource to chemical induction by e.g., excess of glucocorticoids, iron or high fact diet[274], as it happens in mammals. Overall, zebrafish offers a variety of genetic and transgenic lines, systems, and tools amenable to high-throughput screening assays that can be used to rapidly and successfully evaluate drugs against skeletal phenotypes, thus contributing to greatly improve our knowledge on disease mechanisms and to discover new bone-disease therapeutics.

4.4. TOOLS TO IMPROVE SCREENING THROUGHPUT AND REPLICABILITY

Technological innovation applied to the standardization and mass production of the animals, to the robotic handling of animals, plates, and liquids, to the automation of data acquisition and processing can improve screening throughput and data accuracy thus accelerating the use of zebrafish systems for bone anabolic drug discovery (Fig. 4.2). The miniaturization and improvement of various pieces of apparatus have also boosted screening capacity by reducing operational times and the need for biological material. But technological innovation has a cost: it is expensive to set up and to run and therefore requires a massive investment that many research laboratories in academia or small companies cannot afford. A larger implementation of high-throughput zebrafish screening pipelines will only be possible if costs associated to the technologies that accelerate screening speed markedly decrease in the near future.

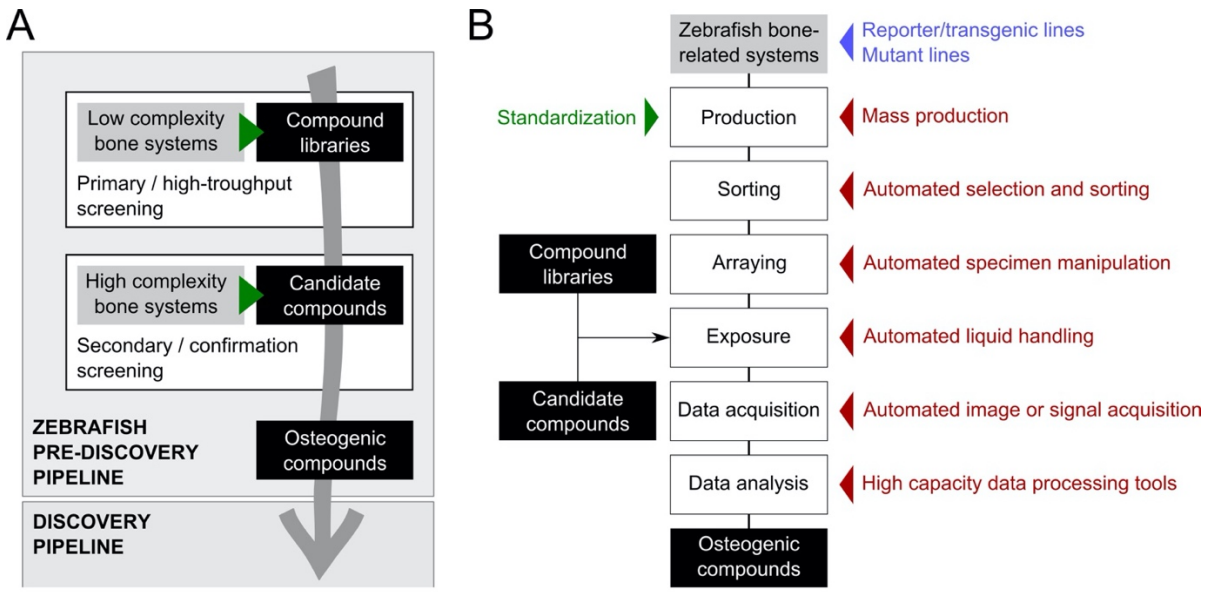

Figure 4.2. Zebrafish pre-discovery pipeline (**A**) and technological innovation applied to the standardization and automation to improve zebrafish screening throughput and data accuracy.

4.4.1. Inbred zebrafish lines

Wild-type zebrafish lines found in pet shops worldwide exhibit a relatively high degree of genetic diversity that triggers some variability in their phenotype, thus some variability in their response to compound exposure[328]. In this regard, several inbred laboratory lines have been developed (e.g., AB and TU lines; see ZFIN for a comprehensive list of wild-type laboratory lines) to reduce genetic diversity and response variability; these strains should be preferentially used in drug discovery pipelines as they will increase data accuracy and therefore reduce the need for higher number of replicate experiments.

4.4.2. Standardized housing and feeding

Animals for screening purposes must be produced under conditions that ensure optimal growth and welfare to provide homogeneous and replicable data. The standards of an “optimal growth and welfare” may vary considerably between wild-type and mutant lines – it largely depends on the severity of the mutant phenotype – and the term “most favourable growth and welfare” is probably more appropriate. To provide optimal/most favourable conditions, housing, husbandry and feeding of the zebrafish has to be adapted to all life stages and standardized. The European community directive 2010/63/EU on the protection of animals used for scientific purposes establishes general guidelines for water quality, chemical and physical parameters applicable to all fish species; however it does not specify zebrafish. Aleström and colleagues[287] recently refined the specific recommendations for housing and husbandry of zebrafish and provided a comprehensive guidance on the best practices for rearing and maintaining zebrafish under optimal growth and welfare conditions. The authors emphasized that standardization of husbandry procedures is essential for improving experimental replicability and provided acceptable ranges for different parameters. In brief, all housing systems should have a filtration system (including mechanical, chemical, and biological filters) and a UV sterilizer to maintain water quality, and light and temperature control. Water temperature should be within a 24-29ºC range (ideally 28.5 ± 0.5ºC) and a fixed light|dark cycle of 14|10-hours is commonly used. The water used to fill the fish tanks should be dechlorinated (ideally reverse osmosis filtered water is used) and slightly alkaline (pH of 6.5-8 is achieved

by supplementing water with a salt mixture). Conductivity should range between 150 to 1700 µS and hardness between 3-8. Nitrogenous compounds must be monitored regularly and kept bellow toxic ranges. Fish density is also a critical parameter to achieve optimal growth and welfare conditions. Although stocking densities of 4-10 adults/L and 25 juveniles/L are commonly used[231,287], lower densities are recommended to keep oxygen levels close to saturation, maximize growth rate and reduce stress thus increasing welfare[329]. High fish density also increased the proportion of males in the breeding stock[330] and decreased the production of eggs[331]. It is therefore important to maintain optimal housing condition for the zebrafish that will be used in screening experiments but also for the breeders that will be used to produce high quality eggs. Several commercial systems

The nutrition of model animals has been recognized as an important variable in research outcomes and the use of 'standard reference diets' has been proposed to improve the replicability of scientific data[332]. Among the several zebrafish facilities dedicated to research worldwide, variations in feeding protocols that could affect growth, health and behavior have been identified; the use of live preys with different nutritional value and the introduction of dry food at different developmental stages are striking examples[225,232,275,329,333–338]. Efforts have been made recently to uniformize zebrafish feeding procedures but also to use standard diets with controlled nutritional composition[234]. In this regard, two microdiets have been recently launched under the name ZEBRAFEED (Sparos Lda) and GEMMA Micro (Skretting); they were formulated to meet the nutritional requirement for all life stages of zebrafish therefore removing the need for live preys (Table 4.1). While both diets provided optimal growth conditions, ZEBRAFEED promoted higher embryo and larval survival and also enhanced reproductive performance[337]. The large-scale usage of a microdiet following an established feeding protocol will certainly contribute towards the standardisation of zebrafish husbandry and the replicability of research data but will also maximize the production and quality of zebrafish embryo/larvae for drug or mutagenesis screenings[337]. In the context of this review, the implementation of a standard reference diet optimized for nutrients essential to the correct development of fish skeletal structures – e.g., fatty acids, phospholipids, vitamins and minerals – will decrease the incidence of skeletal deformities[234,339], providing better conditions for the screening of osteogenic compounds.

4.4.3. Mass production of synchronized embryos

To generate statistically meaningful results, zebrafish high-throughput screening requires the daily production of thousands of synchronized embryos (i.e., at the same developmental stage). To decrease the intensive manual labour that would result from the manipulation of dozens of tanks and hundreds of breeders and increase embryo synchronization, large-scale egg production systems have been developed[345]. Commercial breeding systems such as the Mass Embryo Production System (MEPS; Aquatic Habitats) and iSpawn (Tecniplast) can achieve remarkable spawning rates of up to 800-1000 embryos/minute (Table 4.1). More affordable and with a good spawning capacity (e.g., 10,000 embryos per breeding session using 100-200 pairs of fish), custom-made mass embryo production systems are also available[341]. To maintain an optimal mass production of embryo – both qualitatively and quantitatively – breeders that may suffer some stress incurred by frequent group mattings should be replaced regularly, e.g., using a rotation of 1000 breeders per week.

4.4.4. Target specimen sorting

Targets for drug screening in zebrafish can be cells, tissues, or whole animals (embryo and larvae). While cells – adherent or in suspension – can be easily arrayed in multiwell plates using liquid-handling robots, tissues and whole animals have been typically sorted out under a stereomicroscope using wide-bore transfer pipettes, in a rather laborious process. Automation of this process can be carried out using a fluorescence-gated sorting system – e.g., the COPAS FP-1000/2000 of Union Biometrica (Table 4.1) – that has the capacity to array tissues, embryos and larvae in 96- and 384-well plates but also select them based on viability (dead embryo are discarded), morphology (e.g., size and length) and/or fluorescent signal, and sort a desired number of specimens into individual wells of a microtiter plate. Custom-made systems have also been developed to automatically sort embryos into microplates, e.g., the ZebraFactor of the Swiss Center for Electronics and Microtechnology [340], but also to automatically remove the chorion (a barrier that may prevent or limit embryo exposure to compounds) before sorting, when drug screening is performed in early stages of embryo development [346]. However, none of these custom-made systems

have the ability to sort based on fluorescence or provide morphological information. In the context of this review, larvae from bone-specific transgenic lines expressing a fluorescent reporter protein (see section on transgenic lines) or from wild-type lines stained with bone-specific fluorochromes (e.g., alizarin red S or calcein) can be easily sort out using a fluorescence-gated sorting system as long as the fluorescence signal is strong enough to be detected. Typically, 4-dpf larvae have cranial bone structures sufficiently mineralized to be detected or have already an active expression of bone-related genes. Scales are bone structures that can be easily harvested from the flank of juvenile/adult zebrafish; they have been already used to screen for osteogenic activities, although at low throughput [187,292,303]. The automation of scale sorting based on fluorescent signal (e.g., using *Tg(sp7:mCherry)* line) could be easily achieved using such system, increasing the throughputness of this system.

4.4.5. Compound delivery

Higher screening throughput and higher data accuracy can be achieved using liquid-handling robotics to rapidly dilute and/or dispense precise amounts of the compounds from stock library plates and array targets such as zebrafish embryo and larvae. Robotic solutions are commercialized by different companies (e.g., PerkinElmer, Brand, Hudson Robotics, Labcyte, Gilson) and can be adapted to the several zebrafish systems used to screen for osteogenic compounds. To further increase throughput screening, plate-handling robotic arms can also be used (e.g., PerkinElmer, Hudson Robotics), although their implementation requires a massive investment which probably limit their usage to big Pharma and Biotech companies. If compounds have to be delivered through microinjection, robotic injection systems have been developed: perivitelline injection for embryos [347,348] and intrayolk injection for larvae [349].

4.4.6. Image acquisition

To improve the throughput and quality of screening pipelines, image acquisition has to be automated and use rapid and high-resolution camera. In the case of zebrafish screening, camera should also have the capacity to image large objects such as larvae. While examination of wild-type and mutant/diseased animals for developmental, morphological and functional changes upon compound exposure can

be done, the use of transgenic reporter fish expressing fluorescent proteins can greatly increase the automation of image acquisition. In the regard, fluorescent microscopes with automated stages or microplate readers coupled to high resolution camera will speed-up the examination and imaging of zebrafish embryos or larvae in microtiter plates.

4.4.7. Image analysis

Automated screening systems generate large quantities of images that need to be analysed using specialized algorithms to provide accurate data in a timely manner. Commercial solutions and open-source software are available for automated image analysis, providing macros to count, measure, characterize morphometry and classify objects. Most of them can also be used for image acquisition – providing tools to control microscope and capture images – and all of them can be easily applied to screening pipelines using zebrafish (Table 4.1; see also the review by Mikut et al. (2010)[350]).

Table 4.1. Tools to improve the throughput and accuracy of *in vivo* screenings in zebrafish.

Tool	Standardized diet	Mass production	Sorting	Compound handling	Exposure	Handling	Signal acquisition	Imaging	Data analysis	URL / Reference
ZEBRAFEED	X									www.sparos.pt
GemmaMicro	X									www.skretting.com
MEPS - Mass embryo production systems		X								www.mbki.com
iSPAWN		X								www.tecniplast.it
COPAS FP-1000/2000			X							www.unionbio.com
ZebraFactor			X							(340)
ARQiv - Automated reporter quantification system *in vivo*			X	X		X	X			(341)
ScreenCube					X					(342)
VAST - Vertebrate automated screening technology						X		X	X	www.unionbio.com
HCS LCI							X	X	X	www.leica-microsystems.com
Imaging Machine							X	X	X	www.acquifer.de
ImageXpress							X	X	X	www.moleculardevices.com
IN Cell Investigator Zebrafish Analysis							X	X	X	www.gehealthcare.com
COPAS Vision						X	X	X	X	www.unionbio.com
Micro computed tomography								X	X	www.bruker.com
ZebrafishMiner									X	(343)
ZFIQ zebrafish image quantitator									X	(344)
ImageJ									X	imagej.nih.gov
Image-Pro									X	www.mediacy.com

4.4. CONCLUSIONS

Several assays that have been recently developed in zebrafish to study mechanisms of bone development, repair and regeneration, have the capacity to integrate high-throughput drug discovery pipelines if coupled with technological innovation applied to the standardization and automation of the screening process. However, to the best of our knowledge, a high-throughput screening pipeline using zebrafish for bone anabolic drug discovery has not been yet implemented. It may be related to the scepticism of the pharma/biotech industry about the validity of the zebrafish to model human diseases, in particular bone disorders. Technological features that can further increase replicability and throughput of zebrafish screening pipelines are developing rapidly and should bring an increased interest to this simple and cost-effective vertebrate model in relation its capacity to achieve robust data comparable to those collected in rodents. On a different field of research, zebrafish is gaining momentum as a model for acute/chronic toxicity studies of environmental pollutants (biocides, metals, microplastics, etc.) but also drugs (safety assessment before marketing). Zebrafish assays and technological innovations described here can also be used to screen compounds for osteotoxicity.

Chapter 5

Effects of pristine or contaminated polyethylene microplastics on zebrafish development

Submitted chapter:

Tarasco M, Gavaia PJ, Bensimon Brito A, Cordelières FP, Martins G, Castro DT, Silva N, Cabrita E, Bebianno MJ, Stainier DYR, Cancela ML, Laizé V (2022). Effects of pristine or contaminated polyethylene microplastics on zebrafish development. Submitted to Chemosphere.

PREAMBLE

The majority of zebrafish studies have evaluated the effects of microplastic exposure (pristine or contaminated with organic pollutants) on development, neurotoxicity, behavior, oxidative stress, intestinal damage and microbiome changes. In this regard, while several studies have reporter microplastic toxicity (normally higher in combination with pollutants), others showed limited or no impact. Variability in the biological response may be due to the different type and size of plastic tested, different exposure duration, concentration, and route. Due to laboratory limitations (i.e., static conditions, absence of recirculating housing systems to study microplastic), most of the studies have performed relatively short-term exposure trials (i.e., maximum up to 21 days), mostly throughout waterborne exposure, and limited developmental stages. Thus, the impact of microplastic on zebrafish remain to be better assessed especially upon long exposure times during the full developmental process and its impact in future generations.

In this chapter, we assessed the biological effects of a long-term exposure to polyethylene (PE) microparticles – pristine or contaminated with benzo[α]pyrene (BaP), a model compounds for PAHs – on zebrafish growth, reproduction, and bone development. In this regard, zebrafish at different developmental stages (from larvae throughout adulthood) were fed experimental diets enriched in PE microplastics and expression of selected marker genes, intergenerational effects were evaluated.

5.1. ABSTRACT

The presence of microplastics in the aquatic ecosystem represents a major issue for the environment and human health. The capacity of organic pollutants to adsorb onto microplastic particles raises additional concerns, as it creates a new route for toxic compounds to enter the food web. Current knowledge on the impact of pristine and/or contaminated microplastics on aquatic organisms remains insufficient, and we provide here new insights by evaluating their biological effects in zebrafish (*Danio rerio*). Zebrafish larvae were raised in ZEB316 stand-alone housing systems and chronically exposed throughout their development to polyethylene particles of 20-27 µm, pristine (MP) or spiked with benzo[α]pyrene (MP-BaP), supplemented at 1% w/w in the fish diet. While they had no effect at 30 days post-fertilization (dpf), MP and MP-BaP affected growth parameters at 90 and 360 dpf. Relative fecundity, egg morphology, and yolk area were also impaired in zebrafish fed MP-BaP. Zebrafish exposed to experimental diets exhibited an increased incidence of skeletal deformities at 30 dpf as well as an impaired development of caudal fin/scales, and a decreased bone quality at 90 dpf. An intergenerational bone formation impairment was also observed in the offspring of parents exposed to MP or MP-BaP through a reduction of the opercular bone in 6 dpf larvae. Beside a clear effect on bone development, histological analysis of the gut revealed a reduced number of goblet cells in zebrafish fed MP-BaP diet, a sign of intestinal inflammation. Finally, exposure of larvae to MP-BaP up-regulated the expression of genes associated with the BaP response pathway, while negatively impacting the expression of genes involved in oxidative stress. Altogether, these data suggest that long-term exposure to pristine/contaminated microplastics not only jeopardizes fish growth, reproduction performance, and skeletal health, but also causes intergenerational effects.

5.2. INTRODUCTION

Plastic pollution has greatly increased over the last decades and represents a major issue for both the environment and human health. Pollution with plastic debris is ubiquitous and massive with more than 5.25 trillion particles weighing 268,940 tons floating in the world's oceans[26]. Aquatic ecosystems are particularly impacted by plastic pollution and high densities of plastic particles, in particular microplastics

(<5 mm), which are observed throughout the globe thus raising concerns on the welfare of aquatic organisms[79,194]. Released into the aquatic environment through the runoff of urban/industrial effluents (e.g., nurdles, scrubbers) or the breakdown of larger debris (physical, biological, chemical degradation), microplastics are found in many rivers and oceans worldwide. The presence of microplastics has been reported not only on ocean's surface but also in deep oceans at 10,890 meters[41], and in sediments. Plastic debris have reached even the most remote places on earth such as the Arctic snow[42] and Antarctic ice[43]. Microplastics are heterogeneous in composition (they are manufactured with different polymers, e.g., polyethylene, polystyrene, polyvinylchloride and polyurethane), have different densities (they float, are neutrally-buoyant or sink to the river/ocean floor), and often incorporate additives (fillers, plasticizers, colorants, and stabilizers)[7]. The ingestion of microplastics by aquatic organisms may have a physical impact by disturbing feeding habits, blocking the feeding appendages and the passage of food through the intestine, causing false satiation or damaging the gastrointestinal track, which results in a decrease in food intake[78,79]. On the other hand, microplastics can chemically affect internal organs through the leaching of manufacturing additives (e.g., polybrominated diphenyl ethers, nonylphenol and triclosan), or the release of contaminants (e.g., heavy metals, endocrine-disrupting chemicals, persistent organic pollutants and halogenated organic contaminants) that are easily adsorbed onto microplastic surface before ingestion[80,351].

In this regard, ubiquitous contaminants such as benzo[α]pyrene (BaP) and other polycyclic aromatic hydrocarbons (PAHs) – known to be carcinogenic and to disrupt developmental, reproductive, hepatic, endocrine and immunological processes[72,73], but also to be harmful to skeletal development and bone homeostasis[144,352] – have the ability to adsorb onto the surface of different types of microplastic polymers, especially onto polyethylene[16,60,61]. Upon ingestion of the contaminated microplastics, PAHs can leach out, diffuse throughout animal body and accumulate into a range of tissues[74–77], raising additional concerns about the adverse effects produced by microplastics.

Beside the damage that they may cause to the aquatic life, microplastics (and adsorbed chemicals) pose a threat to human health as they are becoming omnipresent

in the food web and in our daily life (e.g., table salt, drinking water, honey, beer, etc.)[27,45,47,194]. Thus, many international environmental and food agencies (United Nations Environment Programme (UNEP), European Food Safety Authority (EFSA) and Group of Experts on the Scientific Aspects of Marine Environmental Protection (GESAMP)) have placed microplastics as one of the top priority research topics[37–39]. Scientific data evidencing the negative impact of microplastics on the physiology of aquatic organisms is rapidly increasing, however cellular and molecular mechanisms underlying microplastic toxicity are still poorly understood and more data are needed to further support environment management issues. Adverse effects such as growth inhibition[353–355], behavioral disorders[353,356], reproductive dysfunctions[357,358], feeding disorders[359,360] and mortality[353,354] have been described for different trophic levels[194]. However, data on specific biological processes (i.e., development, reproduction, transgenerational studies) and in key species such as fish, are still missing or are controversial to fully assess the environmental and biological risks associated with microplastics and adsorbed pollutants.

Among aquatic organisms that may be exposed to microplastics, fish are central to the ocean food web and to human nutrition, and the presence of microplastics potentially contaminated has been widely reported in fish, including in species marketed for human consumption[48,97], opening a new route for toxicity in humans. To better evaluate adverse effects of microplastics in fish and, by extension, in vertebrates, zebrafish has been widely used to gain insights into the biological effects of microplastic ingestion[122]. It is a well-established ecotoxicological model organism to assess risks associated with toxicity, reproduction and osteotoxicity[120,147], but also to study the cellular and molecular mechanisms underlying toxicant effects.

The majority of the studies performed in zebrafish evaluated the effects of microplastic exposure (pristine or in combination with environmental pollutants) on development[124,128,129,131], neurotoxicity[361,362], behavior[363,364], oxidative stress[127,130,136,140], intestinal damage[133,365] and microbiome changes[130,139] (see also the review by Bhagat et al. (2020)[122] and references therein). In this regard, while several studies have reported microplastic toxicity (normally higher in combination with contaminants), others showed limited or no impact. Variability in biological response

may be due to the different type and size of microplastic tested, different exposure duration, concentration, and route. Due to laboratory limitations (i.e., static conditions, absence of recirculating housing systems to study microplastic), most of the data originated from short-term exposure trials (i.e., up to 21 days), mostly through waterborne exposure, and during specific developmental stages. Thus, the impact of microplastics on zebrafish remain to be better assessed especially upon long-term exposure throughout the full developmental process and on future generations.

In this work, the biological effects of a long-term exposure to polyethylene (PE) microparticles were assessed. Zebrafish were fed from larvae to adulthood with experimental diets supplemented with microplastics pristine or contaminated with BaP, and zebrafish growth, reproduction, bone development, expression of selected marker genes and intergenerational effects were evaluated.

5.3. MATERIALS AND METHODS

5.3.1. Chemicals and materials

All chemicals were bought to Sigma-Aldrich (St. Louis, MI, USA) unless otherwise stated. Plastic material was avoided as much as possible to limit any cross-contamination during experimental procedures and replaced by soda-lime glass or stainless steel material. Fluorescent polyethylene microspheres (20-27 μm; 1.005 g/cc) were purchased from Cospheric (Santa Barbara, CA, USA). Microspheres manufacturing composition: polyethylene (CAS number 9002-88-4; >70% w/w) and proprietary additive (trade secret; <30 % w/w).

5.3.2. Experimental diets

Experimental diets were manufactured by Sparos Lda. (Olhão, Portugal) and used to feed zebrafish throughout the experimental procedures. The commercial microdiet ZEBRAFEED (Sparos) was used as control diet (Ctrl) and as the basis of the diets supplemented with pristine microplastics (MP) or with microplastics spiked with benzo[α]pyrene (MP-BaP). Four different grain sizes – i.e., <125 μm, 125-180 μm, 180-355 μm and 355-700 μm – were prepared for each diet to meet the mouth size of the different developmental stages. Briefly, microplastics (1% w/w) were incorporated and mixed in ZEBRAFEED microdiet (grain size <100 μm), hydrated with 50% of

distilled water, then mixed again until complete homogenization and dried at 60ºC overnight. MP-BaP diet was similarly prepared but with microspheres spiked for 30 h with benzo[α]pyrene (10 µM dissolved in dimethyl sulfoxide, DMSO), washed with distilled water and vacuum dried before being incorporated into the diet (method adapted from previous studies[76,123,138]). The successful incorporation of microplastics into the experimental diets was confirmed in 5 aliquots of each diet size. Diet aliquots of approximately 5 mg were solubilized in 50 mL of distilled water and vacuum filtered through a 11 µm paper filter (Grade 1; Whatman, Maidstone, UK). Fluorescence images of each paper filter Ctrl, MP, and MP-BaP (at different grain size) were acquired using a MZ10F fluorescence stereomicroscope (Leica, Wetzlar, Germany) equipped with GFP filters ET470/40x (EX) and ET525/50m (EM), and a DFC7000T color camera (Leica). The number of microplastic particles present in each aliquot was assessed using the built-in function *Find maxima* in ImageJ 1.52v.[366]

5.3.3. Zebrafish maintenance

Sexually mature zebrafish (AB wild-type strain; ZFIN ID: ZDB- GENO-960809-7) were housed in a ZebTEC housing system (Tecniplast, Buguggiate, Italy) under optimal water quality (i.e., temperature 28 ± 0.1ºC, pH 7.5 ± 0.1, conductivity 700 ± 50 µS, ammonia and nitrites lower than 0.1 mg/L, nitrates at 5 mg/L) and crossed following an in-house breeding program. Breeders were fed twice a day with rotifers (*Brachionus plicatilis* type L; 230 rotifers/mL) enriched with 2 mL of Phytobloom Green Formula (Necton S.A., Olhão, Portugal) and ZEBRAFEED microdiet *ad libitum*. Fertilized eggs (N = 300) were placed into a 1-L breeding tank containing system water and 0.0002% (w/v) methylene blue to prevent fungal growth. At 3 days post-fertilization (dpf), hatched larvae were transferred into 3.5-L glass tanks at a density of 100 larvae/L and maintained under static water conditions (90% of the water renewed every 2 days) at 28ºC. At 15 dpf, post-larvae were distributed into new tanks to achieve a density of 26 post-larvae/L and maintained in a ZEB316 custom-made recirculating housing system[367] with a water flow of 8.4 L/h. At 30 dpf, density was adjusted to 5 juveniles/L. All fish were subjected to a 14-h light/10-h dark photoperiod throughout the duration of the experimental work.

5.3.4. Dietary exposure of zebrafish to microplastics

A total of 600 larvae (200 per replicate in glass tanks) were exposed to experimental diets Ctrl, MP, or MP-BaP – dispensed in similar quantity using stainless steel micro-spoons – throughout development. Larvae from 5 to 8 dpf were fed 3 times a day, twice with enriched rotifers (see above) and once with the experimental diet (size <125 µm, 20% body weight). Larvae from 8 to 30 dpf were fed 3 times a day exclusively with the experimental diet (size 125-180 µm from 8 to 15 dpf and size 180-355 µm from 15 to 30 dpf, 20% body weight). Juveniles and adult fish were fed 2 times a day with experimental diet (size 355-700 µm, 3-5% body weight).

5.3.5. Assessment of growth parameters

Dry weight was determined in 30 dpf juveniles (pools of 6 fish) and 6 dpf larvae (offspring; pools of 30 larvae). Fish pools were placed in 1.5-mL tubes, lyophilized and weight using a precision scale (0.00001 g). Wet weight was determined in 90 and 120 dpf adults (individually) using a precision scale. Total length, standard length, head area and body depth (i.e., the vertical distance from the dorsal margin of the body to the ventral margin of the body measured at the base of the pectoral fin) were assessed in 6 dpf offspring by image analysis of brightfield images using ImageJ.

5.3.6. Assessment of reproduction capacity

Sexually mature zebrafish (>3 months old) fed the different experimental diets were placed 12 h prior to the experiment in breeding tanks (Tecniplast), with males and females separated by a tank divider following a 1:1 sex-ratio. For each breeding experiment, 2 couples were randomly selected from each replicate tank (3 tanks per experimental diet), resulting in 18 independent breeding events. A total of 4 breeding experiments were performed with a resting period of 2 weeks in-between each breading event. Breeding was initiated by removing the divider separating males and females and breeding success was scored as follows: score = 1 when a couple successfully laid eggs and score = 0 when no eggs were laid, or eggs aborted. Eggs from successful breeding events were kept in glass Petri dishes supplemented with fish water at a density of 50 eggs/40 mL. Methylene blue (0.0002% w/v) was added to prevent fungal growth. For each breeding event, all laid eggs were imaged at 0 and

24 hpf (hours post-fertilization) using a Leica MZ10F stereomicroscope equipped with a DFC7000T color camera. Egg number, viability, area, and circularity were assessed through image analysis using a macro developed in ImageJ (See Chapter 3.2, Fig. 3.6). Yolk area was measured at 0 hpf using ImageJ built-in tools. Relative fecundity was calculated as the total number of eggs normalized to female body weight. Hatching rate was calculated as the number of larvae hatched at 3 dpf normalized to the total number of fertilized eggs. Hatched larvae were kept in fish water up to 6 dpf to assess intergenerational effects.

Sperm quality was assessed in 6 males per condition. Fish were anesthetized with 0.6 mM tricaine methanesulfonate, rinsed with phosphate buffered saline (PBS) and sperm was collected using a 25 µL glass capillary tube (Blaubrand, Wertheim, Germany) attached to a mouthpiece while performing an abdominal massage. Sperm (1 to 3 µL per fish) was immediately diluted in 10 µL of 0.2 µm filter-sterilized Hank's balanced salt solution (HBSS) and maintained at 4ºC until further used but no longer than 1 h. Sperm concentration and motility were evaluated using a computer-assisted sperm analysis (CASA) system (Proiser, Valencia, Spain) coupled to a E-200 microscope (Nikon, Tokyo, Japan) equipped with a x10 negative phase contrast objective. Images were captured with a A312f/fc camera (Basler AG, Ahrensburg, Germany) and processed with CASA software. For sperm concentration, samples were diluted 1:20 in HBSS and the number of spermatozoa was determined from 3 field images. For sperm motility analysis, 0.5 µL of sperm was placed on a Makler chamber (Microptics S.L., Barcelona, Spain) and immediately activated with 5 µL of sterilized system water at 28°C. Each sample was measured twice. Sperm motility was characterized from 0 to 60 s post-activation through the acquisition of several parameters i.e., total motility (%), progressive motility (%), curvilinear velocity (µm/s), straight line velocity (µm/s) and linearity (%). To assess sperm viability, 2 µL of sperm were diluted in 200 µL of HBSS in flow cytometry tubes and labelled with 1 µL of propidium iodide (PI; final concentration 5 ng/mL). Labelled sperm was analyzed using a FACS Calibur flow cytometer (BD Biosciences, Franklin Lakes, NJ) equipped with a 488-nm laser for excitation and a 690/50 nm bandpass filter (FL3) for fluorescence emission. Settings for zebrafish spermatozoa acquisition and analysis were previously established.[368] A total of 10,000 events were counted for each sample.

5.3.7. Assessment of osteotoxicity

5.3.7.1. Axial skeleton development

At 30 dpf, a total of 120 juveniles (40 per replicate tank) were randomly collected for each experimental diet (i.e., Ctrl, MP, and MP-BaP) and euthanized with a lethal dose of anesthetic. Juveniles were fixed for 1 h in 4% paraformaldehyde (PFA; prepared in PBS) at room temperature, washed with 1X PBS, preserved in increasing ethanol series (up to 75%) and stored at -20ºC until further used. Fish were rehydrated in increasing 1X PBS series, stained for 2 h in 0.05% alizarin red S (AR-S) prepared in 1% potassium hydroxide (KOH), washed for 12 h with 1% KOH and preserved in increasing glycerol series (up to 75%) until image acquisition. The incidence, typology (such as shape variation, anomalous supernumerary elements, fusions or platyspondyly) and charge of deformities in the axial skeleton were determined through stereomicroscopy observation. The terminology used is according to Bird and Mabee.[369] Representative images were acquired using a LSM 700 confocal microscope (Zeiss, Oberkochen, Germany) equipped with a 10x/0.30 M27 objective. Images were acquired at 1024×1024 pixels using 4% laser power at 555 nm, acquisition speed=7.75 µs, mCherry channel (λex: 587 nm, λem 610 nm) and a GaAsP detector set to gain=650V and digital gain=0.3. Z slices were recorded at 4 µm per section and adjusted to cover the full depth of the region of interest.

5.3.7.2. Caudal fin development

At 90 dpf, a total of 24 adult fish (8 per replicate tank) were randomly collected for each experimental diet (i.e., Ctrl, MP, and MP-BaP). Fish were sacrificed with a lethal dose of anesthetic and their caudal fin amputated, fixed for 1 h in 4% PFA, washed 3 times with 1X PBS, preserved in increasing ethanol series (up to 75 %) and stored at -20ºC until further use. Caudal fins were rehydrated in increasing 1X PBS series, stained for 30 min in 0.1% AR-S prepared in 1% KOH, washed 3 times with 1% KOH and preserved in increasing glycerol series (up to 75%). Caudal fins were imaged using a Leica MZ10F stereomicroscope equipped with a DFC7000T color camera. Total number of rays and number of fused, bended, or developmentally impaired rays were determined in bright-field images.

5.3.7.3. Scale development

At 90 dpf, a total of 3 adult fish (1 per replicate tank) were randomly collected from each experimental diet (i.e., Ctrl, MP, and MP-BaP), sacrificed with a lethal dose of anesthetic and 30-40 ontogenetic scales were plunked from the left flank of each specimen with stainless steel forceps. Scales were fixed for 30 min in 4% PFA at 4ºC, washed 3 times with 1X PBS, preserved in increasing ethanol series (up to 75%) and stored at -20ºC until further used. Mineral deposition was assessed in von Kossa-stained scales. Briefly, scales were rehydrated in increasing 1X PBS series, washed with 1X PBS, immersed in 5% (w/v) silver nitrate, and exposed to U.V. light for 1 h. Scales were then rinsed with distilled water for 5 min and immersed for 5 min in 2.5% (w/v) sodium thiosulfate. Finally, scales were rinsed thoroughly with distilled water and preserved in increasing glycerol series (up to 75%) until image acquisition. Bright-field images of stained scales were acquired using a Leica MZ10F stereomicroscope equipped with a DFC7000T color camera. Scales area, circularity and mineral deposition were assessed through image analysis using ZFBONE ImageJ toolset.[289]

5.3.7.4. Calcium and phosphate content

30-dpf juveniles (n=3 per diet; pools of 6 fish), 90-dpf adults (n=3 per diet), 6-dpf offspring (n=30 per replicate tanks, n=90 per diet) were randomly sampled and sacrificed with a lethal dose of anesthetic. Fish were dried for 24 h at 60°C, placed in quartz digestion vials and their weight was determined. Samples were digested with 6 ml of 65% nitric acid (HNO_3; Fisher Scientific, Pittsburgh, PA, USA) using a Discover SP-D 80 microwave digestion system (CEM, NC, USA). Digested samples were diluted appropriately with ultrapure Milli-Q water (pH 7.4; Merck Millipore, Burlington, MA, USA). Mineral content was determined using a Microwave Plasma-Atomic Emission Spectrometer (MP-AES 4200, Agilent Technologies, Santa Clara, CA, USA). A six-point calibration curve was carried out for each element in 5% HNO_3 (Phosphorus standard, Agilent 213.318; Calcium standard Agilent 393.366). Samples were analyzed in duplicate, and the concentration calculated using the external standard calibration method. Blank samples, containing only the decomposition reagents, were included to control contamination, and results were subtracted from the sample values.

5.3.7.5. Offspring operculum development

Offspring born from multiple breeding events (10 larvae per successful breeding event; see reproduction section) were sacrificed at 6 dpf with a lethal dose of anesthetic. Larvae were stained for 15 min at room temperature with 0.01% AR-S prepared in Milli-Q water and washed twice with Milli-Q water for 5 min (protocol adapted from Bensimon-Brito et al. (2016)[370]). Stained larvae were placed in a lateral plane on top of a 2% agarose gel and imaged using a Leica MZ10F fluorescence stereomicroscope equipped with a with mCherry filters ET560/40x (EX) and ET630/75m (EM), and a DFC7000T color camera. Morphometric analysis of the operculum was performed as described by Tarasco et al. (2020) using ZFBONE ImageJ toolset.[289] Total length and body depth were measured using ImageJ built-in tools.

5.3.8. Histology

Adult zebrafish (n=5) were demineralized for 10 days in 10% ethylenediamine-tetraacetic acid (EDTA) and 1% PFA (pH 7.0) at 4ºC with the demineralizing solution changed every 2 days. Sample were washed in 1X PBS, incubated in 10% sucrose (in 1X PBS) for 1 h then in 30% sucrose (in 1X PBS) for 12 h at 4ºC. Specimens were then embedded for 1 h in 7.5% gelatin (gelatin from porcine skin, gel strength 300, Type A) prepared in 15% sucrose (in 1X PBS). Samples were placed at 4ºC in a histological box until gelatin solidified, then frozen in isopentane cooled in liquid nitrogen. Using a Leica microtome (CM3050S), fish were longitudinally sectioned at 10 µm under constant temperature (-24ºC). Histological sections were then maintained at -20ºC until further used. For intestinal goblet cell staining, sections were thawed for 15 min at room temperature, washed twice in 1X PBS preheated at 37ºC for 10 min. Slides were post-fixed in 4% PFA for 10 min, washed in 1X PBS, incubated in 3% acetic acid for 3 min and finally stained for 30 min with 1% alcian blue (prepared in 3% acetic acid, pH 2.5). Slides were then washed in distilled water and mounted with mowiol mounting medium. The number of goblet cells was assessed in each villus using a macro developed in ImageJ (See Chapter 3.2, Fig. 3.7).

5.3.9. RNA extraction and gene expression analysis by qPCR

For each experimental diet (i.e., Ctrl, MP, and MP-BaP), total RNA was prepared from the whole body of 30-dpf juveniles (n=3, pools of 10 specimen), from tissues (liver, gut, and vertebral column) of 3 months adults (n=3, pools of 5 organs) and from 6 dpf offspring larvae (n=3, pools of 30 larvae) in triplicates. Total RNA was extracted using NZYol (NZYTech, Lisbon, Portugal), following manufacturer instructions. RNA quantity was measured using a NanoDrop One spectrophotometer (Thermo Scientific, Waltham, MA, USA) and integrity was confirmed by running 0.5 µg of total RNA on a 1.5% agarose gel. Total RNA (1 µg) was reverse-transcribed for 1 h at 37°C using M-MLV reverse transcriptase (Invitrogen), oligo-d(T) primer and RiboLock RNase inhibitor (Thermo Scientific) according to manufacturer instructions. All quantitative real-time PCR (qPCR) reactions were performed using SensiFAST SYBR Hi-ROX kit (Meridian Bioscience, Cincinnati, OH, USA) according to manufacturer instructions, 10 µM of gene-specific primers (Supplementary Table 5.1) and 1:10 dilution of reverse-transcribed RNA, in a CFX Connect Real-Time PCR detection system (Bio-Rad, Hercules, CA, USA). PCR amplification was as follows: an initial denaturation step of 2 min at 95°C and 40 cycles of amplification (10 s at 95°C and 20 s at 65°C). Efficiency of amplification was above 95 % for all primer sets. Levels of gene expression were calculated using the ΔΔCt comparative method[371] and normalized using the average of housekeeping genes *eef1a1l1* and *rps18*, previously validated in zebrafish larvae[372].

5.3.10. Statistical analysis

Data were analyzed using Prism version 8.2.1 (GraphPad Software, Inc. La Jolla, CA, USA). One-way analysis of variance (ANOVA) followed by Dunnett's multiple comparison test, or an unpaired Student's t-test were used for data sets presenting a normal distribution. Kruskal-Wallis test followed by Dunn's multiple comparison test were used for data sets that did not follow a normal distribution. In all cases, differences were considered significant for $p < 0.05$.

5.4. RESULTS

5.4.1. Both pristine and contaminated microplastics impair zebrafish growth

Mortality, weight, and total length were determined in zebrafish fed the experimental diets from 8 to 30, 90 or 360 dpf. Fish fed MP and MP-BaP diets exhibited a similar survival rate to that of control fish for the three time-windows considered ($p > 0.05$; data not shown). While at 30 dpf dry weight and total length were not different among diets, wet weight and total length were affected at 90 and 360 dpf (Fig. 5.1). At 90 dpf, fish fed with MP and MP-BaP showed a reduction in their weight (19.1 ± 5.4% and 28.7 ± 6.1%, respectively) and length (7.1 ± 2.0% and 9.3 ± 2.3%, respectively) over the control group. At 360 dpf, fish fed with MP and MP-BaP showed a reduction in their weight (38.5 ± 8.5% and 44.4 ± 8.8%, respectively) and length (15.1 ± 2.9% and 8.7 ± 3.1%, respectively) over the control group. No differences were found between MP and MP-BaP treatments ($p > 0.05$). The analysis of growth parameters in relation to fish gender showed that while weight and length were affected in males, only females fed with MP-BaP showed a reduction in their weight at 90 dpf. Growth parameters were affected at 360 dpf in both males and females fed with MP and MP-BaP diets (Supplementary Fig. 5.1). Altered growth parameters clearly demonstrate the developmental effect of an exposure to pristine and contaminated microplastics in zebrafish.

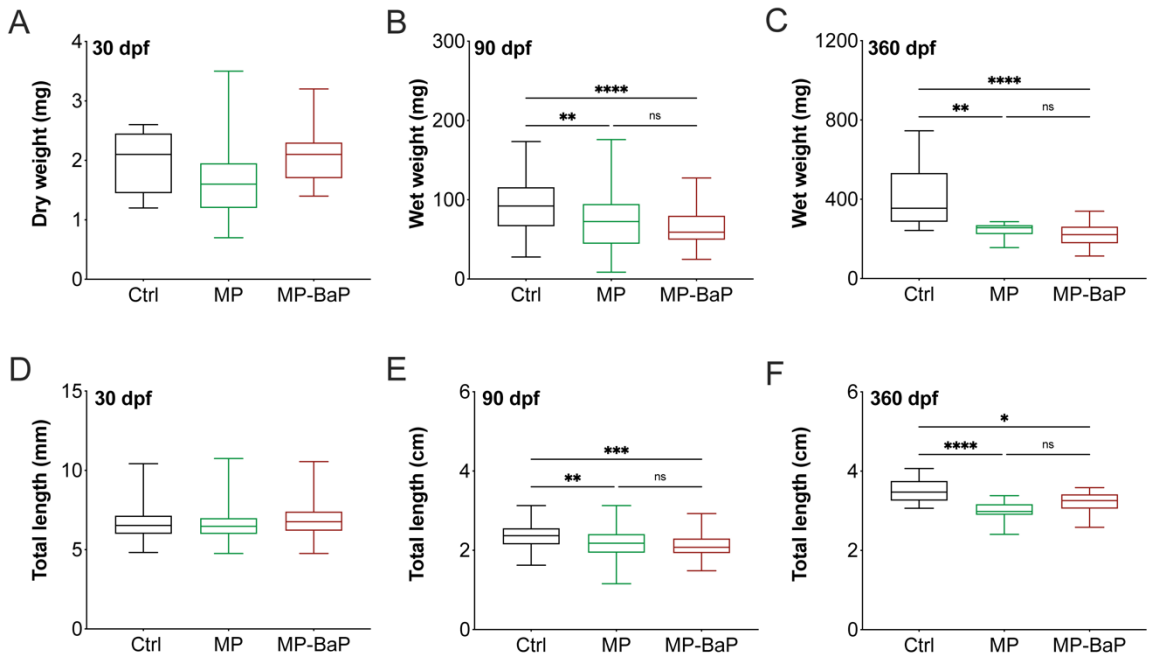

Figure 5.1. Weight (**A-C**) and total length (**D-F**) at 30 (**A, D**), 90 (**B, E**) and 360 (**C, F**) days post-fertilization (dpf) of zebrafish fed from 8 dpf onwards with Ctrl (ZEBRAFEED), MP (ZEBRAFEED supplemented with pristine microplastics) or MP-BaP (ZEBRAFEED supplemented with microplastics spiked with BaP) diets. Asterisks indicate values statistically different between diets according to one-way ANOVA followed by Tukey's multiple comparison test or Kruskal-Wallis test followed by Dunn's multiple comparison test (* $p<0.05$; ** $p<0.01$; *** $p<0.001$; **** $p< 0.0001$). Values are presented as the median ± min and max value. At 30 dpf, n=9 for dry weight and n=54 for total length; at 60 dpf, n≥66 for both wet weight and total length; at 360 dpf, n≥13 for both wet weight and total length.

5.4.2. Contaminated microplastics affect female reproductive capacity

Fish fed the experimental diets until sexual maturity were evaluated for their reproductive performances i.e., breeding success, egg shape parameters (egg area, yolk area and circularity), relative fecundity and egg hatching rate in females, and sperm viability and motility parameters in males. While egg viability, area (at 2 and 24 hpf) and hatching rate were not altered by any of the experimental diets (Supplementary Fig. 5.4A-B-D), other parameters were affected in fish fed MP-BaP. In this regard, the success of breeding events was slightly reduced by 26.3 ± 16.1% (although not statistically different) (Fig. 5.2A) and the relative fecundity of the females fed MP-BaP was reduced by 53.0 ± 18.4% towards the control diet (Fig. 5.2B). Egg circularity at 2 hpf (Fig. 5.2C) and 24 hpf (Supplementary Fig. 5.2C) and yolk area at 2 hpf (Fig. 5.2D) were also affected when parents were fed MP-BaP, showing a reduction of 3.8 ± 1.4%, 2.1 ± 0.9% and 8.0 ± 2.2%, respectively, compared to the control group. Neither sperm viability nor motility parameters (total motility,

progressive motility, curvilinear velocity, straight line velocity and linearity) were affected by the experimental diets (Supplementary Fig. 5.3). No differences were found between zebrafish fed MP and MP-BaP. These data show that long-term exposure to contaminated microplastics may impair egg quality.

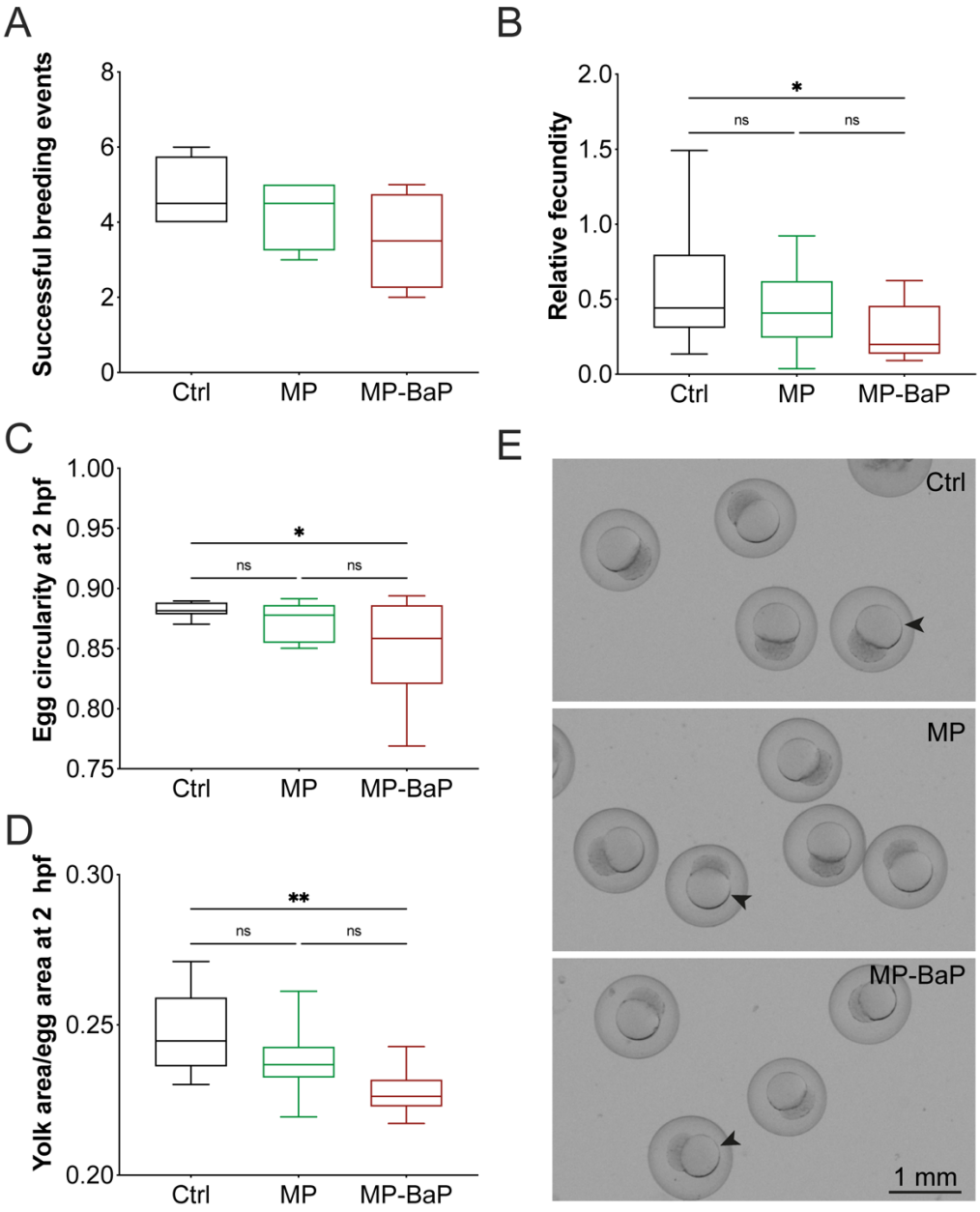

Figure 5.2. Reproductive performance of sexually mature 3-4 months zebrafish fed from 8 dpf onward with Ctrl (ZEBRAFEED), MP (ZEBRAFEED supplemented with pristine microplastics) or MP-BaP (ZEBRAFEED supplemented with microplastics spiked with BaP). (**A**) Average number of successful breeding events. A value of 0 or 1 was given to breeding events for which couples did not lay eggs (or eggs aborted) or for which couples successfully laid eggs, respectively (n=4). (**B**) Relative fecundity calculated as the total number of eggs/female body weight (n≥14). (**C**) Egg circularity and (**D**) yolk area assessed at 2 hours post fertilization (hpf) through the morphometric analysis of bright-field images. Yolk area was normalized using egg area (n≥8; pools of 20 eggs each). (**E**) Representative images of eggs at 2 hpf collected from breeding events. Arrowheads indicate egg yolk. Asterisks indicate values statistically different between diets according to one-way ANOVA followed by Tukey's multiple comparison test (* $p<0.05$; ** $p< 0.01$). Values are presented as the median ± min and max value.

5.4.3. Microplastic exposure leads to osteotoxicity

5.4.3.1. Microplastic affects the development of zebrafish axial skeleton

AR-S stained zebrafish juveniles fed the experimental diets for 22 days (i.e., from 8 to 30 dpf) were examined to assess the effects of microplastic exposure during development of the axial skeleton. Fish fed MP and MP-BaP presented an increased incidence of deformed fish (75.0 ± 2.5% and 88.3 ± 2.3%, respectively) compared to control fish (53.0 ± 0.7% of deformed fish), and fish fed MP-BaP were significantly more deformed (13.3 ± 1.6%) than fish fed MP (Fig. 5.3A). The number of skeletal deformities per fish also increased in fish fed MP and MP-BaP, with a majority of fish presenting more than two deformed skeletal structures, while control fish had more cases with only one deformed structure (Fig. 5.3B). Several types of deformities were observed – e.g., partial/total fusion of the vertebrae or neural/hemal arches and malformations of the operculum, urostyle, parhypural and hypurals – and while most of the axial skeleton regions presented a similar distribution of the deformities among treatments, the caudal fin complex was the region more differentially affected by MP and MP-BaP diets, with an increased number of deformities of 300.0 ± 50.0% over the control diet (Fig. 5.3C). These data show that chronic exposure to pristine microplastic affects zebrafish skeletal development and incidence of skeletal deformities increases when microplastics are contaminated with BaP.

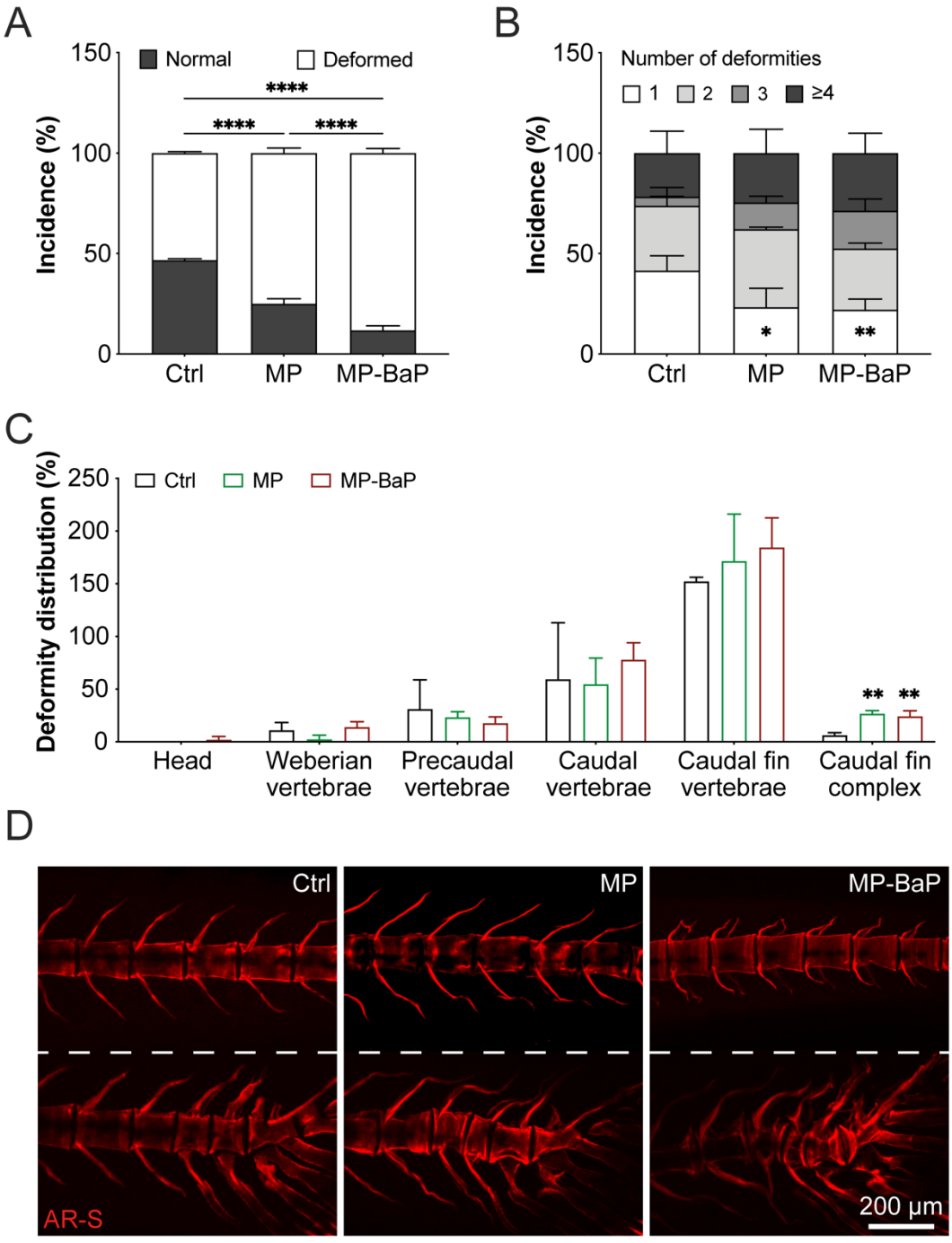

Figure 5.3. Deformities in the axial skeleton of 30 dpf zebrafish fed from 8 dpf onwards with Ctrl (ZEBRAFEED), MP (ZEBRAFEED supplemented with pristine microplastics) or MP-BaP (ZEBRAFEED supplemented with microplastics spiked with BaP). (**A**) Percentage of normal and deformed fish. (**B**) Percentage of deformities per deformed larvae. (**C**) Distribution of the deformities along the axial skeleton. Deformed structures of each individual were summed and divided by the number of fish. (**D**) Representative fluorescence images of AR-S stained skeletal structures in fish fed experimental diets. In A and B, asterisks indicate values statistically different between diets according to two-way ANOVA, followed by Šídák's multiple comparisons test, (* $p<0.05$; ** $p< 0.01$, **** $p< 0.0001$). In C, asterisks indicate values statistically different between diets according to one-way ANOVA, followed by Tukey's multiple comparisons test, (** $p< 0.01$), n=120.

5.4.3.2. Caudal fin structure is impaired in adult zebrafish fed with microplastics

Because the caudal fin complex was severely deformed in 30 dpf juveniles exposed to both pristine and contaminated microplastics, the structure of the caudal fin was further assessed in 90 dpf adults fed the experimental diets through the determination of the number of rays and the number of fused, bended, or developmentally impaired rays. Microscopic examination of AR-S stained fish revealed an increased incidence of caudal fins showing a reduced number of rays in zebrafish fed MP-BaP (29.2 ± 5.9% and 16.7 ± 5.9% over Ctrl and MP, respectively; Fig. 5.4A). The number of fused rays – but not the number of bended or developmentally impaired rays (a slight effect was seen though) – also increased in the caudal fin of fish fed MP and MP-BaP (20.8 ± 5.9% over Ctrl; Fig. 5.4B-D). These data indicate that pristine or contaminated microplastics also trigger skeletal defects in the caudal fin of adult fish chronically exposed since larval stage.

5.4.3.3. Microplastic exposure affects ontogenetic scales

Since scales are central to fish mineral homeostasis, morphological parameters such as total area, circularity, and extent of demineralized area were assessed in ontogenetic scales, plunked from 90 dpf adult zebrafish fed the experimental diets. Scale area was reduced by 17.8 ± 1.9% and 12.9 ± 2.0% over Ctrl in fish fed with MP and MP-BaP, respectively, and this decrease was significantly more pronounced in fish exposed to MP (Fig. 5.5A). On the contrary, scale circularity was slightly increased in fish fed MP-BaP (0.7 ± 0.2% over Ctrl and by 0.7 ± 0.2% over MP; Fig. 5.5B). Finally, the demineralized area was increased by 639.2 ± 31.2% over Ctrl and by 618.4 ± 29.9% over MP in fish fed MP-BaP (Fig. 5.5C). These data suggest that exposure to microplastics reduces scale growth, and that the presence of BaP induces a strong demineralization of the scales.

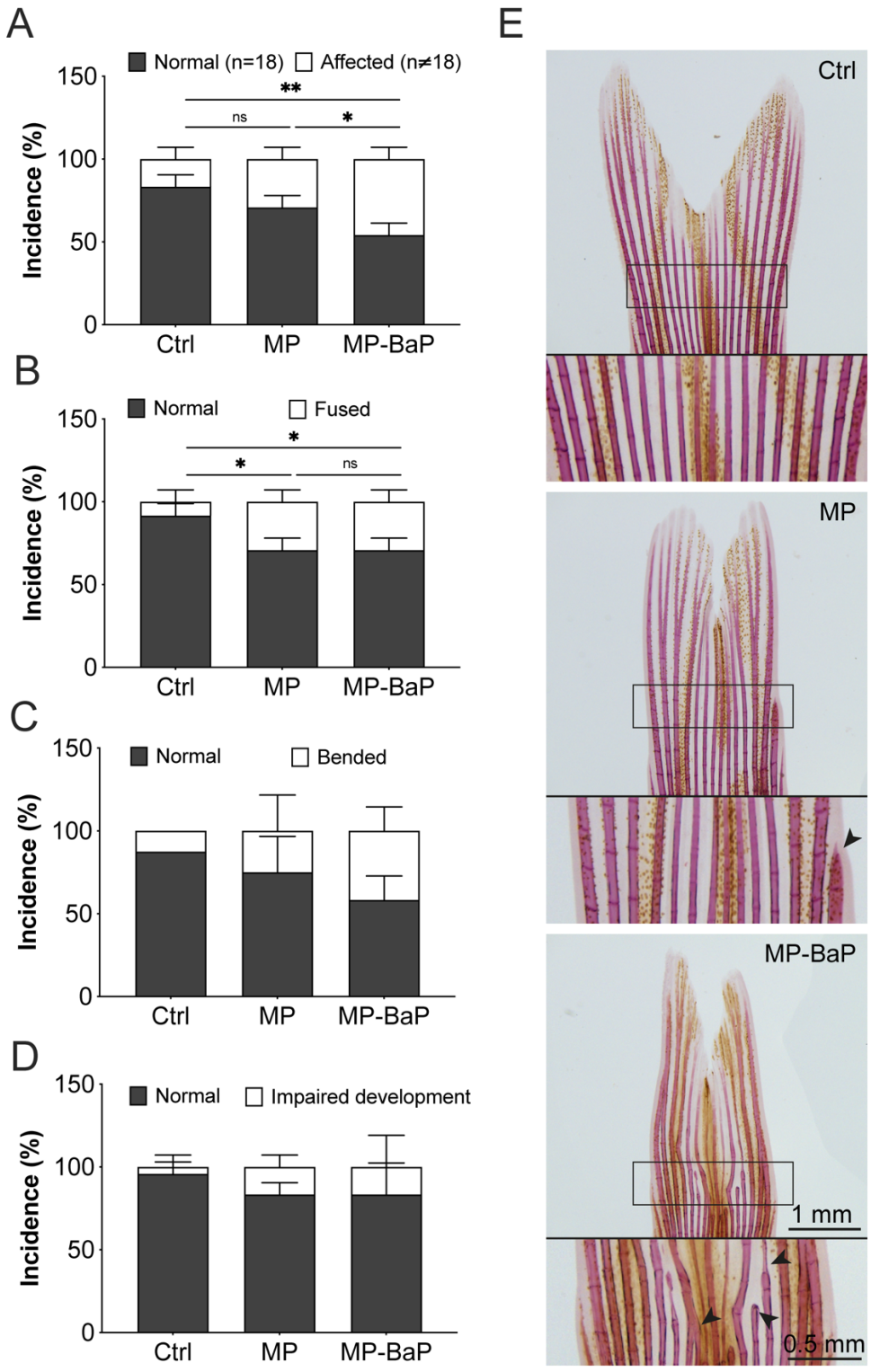

Figure 5.4. Deformities in the caudal fin of 90 dpf zebrafish fed from 8 dpf onwards with Ctrl (ZEBRAFEED), MP (ZEBRAFEED supplemented with pristine microplastics) or MP-BaP (ZEBRAFEED supplemented with microplastics spiked with BaP). (**A**) Percentage of caudal fin with a normal number of rays (equal to 18) or not (number of rays different from 18). (**B**) Percentage of caudal fin with individualized rays or presenting fused rays. (**C**) Percentage of caudal fin with rays normally shaped or presenting bended rays. (**D**) Percentage of caudal fin with normally developed rays or presenting rays with an impaired development. (**E**) Representative bright-field images of AR-S stained caudal fin from fish fed experimental diets. Asterisks indicate values statistically different between diets according to two-way ANOVA, followed by Šídák's multiple comparisons test, (* $p<0.05$; ** $p< 0.01$), n=24.

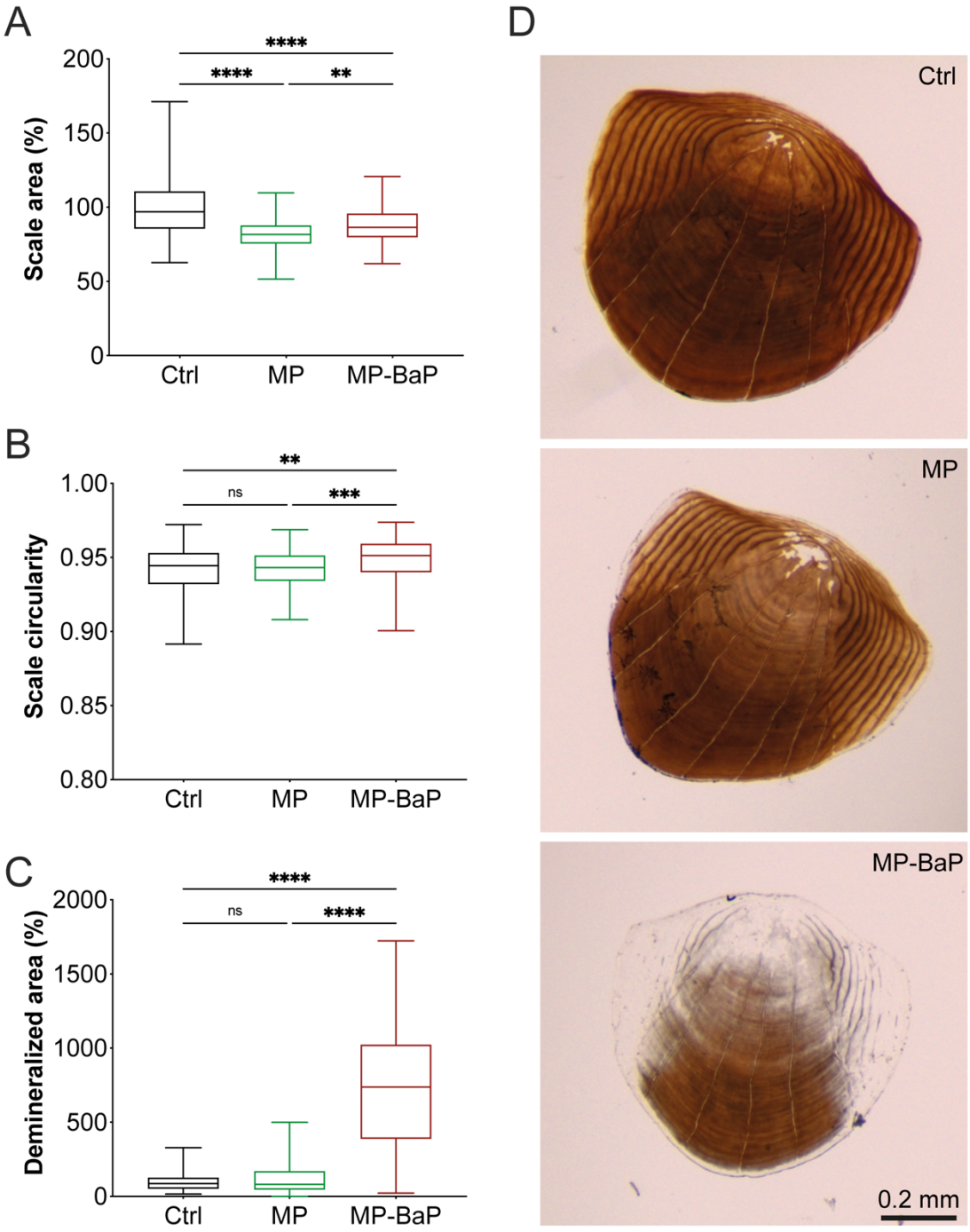

Figure 5.5. Morphology and mineral content of ontogenetic scales from 90 dpf zebrafish fed from 8 dpf onwards with Ctrl (ZEBRAFEED), MP (ZEBRAFEED supplemented with pristine microplastics) or MP-BaP (ZEBRAFEED supplemented with microplastics spiked with BaP). (**A**) Scale area and (**B**) circularity were assessed through the morphometric analysis of ontogenetic scales in bright-field images. (**C**) Mineral content was evaluated through von Kossa staining. (**D**) Representative images of von Kossa stained scales collected from fish fed experimental diets. Asterisks indicate values statistically different between diets according to Kruskal-Wallis test followed by Dunn's multiple comparison test (** $p<0.01$; *** $p<0.001$; *** $p<0.0001$). Values are presented as the median ± min and max value. $n \geq 112$.

5.4.3.4. Exposure to contaminated microplastics decreases calcium to phosphorus ratio

To further investigate the reduction in bone mineralization observed in ontogenetic scales, calcium and phosphorus contents were assessed in the whole body of 30 dpf juveniles and 90 dpf adults fed the experimental diets, and calcium to phosphorus ratio – a proxy for bone quality – was determined. While calcium and phosphorus contents were not significantly altered in fish exposed to pristine or contaminated microplastics at any of the developmental stages evaluated (results not shown), Ca/P ratio was reduced by 8.3 ± 3.1% over Ctrl in fish exposed to MP-BaP until 90 dpf. There was however no difference in the Ca/P ratio calculated for fish fed MP and MP-BaP (Fig. 5.6B). These data show that a long-term exposure (i.e., up to 90 dpf) to BaP-contaminated microplastics affects body Ca/P ratio, and suggests that bone of fish chronically exposed may suffer from a reduced mineral density and thus may be of lower quality, which could trigger skeletal deformities.

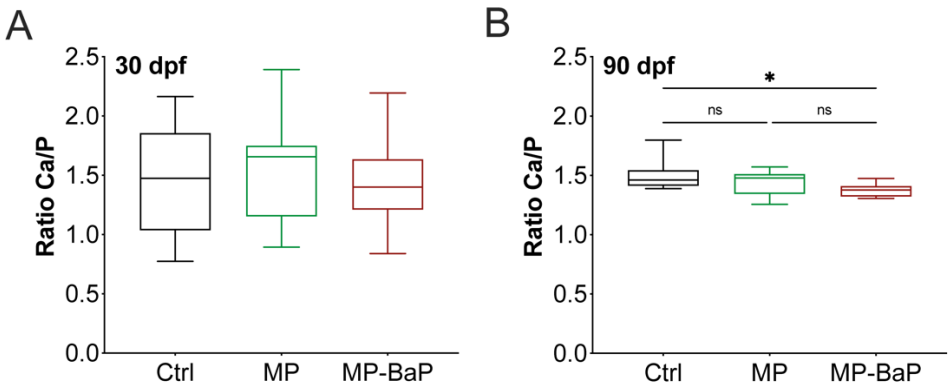

Figure 5.6. Calcium to phosphorus ratio (Ca/P) in 30 dpf juveniles (**A**) and 90 dpf adults (**B**) fed from 8 dpf onwards with Ctrl (ZEBRAFEED), MP (ZEBRAFEED supplemented with pristine microplastics) or MP-BaP (ZEBRAFEED supplemented with microplastics spiked with BaP). At 30 dpf, n=9, pools of 6 fish; at 90 dpf, n=9 dpf. *Asterisks* indicate values statistically different between diets according to one-way ANOVA followed by Tukey's multiple comparison test (* p<0.05). Values are presented as the median ± min and max value.

5.4.3.5. Parental exposure to microplastics affects offspring bone growth

To assess the intergenerational effect of microplastics exposure, in particular on fish development and bone growth, operculum area, head area and body standard length and depth were determined through morphometric analysis of 6 dpf offspring larvae born from parents fed the experimental diets. While standard length and head

area were not affected in offspring of parents exposed to pristine or contaminated microplastics, body depth (trunk height) was reduced in offspring of parents fed MP-BaP by 4.4 ± 1.7% (Fig 5.7B), suggesting that larvae fitness may be affected. The corrected operculum area was also reduced by 12.1 ± 3.8% and 23.4 ± 3.9% over Ctrl in larvae born from parents fed MP and MP-BaP, respectively, suggesting that microplastics osteotoxicity is inherited by future generations. Reduction was more pronounced in offspring of parents fed MP-BaP, indicating that BaP osteotoxicity can also be transmitted by exposed parents to unexposed offspring, but also that microplastics and BaP have additive osteotoxic effects.

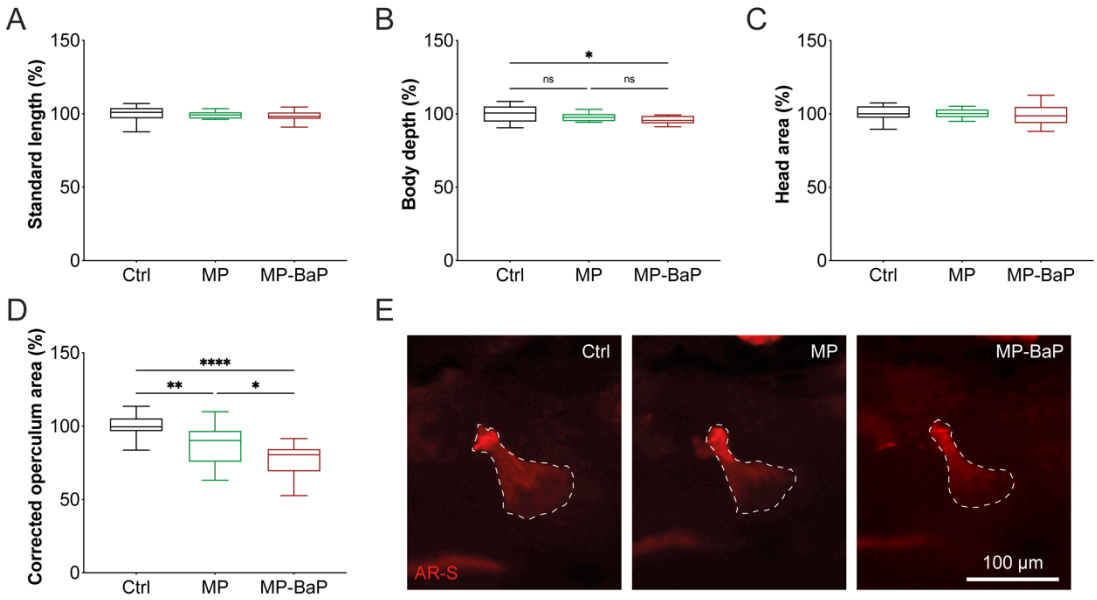

Figure 5.7. Growth parameters of 6 dpf offspring larvae born from parents fed from 8 dpf onwards with Ctrl (ZEBRAFEED), MP (ZEBRAFEED supplemented with pristine microplastics) or MP-BaP (ZEBRAFEED supplemented with microplastics spiked with BaP). Standard length (**A**) and body depth (**B**) were assessed through the morphometric analysis of bright-field images. Head area (**C**) and operculum growth (**D**) were assessed through the morphometric analysis of fluorescence images. (**E**) Representative images of AR-S stained operculum of 6 dpf offspring larvae. *Asterisks* indicate values statistically different between diets according to one-way ANOVA followed by Tukey's multiple comparison test (* p<0.05; ** p<0.01; **** p<0.0001). Values are presented as the median ± min and max value, n≥14, 10 larvae from each breeding event.

5.4.4. Exposure to contaminated microplastics decreases intestinal goblet cell number

Following recent studies in zebrafish[364] and European seabass[373] showing alterations in the population of intestinal goblet cells upon exposure to microplastics, the intestine of 90 dpf adult zebrafish fed the experimental diets was examined for the number of goblet cells per villus (Fig. 5.8). While the number of goblet cells was not

significantly different in fish fed MP versus Ctrl (p >0.05), it was reduced by 32.1 ± 10.7% in fish fed MP-BaP versus Ctrl, suggesting that contaminated microplastics alter intestinal homeostasis and trigger inflammation.

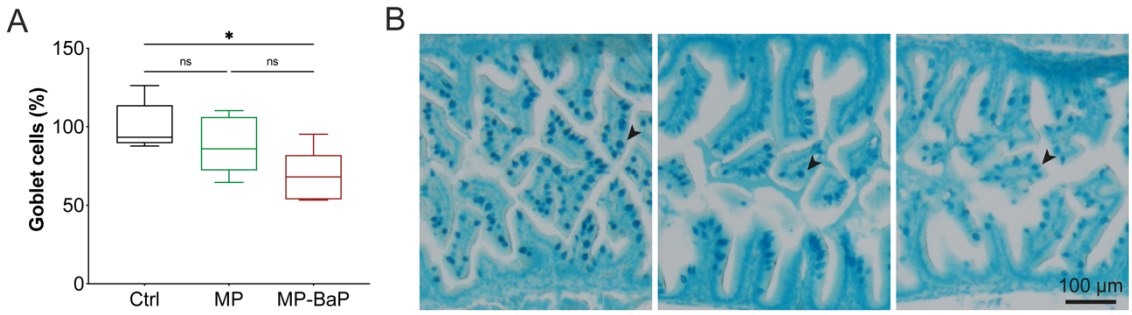

Figure 5.8. Number of goblet cells in 90 dpf zebrafish fed from 8 dpf onwards with Ctrl (ZEBRAFEED), MP (ZEBRAFEED supplemented with pristine microplastics) or MP-BaP (ZEBRAFEED supplemented with microplastics spiked with BaP). (**A**) Number of goblet cells/villus expressed in % over Ctrl. (**B**) Representative images of intestine cryosections stained with alcian blue to mark goblet cells (arrowheads). Asterisks indicate values statistically different between diets according to one-way ANOVA followed by Tukey's multiple comparison test (* p<0.05). Values are presented as the median ± min and max value, n=5.

5.4.5. Gene expression

To gain insights into the molecular mechanisms underlying the effects of pristine and contaminated microplastics on zebrafish, the expression of several marker genes was assessed by qPCR in 30 dpf juveniles and 6 dpf offspring larvae, and in tissues (i.e., gut, liver, and vertebral column) of 90 dpf adults (Fig. 5.9 and Supplementary Fig. 5.4). At a first glance, gene expression was highly variable among different tissues and treatments. A closer look at the expression data revealed that the pregnane X receptor gene (*nr1i2*; xenobiotic receptor) was upregulated in the vertebral column and in the liver (3.38 fold-change over control) of adult zebrafish fed MP-BaP and in offspring born from parents fed MP-BaP, suggesting the activation of xenobiotic signaling in response to BaP. Interestingly, the expression of cytochrome P450 1A gene (*cyp1a*; phase I metabolizing enzyme) was upregulated in offspring born from parents fed MP and MP-BaP, while it was downregulated in gut, liver and vertebral column of adult zebrafish fed the experimental diets, indicating a different regulation depending on the tissue involved. Expression of genes involved in oxidative stress (*cat*, *gpx1a*, *sod1* and *sod2*) were downregulated in tissues of adult fish fed MP and MP-BaP, suggesting an impaired antioxidant response. In contrast, the expression of osteoblast differentiation marker genes (*sp7* and *oc2*) and genes involved in ECM

mineralization (*spp1*, *col1a1* and *col10a1*) were upregulated in 30 dpf zebrafish fed MP-BaP, indicating a feedback response to MP osteotoxicity. Additionally, the expression of cellular stress marker genes (*hsp70* and *hsp90*) was downregulated in most of the treatments, indicating an alteration in cellular homeostasis.

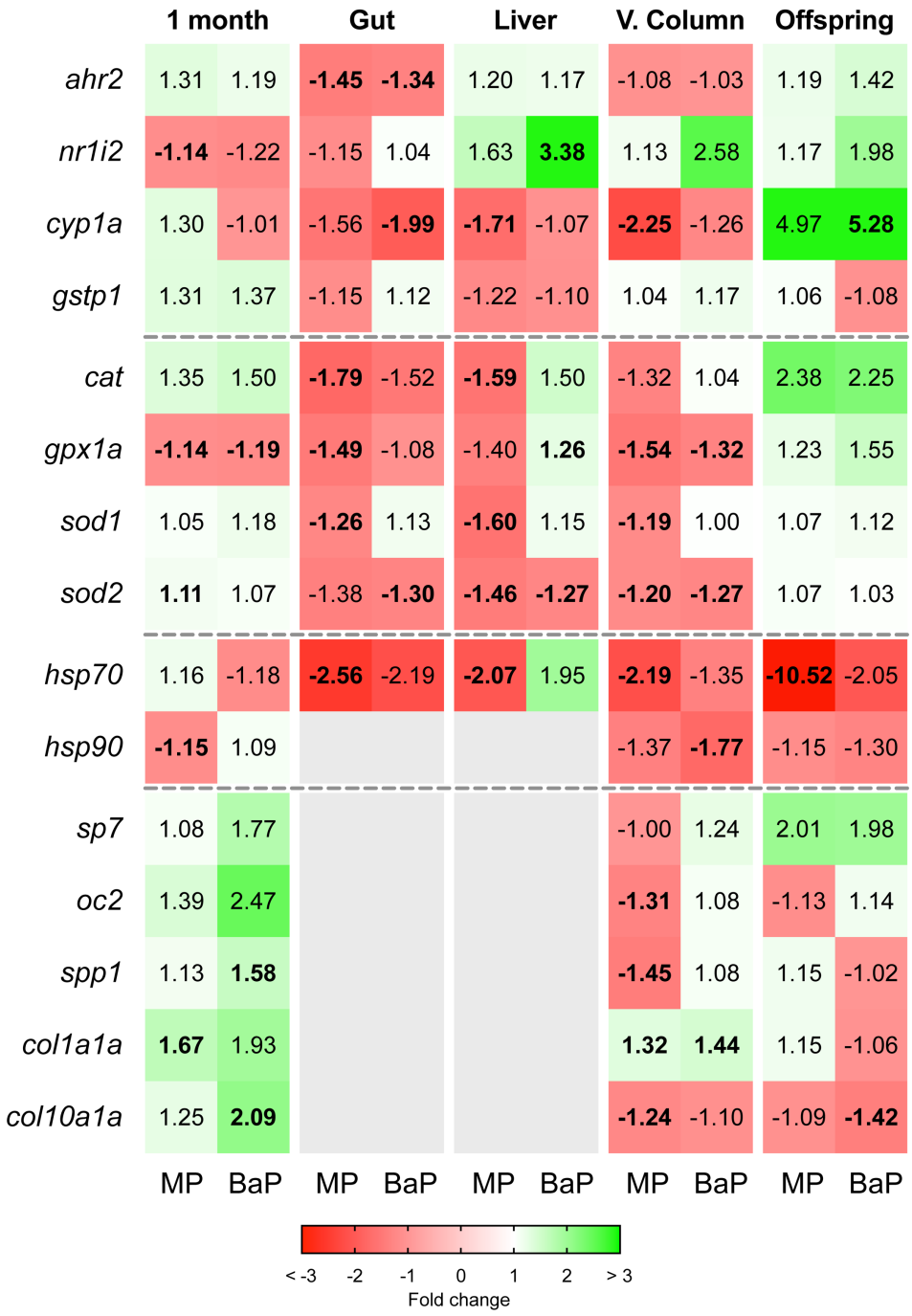

Figure 5.9. Heatmap representation of gene expression levels in 30 dpf juveniles (1 month) and tissues (gut, liver, and vertebral column) of 90 dpf adult zebrafish fed from 8 dpf onwards with Ctrl (ZEBRAFEED), MP (ZEBRAFEED supplemented with pristine microplastics) or BaP (ZEBRAFEED supplemented with microplastics spiked with BaP), and in 6 dpf offspring larvae born from parents fed experimental diets. The averaged expression of *eef1a1l1* and *rps18* housekeeping genes was used to normalize gene expression levels. Values in *bold* are statistically different from Ctrl values according to Student's t-test ($p<0.05$). Values are presented as fold-change over the control, n=3.

5.5. DISCUSSION

Microplastic pollution is one of the biggest threats to the aquatic environment, and effects on aquatic organisms have been subject to increased scrutiny over the past decade. The present work is an additional contribution to the already long list of the adverse effects of microplastics in fish and provides new insights on parameters that have been overlooked such as long-term exposure, nutritional route for microplastics exposure, contamination of the microplastics with adsorbed organic pollutants and a focus on osteotoxic effects.

Exposure to experimental diets supplemented with pristine and contaminated microplastics affected zebrafish growth at 90 and 360 dpf. Effects of microplastics on growth parameters such as body length and weight have already been assessed using aquatic model species (e.g., zebrafish and medaka) or farmed species (e.g., gilthead seabream and European seabass)[127,131,138,374–380], but most of these studies reported a limited impairment, if any. Among the studies that support the effect observed here, a reduction of body length or weight was observed in zebrafish larvae exposed (waterborne) to 1-5 µm microplastics (polymer not specified, pristine or spiked with copper) from 2 hpf to 14 dpf or to 5-µm polystyrene microparticles (pristine or spiked with F-53B) from 6 to 13 dpf, respectively[127,375,376]. Similarly, body length was reduced in Japanese medaka (*Oryzias latipes*) larvae fed from 3 days after hatching for 30 days with a diet supplemented with a mix of commercial microplastics (PP, PS, HDPE and LDPE) or microplastics sampled in natural environments[377]. The duration of the exposure seems to be a critical aspect of impaired fish growth by microplastics as most of the published data available to date was collected from relatively short-term exposures (maximum 21 days or 30 days of exposure for zebrafish or medaka, respectively). In this manner, the present study confirmed that a short exposure from 8 to 30 dpf does not affect zebrafish growth, while longer exposures (i.e., up to 90 and 360 dpf) triggered a reduction in body weight and total length. Using exposure parameters similar to those used in the present study (i.e., nutritional exposure through a diet supplemented with 1% w/w of 11–13 µm polyethylene particles), Cormier et al. (2021) reported that the growth of the zebrafish and marine medaka (*Oryzias melastigma*) was not impaired in fish fed the experimental diets for 60 days[121]. Although this needs to be clarified, we propose that nutritional exposure to

microplastics (1% w/w) only impact fish growth if exposure time is equal or longer than 3 months. It is worth noting that the deleterious growth effect of pristine microplastics did not increase upon contamination with organic pollutants (e.g., BaP, BP3 or PFOS)[121]. We propose that the growth effect of microplastics may be related to their ingestion and an impression of false satiation, reducing feeding activity and impairing energy balance[79,121,139,381,382].

Exposure to pristine microplastics did not impair female reproduction capacity, but relative fecundity and egg quality were both affected when microplastics were contaminated with BaP. Importantly, sperm quality was not affected by pristine or contaminated microplastics. Reproduction success plays an important role in the survival of living organisms and understanding the effects of microplastic on fish reproductive capacity can provide important information on what may happen in future generations. Studies on the effects of ingested microplastics are still scarce, and most of the data available in the literature have only assessed the effect of polystyrene waterborne exposure using the Japanese medaka. In this regard, waterborne exposure of sexually mature medaka to 2-µm polystyrene particles for 21 days had no impact on the number of eggs and embryo survival[383], but dietary exposure of medaka during maturation (from 28 dpf juveniles to spawning adults) to bigger polystyrene particles (10 µm) for 10 weeks showed a decrease in egg number.[382] A delayed maturation of the gonads and decreased fecundity were also reported in 3 month old marine medaka exposed to 10 µm polystyrene particles for 60 days, while hatching rate and offspring body length were also affected.[384]

In the present work, relative fecundity (number of spawned eggs) and egg quality was affected in fish fed MP-BaP but not MP, suggesting that BaP may play a critical role in disrupting female reproductive performance. In this regard, waterborne exposure to BaP decreased the number of spawned eggs, the fertilization rate and the hatching success in both zebrafish and medaka [385–387]. In agreement with the present data, Cormier et al. (2021) reported a decrease in the number of eggs produced by zebrafish and medaka females fed diets supplemented with 1% w/w of pristine and contaminated microplastics (e.g., BaP, BP3 or PFOS).[121] In that study, PVC (125–250 µm) appeared more toxic than PE (11–13 µm), and microplastics spiked with PFOS and BP3 showed a stronger impairment than microplastics spiked with BaP. In

the present work, the reproductive capacity of sexually mature 3-4-months fish exposed to pristine microplastics was not impacted (although a tendency was observed for most of the parameters evaluated). The microplastic particles used by Cormier et al. (2021) were smaller than those used in this study (11-13 *vs* 20-27 µm) and could have a stronger impact on fish reproductive capacity since a higher number might have been ingested and accumulated. Our data also indicated that the yolk area was reduced in eggs laid by females fed MP-BaP. Those eggs also presented a slight decrease in their circularity, probably a consequence of the reduced yolk area. The (zebra)fish yolk contains a finite supply of nutrients, such as proteins and lipids, which are critical to the survival and development of the embryo and larvae, thus yolk fitness has important implications for next generations. When yolk reserves are disrupted, it is more likely that offspring development will be impaired, resulting in reduced hatching rate and morphological deformities which may lead to their death[388].

In the present study, the only growth parameter affected in the offspring born after parental exposure was the body depth, which was reduced in larvae from parents fed MP-BaP (i.e., larvae were slimmer), while standard length and head area were not affected. Reduced body depth could be related to the reduced yolk area observed in eggs from females fed MP-BaP and consequently a shortage in the nutrients to meet the metabolic requirements needed for a healthy development. Interestingly, growth of the opercular bone was also impaired in offspring born from parents fed pristine/contaminated microplastics, indicating that microplastic and BaP osteotoxicity can be inherited by future generations. Although BaP levels were not determined in the eggs, impaired operculum growth in offspring larvae born from parents fed MP-BaP is similar to the effect recently observed in larvae exposed to BaP waterborne[389], indicating the probable presence of BaP in egg yolk. In this regard, it has been shown that eggs are able to accumulate lipophilic xenobiotics into their yolk by maternal or waterborne exposure[388]. Epigenetic mechanisms may also be involved into intergenerational BaP osteotoxicity as recently proposed by Mo et al. (2021)[390] Operculum growth was also reduced in offspring born from parents fed MP, suggesting that additives used in the preparation of the microplastics could also impact bone development or that microplastics may have intergenerational bone effects through mechanisms that remain to be determined.

The present study also provides clear evidence that pristine and contaminated microplastics have the potential to affect the development of zebrafish axial skeleton resulting in an increased incidence of skeletal deformities, in particular in the caudal fin region. Although the adverse effects of microplastics have been reported in many biological processes, only scarce data are available on a possible osteotoxic effect, i.e., impaired bone formation that may lead to skeletal defects and altered mineral density. Assessing osteotoxic effects is critical as bone defects may impair fish swimming performance and thus their feeding activity and their capacity to escape predation. In this regard, Zhao et al. (2020) reported that the exposure of 4 hpf zebrafish embryos for 7 days to polystyrene microplastics spiked with butylated hydroxyanisole (BHA), a synthetic antioxidant widely used to prevent aging of plastics, increased the rate of morphological deformities (i.e., pericardial edema, yolk sac edema, hyperemia and spinal deformity), while pristine microplastics (MPs) did not show any defects[129]. A longer exposure (12 days) to smaller contaminated particles (0.065 µm) caused a decrease in the number of calcified vertebrae, while pristine MPs had again no effect. Zhao et al. (2020) proposed that the osteotoxic effect observed upon the exposure of fish to contaminated microplastics may be related to thyroid-stimulating hormone (TSH) which was increased upon microplastic exposure. Although TSH levels were not determined here, BaP was shown to increase TSH also in Abu mullet[391] and we propose that microplastics contaminated with BaP may exert their osteotoxic effect through a mechanism that may involve TSH. In this regard, it has been shown that TSH is a negative regulator of skeletal remodeling in mice, which can inhibit osteoblast differentiation[392]. Impaired osteoblast maturation could also be at the origin of the osteotoxic effects – i.e., impaired development of the axial skeleton and caudal fin, impaired scale mineralization, and reduced bone quality – observed in fish fed microplastics contaminated with BaP. In this regard, waterborne exposure of zebrafish to BaP impaired osteoblast maturation and affected bone remodeling through the activation of the xenobiotic and metabolism pathways and an increase in inflammatory response[352]. Although the presence of BaP in bony tissues or in the surrounding tissues was not evaluated, we propose that, upon their ingestion, contaminated microplastics may release BaP in the stomach and/or intestinal tissues; once unbound to the microplastic particles, BaP diffuses throughout the fish body as already showed for zebrafish and bivalves[74–77] and may affect organism physiology, such as bone homeostasis.

Although to a lower extent, pristine microplastics also increased the incidence of deformities in the axial skeleton and the caudal fin and triggered a reduction in scale mineralization. While we cannot exclude that PE manufacturing additives may have leached, those findings suggest that other mechanisms – not associated with organic pollutants – are involved into the osteotoxic effects observed. In this regard, abnormal bone homeostasis can result from many different factors such as temperature, water acidification, water flow, genetic background, nutrition, and exposure to environmental pollutants[141–145], thus an impact upon microplastic ingestion cannot be excluded. In this study, the exposure to contaminated microplastics caused a depletion of goblet cells at 90 dpf, suggesting that intestinal homeostasis may be impaired by BaP. Although less pronounced, exposure to pristine microplastics also affected goblet cell numbers. A similar effect was observed in European seabass larvae fed a diet supplemented with 0.1 or 0.5% w/w of PE (40-150 µm) for 21 days[373] and in adult zebrafish fed pristine HDPE+PS microplastics (25-90 µm) for 20 days, which additionally showed alterations of the intestinal mucosa, such as epithelial detachment and mucous hypersecretion.[364] Goblet cells maintain the intestinal mucosal barrier through the secretion of mucin which protects the intestine from pathogens and chemical injury[393,394]. Depletion of goblet cells was shown to increase inflammation and cause disruption of the intestinal homeostasis, which is essential for digestion and nutrient absorption[395,396]. Although nutrient absorption was not measured, impairment of the intestinal barrier may jeopardize zebrafish growth.

Finally, the expression of several marker genes was assessed to gain insights into the molecular mechanisms underlying the effects of pristine and contaminated microplastics on zebrafish. Although gene expression levels were variable among the different tissues and treatments, genes involved in antioxidant response were generally downregulated in zebrafish exposed to the experimental diets up to 90 dpf. Oxidative stress occurs when there is an imbalance between the production of reactive oxygen species (ROS) and the activity of antioxidant defenses. In this sense, when the activity of antioxidant enzymes such as catalase (CAT), superoxide dismutase (SOD), glutathione-S-transferase (GST) and glutathione peroxidase (GPx) is inhibited, ROS accumulation may cause physiological impairments[397,398]. In agreement with the data presented here, a downregulation of *cat*, *sod1*, *gpx1a* was reported in brain/liver[399] and gills[400] of adult zebrafish waterborne exposed to polystyrene (PS)

microparticles (0.10-0.12 μm) for 35 days and in liver of marine medaka exposed to PS microparticles (10 μm) for 60 days[384]. Enzymatic inhibition of CAT and SOD activity was also reported in the liver of adult zebrafish exposed to PE microparticles (146.20 ± 8.86 μm) for 10 days[401] and European seabass larvae fed PE (40-150 μm) for 3 weeks[373]. We propose that long-term exposure to microplastics impairs the activity of antioxidant enzymes and leads to increase oxidative stress, which has been associated also with an impairment of bone cells function and quality[402,403]. Interestingly, expression of cellular stress marker genes (*hsp70* and *hsp90*) was down-regulated in zebrafish fed MP and MP-BaP, both in individual tissues and whole specimen. In agreement with the present data, expression of *hsp70* was down-regulated in European seabass fed PE-MPs for 21 days[373] and in *Daphnia magna* exposed to a mix of MPs for 48 h[404]. In fish, the expression of heat shock-proteins is normally increased to restore the cell status upon exposure to stressful conditions (i.e., heat, salinity, and environmental pollutants)[405]. Therefore, we cannot exclude that a decrease in the expression of proteins involved in cell repair may have impaired fish physiology upon exposure to MPs, leading to an increase in oxidative damage.

Genes related to xenobiotic metabolism were also differentially regulated in zebrafish exposed to experimental diets. In particular, *nr1i2,* a nuclear receptor known to be activated by BaP and other PAHs[144,389] and responsible for the activation of detoxifying mechanism, was up-regulated in liver and vertebral column of adult zebrafish fed MP-BaP, another indication of the possibility that BaP may have leached from MP and accumulate in surrounding tissues. In the offspring, we observed a general increase in expression of genes related to xenobiotic metabolism, such as nuclear receptors and a stronger up-regulation of *cyp1a,* suggesting that xenobiotic metabolism may be activated and may cause intergenerational effects. Surprisingly, *cyp1a,* which is expected to be activated upon exposure to environmental pollutants, was down-regulated in gut, liver and vertebral column of zebrafish exposed to pristine and contaminated MPs up to 90 dpf. On the contrary, several studies have reported increased activity or transcription of *cyp1a* in zebrafish exposed to pristine or contaminated MPs[75,123,137,140] from 1 to 21 days, depending on the study. In agreement with our data, Xia et al. (2020) showed that *Cyprinus carpio* larvae exposed to PVC microplastics (100–200 μm) for up to 60 days had *cyp1a* expression upregulated after 30 days of exposure but downregulated at the end of the

experiment[406]. We propose that effects of short-term exposures to MPs may be counteracted by xenobiotic metabolism enzymes, while longer exposures may be more effective due to the impairment of cellular detoxifying mechanisms. To the best of our knowledge, this is the first time that an effects of pristine/contaminated MPs is reported on bone related gene expression, i.e., a general upregulation in zebrafish larvae fed MP and MP-BaP and a downregulation of *col10a1*a, *oc2* and *spp1* in adult vertebral column. However, this is not the first time that genes involved in bone metabolism are differentially regulated in zebrafish exposed to PAHs. Indeed, bone marker genes were upregulated in zebrafish larvae exposed (waterborne) to 3-methylcholanthrene (i.e., *fgf20a*, *vdrb*, *bmp2a* and *alpl*)[144] and to BaP (i.e., *vdrb* and *alpl*)[389]. Furthermore, waterborne exposure to BaP also increased proliferation of immature osteoblast as reported by the increased number in *sp7* positive cells. As already seen for marker genes involved in xenobiotic response pathway (see above), it seems that short-term and long-term exposure to MPs elicit opposite effects on the expression of bone related genes. This may indicate that the transcriptional machinery will initially answer the osteotoxic signal through a compensatory/feedback mechanism, which will be override by the toxic signal in the long run. It is also possible that long-term microplastic osteotoxicity initiates indirect mechanisms such as oxidative damage and activation of xenobiotic metabolism. Further studies should aim at gaining additional knowledge on the mechanisms underlying short and long-term osteotoxicity of microplastics leading to an impairment of bone homeostasis.

5.6. CONCLUSIONS

This study demonstrated that long-term dietary exposure to pristine/contaminated polyethylene microplastics has the potential not only to jeopardize fish growth and reproductive performance, but also to produce an intergenerational effect. The data presented here also provided the first evidence of adverse effects on fish axial skeleton and bone compartment upon the ingestion of microplastics, with osteotoxic outcomes aggravated by the presence of organic contaminants adsorbed on the surface of the microplastics. Gene expression analysis evidenced an involvement of the xenobiotic pathway and antioxidant response in the mechanisms underlying the harmful effects triggered by pristine and/or contaminated microplastics. Future studies should aim at providing additional evidence on the

adverse effects following a long-term exposure of fish to microplastics, and at testing a wider range of plastic polymers and contaminants with the capacity to absorb onto microplastics.

Chapter 6

New insights into benzo[α]pyrene osteotoxicity in zebrafish

Published chapter:

Tarasco M, Gavaia PJ, Bensimon Brito A, Cardeira da Silva J, Ramkumar S, Cordelières FP, Günther S, Bebianno MJ, Stainier DYR, Cancela ML, Laizé V (2021). New insights into benzo[α]pyrene osteotoxicity in zebrafish. Ecotoxicology and Environmental Safety, 226, 112838

PREAMBLE

Following the results presented in Chapter 5, evidencing an impairment of bone development in zebrafish exposed to microplastic spiked with benzo[α]pyrene, we decided to gain insights into the mechanism of BaP osteotoxicity by exposing zebrafish to waterborne BaP in static conditions using a wide range of concentrations.

To better understand the osteotoxic effects of BaP in developing and regenerating zebrafish bone structures, we evaluated bone cell activity using transgenic reporter lines, and quantified xenobiotic signaling and bone marker gene expression. Following recent *in vitro* data providing evidence of interaction between neutrophils and bone forming/resorbing cells, their involvement in the mechanisms of BaP osteotoxicity was also addressed.

6.1. ABSTRACT

Persistent and ubiquitous organic pollutants, such as the polycyclic aromatic hydrocarbon benzo[α]pyrene (BaP), represent a major threat to aquatic organisms and human health. Beside some well-documented adverse effects on the development and reproduction of aquatic organisms, BaP was recently shown to affect fish bone formation and skeletal development through mechanisms that remain poorly understood. In this work, zebrafish bone-related *in vivo* assays were used to evaluate the osteotoxic effects of BaP during bone development and regeneration. Acute exposure of zebrafish larvae to BaP from 3 to 6 days post-fertilization (dpf) induced a dose-dependent reduction of the opercular bone size and a depletion of *osteocalcin*-positive cells, indicating an effect on osteoblast maturation. Chronic exposure of zebrafish larvae to BaP from 3 to 30 dpf affected the development of the axial skeleton and increased the incidence and severity of skeletal deformities. In young adults, BaP affected the mineralization of newly formed fin rays and scales, and impaired fin ray patterning and scale shape, through mechanisms that involve an imbalanced bone remodeling. Gene expression analyses indicated that BaP induced the activation of xenobiotic and metabolic pathways, while negatively impacting extracellular matrix formation and organization. Interestingly, BaP exposure positively regulated inflammation markers in larvae and increased the recruitment of neutrophils. A direct interaction between neutrophils and bone extracellular matrix or bone forming cells was observed *in vivo*, suggesting a role for neutrophils in the mechanisms underlying BaP osteotoxicity. Our work provides novel data on the cellular and molecular players involved in BaP osteotoxicity and brings new insights into a possible role for neutrophils in inflammatory bone reduction.

6.2. INTRODUCTION

Polycyclic aromatic hydrocarbons (PAHs) are persistent organic pollutants (POPs) produced by incomplete combustion of organic compounds. Their presence in the environment typically results from natural events, such as volcanic activity and forest fires, and anthropogenic activity, such as car exhaust, petroleum exploration, residential waste burning and manufacturing of carbon, coal tar pitch and asphalt[63,64]. Because they are hydrophobic and chemically stable compounds[407], PAHs are

persistent in the environment and are detected in the atmosphere, water-bodies and sediments. The lipophilic nature of PAHs facilitates their accumulation in fatty tissues of aquatic organisms thus their entry in the food web, raising concerns for human health[70,71]. In this regard, people living in urban areas, smokers, grill and coke oven workers are daily exposed to PAHs and several studies have revealed the presence of PAH compounds in urine, blood and breast milk[408–411].

Benzo[α]pyrene (BaP) – a model compound of the PAH family – has been widely used to assess the toxic effects of this class of POPs on terrestrial and aquatic organisms. In fish, exposure to BaP can occur through dermal exposure, respiration, or consumption of contaminated prey or sediments. BaP is carcinogenic and has been included in the priority list of substances that, due to their persistence, bioaccumulation and toxicity, need to be monitored and environmentally risk assessed both in Europe and in the United States (lists are available from the European Environmental Agency at www.eea.europa.eu and from Environmental Protection Agency at www.epa.gov). In the aquatic environment, BaP concentrations range from 6.3×10^{-7} to 4.5×10^{-5} µM[412–414] and in some extreme cases can reach 1.9×10^{-2} µM[415]. Several studies have revealed the adverse effects of BaP and other PAHs on developmental, reproductive, hepatic, endocrine and immunological processes in exposed vertebrates (reviewed by Collier et al. in 2013 and Williams et al. in 2015)[72,73]. Beside these well-documented toxic effects, BaP and other PAHs have also been shown to affect bone homeostasis (e.g., in the zebrafish *Danio rerio*, European seabass *Dicentrarchus labrax* and mouse *Mus musculus*)[144,416–418] by decreasing bone formation or increasing bone resorption. Bone is a dynamic tissue undergoing constant remodeling, a process coordinated by the concerted action of osteoblasts (bone formation) and osteoclasts (bone resorption) and critical to calcium and phosphate homeostasis, micro-fracture repair, and adaptation of the skeleton to mechanical loading[149]. Imbalanced remodeling may result in a bone with altered microarchitecture and structure (i.e., a weaker bone) and may lead to a skeleton with deformities. In humans, epidemiological studies indicate that exposure to PAHs through smoking or cooking activities can lead to bone diseases such as osteoporosis, which results in bones with reduced mineral density and prone to fractures[419–421].

In fish, such defects may affect swimming performance, impair feeding activity and consequently reducing welfare, or further increasing mortality or susceptibility to predation[143,422]. Therefore, the osteotoxic effects of PAHs have been assessed in various teleost fishes. For example, experimental oil spills containing PAHs were found to alter the expression of transcripts encoding proteins involved in bone resorption (up-regulation) and bone formation (down-regulation) in the Atlantic cod *Gadus morhua*[423] and to decrease vertebrae mineralization in the European seabass[416]. In the rainbow trout *Oncorhynchus mykiss* and the pink salmon *Oncorhynchus gorbuscha*, PAHs mixtures have been shown to increase craniofacial and spinal deformities[424,425], and 3-methylcholanthrene (another well-studied PAH compound) has been shown to increase skeletal malformations as well as decrease bone mineralization and regeneration in the zebrafish[144]. In the false kelpfish *Sebastiscus marmoratus*, BaP has been shown to alter the expression of bone marker genes related to Shh signaling, thus leading to skeletal deformities such as spinal curvature and jaw defects[426]. BaP has also been shown to trigger transgenerational effects (F1-F3 generations) on bone of the Japanese medaka *Oryzias latipes*, in particular an increase in vertebrae compression, as well as a reduction of bone integrity and thickness, bone formation and osteoblast numbers[422,427]. Multigenerational deformities (F1-F2 generations) were also observed in BaP exposed zebrafish larvae, in particular in the caudal and pectoral fins and craniofacial structures[428]. Torvanger et al.[186] recently reported a reduction in osteoblast and osteoclast activity in *ex vivo* scales of zebrafish and goldfish *Carassius auratus* after exposure to BaP.

Due to numerous technical advantages, similarities in bone biology with mammalian systems, availability of genetic tools, live imaging, and its capacity to regenerate skeletal structures, zebrafish is deemed a suitable organism for ecotoxicological studies and to investigate bone processes during development and regeneration[120,147]. In this work, we aimed at better understanding the osteotoxic effects of BaP by assessing bone formation, mineralization and patterning in developing and regenerating zebrafish bone structures[147,184,185,187], evaluating bone cell activity using transgenic reporter lines, and quantifying xenobiotic signaling and bone marker gene expression. Following recent *in vitro* data providing evidence of

interaction between neutrophils and bone forming/resorbing cells[429–432], their involvement in the mechanisms of BaP osteotoxicity will also be addressed.

6.3. MATERIALS AND METHODS

6.3.1. Chemical solutions

All chemicals were purchased from Sigma-Aldrich (St. Louis, MI, USA) unless otherwise stated. A stock solution of benzo[α]pyrene (BaP) was prepared at 31.6 mM in dimethyl sulfoxide (DMSO, 100%) and stored at -20ºC in a glass flask. It was freshly diluted to selected concentrations prior to each experiment.

6.3.2. Zebrafish maintenance

Zebrafish – AB wild-type strain, and transgenic lines *Tg(Ola.Sp7:mCherry-Eco.NfsB)*^{pd46} [166], *Tg*(*Ola.osteocalcin:EGFP*)^{hu4008} [165] and *TgBAC*(*mpx:GFP*)^{i114} [433], referred to as *Tg(sp7:mCherry)*, *Tg(osteocalcin:GFP)* and *Tg(mpx:GFP)* – were maintained in a ZebTEC (Tecniplast, Buguggiate, Italy) recirculating system with controlled water parameters (i.e., temperature 28 ± 0.1°C, pH 7.5 ± 0.1, conductivity 700 ± 50 μS, ammonia and nitrites lower than 0.1 mg/L, nitrates at 5 mg/L) under a 14-10 h light-dark photoperiod. System water was prepared by adding, using an automatic dosing system, salt (35 g/L; Instant Ocean, Blacksburg, VA, USA) and sodium bicarbonate (30 g/L; Fisher Scientific, MA, USA) to reverse osmosis treated water in order to achieve the desired pH and conductivity set in the ZebTEC system. System water was automatically replaced (10%) every day. Fish were fed twice a day with *Artemia* nauplii (strain AF480 from INVE Aquaculture, Dendermonde, Belgium) and ZEBRAFEED microdiet (Sparos Lda, Olhão, Portugal) *ad libitum*.

6.3.3. Experimental design

Parameters (e.g., developmental stages, duration of BaP exposure, frequency of treatment renewals, endpoints for each assay) associated with zebrafish experimentation are summarized in Fig. 6.1.

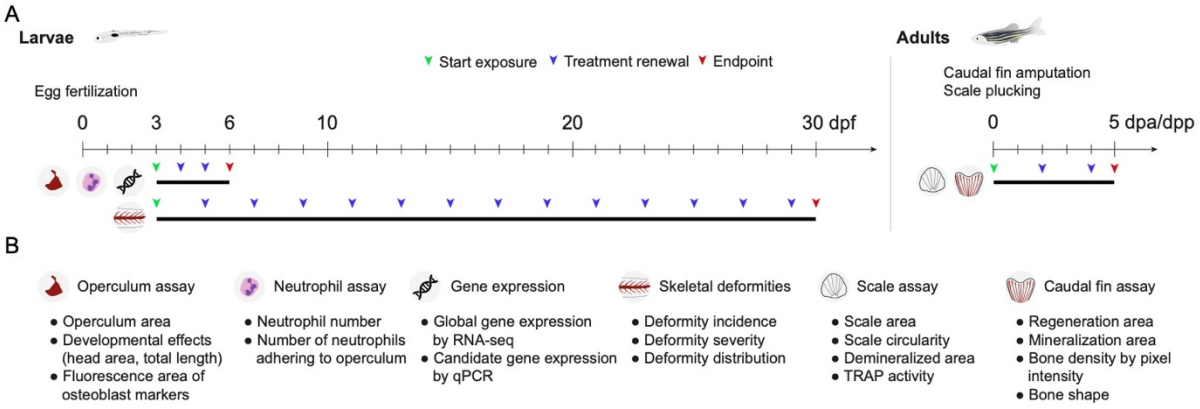

Figure 6.1. Experimental design of the zebrafish assays used to assess the effects of BaP exposure on bone throughout development and regeneration. (**A**) Time course of the *in vivo* assays performed using larval (*left panel*) and adult stages (*right panel*), including information on the onset of BaP exposure and the schedule for treatment renewals and endpoint collection. *dpf*, days post-fertilization; *dpa*, days post-amputation; *dpp*, days post-plucking. (**B**) Biological parameters evaluated at each endpoint for each assay.

6.3.4. Operculum growth assay

Sexually mature zebrafish aged between 6 and 18 months were crossed (1:2 male:female sex ratio) and fertilized eggs (approximately 200 eggs per breeding event) were transferred into a 1-L nursing tank (Tecniplast) and cultured under static water conditions. Methylene blue (0.0002% w/v) was added to prevent fungal growth. At 3 days post-fertilization (dpf), larvae were randomly transferred into borosilicate glass flasks (15 larvae in 10 mL of fish water) and exposed to BaP at concentrations ranging from 0.01 to 31.6 µM, calcitriol (1α,25-dihydroxyvitamin D_3) at 10 pg/mL, or DMSO and ethanol (vehicle for BaP and calcitriol, respectively) at 0.1%. About 70% of the fish water was renewed daily until the end of the treatment. At 6 dpf, larvae were euthanized with a lethal dose of anesthetic (tricaine; MS222), stained for 15 min at room temperature with 0.01% alizarin red S (AR-S; pH 7.4) prepared in Milli-Q water (Merck Millipore, Darmstadt, Germany), and washed twice with Milli-Q water for 5 min (method adapted from Bensimon-Brito et al.[370]). Stained larvae were placed in a lateral plane on top of a 2% agarose gel, imaged and analyzed. To evaluate the effects of BaP on the expression of immature and mature osteoblast markers, larvae of the transgenic zebrafish lines *Tg(sp7:mCherry)* and *Tg(osteocalcin:GFP)* were exposed to 1 µM BaP and 0.1% DMSO from 3 to 6 dpf. The fluorescence area was measured and corrected by the area of the operculum stained with either 0.2% calcein or 0.01% AR-S in combination with *Tg(sp7:*mCherry*)* and *Tg*(*osteocalcin:GFP)* transgenes, respectively. Images were acquired using a MZ10F fluorescence stereomicroscope

(Leica, Wetzlar, Germany) equipped with either mCherry (ex: ET560/40x; em: ET630/75m) or GFP (ex: ET470/40x; em: ET525/50m) filters and a DFC7000T color camera (Leica). Images were acquired using the following parameters: exposure time 600 ms, gamma 1.00, image format 1920×1440 pixels and binning 1×1. Experimental settings and morphometric analysis were performed as described by Tarasco et al.[184] using ZFBONE ImageJ toolset[289].

6.3.5. Axial skeleton development assay

For this assay, fish were exposed to BaP from 3 dpf (onset of bone development) until 30 dpf (when all the bony structures of the axial skeleton are fully developed). 3-dpf zebrafish larvae were randomly placed into 1.5-L EPA-certified soda-lime glass jars (Thermo Fisher Scientific, Waltham, MA, USA) at a density of 100 larvae per jar and exposed for 27 days to BaP at concentrations ranging from 0.01 to 10 µM, or DMSO at 0.1%. About 80% of the fish water was renewed every second day until the end of the treatment. At 30 dpf, larvae were euthanized with a lethal dose of anesthetic (see above) and stained with 0.05% AR-S prepared in 1% potassium hydroxide, cleared using 1% potassium hydroxide and preserved in increasing series of glycerol up to 75%, as described by Walker and Kimmel[434]. The incidence, typology (such as shape variation, anomalous supernumerary elements, fusions or platyspondyly) and charge of deformities in the axial skeleton were determined through stereomicroscopy observation and structures classified according to Bird and Mabee[369]. Representative images were acquired using a LSM 800 confocal microscope (Zeiss, Oberkochen, Germany) equipped with a 10x/0.45 M27 objective. Images were acquired at 1024×1024 pixels using 15% laser power at 561 nm, acquisition speed=8.26 µs, mCherry channel (λex: 587, λem 610) and a GaAsP detector set to gain=650V and digital gain=0.3. Z slices were recorded at 4 µm per section and adjusted to cover the full depth of region of interest.

6.3.6. Caudal fin regeneration assay

Young adult zebrafish (3-months old) were anesthetized with 0.6 mM tricaine (MS222) and placed on the stage of a stereomicroscope. Caudal fin was carefully deployed, flattened, and amputated 1–2 segments anterior to the bifurcation of the most peripheral branching lepidotrichia using a sterile scalpel in a single downward

movement. Fish were allowed to recover and then placed randomly into a 1.5-L EPA-certified soda-lime glass jar (8 fish per jar) containing water from the rearing system and maintained at 33 ± 0.1°C. Fish regenerating their caudal fin were exposed for 5 days to BaP at concentrations ranging from 0.01 to 10 µM, or DMSO at 0.1%. About 80% of the fish water was renewed every second day until the end of the experiment. At 5 days post-amputation (dpa), fish were stained for 20 min with 0.01% AR-S (pH 7.4, prepared in system water) and euthanized with a lethal dose of anesthetic (see above). Images were acquired using a Leica MZ10F fluorescence stereomicroscope equipped with a mCherry filter (ex: ET560/40x; em: ET630/75m) and a Leica DFC7000T color camera, and the following parameters: exposure time 600 ms, gamma 1.00, image format 1920×1440 pixels and binning 1×1. Caudal fin regeneration, *de novo* bone formation and patterning were assessed through the morphometric analysis of regenerated areas as described by Cardeira et al.[185] and using ZFBONE ImageJ toolset[289]. The percentage of fin bifurcation is defined as the ratio between the distance from the stump to the bifurcation point and the distance from the stump to the ray tip. For each fin, 8 rays were measured (4 rays for each fin lobe) and averaged. The mineral density of newly formed bone was assessed in regenerating fin (5 fins per condition) exposed to 1 µM BaP or 0.1% DMSO, and scanned with a SkyScan 1272 high-resolution 3D X-ray microscope based on micro computed tomography (micro-CT) technology (Bruker, Kontich, Belgium) using a 60-kV voltage, a 166-µA current and a 0.25-mm thick aluminium filter. For each sample, 800 projections with an isotropic voxel size of 3 µm were acquired over a rotation range of 360° with a rotation step of 0.45°. The cross-sectional images (4904×4904 pixels) were reconstructed from the X-ray projections using the NRecon software v1.6.10.2 (Bruker). During reconstruction, the following parameters were used: compensate for misalignment (82), smoothing (2) and beam hardening (50%). Images were imported in FIJI software for background subtraction (Rolling ball radius: 25 pixel) and stack merging through average projection. The pixel intensity of 8 lepidotrichia per fin was assessed using ZFBONE ImageJ toolset[289].

6.3.7. Scale regeneration assay

Young adult zebrafish (3-months old) were anesthetized with 0.6 mM tricaine and placed on the stage of a stereomicroscope. Ontogenetic scales (around 20-30 per

fish) were carefully plucked from the left flank of the body using thin stainless-steel forceps. Fish were allowed to recover and then randomly placed into a 1.5-L EPA-certified soda-lime glass jar (8 fish per cup) containing water from the rearing system and maintained at 33 ± 0.1°C. Fish were exposed for 5 days to BaP at concentrations ranging from 0.01 to 10 µM, or DMSO at 0.1%. About 80% of the fish water was renewed every second day until the end of the experiment. At 5 days post-plucking (dpp), fish were euthanized with a lethal dose of anesthetic (see above) and regenerating scales were collected (same procedure as above), washed in phosphate-buffered saline (PBS) and fixed for 30 min at 4°C in 4% formaldehyde (prepared in PBS, pH 7.4). Scales were dehydrated through ice-cold increasing series of ethanol up to 100% and preserved at -20°C. Osteoclast enzymatic activity was assessed through tartrate-resistant acid phosphatase (TRAP) staining. Scales were rehydrated, washed with PBS and incubated at room temperature in a 0.1 M sodium acetate buffer (pH 5.1) containing 50 mM of L(+)-tartaric acid. Scales were then incubated in the dark until TRAP signal was revealed (approximately 1 h) using naphthol AS-TR phosphate as substrate and hexazotized pararosaniline, as described by Witten[435]. Scales were rinsed twice in water and then preserved through an increasing series of glycerol (Biochem Chemopharma, Cosne sur loire, France) up to 75% until image acquisition. Mineral deposition was assessed in von Kossa stained scales. Briefly, scales were rehydrated, washed with PBS, and incubated for 1 h in 5% silver nitrate, under UV light. Scales were then rinsed with distilled water for 5 min and immersed for 5 min in 2.5% sodium thiosulfate. Finally, scales were rinsed thoroughly with distilled water and preserved in increasing series of glycerol up to 75% until image acquisition. Bright-field images of TRAP and von Kossa stained scales were acquired using a SteREO Lumar.V12 stereomicroscope and the following parameters: 16-bit RGB image, exposure time 100 ms, gamma 1.00, image format 1384×1040 pixel and binning 1×1. Scales area, circularity, osteoclast activity and mineral deposition were assessed throughout morphometric analysis using ZFBONE ImageJ toolset[289].

6.3.8. RNA preparation and gene expression analysis

Total RNA was isolated from 6-dpf zebrafish larvae exposed to 1 µM BaP or 0.1% DMSO (4 biological replicates per condition, prepared from pools of 30 larvae) using NZYol (NZYTech, Lisbon, Portugal) and treated with RQ1 RNase-Free DNase

(Promega, WI, USA) to avoid contamination by genomic DNA. RNA integrity and quantity were confirmed using an Experion Automated Electrophoresis system (Bio-Rad, Hercules, CA, USA) and only RNA with a RIN > 9.8 was further used. RNA-seq – a single readout of the pooled replicates – was first used to gain insights into the molecular mechanisms involved in BaP osteotoxicity; qPCR analysis of the 4 biological replicates was later used to confirm the differential expression of candidate genes.

6.3.9. Gene expression analysis by RNA-seq

RNA and library preparation integrity were verified with LabChip Gx Touch 24 (Perkin Elmer). 200 ng of total RNA was used as input for VAHTS Stranded mRNA-seq Library preparation following manufacture's protocol (Vazyme). Sequencing was performed on NextSeq500 instrument (Illumina) using v2 chemistry, resulting in average of 27M reads per library with 1x75bp single end setup. The resulting raw reads were assessed for quality, adapter content and duplication rates with FastQC[436]. Trimmomatic version 0.38 was employed to trim reads after a quality drop below a mean of Q20 in a window of 5 nucleotides[437]. Only reads between 30 and 150 nucleotides were cleared for further analyses. Trimmed and filtered reads were aligned versus the Ensembl zebrafish genome version DanRer11 (GRCz11.92) using STAR 2.6.1d with the parameter "--outFilterMismatchNoverLmax 0.1" to increase the maximum ratio of mismatches to mapped length to 10%[438]. The number of reads aligning to genes was counted with featureCounts 1.6.3 tool from the Subread package[439]. Only reads mapping at least partially inside exons were admitted and aggregated per gene. Reads overlapping multiple genes or aligning to multiple regions were excluded. Gene ontology analyses were performed using PANTHER (Protein Analysis THrough Evolutionary Relationships) and pathway enrichment was determined using REACTOME classification system. Ensembl zebrafish gene IDs of differentially expressed genes exhibiting a fold change greater than 2 and lower than 0.5 in RNA-seq dataset were used as input data. Over-representation was tested using Bonferroni correction for multiple testing. In this regard, the number of differentially expressed genes (in this study) is compared to the zebrafish reference list (all genes in the database) and P-value is calculated using the binomial test to determine whether the over- or under- representation is significant or not. RNA-seq data have been

deposited in NCBI Gene Expression Omnibus under the GEO Series accession number GSE174529 (https://www.ncbi.nlm.nih.gov/geo/).

6.3.10. Gene expression analysis by qPCR

Total RNA (1 µg) was reverse-transcribed for 1 h at 37°C using M-MLV reverse transcriptase (Invitrogen, Carlsbad, CA, USA), oligo-d(T) primer and RiboLock RNase inhibitor (Thermo Fisher Scientific). All quantitative real-time PCR (qPCR) reactions were performed using SensiFAST SYBR Hi-ROX kit (Meridian Bioscience, Cincinnati, OH, USA), 10 µM of gene-specific primers (Supplementary Table 1) and 1:10 dilution of reverse-transcribed RNA, in a CFX Connect Real-Time PCR detection system (Bio-Rad). PCR amplification was as follows: an initial denaturation step of 2 min at 95°C and 40 cycles of amplification (10 s at 95°C and 20 s at 65°C). Efficiency of amplification was above 95% for all primer sets. Levels of gene expression were calculated using the ΔΔCt comparative method[371] and normalized using the average of two housekeeping genes (i.e., *eef1α1l1* and *rps18*) previously validated in zebrafish larvae[372].

6.3.11. Neutrophil quantification

Adults of the *TgBAC*(*mpx:GFP*)^{i114} line (where neutrophils are labeled with green fluorescence) were crossed and fertilized eggs (approximately 200 eggs) were transferred into a 1-L nursing tank (Tecniplast) with static water conditions. Methylene blue (0.0002% w/v) was added to prevent fungal growth. At 3 dpf, larvae were randomly transferred into borosilicate glass flasks (30 larvae in 25 mL of fish water) and exposed to 1 µM BaP or 0.1% DMSO. About 70% of the fish water was renewed daily until the end of the treatment. At 6 dpf, larvae were euthanized with a lethal dose of anesthetic (see above), then stained for 15 min at room temperature with 0.01% AR-S and washed twice with fish water for 5 min. Stained larvae were embedded in 1% low melting agarose for imaging. Representative images were acquired using an Axio Observer.Z1.7 spinning disk confocal microscope (Zeiss, Oberkochen, Germany) equipped with a 40x/1.1 W Korr UV VIS IR water immersion objective. Images were acquired at 804×804 pixels using 8% laser power at 488 nm excitation with 50 ms exposure time for EGFP channel and 30% laser power at 587 nm excitation with 100

ms exposure time for mCherry channel. Z slices were recorded at 1 µM per section and adjusted to cover the depth of the operculum.

6.3.12. Statistical analysis

Data were analyzed using Prism version 8.2.1 (GraphPad Software, Inc. La Jolla, CA, USA). One-way analysis of variance (ANOVA) followed by Dunnett's multiple comparison test or an unpaired t-test with Welch's correction were used for data sets presenting a normal distribution. Kruskal-Wallis test followed by Dunn's multiple comparison test was used for data sets that did not follow a normal distribution. A chi-squared test, 1 degree of freedom, was used to analyze data sets related to skeletal deformity. In all cases, differences were considered significant for $p < 0.05$. Blind analyses were performed whenever possible to reduce the bias associated to experimenters.

6.4. RESULTS

6.4.1. Benzo[α]pyrene impairs operculum growth by affecting osteoblast maturation

To understand the effect of BaP on bone formation, zebrafish larvae were exposed for 3 days to BaP (from 0.01 to 31.6 µM) and operculum area, head area and standard body length were determined through morphometric analysis. Head area was used to normalize the area of the operculum while standard body length was assessed to evaluate larvae developmental impairment. We observed that only BaP concentrations higher than 0.1 µM inhibited operculum growth (Fig. 6.2A). When the corrected operculum area of BaP-treated larvae was compared with the control value (0.1% DMSO), reductions of 13.8 ± 2.7% and 45.5 ± 3.2% were observed at the lowest effective concentration (0.1 µM) and at the highest non-lethal concentration (31.6 µM), respectively, following a dose-dependent response. In all experiments, the corrected operculum area of calcitriol-treated larvae (positive control) increased by 54.5 ± 4.7%, confirming the fitness of the embryo batch and the responsiveness of the assay. Head area and body standard length were slightly reduced at the two highest concentrations (Supplementary Fig. 6.1), indicating that BaP affected larval development in a more general manner at concentrations higher than 10 µM. To gain insights into the

mechanisms underlying BaP effects on bone cells and their maturation, the expression of marker transgenes for immature and mature osteoblasts (i.e., *Tg(sp7:mCherry)* and *Tg(osteocalcin:GFP)*, respectively) was monitored in the operculum of larvae exposed to 1 µM BaP for 3 days. The intra-operculum fluorescent signal area increased by 8.80 ± 2.27% (Fig. 6.2B) for *Tg(sp7:mCherry)* and decreased by 64.89 ± 7.61% (Fig. 6.2C) for *Tg(osteocalcin:GFP)*, when compared to control, suggesting that BaP impairs osteoblast maturation, i.e., by blocking the transition of immature osteoblasts (*sp7*-positive cells) to a mature state (*osteocalcin*-positive cells). It is worth to mention that the operculum area determined by calcein/AR-S staining was also reduced in BaP-treated versus control transgenic larvae (Supplementary Fig. 6.2) indicating that results with reporter lines relate to the morphological phenotype observed in wild-type line.

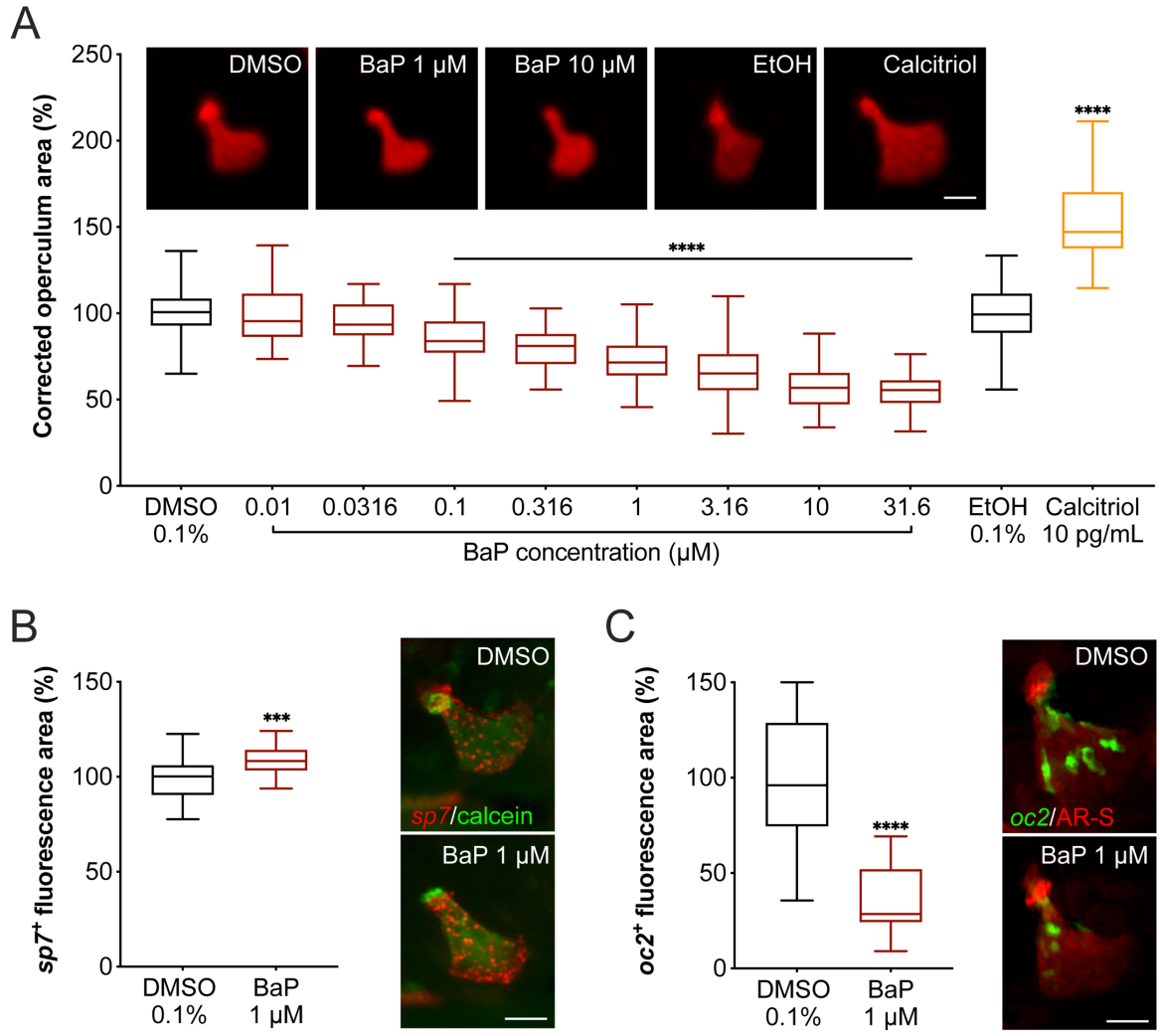

Figure 6.2. (**A**) Operculum growth in zebrafish larvae exposed to increasing concentrations of BaP from 3 to 6 dpf. Regions of interest (operculum and head area) were determined through the morphometric analysis of AR-S stained bone structures imaged by fluorescence microscopy. Representative images

of AR-S stained operculum are presented on the top of the graph (background was removed using image processing software to highlight operculum structure). Dimethyl sulfoxide (DMSO) and ethanol (EtOH) were used as vehicle for BaP and calcitriol, respectively. Scale bar is 50 µm. P-value calculated using one-way ANOVA followed by Dunnett's multiple comparison test for BaP/DMSO and Student's t-test for calcitriol/EtOH. Values are presented as median and quartiles (n ≥ 25). (**B, C**) Expression of osteoblast marker genes in the operculum of zebrafish larvae exposed to 1 µM BaP or 0.1% DMSO from 3 to 6 dpf. (**B**) osterix (sp7), a marker of immature osteoblasts, appears in red in the *Tg(Ola.Sp7:mCherry-Eco.NfsB)*^{pd46} line; operculum is counter-stained with calcein. (**C**) osteocalcin (oc2), a marker of mature osteoblasts, appears in green in the *Tg(Ola.osteocalcin:EGFP)*^{hu4008} line; operculum is counter-stained with AR-S. Representative images of the operculum are presented on the right side of the respective graph. Scale bar is 50 µm. P-value calculated using Student's t-test. Values are presented as median and quartiles (n ≥ 21).

6.4.2. Benzo[α]pyrene affects zebrafish axial skeleton development

To assess the effect of BaP on skeletogenesis, the axial skeleton of zebrafish juveniles exposed for 27 days to BaP (from 0.01 to 10 µM) was evaluated for the incidence of deformed fish, the number of deformities per fish and their distribution along the axial skeleton. At the two highest concentration (i.e., 3.16 and 10 µM) all the fish died after 5 days of exposure and no data was retrieved. Fish exposed to the other concentrations presented an increasing incidence of deformities, starting from 70% at 0.01 µM BaP and reaching 100% at 1 µM BaP (Fig. 6.3A). An increasing number of skeletal malformations correlated to increasing concentrations of BaP. We observed a minimum of 4 deformed axial skeletal structures per fish upon exposure to 1 µM BaP (Fig. 6.3B). BaP affected several structures of the axial skeleton and several types of deformities were reported, e.g., partial/total fusion of the vertebrae or neural/hemal arches and malformations of the operculum, urostyle, parhypural and hypurals (Fig. 6.3D). The caudal vertebrae, caudal fin vertebrae and caudal fin complex were the most affected regions. Only the highest concentrations of BaP (0.316 and 1 µM) affected skeletal structures in the head region (Fig. 6.3C). This data confirms the osteotoxic effect of BaP during skeletal development upon chronic exposure.

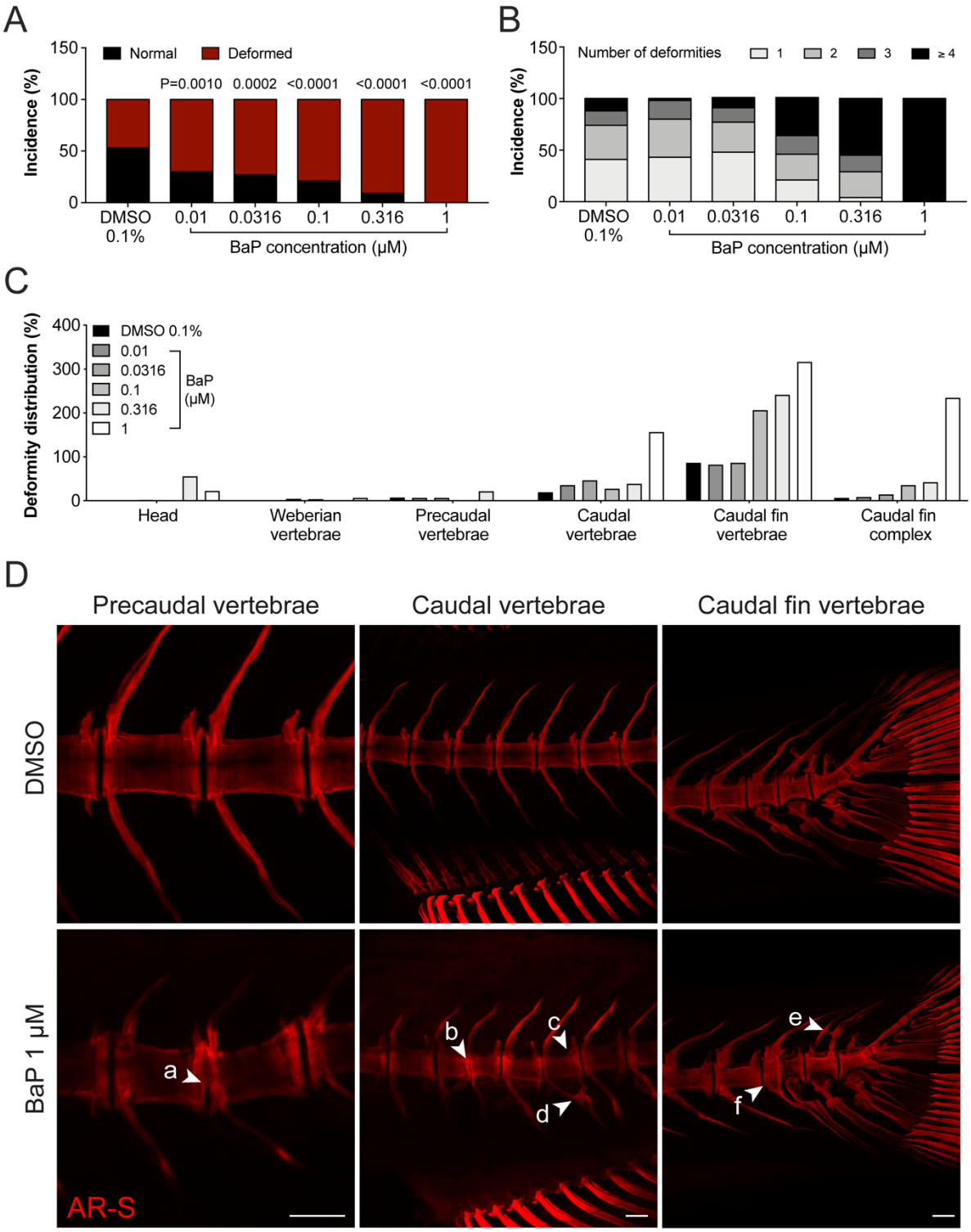

Figure 6.3. Deformities in the axial skeleton of 30 dpf juvenile zebrafish exposed to increasing concentration of BaP throughout their development. (**A**) Percentage of normal and deformed zebrafish. (**B**) Percentage of deformities per deformed larvae. (**C**) Distribution of the deformities along the axial skeleton. Deformed structures of each individual were summed and divided by the number of fish. (**D**) Representative fluorescence images of AR-S stained skeletal structures exposed to 0.1% DMSO or 1 µM BaP. Arrowheads point to: a, partially fused vertebrae; b, fused vertebrae; c, deformed vertebrae; d, fused hemal arches; e, ectopic mineralization; f, platyspondyly. Scale bar is 100 µm. P-value calculated using chi-squared test, 1 degree of freedom. n≥65, except for BaP 1 µM (n=18).

6.4.3. Benzo[α]pyrene impairs bone mineral density and patterning

To evaluate the effect of BaP on *de novo* bone formation, adult zebrafish were finectomized and exposed for 5 days to BaP (from 0.01 to 10 μM). Caudal fin regeneration, *de novo* bone formation and ray patterning were assessed through morphometric analysis. Fish exposed to 1, 3.16 and 10 μM BaP showed a reduction in regenerated caudal fin tissues of 19.10 ± 5.7%, 21.10 ± 6.0% and 30.50 ± 6.4% over control, respectively (Fig. 6.4A). Lower concentrations also triggered a decrease in fin regeneration although to an extent not statistically significant. While none of the concentrations tested altered the extent of *de novo* bone formation (Fig. 6.4B), we observed that the patterning of newly formed rays was strongly affected at these concentrations. Rays bifurcated earlier (24.2 ± 5.0%) in BaP-treated versus control fish, modifying the shape of the fin through the proximalization of ray branching (Fig. 6.4C, D). Bone mineral density was then evaluated by micro-computed tomography (μCT) in adult zebrafish regenerating their caudal fins upon exposure to 1 μM BaP for 5 days. Pixel intensity was assessed in μCT images of regenerating rays (Fig. 6.4F). Pixel intensity was lower in BaP-treated versus control fish, from the amputation plane along all the ray length (Fig. 6.4E) and the assessment of the total area under the intensity curve showed a reduction of 29.81 ± 4.90% (Fig. 6.4G), indicating an impairment of *de novo* bone mineralization.

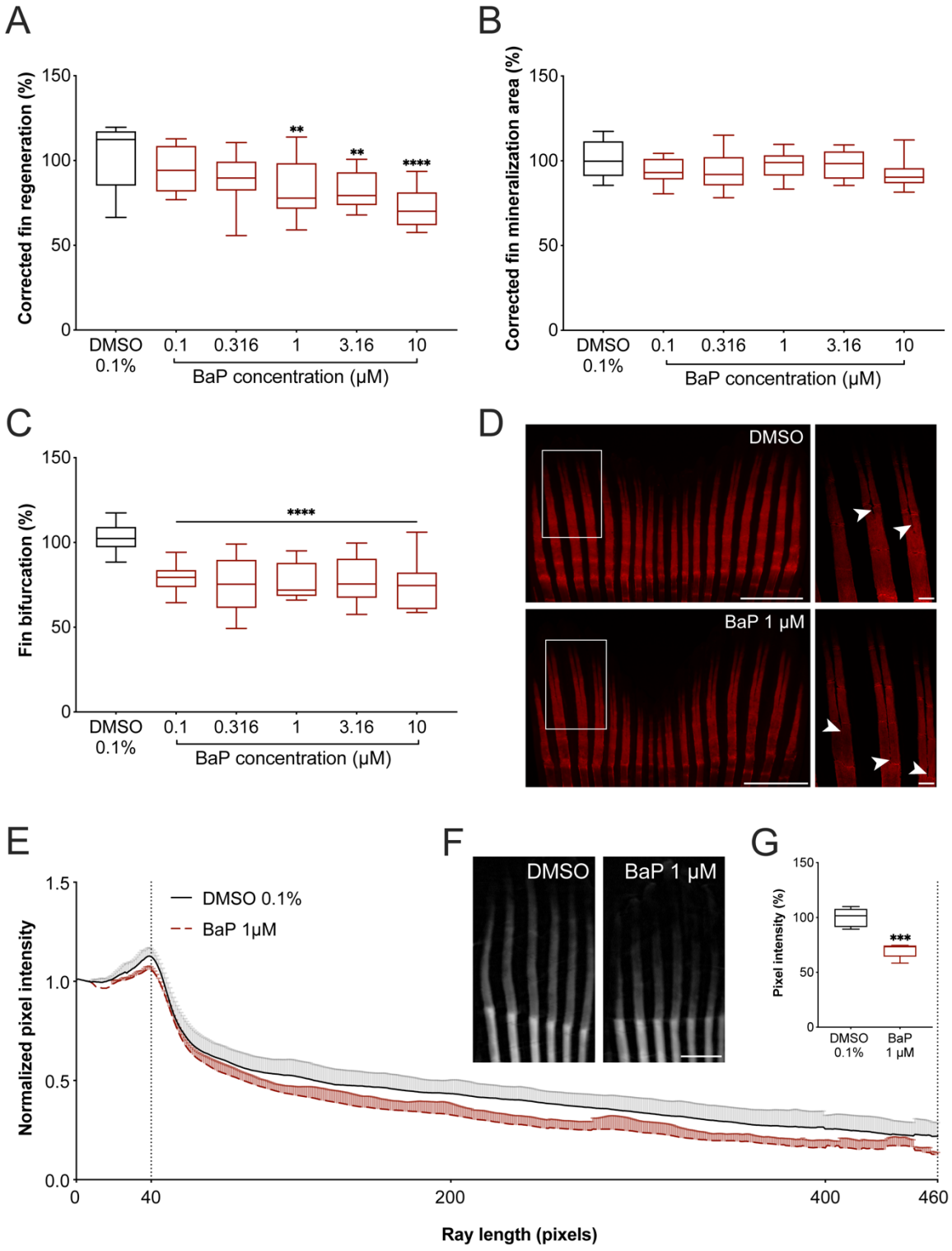

Figure 6.4. Regeneration of the caudal fin in adult zebrafish exposed to increasing concentrations of BaP for 5 days after finectomy. (**A**) Caudal fin tissue regeneration, (**B**) de novo bone formation and (**C**) ray bifurcation was assessed through morphometric analysis of the fin structures in bright-field and fluorescence images. Fin bifurcation corresponds to the ratio between the distance from the stump to the bifurcation point / distance from stump to ray tip (**D**) Representative images of the regenerating caudal fin rays exposed to 0.1% DMSO or 1 µM BaP. Magnification of the boxed area is presented in the right panel. Arrowheads point to ray bifurcation point. Scale bar is 1 mm in left panels and 0.1 mm in right panels. P-value calculated using one-way ANOVA followed by Dunnett's multiple comparison test. Values are presented as median and quartiles (n≥9). (**E-G**) Density of regenerating caudal fin rays

from adult zebrafish exposed to BaP for 5 days after finectomy assessed through ray pixel intensity micro–computed tomography (µCT) images. (**E**) Averaged normalized pixel intensity along regenerated rays from 40 (amputation plane) to 460 pixels. (**F**) Representative µCT images of the regenerating caudal fin rays exposed to 0.1% DMSO or 1 µM BaP. Scale bar is 1 mm. (**G**) Area under curve (40-460 pixels). P-value calculated using Student's t-test. Values are presented as median and quartiles (n=5).

6.4.4. Benzo[α]pyrene inhibits scale mineralization and increase osteoclast activity during regeneration

To validate BaP inhibition of bone mineralization during regeneration, we assessed scale area, circularity, TRAP signal and demineralized area in adult zebrafish regenerating scales upon exposure to BaP (from 0.01 to 10 µM) for 5 days. All parameters were affected by BaP at all tested concentrations (Fig. 6.5E). We observed that scale area was reduced by 36.84 ± 3.03% and 54.41 ± 4.24% at the lowest (0.01 µM) and highest (10 µM) concentrations, respectively (Fig. 6.5A) indicating a reduction in mineralization. Scale circularity was reduced by 2.68 ± 0.47% and of 6.52 ± 0.59% at the lowest and highest concentrations, respectively, further confirming their affected morphology (Fig. 6.5B). TRAP signal was increased by 920.10 ± 330.90% and 2884.00 ± 406.30% at the lowest and highest concentrations, respectively (Fig. 6.5C). Finally, demineralized area was increased by 86.28 ± 25.61% and 226.90 ± 43.74% at the lowest and highest concentrations, respectively (Fig. 6.5D). Together, our data show that BaP decreases bone formation while increasing osteoclast activity during scale regeneration.

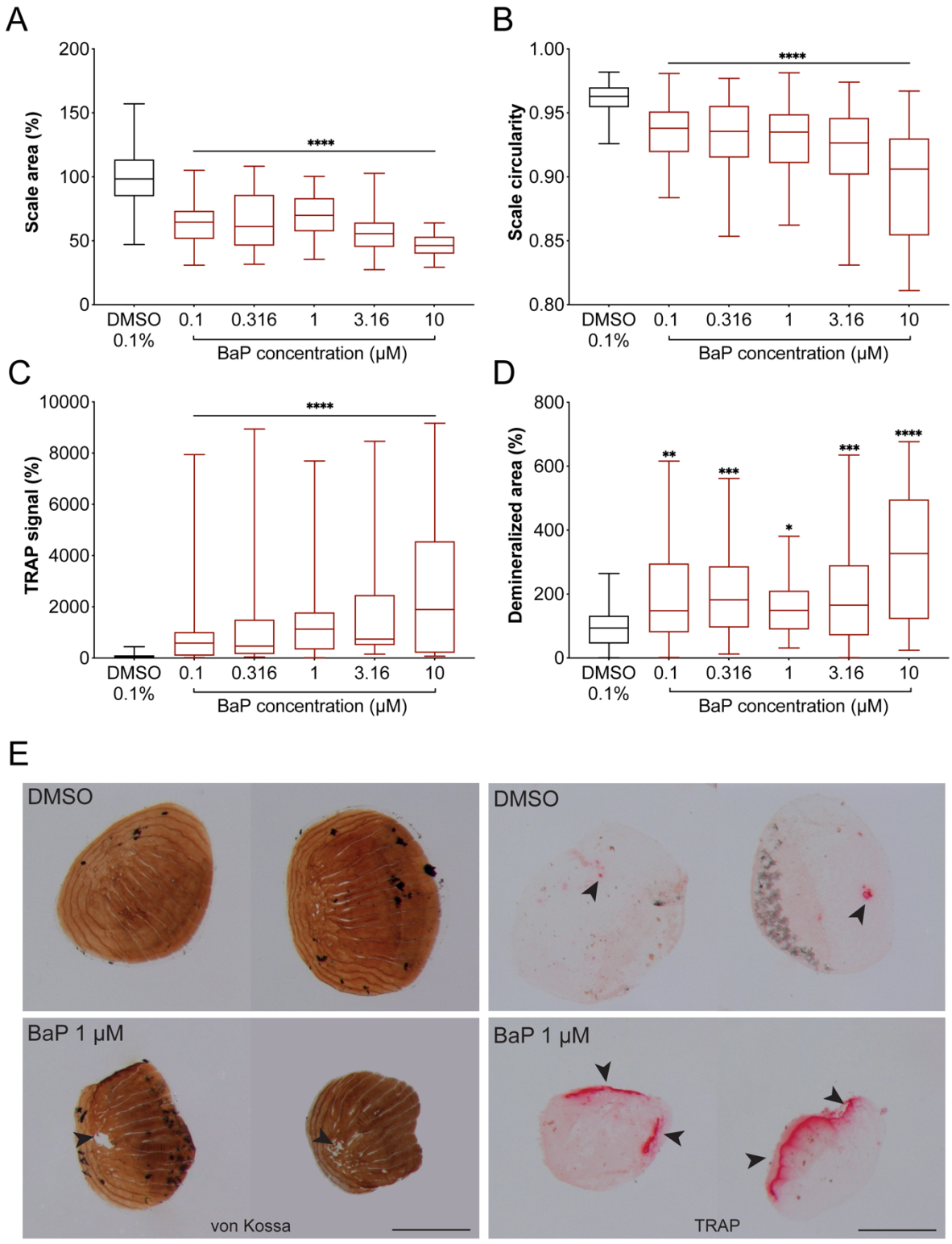

Figure 6.5. Morphology, mineral content, and osteoclast activity of regenerating scales from adult zebrafish exposed to increasing concentration of BaP for 5 days after plucking. (**A**) Scale area and (**B**) circularity were assessed through morphometric analysis of regenerating scales in bright-field images. (**C**) Osteoclast activity was assessed through TRAP (Tartrate-Resistant Acid Phosphatase) staining while (**D**) mineral content was evaluated through von Kossa staining. (**E**) Representative images of von Kossa (left panels) and TRAP (right panels) stained scales collected from adults exposed to either 0.1% DMSO or 1 μM BaP. Arrowheads point to demineralized areas or regions of TRAP signal. Scale bar is 0.5 mm. P-value calculated using Kruskal-Wallis test followed by Dunn's multiple comparisons test for

TRAP activity and one-way ANOVA followed by Dunnett's multiple comparison test for scale area, scale circularity and demineralized area. Values are presented as median and quartiles (n≥20; n=9 at BaP 10 µM in Demineralized area).

6.4.5. Analysis of gene expression in BaP-treated larvae

To understand the molecular mechanisms behind BaP osteotoxic effects, 3-dpf larvae were exposed for 3 days to 1 µM BaP and their transcriptome was first determined by RNA-seq and compared to that of larvae exposed to 0.1% DMSO. Note that RNA-seq analysis was based on a single readout (pooled replicates) for each condition, to get insights into gene networks involved. A selection of differentially expressed genes was further analyzed by qPCR using the 4 biological replicates. Analysis of differentially expressed genes revealed that pathways related to xenobiotic response (e.g., glutathione conjugation, phase II conjugation of compounds, phase I functionalization of compounds, metabolism, and biological oxidations) and to extracellular matrix degradation, formation and organization (e.g., collagen chain trimerization, collagen synthesis, formation and degradation, ECM degradation and formation, activation of metalloproteinases) were enriched in BaP-treated larvae. Interestingly, pathways related to neutrophil metabolism (e.g., neutrophil degranulation) were also enriched in BaP-treated larvae (Supplementary Fig. 6.3). The most enriched biological processes were related to xenobiotic response such as cellular detoxification and response to toxic substances, metabolic processes, and ECM organization (Supplementary Fig. 6.4).

To confirm RNA-seq data, the expression of several marker genes was assessed by qPCR (Fig. 6.6). We observed that expression of xenobiotic nuclear receptors and transcription factors (*ahr2*, *nr1i2* and *nr1i2 X2*) was up-regulated in BaP-treated larvae by 1.44, 1.91 and 1.53 respectively. Similarly, Phase I and II metabolizing enzymes (*cyp1a* and *gstp1*) were also up regulated by 46.90 and 7.56 folds, respectively. In contrast, while the expression of osteoblast differentiation marker genes (*runx2b*, *sp7*, and *bmp2b*) was not affected upon BaP exposure, expression of those involved in ECM mineralization (*oc2,* also known as *bglapl,* and *spp1*) was down regulated by 1.40 and 1.56 fold, respectively. Osteoblast signaling receptor (*vdrb*) was up regulated by 1.14 fold. Additionally, the expression of collagenous ECM components (*col1a1a*, *col2a1a* and *col10a1a*) was also down regulated by 1.92, 1.82 and 2.33 fold while *alpl* expression was up regulated by 1.19 fold. Expression of genes involved in

osteoclastogenesis (*acp5a*, *acp5b*, *ctsk* and *fosab*) was up regulated in BaP-treated larvae by 2.20, 2.00, 1.70 and 1.82 fold, respectively, similarly to genes involved in osteoclast activity/ECM degradation (*mmp9* and *mmp13*) which were strongly up regulated by 7.53 and 10.67 fold, respectively. Inflammation and neutrophils marker genes (*il-6*, *il-1β*, *mpx* and *lyz*) were also upregulated by 1.50, 4.50, 3.00 and 2.80 fold, respectively. In a general manner, the expression levels of selected marker genes determined by qPCR confirmed pathway enrichment revealed by transcriptomic analysis.

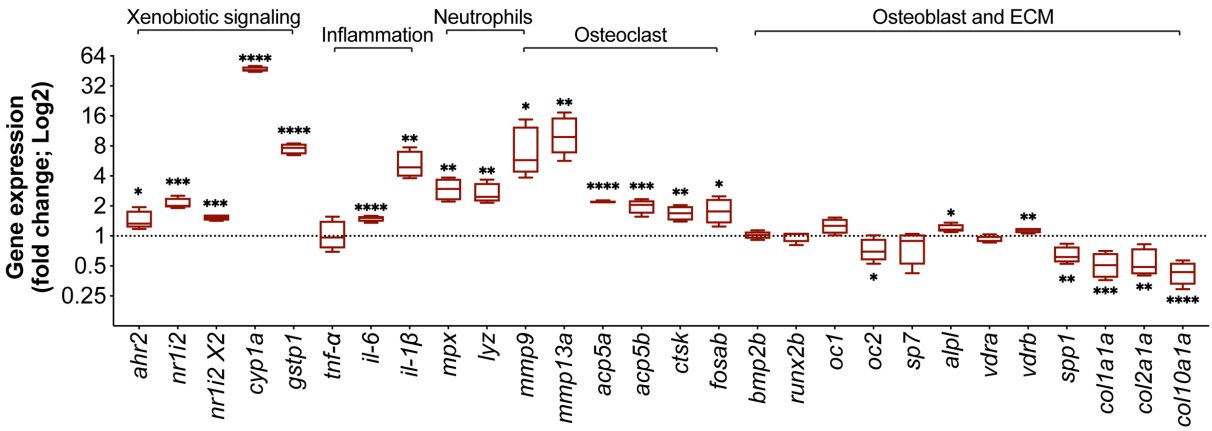

Figure 6.6. Gene expression levels in zebrafish larvae exposed to 1 µM BaP from 3 to 6 dpf. The averaged expression of *eef1a1l1* and *rps18* housekeeping genes was used to normalize gene expression levels. P-value calculated using Student's t-test. Values are presented as median and quartiles expressed in Log2 over the control (0.1% DMSO) (n=4).

6.4.6. Neutrophil recruitment and their interaction with bone increases upon BaP exposure

Our data showed an increase in expression of inflammation and neutrophil marker genes upon BaP exposure, and following recent *in vitro* studies[429–432] suggesting that neutrophils can interact with bone cells, we assessed the number of neutrophils and their interaction with the developing operculum in *Tg*(*mpx:GFP*) larvae exposed for 3 days to 1 µM BaP. The number of mpx:GFP positive neutrophils was significantly increased in BaP-treated larvae (Supplementary Fig. 6.5). This phenotype was particularly strong in the region of the trunk above the hematopoietic tissue, where neutrophil population was 2.5 times larger in BaP-treated fish than in controls (Fig. 6.7A, B). Confocal microscopy showed that the number of neutrophils observed at the surface of the opercular bone doubled in larvae exposed to BaP (Fig. 6.7C, D). A

closer look at these images revealed that BaP-treated larvae presented fewer cases of operculum without neutrophils (17.78 ± 9.33%) and more cases of operculum with a single neutrophil (7.26 ± 5.16%). Similarly, while control fish opercular bones had a maximum of two neutrophils on their surface simultaneously, 10.52 ± 3.17% of larvae exposed to BaP had more than three neutrophils on the operculum surface (Fig. 6.7E). This observation suggests that neutrophils can interact with bone structures and may play a role in BaP osteotoxic effect.

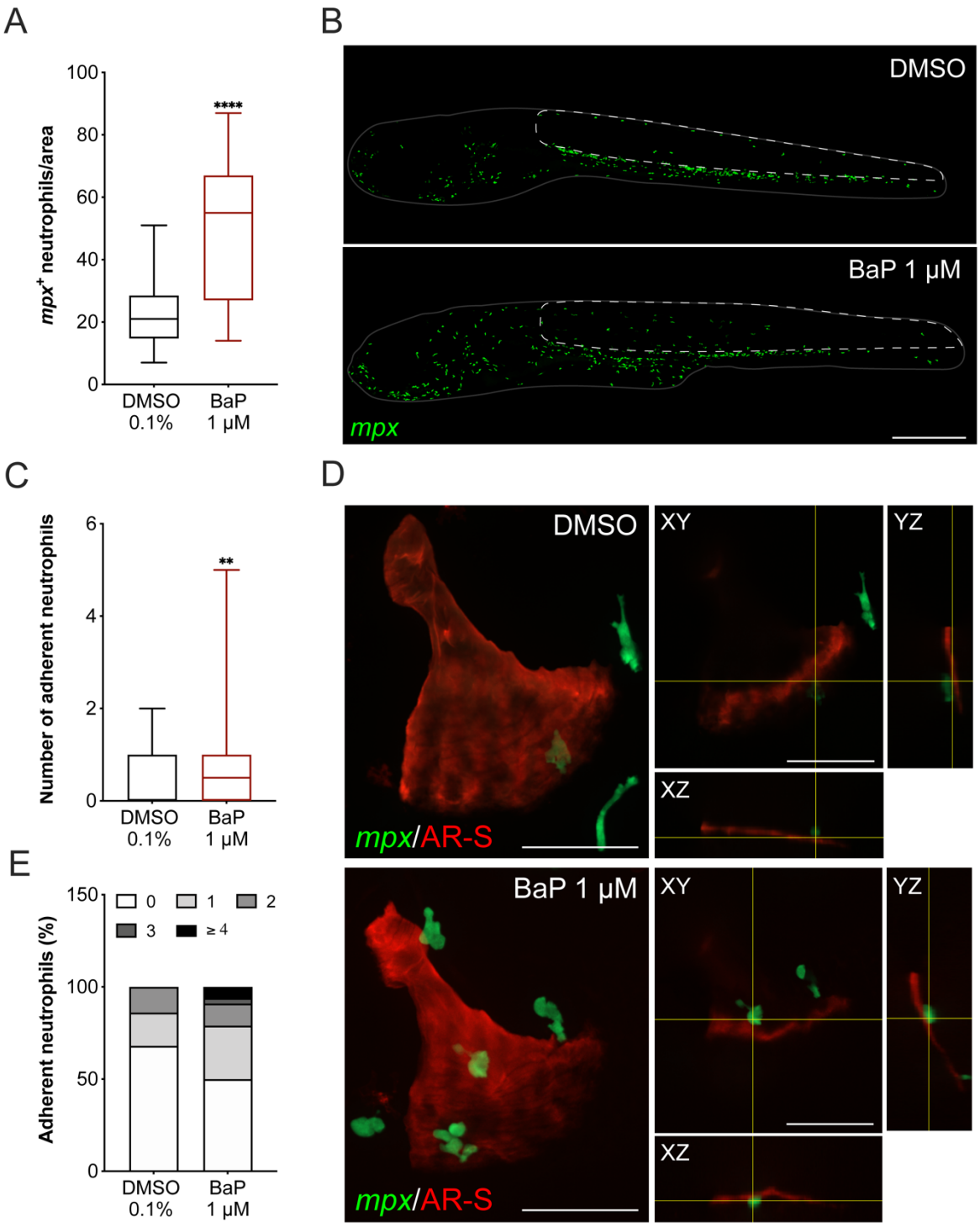

Figure 6.7. Number of neutrophils in *TgBAC(mpx:EGFP)^{i114}* zebrafish larvae exposed to BaP from 3 to 6 dpf. (**A**) Number of neutrophils in the region of interest (ROI) expressed in % over control. (**B**) Representative images of transgenic larvae exposed to 0.1% DMSO or 1 μM BaP, where *TgBAC(mpx:EGFP)^{i114}* positive cells are in green. ROI is outlined with a white dashed line, while larvae is outlined with a grey line. Scale bar is 500 μm. P-value calculated using Student's t-test. Values are presented as median and quartiles (n=18). (***C***) Number of adherent neutrophils on the opercular bone stained with AR-S. P-value calculated using Mann Whitney test. Values are presented as median and quartiles (n=109). (**D**) Representative images of adherent neutrophils on the operculum of larvae exposed to 0.1% DMSO or 1 μM BaP, where *TgBAC(mpx:EGFP)^{i114}* positive cells are in green and operculum is in red. On the right side of the representative images, orthogonal projections of the planes (XY, YZ and XZ) marked with the yellow lines. Scale bar is 50 μm. (**E**) Percentage of adherent neutrophils at 6 dpf per opercular bone. Colors indicate the number of *TgBAC(mpx:EGFP)^{i114}* positive cells per operculum.

6.5. DISCUSSION

In this study, several zebrafish *in vivo* systems were used cooperatively to assess benzo[a]pyrene osteotoxicity during bone development and regeneration. A short exposure (3 days) to BaP impaired the growth of the opercular bone and decreased osteoblast differentiation during larval development. A long exposure (27 days) to BaP affected the development of the axial skeleton, increasing incidence, charge, and severity of skeletal deformities. During regeneration, BaP affected the mineralization of newly formed fin rays and scales, while it impaired fin ray patterning and scale shape. Expression data indicated that BaP activated xenobiotic and metabolic pathways, while negatively affecting extracellular matrix formation and organization. A role of the neutrophils in the mechanisms underlying BaP effect on bone formation and regeneration through their interaction with bone extracellular matrix or bone forming cells, the osteoblasts, was also evidenced. This is not the first time that PAHs are associated with adverse effects on bone formation and regeneration. An impaired growth of the operculum was recently evidenced in larvae exposed to 3-methylcholanthrene (3-MC)[144], another member of the PAH family, and effective concentrations for 3-MC are in the same range of those determined here for BaP, although a bit higher (from 3.7 to 117 μM). This comparable effect could be related to their close molecular structure, which differs only in 1 carbon and 4 hydrogen atoms. It is also worth mentioning that larvae exposed to concentrations higher than 10 μM displayed a decrease in total length and head area, thus BaP may also trigger a more general growth retardation at higher concentrations, besides a specific effect on bone. The BaP action on bone mineral density evidenced here in newly formed fin rays and scales was also described in the Japanese medaka (*Oryzias latipes*). It was

shown that parental administration of BaP was able to inhibit centra mineralization in offspring larvae (F1-F3 generations), suggesting that BaP osteotoxicity can affect a large range of bone structures and also be inherited by next generations[427,440]. Delay in caudal vertebrae ossification was also reported during rat development following parental dietary exposure to BaP.[441] *In vitro* data collected from mammalian cell systems also evidenced that BaP can reduce mineral deposition in human periodontal ligament (HPDLC) and mesenchymal stem cells (C3H10T1/2, MEF, HCT116 and hBM-MSCs)[442–444], confirming not only the anti-mineralogenic effect of BaP, but also that mechanisms of action may be conserved throughout vertebrate evolution, from fish to human. The strong reduction of the fluorescence signal associated with *osteocalcin* expression, a marker of mature osteoblasts[445], indicated that BaP osteotoxicity in the operculum may be related to an impairment of osteoblast differentiation. A reduction in *osteocalcin* expression was also confirmed by qPCR in BaP-treated zebrafish larvae (this study) and mesenchymal stem cell cultures[443]. Osteocalcin is a bone matrix protein mainly produced by osteoblasts, which is involved in bone matrix formation and mineralization[156,446]. Impaired osteoblast differentiation associated with a reduced number of mature osteoblasts and a reduced production of osteocalcin could be the basis for the reduced bone growth and mineralization observed upon BaP exposure. Interestingly, the fluorescence signal associated with *osterix* expression, a marker of immature osteoblasts[164], was not reduced upon larvae exposure to BaP – it was even slightly increased – while qPCR data showed no effect of BaP exposure on *osterix* expression (this study). The apparent absence of effect on immature osteoblast would indicate that BaP specifically targets late osteoblast maturation. On the contrary, BaP parental exposure reduced *col10* and *sp7* fluorescence signals in vertebrae of 26-dpf medaka from F1-F3 generations[440] and *sp7* expression in 17 days post-hatching (dph) medaka larvae from F2 and F3 generations[422]. These differences may be related to the different animal model (i.e., zebrafish vs medaka), type of exposure (i.e., direct vs parental), bone structure assessed (i.e., operculum vs vertebrae) and the different endpoint (i.e., 6 dpf vs 17/26 dpf). It is important to mention that, while *sp7* expression was reduced in medaka F2 and F3 generations, it was not affected in medaka F1 generation, emphasizing the complexity of BaP effect on this marker gene. In this regard, the same two studies show that other markers of osteoblast proliferation, *runx2* and *bmp2*, were up-regulated upon BaP exposure[422,427].

Based on our experimental results, we propose that BaP osteotoxic effect on the operculum growth is the result of an inhibition of the final step of osteoblast maturation, which leads to a decrease in operculum growth and mineralization. The slight increase of immature osteoblasts in zebrafish larval operculum may be a feedback response to BaP osteotoxic effect or an accumulation of immature cells that failed to differentiate. Few studies have reported the occurrence of skeletal anomalies upon BaP exposure. While no skeletal effects were observed in rat fetus after parental dietary exposure[441], BaP triggered spinal curvatures and jaw defects in the false kelpfish *Sebastiscus marmoratus* after 7 days of waterborne exposure[426] and multigenerational bone deformities in medaka F1-F3 generations[422,427] and zebrafish F1-F2 generations[428] after parental dietary exposure. Our data collected in zebrafish juveniles exposed for 27 days to waterborne BaP further supports the skeletotoxic effect of BaP and revealed that 100% of the fish were deformed at the highest non-lethal concentration (1 µM). Most of the BaP concentrations found in the environment fall within the range of 6.3×10^{-7} to 4.5×10^{-5} µM[412–414] and are below the lowest effective concentration determined in this study, although much higher concentrations (i.e., 1.9×10^{-2} µM) have been reported[415]). Still, an exposure to sub-effective concentrations for periods longer that those reported here, a situation that may regularly occur in the environment, could lead to skeletal anomalies at concentrations lower than 0.01 µM.

It is important to mention that the incidence of deformities observed in the control group (50%) is within the normal range (45–65%) for wild-type zebrafish[234,447]. BaP exposure affected different skeletal structures, but no particular pattern was identified, except for the occurrence of anomalies in the head structures (e.g., opercular bones) in the higher concentrations tested. The most common anomalies were fusions of vertebrae and arches, deformed vertebrae and arches, cases of platyspondyly or ectopic mineralization. Our data also revealed that the regions of the axial skeleton mostly affected by BaP were the caudal vertebrae, caudal fin vertebrae and the caudal fin complex. These regions were also found to be more prone to deformities in other studies in zebrafish[234,448] and also in other fish species[143], for reasons that remain to be better understood, but could be related to their central role in locomotion, their close position to the swimming bladder and other developmental factors.[449–451] It is worth mentioning that several of the fish exposed to the highest

concentrations of BaP also presented a deformed operculum. Therefore, BaP-exposed fish may develop deformities that could affect locomotion and fitness, thus reducing their ability to feed or avoid predation in the nature. Although this should be further investigated, an increase on the incidence of skeletal deformities upon BaP exposure may result from an unbalanced resorption and formation during bone remodeling process or alteration in extracellular matrix components and organization[144,452–454].

Scale regeneration in zebrafish is achieved through a succession of differentiation, proliferation, and parallel routes of shape change or cell death of the osteoblast.[455] Our data showed smaller regenerated scales in fish exposed to BaP, which is consistent with a reduced bone formation by osteoblasts. It is also in agreement with published data showing that an exposure of *ex vivo* cultured zebrafish scales to 5 and 50 µM BaP (concentrations higher than those tested in this study) inhibited Sp7 activity, evidencing an effect on osteoblast differentiation that may be related to a reduced bone formation[186]. Similarly, exposure of *ex vivo* cultured goldfish scales to seawater polluted with a mixture of PAHs (including BaP at concentrations ranging from 26 to 49 ng/L) showed that osteoblast activity and marker genes were strongly affected[456]. Our data showing intense TRAP activity and regions of strong demineralization also indicated that BaP may stimulate osteoclast activity thus the resorption of the mineralized matrix. Data from literature is scarce and limited to *ex vivo* cultures of goldfish scales. While TRAP activity was unaltered in scales exposed to a mixture of PAHs[456], Mmp9 activity was decreased in scales exposed to BaP, suggesting reduced bone resorption[186]. Discrepancy on the effect of BaP on osteoclast activity and bone resorption may be related to the species (i.e., zebrafish vs goldfish), exposure time (5 vs 2 days), and biological material (i.e., regenerating vs *ex vivo* scales) used in the different studies. Based on available data, we propose that BaP exerts its osteotoxic effect through a dual action on bone cells: an impaired osteoblast differentiation resulting in a reduced scale regeneration and an increased osteoclast activity resulting in an increased scale demineralization. The combined effect would result in an abnormal bone formation and remodeling leading to smaller and misshaped scales.

BaP was also found to affect caudal fin regeneration and *de novo* bone formation. As for scale, the size of the regenerated fin and the mineralization and shape of the newly formed bone were impaired, indicating that similar mechanisms may be involved. Other toxicants have been previously shown to affect zebrafish caudal fin regeneration. TCDD inhibited caudal fin tissue regeneration in larvae at 5 dpf[457] (exposed for 3 days after amputation at 2 dpf) and in adult up to 21 dpa[458], while 3-MC not only affected tissue regeneration in adults regenerating their caudal fin but also impaired calcification[144]. However, previous studies did not evaluate the effects of PAHs on regeneration of caudal fin rays, patterning, and total mineralization area. Although the mineralized bone area of the caudal fin was not affected upon BaP exposure at all concentrations tested, analysis of µCT images revealed that the mineral density of the rays was affected from the amputation plane throughout the ray. This could be related to impaired osteoblast differentiation and/or deposition of matrix mineral. Shaping of the caudal fin rays was also affected at all concentrations tested, resulting in a proximalization of the point of the first bifurcation. Although the mechanisms of ray bifurcation during development or regeneration are not fully understood, recent studies have shown that ray branching may be controlled by either Shh/Smo (Sonic hedgehog/Smoothened) signaling[459], levels of thyroid hormone[460] and even water temperature[461]. Interestingly, hyperthyroid fish display a proximalization of the bifurcation points. In this regard, BaP is a known endocrine disruptor and several studies have shown that an exposure to BaP increases levels of thyroid hormone in rat hepatocytes[462] and of thyroid stimulating hormone (TSH) in Abu mullet[391]. Although this should be further tested, BaP effect on ray bifurcation could be related to its action on thyroid hormone homeostasis. It will be also interesting to evaluate, in future studies, which genes are involved in ray patterning plasticity that may be affected by external stressors such as temperature or contaminants (BaP in the case of this study). The lesser extent of fin regeneration in fish exposed to BaP may result from an inhibition of the pathways involved in fin regenerative outgrowth (as also suggested for TCDD[458]), a hypothesis that we did not explore in this work. Although not quantified, an hyperpigmentation was observed in regenerated fin exposed to BaP, indicating that BaP may stimulate melanocytes differentiation or proliferation, possibly through the activation of the AHR receptor as reported for TCDD[458] and ambient particulate matter, which is known to absorb many PAHs and metals[463].

To gain insights into the mechanisms of BaP osteotoxicity, transcriptomic data was collected from larvae exposed to DMSO or BaP for 3 days. Pathway enrichment of differentially expressed genes confirmed the role of xenobiotic related pathways such as phase I functionalization of compounds, phase II conjugation of compounds, glutathione conjugation, metabolism and biological oxidation, in particular the marker genes *ahr2*, *nr1i2*, *cyp1a* and *gstp1*, all up-regulated upon BaP exposure. A similar trend was reported in several *in vitro* and *in vivo* systems upon exposure to BaP but also to other PAHs. AHR and NR1I2 are xenobiotic-dependent transcription factors involved in the regulation of phase I and phase II metabolizing enzymes, which detoxify harmful compounds in order to protect the organisms. An up-regulation of these genes was also observed in zebrafish exposed to 3-MC, although to a lower extent, probably due to the different concentrations tested[144]. Besides mediating xenobiotic toxic effects, AHR has been shown to regulate several physiological and pathological processes (e.g., hematopoiesis, inflammation, immune response, detoxification and cancer) and of interest to this study, bone metabolism[464,465]. AHR is in fact expressed in osteoblast and osteoclast cells and it also plays a role in ECM homeostasis[466–468]. In this work, *ahr2* expression was assessed globally and it is therefore not possible to associate its upregulation to any specific process. Pathways related to extracellular matrix degradation, formation, and organization (e.g., collagen chain trimerization, collagen synthesis, formation and degradation, ECM degradation and formation, activation of metalloproteinases) were also enriched in BaP-treated larvae. In this regard, the altered expression of bone marker genes (i.e., *oc2*, *col1a1a*, *col2a1a*, *col10a1a* and *spp1*) coding for extracellular matrix proteins involved in bone formation and mineralization is consistent with impaired osteoblast differentiation and reduced bone formation observed in BaP-treated larvae. As observed in zebrafish exposed to 3-MC[144], BaP exposure induced, albeit only slightly, the expression of *vdrb* and *alpl*. In mammals and fish, vitamin D receptor (VDR) and alkaline phosphatase (ALP) are central to osteoblast function, activity and bone formation[469–471], and their increased expression in BaP-treated larvae may not fit the osteotoxic effect observed here. An increase of *vdrb* could however be related to its role in xenobiotic response since, in fact, VDR transactivation can be a target for several xenobiotics (such as 7-methylbenzo[α]pyrene)[472] and induce the transcription of metabolizing enzymes[473,474]. In this regard, induction of CYP1A expression by VDR activation was only reported in human monocyte/macrophage-derived cells to respond

to BaP-mediated toxicity[475,476]. Increased expression of *alpl* is probably related to liver damage as reported in fish exposed to other PAH[477]. The molecular mechanisms underlying the activation of osteoclast differentiation by BaP have never been reported in fish. In mouse *in vitro* system, BaP stimulated osteoclastogenesis through the activation of AhR and the involvement of a RANKL/AhR/c-Fos signaling axis[478,479]. Our expression data is consistent with this mechanism, with genes involved in osteoclast differentiation (*fosab*, *ctsk*) and activity (*acp5a/b* and *mmp9/13*) up regulated in BaP-treated larvae. Thus, the role of AHR/c-Fos signaling pathway in the stimulation of osteoclast activity by BaP may have been conserved throughout vertebrate evolution.

Finally, transcriptomic analysis showed a 2-fold enrichment in genes related to neutrophil degranulation. At the beginning of an acute inflammation that may result from a bacterial infection, cancers and exposure to environmental pollutants, neutrophils migrate to site of inflammation, where they release factors such as chemokine/cytokines to help other cell respond with a proper immune response, or undergo degranulation[480–482]. During degranulation, proteins such as myeloperoxidase, elastase, gelatinase, and collagenase present in the granules are released into the extracellular environment. Excessive neutrophil degranulation has been described in many inflammatory disorders, such as lung injury[483], severe asthma[484] and rheumatoid arthritis[485]. Several *in vitro/in vivo* studies in mammalian and fish systems have shown that exposure to BaP can trigger an inflammatory response[486–489], a situation confirmed here with the increased expression of well-established inflammatory markers such as *il-6* and *il-1β* in BaP-treated larvae. Our data also indicate that the number of neutrophils increased upon BaP exposure in the whole-larvae and in the fish trunk. Again, expression data further supported BaP effect on neutrophils, as neutrophil marker genes such as *mpx*, *lyz* and *mmp9* were up regulated in BaP-treated larvae. Further studies should determine whether neutrophil activation results from BaP-induced inflammation or AHR activation in fish. Several studies in mammalian models have shown that AHR signaling stimulates neutrophils recruitment[490,491] and, recently, that Ahr is functional in teleost (e.g., rainbow trout) immune cells[492]. An interaction between neutrophils and the opercular bone was observed in our study. Interestingly, the number of interacting neutrophils increased in fish exposed to BaP. This is to the best of our knowledge, the first evidence (in fish

and in any *in vivo* model) that neutrophils may interact directly with bone structures. Whether they interact with osteoblasts or ECM remains to be established in our system, but *in vitro* studies can already give us some hints. Allaeys et al. (2011)[429] showed that exposure of human osteoblast (grown from trabecular bone explants) to monosodium urate (crystal deposited in chronic gut disease) promoted neutrophils adherence to osteoblast. It has also been suggested that neutrophils induced osteoblast retraction leaving the ECM more vulnerable to active osteoclast, a process that leads to an imbalanced bone formation/resorption. A more recent study by Bastian et al. (2018)[430] showed that neutrophils inhibited the synthesis of ECM mineralization by human bone marrow stromal cells (BMSCs). These authors also showed that co-culture of BMSCs with neutrophils induced a decrease in cell density and both ALP activity and ECM mineralization were significantly reduced. A stimulation of osteoclast differentiation by neutrophils was also reported in mice, both *in vivo* and *in vitro*. In this regard, Kim et al. (2020)[431] showed in a mouse periodontitis and air pouch model, that the presence of neutrophils could induce RANKL expression in periodontal tissue and stimulate osteoclast formation. Sugisaki et al. (2020)[432] showed that human neutrophils enhanced osteoclast differentiation in co-cultures of mouse bone marrow cells and osteoblasts. We propose that neutrophils play a major role in BaP osteotoxicity through a mechanism that probably involves an initial inflammatory event induced by BaP, a recruitment of neutrophils following inflammation and an increased interaction of neutrophils with bone structures, resulting in less bone formed or more bone lost. A simple scheme of the molecular mechanisms of BaP osteotoxicity in zebrafish is presented in Fig. 6.8, where the activation of AHR and PXR signaling pathways regulates not only the expression of xenobiotic metabolizing enzymes but also genes involved in the differentiation and function of bone forming and resorbing cells and neutrophils.

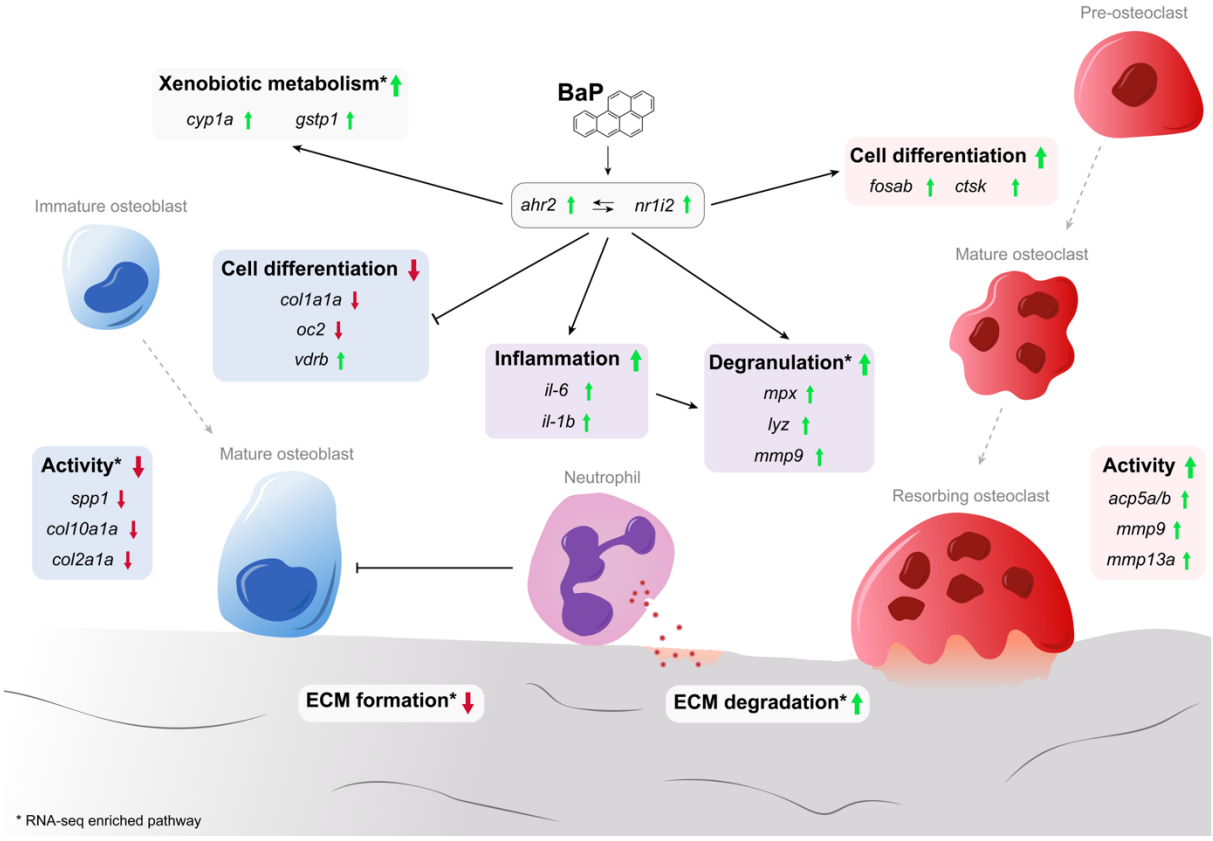

Figure 6.8. Schematic overview of the possible mechanisms underlying the BaP osteotoxicity in zebrafish larvae. Vertical arrows after gene names indicate increased (upward pointing green arrow) and decreased (downward pointing red arrow) gene expression. Asterisks indicate enriched pathways supported by RNA-seq.

6.6. CONCLUSIONS

This study demonstrated the strong osteotoxic effects of BaP throughout zebrafish development and regeneration. By inhibiting osteoblast maturation and ECM mineralization and stimulating osteoclast activity, BaP impacted both bone formation and resorption, thus bone remodeling. Consequences of BaP on bone remodeling were seen both after a long exposure (27 days) in developing larvae, i.e., an increased incidence and severity of skeletal deformities in the axial skeleton, and after a short exposure (5 days) in regenerating adults, leading to misshaped and demineralized newly formed fin rays and scales. Transgenic and transcriptomic approaches helped us to gain insights into cellular and molecular mechanisms underlying BaP osteotoxicity. We believe that, besides the activation of xenobiotic and metabolic pathways through Ahr2 and/or Pxr, which may negatively impact extracellular matrix formation and organization, BaP activates inflammatory mechanisms that recruit neutrophils, which affect both osteoblast and osteoclast activity, possibly through a direct interaction of the neutrophils with the bone matrix. Future studies should aim at further exploring the crosstalk mechanisms between immune system and bone, in particular characterizing the role of neutrophils in bone homeostasis. In a more global context, it would be of utmost interest to investigate whether pollutants of the PAH family, especially those with 2 or 3 rings (e.g., naphthalene and anthracene) or those with a more complex structure, have a similar effect on fish bone.

Chapter 7

Conclusions and perspectives

There is compiling evidence that the increasing presence of microplastics in the aquatic ecosystem represents a major issue for aquatic organisms, the environment and eventually for human health. Beside the necessity to drastically reduce plastic pollution, there is also the need to assess the biological effects of this pollution and get new knowledge as scientific data are required to support environmental regulations and policies. Ongoing research effort should also address the raising concern related to the capacity of the organic pollutants cohabiting with the microplastics in the aquatic environment to adsorb onto plastic particles, creating a new route for toxic compounds to enter the food web. To contribute to the acquisition of knowledge on the adverse effects of (micro)plastics in fish, we assessed developmental and biological effects of a long-term exposure to PE microparticles – pristine or contaminated with BaP – on zebrafish development. A stand-alone housing system useful to the scientific community to perform state-of-the-art toxicological studies in small teleosts and ImageJ macros useful to the automatization and standardization of image analysis and the production of accurate data on the morphology of developing or regenerating bone structures were developed. Using these tools, data relevant to microplastic and benzo[a]pyrene osteotoxicity were generated and evidence of intergenerational effect were collected.

7.1. ZEB316, a stand-alone housing system to perform state-of-the-art studies on microplastics and organic pollutants

The first challenge encountered at the beginning of this work was to maintain in optimal water conditions the zebrafish larvae, juveniles, and adults during a long-term exposure to microplastics. Indeed, most of the studies that evaluated microplastics effect on fish have used static water conditions, which are generally associated with poor water quality due to the accumulation of molecules produced by fish metabolism (e.g., ammonium, nitrites and nitrates), conditions not compatible with a long-term exposure. To avoid the deterioration of water quality, large volumes of water have to be regularly renewed or water has to be cleaned using mechanical and biological filters in a water recirculation system. Unsatisfied with the commercial solutions available to us – these housing systems are made with plastic materials that may interfere with the experiments – we designed and developed the ZEB316, a stand-alone housing system built with inert materials to perform state-of-the-art

toxicological studies. ZEB316 system was showed to provide optimal water parameters and promote adequate fish growth, while efficiently retaining microplastic particles introduced into the system through the food diet, thus preventing particle accumulation which may interfere with experimental conditions. We could demonstrate that ZEB316 system is a cost-effective, easy-to-build and easy-to-maintain alternative to commercial housing systems, and is also an effective solution to perform state-of-the-art toxicological experiments aiming at studying the environmental pollution by microplastics and their effect on aquatic organisms. Design and building parameters were made freely available to the scientific community and the supplier of commercial housing systems for zebrafish has already contacted us to enquire about the possibility to produce it at an industrial scale. There is still room for some improvements and the future version of the ZEB316 system should try to get rid of the few plastic parts that are still used in the current version, e.g., by favoring plastic-free equipment (water pump, heater, and UV sterilizer) and by developing silicone-free glass tanks. Electronic components could also be implemented to automatically monitor or adjust water parameters and sump water level.

7.2. ZFBONE, a toolset of ImageJ macros to perform semi-automatic morphometric analysis

The second challenge encountered during this work was to analyze the numerous bright-field/fluorescence microscopy images acquired throughout the different experimental assays and at the origin, of most of the data presented in this dissertation. While imaging is now a common technique in most research laboratories, generating a large amount of data, image analysis is often a bottleneck due to the lack of dedicated automatic/semi-automatic tools to speed up the process of data acquisition. In the absence of tools to process our images and analyze zebrafish bone structure morphometrics, we designed and developed macros using the freely available ImageJ platforms. Our aim was also to reduce user bias to increase data reproducibility, toward the standardization of experimental methodologies. Macros are assembled in ZFBONE toolset freely available to the scientific community through GitHub. They allow users to assess, from 2D images, morphometric parameters of several bone structures (e.g., operculum, caudal fin rays and scales) but also the extent and the intensity of bone-specific colorations. Other macros – not included in

ZFBONE toolset – were developed to acquire, for example, morphometric parameters from fish eggs, or to identify and count goblet cells in histological sections. Macros developed within the scope of this work, provide the zebrafish community a set of simple and robust tools to acquire, in a timely manner, meaningful and accurate data. Macros of ZFBONE toolset have been successfully implemented in several research laboratories across Europe and some labs have contacted us to develop macros dedicated to the morphometric analysis of non-calcified fish tissues (e.g., heart) or fish staining (e.g., marking dyes). In the future ZFBONE toolset should be enriched with new functionalities, e.g., a macro to analysis skeletal deformities or a macro that uses landmarks to assess whole skeleton morphometrics and not only the morphology of individual structures. ZFBONE, could also be re-developed in a more advance programming language (e.g., Java) to overcome the limitations of the ImageJ scripting language and provide more versatile tools, e.g., a more friendly and sophisticated graphical user interface and a better handling of wrong or unexpected user inputs.

7.3. Polyethylene microplastics have an impact on zebrafish development

Data on the effect of microplastic ingestion in fish are controversial, with some studies reporting adverse effects on fish development, behavior, oxidative stress and intestinal damage (normally higher in combination with pollutants), while others showed limited or no impact. A comprehensive analysis of literature data revealed several bottlenecks related to fish housing conditions (i.e., experiments using static water conditions with poor water quality or experiments using housing systems with plastic components), duration of the exposure (i.e., mostly short-term exposure trials of variable duration), type of exposure (i.e., mostly waterborne exposure with heterogenous levels of ingestion), and developmental stages (mostly larval stages, rarely throughout a complete developmental window). We decided to perform an experiment using zebrafish, housed in a water recirculating system specifically designed for microplastic toxicological studies, fed diets supplemented with PE microplastics over a long period of time covering larvae, juvenile and adult stages. To address a possible synergistic toxicity between microplastics and organic pollutants, biological effects of microplastics contaminated with BaP were also assessed. We demonstrated that long-term dietary exposure to pristine/contaminated polyethylene

microplastics has the potential not only to jeopardize fish growth and reproductive performance, but also to produce intergenerational effects. We also provided the first evidence of adverse effects of microplastics on fish axial skeleton and bone compartment, with osteotoxic outcomes aggravated by the presence of organic contaminants adsorbed on the surface of the microplastics. Gene expression analysis evidenced a role for the xenobiotic pathway and antioxidant response in the mechanisms underlying the harmful effects triggered by pristine and/or contaminated microplastics. Future studies should aim at confirming the adverse effects of pristine/contaminated microplastics on bone homeostasis but also at assessing a possible effect on bone remodeling and shaping using *in vivo* systems currently being optimized. A deeper knowledge of the mechanisms underlying microplastic osteotoxicity should also be sought, for example through the global analysis of gene expression by RNA-Seq instead of a candidate gene approach. The use of transgenic reporter lines for bone marker genes instead of a wild-type line could also bring more meaningful data on the molecular players of microplastic toxicity. Finally, future studies should also aim at testing a wider range of plastic polymers and contaminants with the capacity to absorb onto microplastics.

7.4. New insights into BaP osteotoxicity

To follow up the results collected from the dietary exposure of zebrafish to microplastics showing an increased osteotoxicity upon MP contamination by BaP and to gain insights into the mechanisms underlying BaP effect on bone, we simplified the experimental procedures and exposed zebrafish directly to BaP without using microplastics and fish feed as vehicles. Waterborne exposure to BaP was performed in static water conditions (short-term exposure) and a wide range of concentrations was used to determine lethal and effective concentrations. We evaluated mineralization status, bone cell activity using transgenic reporter lines, transcriptomics, and bone marker gene expression, and could confirm the strong osteotoxic effect of BaP throughout zebrafish development but also on bone regeneration. At a cellular level, we demonstrated that BaP affects bone homeostasis by inhibiting osteoblast maturation and ECM mineralization and stimulating osteoclast activity, but also by activating inflammatory mechanisms that recruit neutrophils. We also provided for the first time evidence of a direct interaction of the neutrophils with

the bone matrix. At a molecular level, we demonstrated the activation of xenobiotic and metabolic pathways through Ahr2 and/or Pxr, and confirmed BaP effect on the expression of inflammation markers and neutrophil degranulation genes. Future studies should aim at further exploring the crosstalk mechanisms between immune/inflammation system and bone, in particular characterizing the role of neutrophils in bone homeostasis. It would be of utmost interest to investigate whether neutrophil ablation would rescue the bone phenotype observed in this work and which biochemical signal is involved in their interaction with bone structures.

Appendix

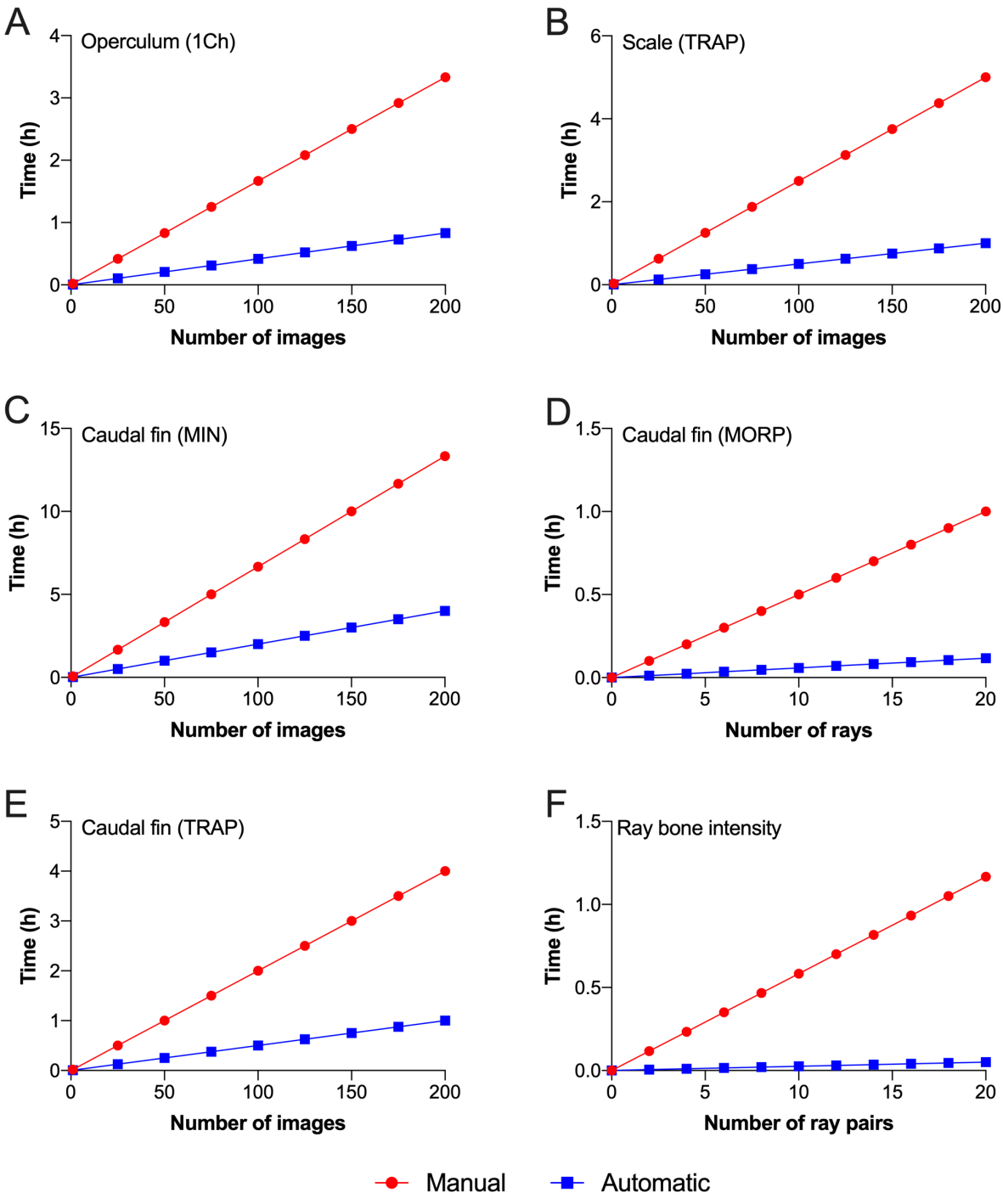

Supplementary Figure 3.1. Predicted time benefit of automatic (using ZFBONE toolset) *vs.* manual (using built-in ImageJ tools) analysis. Time spent to analyze: (**A**) fluorescence images of a developing operculum stained with AR-S; (**B**) bright-field images of a regenerating scale stained with TRAP; (**C**) bright-field images of a regenerating caudal fin stained with AR-S; (**D**) fluorescence images of a regenerating caudal fin stained with AR-S, where a single ray was analyzed for each image; (**E**) bright-field images of a regenerating caudal fin stained with TRAP; (**F**) radiographic images of a caudal fin, where the intensity of a single ray was measured for each image.

Supplementary data – Chapter 5

Supplementary table 5.1. Gene-specific primers used to analyze gene expression by qPCR.

Genes		Sequence (5′-3′)	GenBank accession no.
ahr2	Fw:	CCAACAACCATCAATCAGTCAGAAC	NM_131264
	Rev:	TGCCAGCCAGGCGGTCCTGC	
nr1i2	Fw:	TAGGCAACGGCAGCATTCGC	NM_001098617
	Rev:	CATCACGAGCAGACACGGCG	
cyp1a	Fw:	CTGCGAACATTTTCAACGGTG	NM_131879
	Rev:	CCATCGGCTTTCATAACAGAGTG	
gstp1	Fw:	GTGCTGTTTCAGTCCAACGCC	NM_131734
	Rev:	CGTCGTTCATCACGTCAATGAGGG	
cat	Fw:	TATCAGGGATACGCTTCTGTTTCCG	NM_130912
	Rev:	ACTGAACAGGAAAGACACCTGGTG	
gpx1a	Fw:	GAGGCACAACAGTCAGGGATT	NM_001007281
	Rev:	CTTCATTCTTGCAGTTCTCCTGGT	
sod1	Fw:	TCCTTCTCATGAATCACCATGGTCC	NM_131294
	Rev:	GCCAACCGATAGTGTGAGACACG	
sod2	Fw:	AGGCTCTGGCCAAGGGTGATG	NM_199976
	Rev:	TCCAACAGCTCACCCTGTGGTTC	
hsp70	Fw:	GCACAAGAAGGACATCAGTCAGA	NM_131397
	Rev:	GGATGCCCTCGTACAGAGAGT	
hsp90	Fw:	GGTACCAAAGTCATTCTCCACCTT	NM_131328
	Rev:	CCTCAAGATCCACCTCTTTTTCTC	
sp7	Fw:	GCTAAGTCCAGGGCAGGCTCAG	NM_212863
	Rev:	CAATGGCGTGAAATCAGGAGTGTAAC	
oc2	Fw:	CCAACTCCGCATCAGACTCCGCATCA	NM_001291889
	Rev:	AGCAACACTCCGCTTCAGCAGCACAT	
spp1	Fw:	CACAGACAGCGCAGATGACACT	NM_001002308
	Rev:	CCCCGGCCTGTGTTGATAATG	
col1a1a	Fw:	GCTTCATTGCCCAGCCACAGGA	NM_199214
	Rev:	GCAGGGTTCTTCTTGGTGCCGTCT	
col10a1a	Fw:	ATACCCAGTTCTTGTCAAAAGTCCA	NM_001083827
	Rev:	GATCATAATGCTGCTCTGCGTT	
mmp9	Fw:	CTGAACCCACTGCTCCTCAACC	NM_213123
	Rev:	CCGTCCTTGAAGAAGTGAAGCTCC	
eef1a1l1	Fw:	TTGAGAAGAAAATCGGTGGTGCTG	NM_131263
	Rev:	GGAACGGTGTGATTGAGGGAAATTC	
rps18	Fw:	AACACGAACATTGATGGAAGACG	NM_173234
	Rev:	ATTAGCAAGGACCTGGCTGTATTT	

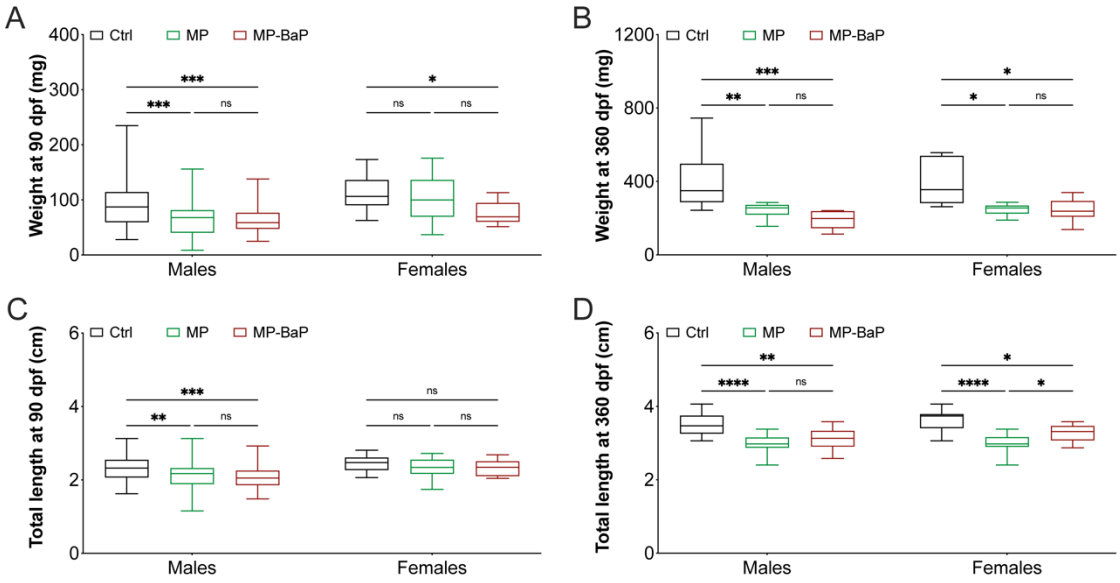

Supplementary Figure 5.1. Weight (**A, B**) and total length (**C, D**) at 90 dpf (**A, C**) and 360 dpf (**B, D**) of males and females zebrafish fed from 8 dpf onwards with Ctrl (ZEBRAFEED), MP (ZEBRAFEED supplemented with pristine microplastics) or MP-BaP (ZEBRAFEED supplemented with microplastics spiked with BaP). Asterisks indicate values statistically different between diets according to two-way ANOVA followed by Tukey's multiple comparison test (* $p<0.05$; ** $p<0.01$; *** $p<0.001$; **** $p<0.0001$). Values are presented as the median ± min and max value. At 90 dpf, n≥55 for males and n≥9 for females; at 360 dpf, n≥11 for males and n≥9 for females.

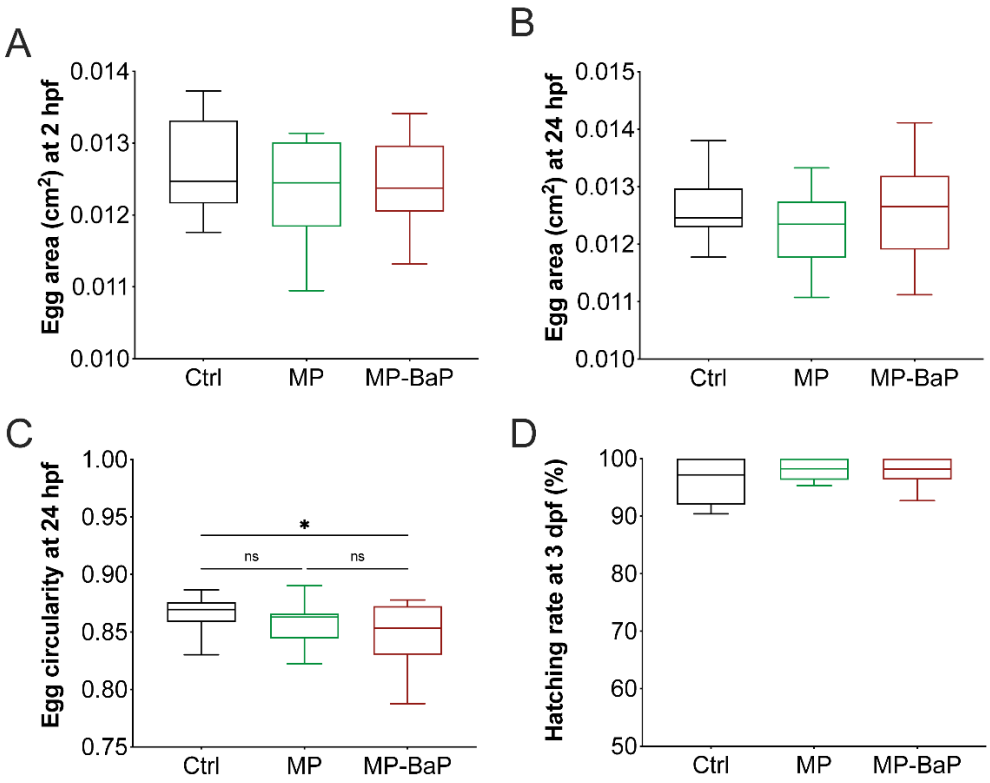

Supplementary Figure 5.2. reproductive performance of sexually mature 3-4-months zebrafish fed from 8 dpf onward with Ctrl (ZEBRAFEED), MP (ZEBRAFEED supplemented with pristine microplastics) or MP-BaP (ZEBRAFEED supplemented with microplastics spiked with BaP). (**A, B, C**) Egg area at 2 and 24 hpf and egg circularity at 24 hpf assessed through the morphometric analysis of bright-field images (n≥8; pools of 20 eggs each). (**D**) Egg hatchability (i.e., number of hatched eggs/number of fertilized eggs) at 3 dpf expressed in % over Ctrl (n≥8). Asterisks indicate values statistically different between diets according to one-way ANOVA followed by Tukey's multiple comparison test (* $p<0.05$) Values are presented as the median ± min and max value.

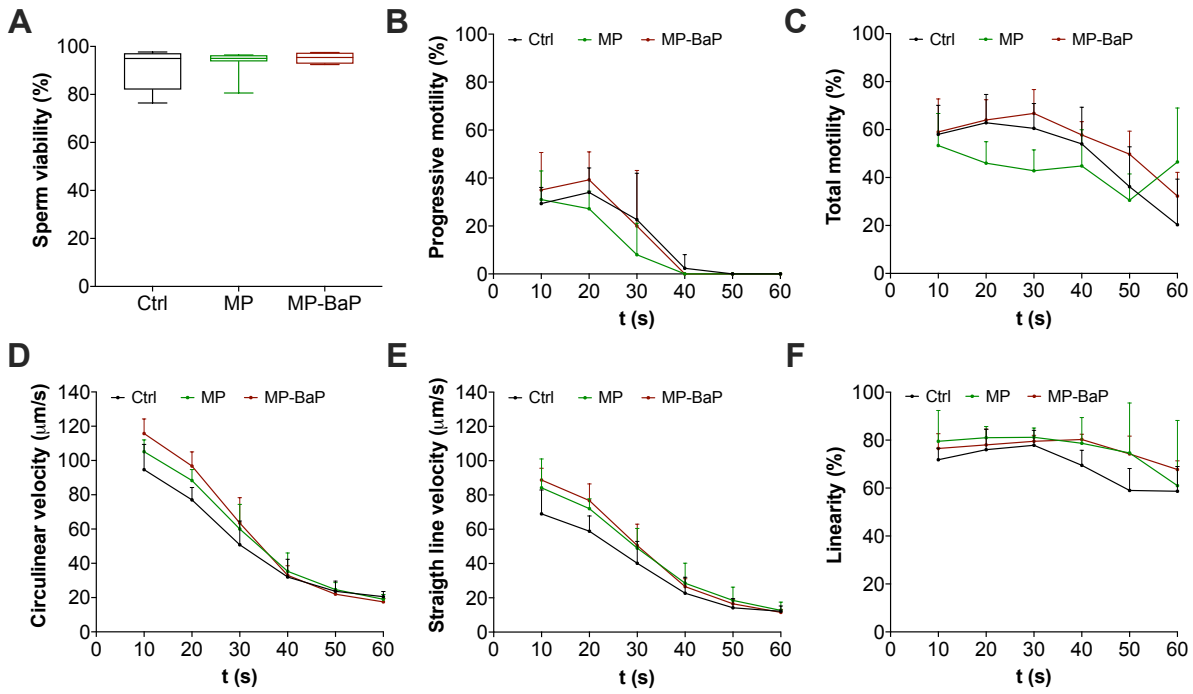

Supplementary Figure 5.*3*. Sperm quality of sexually mature 3-4 months males fed from 8 dpf onward with Ctrl (ZEBRAFEED), MP (ZEBRAFEED supplemented with pristine microplastics) or MP-BaP (ZEBRAFEED supplemented with microplastics spiked with BaP). Sperm viability (**A**), progressive motility (**B**), total motility (**C**), curvilinear velocity (**D**), straight line velocity (**E**) and linearity (**F**). While sperm viability was assessed throughout cell sorting, all the other sperm parameters were assessed throughout CASA system. Sperm was monitored from 0 to 60 s, n≥6.

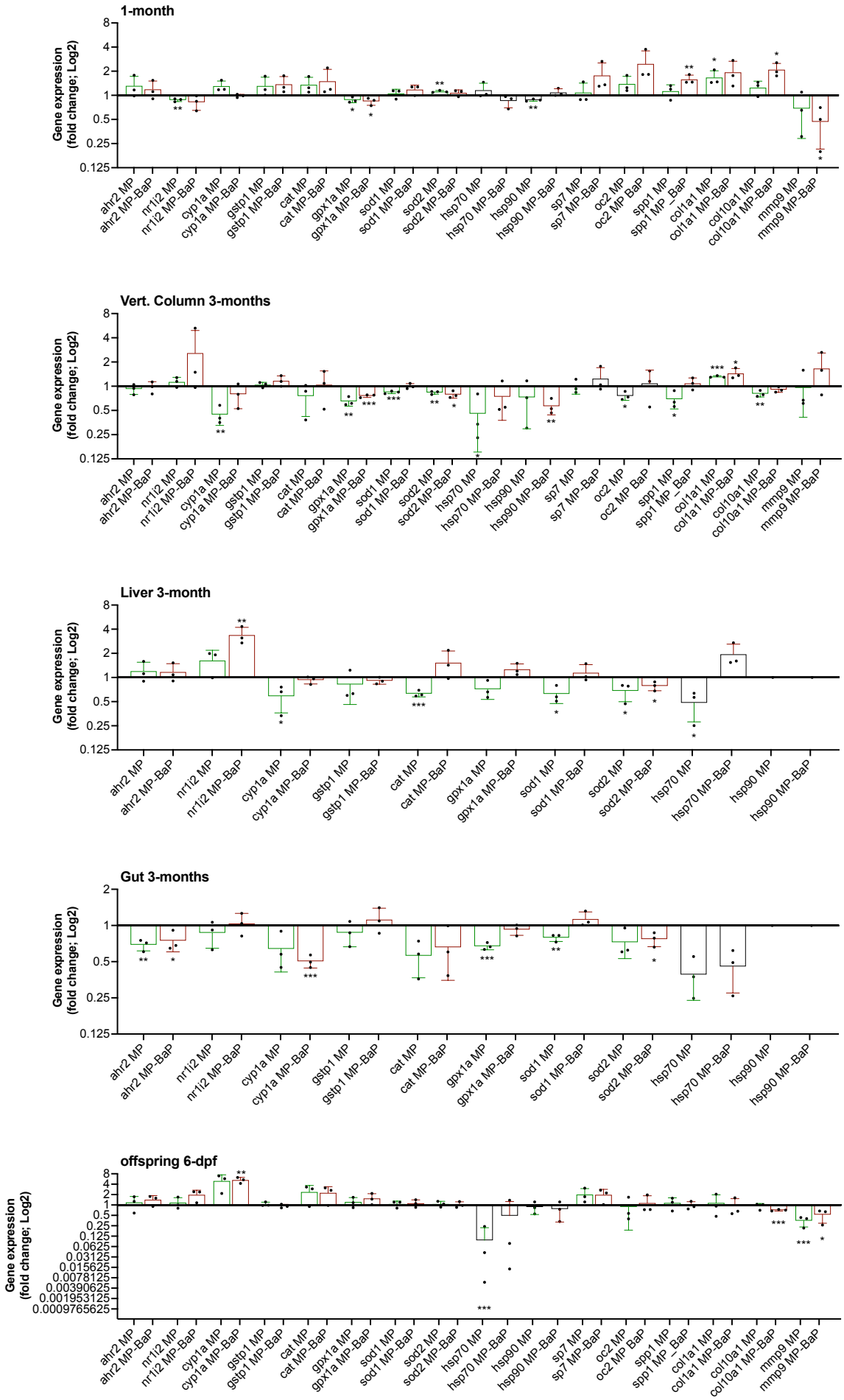
1-month
Vert. Column 3-months
Liver 3-month
Gut 3-months
offspring 6-dpf
Gene expression (fold change; Log2)
ahr2 MP
ahr2 MP-BaP
nr1i2 MP
nr1i2 MP-BaP
cyp1a MP
cyp1a MP-BaP
gstp1 MP
gstp1 MP-BaP
cat MP
cat MP-BaP
gpx1a MP
gpx1a MP-BaP
sod1 MP
sod1 MP-BaP
sod2 MP
sod2 MP-BaP
hsp70 MP
hsp70 MP-BaP
hsp90 MP
hsp90 MP-BaP
sp7 MP
sp7 MP-BaP
oc2 MP
oc2 MP BaP
spp1 MP
spp1 MP _BaP
col1a1 MP
col1a1 MP-BaP
col10a1 MP
col10a1 MP-BaP
mmp9 MP
mmp9 MP-BaP

Supplementary Figure 5.4. Gene expression levels in 30 dpf juveniles and tissues (gut, liver, and vertebral column) of 90 dpf adult zebrafish fed from 8 dpf onwards with Ctrl (ZEBRAFEED), MP (ZEBRAFEED supplemented with pristine microplastics) or MP-BaP (ZEBRAFEED supplemented with microplastics spiked with BaP), and in 6-dpf offspring larvae born from parents fed experimental diets. The averaged expression of eef1a1l1 and rps18 housekeeping genes was used to normalize gene expression levels. Asterisks indicate values statistically different between diets according to Student's t-test (* $p<0.05$; ** $p<0.01$; *** $p<0.001$). Values are presented as mean expressed in Log2 over the control, n=3.

Supplementary data – Chapter 6

Supplementary table 6.1. Gene-specific primers used to analyze gene expression by qPCR.

Genes		Sequence (5′-3′)	GenBank accession no.
ahr2	Fw:	CCAACAACCATCAATCAGTCAGAAC	NM_131264
	Rev:	TGCCAGCCAGGCGGTCCTGC	
cyp1a	Fw:	CTGCGAACATTTTCAACGGTG	NM_131879
	Rev:	CCATCGGCTTTCATAACAGAGTG	
gstp1	Fw:	GTGCTGTTTCAGTCCAACGCC	NM_131734
	Rev:	CGTCGTTCATCACGTCAATGAGGG	
nr1i2	Fw:	TAGGCAACGGCAGCATTCGC	NM_001098617
	Rev:	CATCACGAGCAGACACGGCG	
nr1i2 X2	Fw:	TGCCCTGAAGAACACACTGC	XM_021478724
	Rev:	TCAACGGCGGAATGCTGAAA	
mmp9	Fw:	CTGAACCCACTGCTCCTCAACC	NM_213123
	Rev:	CCGTCCTTGAAGAAGTGAAGCTCC	
mmp13a	Fw:	TGTCAGTGGCAGAGGTGGATGACTC	NM_001290479
	Rev:	CGCCACCAGGAACAGATTGTAATATTGAG	
tnfα	Fw:	AACAAGATGGAAGTGTGCTGAGAC	NM_212859.2
	Rev:	TGGTCATCTCTCCAGTCTAAGGTC	
il6	Fw:	TGAAGACACTCAGAGACGAGCAGTT	NM_001261449
	Rev:	AGGTTTGAGGAGAGGAGTGCTGAT	
il1ß	Fw:	ATGGCGAACGTCATCCAAGAGCG	NM_212844
	Rev:	CATGCTGAAGCGCACTTTCAAGTCG	
mpx	Fw:	GATGAACAACACTGAACTAGCCC	NM_001351837
	Rev:	CAAACCACAACCTATCGCCA	
lyz	Fw:	AGTGGCCTGTTCAGACTTGCTTAAC	NM_139180
	Rev:	AGAATCCCAGGTTTCCCATGATTTC	
acp5a	Fw:	ATAGAGACCGCTACAGCCCGCA	NM_214773
	Rev:	TGCCAGCAATGACGTACCAAGG	
acp5b	Fw:	GTGGTTGGTCACTATCCCATCTG	NM_001002452
	Rev:	GAACGAACTCCCATCATCCTCTCT	
ctsk	Fw:	GGATTCCCTCTGCTGGTGCTG	NM_001017778
	Rev:	GCATGTTCTTCTCCCAAATCGTCC	
fosab	Fw:	CAATCACGACCTCTTCCAGCAGCC	NM_205569
	Rev:	AACCGAGCGAGCCGTTTCCA	
bmp2b	Fw:	GAGGAACTTAGGAGACGACGGGAACGC	NM_131360
	Rev:	TCTCGGGAATGAGTCCAACGGCAC	
runx2b	Fw:	TCAGGAATGCCTCAGGGGTTATG	NM_212862
	Rev:	CTTGCGGTGGGTTTGTGAATACT	
oc1 / bglap	Fw:	TTTATAGGCGGCGATGATTCC	NM_001083857
	Rev:	GAAGCGAACATGAAGAGTCTGACAGTCC	
oc2 / bglapl	Fw:	CCAACTCCGCATCAGACTCCGCATCA	NM_001291889
	Rev:	AGCAACACTCCGCTTCAGCAGCACAT	
sp7	Fw:	GCTAAGTCCAGGGCAGGCTCAG	NM_212863
	Rev:	CAATGGCGTGAAATCAGGAGTGTAAC	
alpl	Fw:	TTCCTCTGCGGTGTCAAAGCCAA	XM_005169273
	Rev:	AAGCAGCACTCGGGGTGGCAT	
vdra	Fw:	GAATCCACAGTAAACGGTGATGCC	NM_130919
	Rev:	TCATACTGCGCCTGAAGAAACCC	
	Fw:	TCAAGTGCCAGATGAGTTCGACC	

Genes		Sequence (5′-3′)	GenBank accession no.
vdrb	Rev:	TGAAGAAGCCTTTGCAGCCCT	NM_001159985
spp1	Fw:	CACAGACAGCGCAGATGACACT	NM_001002308
	Rev:	CCCCGGCCTGTGTTGATAATG	
col1a1a	Fw:	GCTTCATTGCCCAGCCACAGGA	NM_199214
	Rev:	GCAGGGTTCTTCTTGGTGCCGTCT	
col2a1a	Fw:	CAGGAAGAGTTTGGCGGCTGT	NM_131292
	Rev:	GACACGGCACGGTTCTGGTT	
col10a1a	Fw:	ATACCCAGTTCTTGTCAAAAGTCCA	NM_001083827
	Rev:	GATCATAATGCTGCTCTGCGTT	
eef1a1l1	Fw:	TTGAGAAGAAAATCGGTGGTGCTG	NM_131263
	Rev:	GGAACGGTGTGATTGAGGGAAATTC	
rps18	Fw:	AACACGAACATTGATGGAAGACG	NM_173234
	Rev:	ATTAGCAAGGACCTGGCTGTATTT	

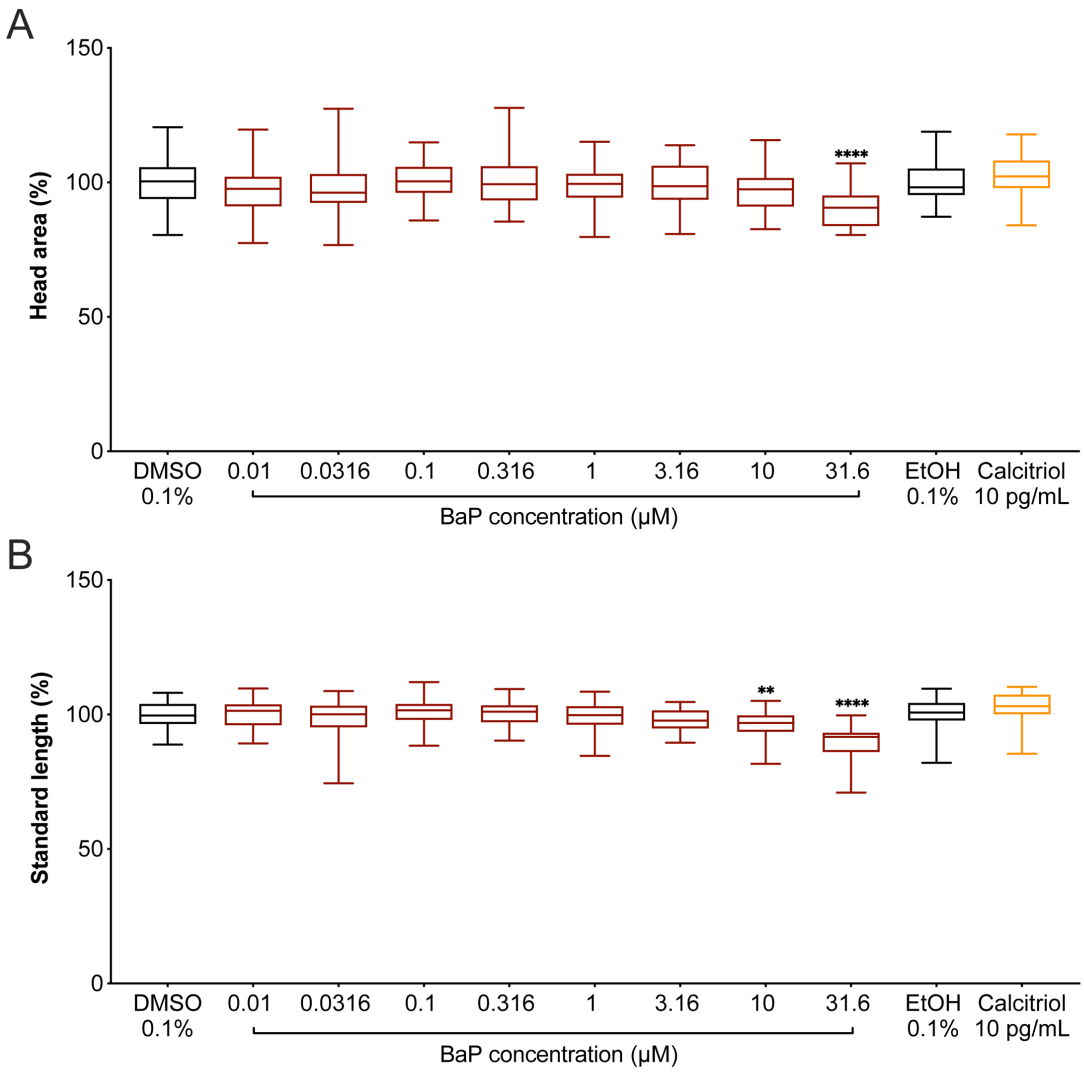

Supplementary Figure 6.3. Head area (**A**) and standard length (**B**) of zebrafish larvae exposed to increasing concentrations of BaP from 3 to 6 dpf. Data was determined through morphometric analysis of fluorescence images of AR-S stained larvae (head area) and bright-field images (standard length). DMSO and ethanol were used as vehicle for BaP and calcitriol, respectively. P-value calculated using one-way ANOVA followed by Dunnett's multiple comparison test for BaP/DMSO and Student's t-test for calcitriol/ethanol. Values are presented as median and quartiles (n ≥ 25).

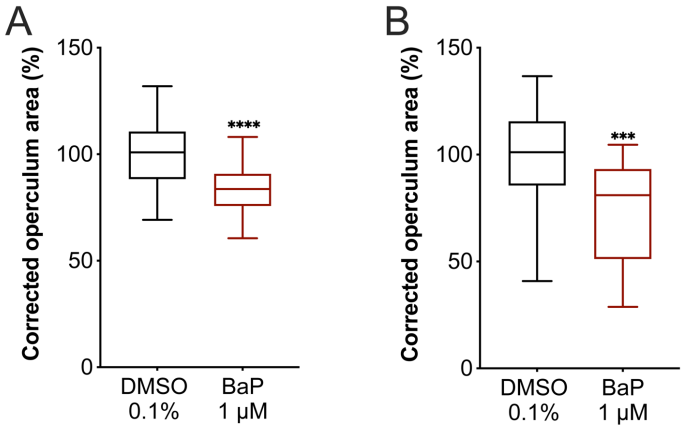

Supplementary Figure 6.2. Operculum growth in zebrafish transgenic larvae exposed to 1 µM BaP or 0.1% DMSO from 3 to 6 dpf. (**A**) Area of the operculum in *Tg(Ola.Sp7:mCherry-Eco.NfsB)*^{pd46} larvae determined through morphometric analysis of calcein stained larvae and corrected by the area of the head. (**B**) Area of the operculum in *Tg(Ola.osteocalcin:EGFP)*^{hu4008} determined through morphometric analysis of AR-S stained larvae and corrected by the area of the head. Asterisks indicate values significantly different from control values (Student's t-test; ***p < 0.001; ****p < 0.0001). Values are presented as mean ± SD (n ≥ 18).

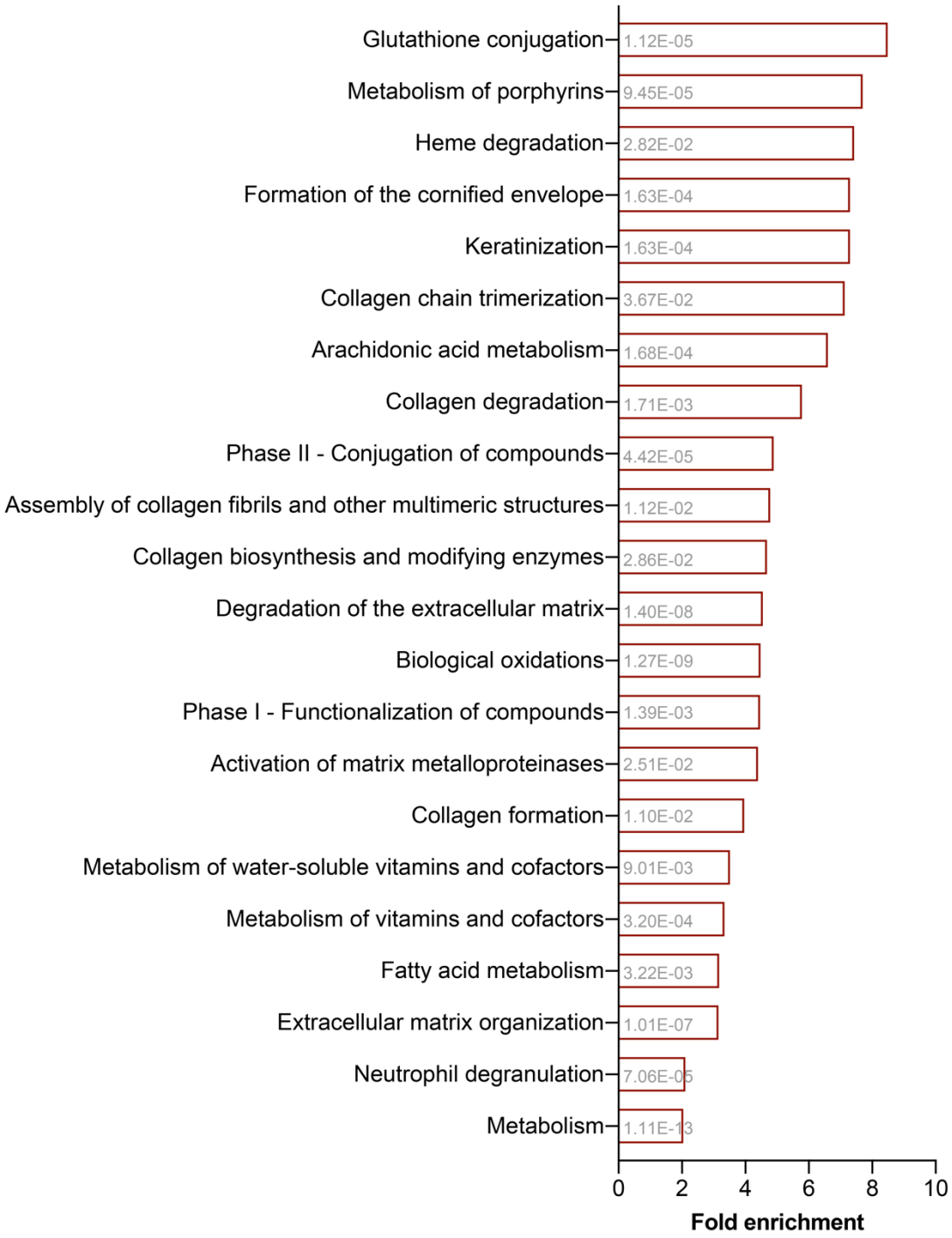

Supplementary Figure 6.3. Pathway enriched in zebrafish larvae exposed to 1 µM BaP from 3 to 6 dpf. Gene ontology analyses were performed using PANTHER (Protein Analysis THrough Evolutionary Relationships) and pathway enrichment was determined using REACTOME classification system. Ensembl zebrafish gene IDs of differentially expressed genes exhibiting a fold change greater than 2 and lower than 0.5 in RNA-seq dataset were used as input data. Over-representation was tested using Bonferroni correction for multiple testing, p-value appears in grey.

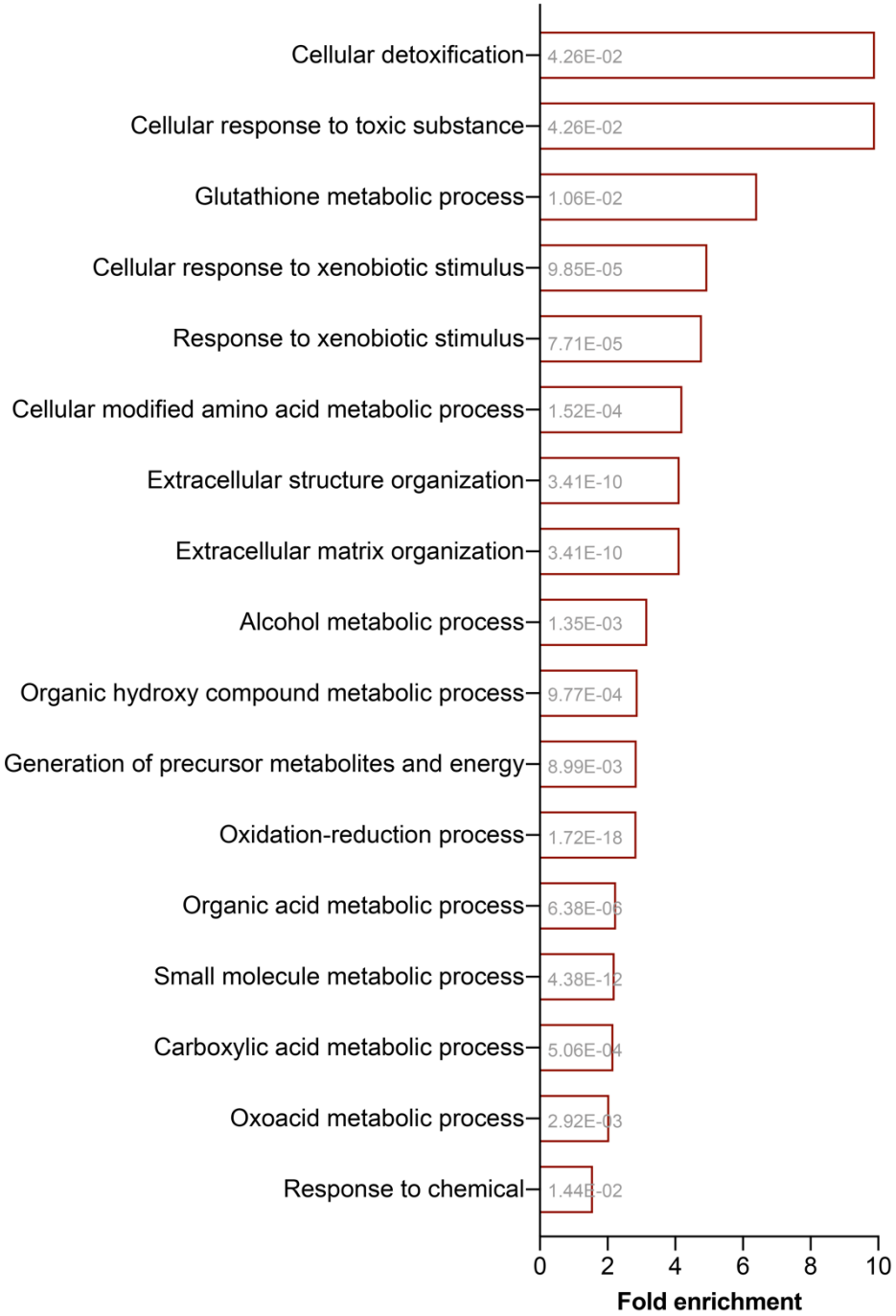

Supplementary Figure 6.4. Over-represented biological processes in zebrafish larvae exposed to 1 µM BaP from 3 to 6 dpf. Gene ontology analyses were performed using PANTHER (Protein Analysis THrough Evolutionary Relationships) and biological processes were determined using Gene Ontology (GO) classification system. Ensembl zebrafish gene IDs of differentially expressed genes exhibiting a fold change greater than 2 and lower than 0.5 in RNA-seq dataset were used as input data. Over-representation was tested using Bonferroni correction for multiple testing, p-value appears in grey.

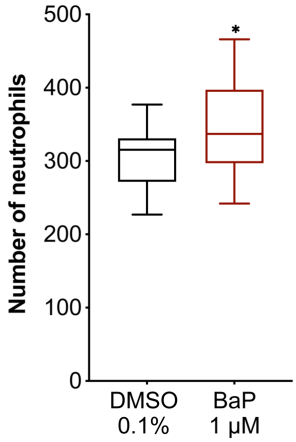

Supplementary Figure 6.5. Number of neutrophils in *TgBAC(mpx:EGFP)*^{i114} zebrafish whole-larvae exposed to BaP from 3 to 6 dpf. P-value calculated using Student's t-test. Values are presented as median and quartiles (n=18).

References

1. Plastics Europe - Association of Plastic Manufacturers (Organization). Plastics – the Facts 2020. An analysis of European plastics production, demand and waste data. PlasticEurope. 2020.
2. Geyer R. Production, use, and fate of synthetic polymers. In: Plastic Waste and Recycling. Elsevier; 2020. p. 13–32.
3. Geyer R. A Brief History of Plastics. In: Mare Plasticum - The Plastic Sea. Cham: Springer International Publishing; 2020. p. 31–47.
4. Lili F, Matthew F, editors. Plastic atlas. Facts and figures about the world of synthetic polymers. [Internet]. Second edi. Heinrich Böll Foundation. 2019. 52 p.
5. Wayman C, Niemann H. The fate of plastic in the ocean environment-a minireview. Environ Sci Process Impacts. 2021;23(2):198–212.
6. Geyer R, Jambeck JR, Law KL. Production, use, and fate of all plastics ever made. Sci Adv. 2017;3(7):e1700782.
7. Cole M, Lindeque P, Halsband C, Galloway TS. Microplastics as contaminants in the marine environment: A review. Mar Pollut Bull. 2011;62(12):2588–97.
8. Brydson JA. Plastics Materials 7th Edition. Vol. 7, Elsevier. 1999.
9. Ronca S. Polyethylene. In: Brydson's Plastics Materials. Elsevier; 2017. p. 247–78.
10. Erni-Cassola G, Zadjelovic V, Gibson MI, Christie-Oleza JA. Distribution of plastic polymer types in the marine environment; A meta-analysis. J Hazard Mater. 2019;369:691–8.
11. de Haan WP, Sanchez-Vidal A, Canals M. Floating microplastics and aggregate formation in the Western Mediterranean Sea. Mar Pollut Bull. 2019;140:523–35.
12. Shahul Hamid F, Bhatti MS, Anuar N, Anuar N, Mohan P, Periathamby A. Worldwide distribution and abundance of microplastic: How dire is the situation? Waste Manag Res. 2018;36(10):873–97.
13. Pabortsava K, Lampitt RS. High concentrations of plastic hidden beneath the surface of the Atlantic Ocean. Nat Commun. 2020;11(1):1–11.
14. Pascall MA, Zabik ME, Zabik MJ, Hernandez RJ. Uptake of polychlorinated biphenyls (PCBs) from an aqueous medium by polyethylene, polyvinyl chloride, and polystyrene films. J Agric Food Chem. 2005;53(1):164–9.
15. Agboola OD, Benson NU. Physisorption and Chemisorption Mechanisms Influencing Micro (Nano) Plastics-Organic Chemical Contaminants Interactions: A Review. Front Environ Sci. 2021;9(May):1–27.
16. Rochman CM, Hoh E, Hentschel BT, Kaye S. Long-term field measurement of sorption of organic contaminants to five types of plastic pellets: Implications for plastic marine debris. Environ Sci Technol. 2013;47(3):1646–54.
17. Hahladakis JN, Velis CA, Weber R, Iacovidou E, Purnell P. An overview of chemical additives present in plastics: Migration, release, fate and environmental impact during their use, disposal and recycling. J Hazard Mater. 2018;344:179–99.
18. Godwin AD. Plasticizers. In: Applied Plastics Engineering Handbook. Elsevier; 2017. p. 533–53.
19. Wexler P. Encyclopedia of toxicology. Encyclopedia of Toxicology. 2005.
20. Bhunia K, Sablani SS, Tang J, Rasco B. Migration of chemical compounds from packaging polymers during microwave, conventional heat treatment, and storage. Compr Rev Food Sci Food Saf. 2013;12(5):523–45.
21. Poisson C, Hervais V, Lacrampe MF, Krawczak P, Falher T, Gondard C, et al. Optimization of polyethylene/binder/polyamide extrusion blow-molded films. III. Slippability improvement with fatty acid amides. J Appl Polym Sci. 2010;115(4).
22. de Boer J, El-Sayed A, Fiedler H, Legler J, Muir DCG, Nikiforov VA, et al. Chlorinated paraffins. In: The Handbook of Environmental Chemistry. Chlorinated Paraffins. Vol. 10, Springer-Verlag, Berlin/ Heidelberg. 2010.
23. D'Arcy N. Antimicrobials in plastics: a global review. Plast Addit Compd. 2001;3(12):12–5.
24. Jambeck JR, Geyer R, Wilcox C, Siegler TR, Perryman M, Andrady A, et al. Plastic waste inputs from land into the ocean. Science. 2015;347(6223):768–71.
25. Lechthaler S, Waldschläger K, Stauch G, Schüttrumpf H. The way of macroplastic through the environment. Environ - MDPI. 2020;7(10):1–30.
26. Eriksen M, Lebreton LCM, Carson HS, Thiel M, Moore CJ, Borerro JC, et al. Plastic Pollution in the World's Oceans: More than 5 Trillion Plastic Pieces Weighing over 250,000 Tons Afloat at Sea. PLoS One. 2014;9(12):1–15.
27. Avio CG, Gorbi S, Regoli F. Plastics and microplastics in the oceans: From emerging pollutants to emerged threat. Mar Environ Res. 2016;
28. Prokić MD, Gavrilović BR, Radovanović TB, Gavrić JP, Petrović TG, Despotović SG, et al. Studying microplastics: Lessons from evaluated literature on animal model organisms and

experimental approaches. J Hazard Mater. 2021;414:125476.
29. Rech S, Borrell Y, García-Vazquez E. Marine litter as a vector for non-native species: What we need to know. Mar Pollut Bull. 2016;113(1–2).
30. Canals M, Pham CK, Bergmann M, Gutow L, Hanke G, van Sebille E, et al. The quest for seafloor macrolitter: A critical review of background knowledge, current methods and future prospects. Environ Res Lett. 2021;16(2).
31. Zhang K, Hamidian AH, Tubić A, Zhang Y, Fang JKH, Wu C, et al. Understanding plastic degradation and microplastic formation in the environment: A review. Environ Pollut. 2021;274.
32. Lim X. Microplastics are everywhere — but are they harmful? Nature. 2021;593(7857):22–5.
33. Cózar A, Echevarría F, González-Gordillo JI, Irigoien X, Úbeda B, Hernández-León S, et al. Plastic debris in the open ocean. Proc Natl Acad Sci U S A. 2014;111(28):10239–44.
34. Auta HS, Emenike CU, Fauziah SH. Distribution and importance of microplastics in the marine environmentA review of the sources, fate, effects, and potential solutions. Environ Int. 2017;102:165–76.
35. Hale RC, Seeley ME, La Guardia MJ, Mai L, Zeng EY. A Global Perspective on Microplastics. J Geophys Res Ocean. 2020;125(1):1–40.
36. Yu Q, Hu X, Yang B, Zhang G, Wang J, Ling W. Distribution, abundance and risks of microplastics in the environment. Chemosphere. 2020;249:126059.
37. Kass G, Moon J, Robinson T. Horizon 2020: EFSA's Priority Research Topics. EFSA Support Publ. 2017;14(1):1166E.
38. GESAMP (2016). "Sources, fate and effects of microplastics in the marine environment: part two of a global assessment" (Kershaw, P.J., and Rochman, C.M., eds). (IMO/FAO/UNESCO-IOC/UNIDO/WMO/IAEA/UN/ UNEP/UNDP Joint Group of Experts on the Scientific Aspec.
39. UNEP (2016). Marine plastic debris and microplastics – Global lessons and research to inspire action and guide policy change. United Nations Environment Programme, Nairobi.
40. Boucher J, Friot D. Primary microplastics in the oceans: A global evaluation of sources [Internet]. IUCN International Union for Conservation of Nature; 2017.
41. Jamieson AJ, Brooks LSR, Reid WDK, Piertney SB, Narayanaswamy BE, Linley TD. Microplastics and synthetic particles ingested by deep-sea amphipods in six of the deepest marine ecosystems on Earth. R Soc Open Sci. 2019;6(2).
42. Bergmann M, Mützel S, Primpke S, Tekman MB, Trachsel J, Gerdts G. White and wonderful? Microplastics prevail in snow from the Alps to the Arctic. Sci Adv. 2019;5(8):1–11.
43. Kelly A, Lannuzel D, Rodemann T, Meiners KM, Auman HJ. Microplastic contamination in east Antarctic sea ice. Mar Pollut Bull. 2020;154:111130.
44. Napper IE, Davies BFR, Clifford H, Elvin S, Koldewey HJ, Mayewski PA, et al. Reaching New Heights in Plastic Pollution—Preliminary Findings of Microplastics on Mount Everest. One Earth. 2020;3(5):621–30.
45. Diaz-Basantes MF, Conesa JA, Fullana A. Microplastics in honey, beer, milk and refreshments in Ecuador as emerging contaminants. Sustain. 2020;12(12).
46. Kedzierski M, Lechat B, Sire O, Le Maguer G, Le Tilly V, Bruzaud S. Microplastic contamination of packaged meat: Occurrence and associated risks. Food Packag Shelf Life. 2020;24.
47. Zhang Q, Xu EG, Li J, Chen Q, Ma L, Zeng EY, et al. A Review of Microplastics in Table Salt, Drinking Water, and Air: Direct Human Exposure. Environ Sci Technol. 2020;54(7):3740–51.
48. Neves D, Sobral P, Ferreira JL, Pereira T. Ingestion of microplastics by commercial fish off the Portuguese coast. Mar Pollut Bull. 2015;101(1):119–26.
49. Bridson JH, Gaugler EC, Smith DA, Northcott GL, Gaw S. Leaching and extraction of additives from plastic pollution to inform environmental risk: A multidisciplinary review of analytical approaches. J Hazard Mater. 2021;414:125571.
50. Paluselli A, Fauvelle V, Galgani F, Sempéré R. Phthalate Release from Plastic Fragments and Degradation in Seawater. Environ Sci Technol. 2019;53(1):166–75.
51. Sørensen L, Groven AS, Hovsbakken IA, Del Puerto O, Krause DF, Sarno A, et al. UV degradation of natural and synthetic microfibers causes fragmentation and release of polymer degradation products and chemical additives. Sci Total Environ. 2021;755:143170.
52. Aminot Y, Lanctôt C, Bednarz V, Robson WJ, Taylor A, Ferrier-Pagès C, et al. Leaching of flame-retardants from polystyrene debris: Bioaccumulation and potential effects on coral. Mar Pollut Bull. 2020;15:1–7.
53. Amelia TSM, Khalik WMAWM, Ong MC, Shao YT, Pan HJ, Bhubalan K. Marine microplastics as vectors of major ocean pollutants and its hazards to the marine ecosystem and humans. Prog Earth Planet Sci. 2021;8(1).
54. Chen CF, Ju YR, Lim YC, Hsu NH, Lu KT, Hsieh SL, et al. Microplastics and their affiliated PAHs

in the sea surface connected to the southwest coast of Taiwan. Chemosphere. 2020;254.
55. Fraser MA, Chen L, Ashar M, Huang W, Zeng J, Zhang C, et al. Occurrence and distribution of microplastics and polychlorinated biphenyls in sediments from the Qiantang River and Hangzhou Bay, China. Ecotoxicol Environ Saf. 2020;196.
56. Liu S, Shi J, Wang J, Dai Y, Li H, Li J, et al. Interactions Between Microplastics and Heavy Metals in Aquatic Environments: A Review. Front Microbiol. 2021;12:1–14.
57. Cao Y, Zhao M, Ma X, Song Y, Zuo S, Li H, et al. A critical review on the interactions of microplastics with heavy metals: Mechanism and their combined effect on organisms and humans. Sci Total Environ. 2021;788:147620.
58. Santos LHMLM, Rodríguez-Mozaz S, Barceló D. Microplastics as vectors of pharmaceuticals in aquatic organisms – An overview of their environmental implications. Case Stud Chem Environ Eng. 2021;3:100079.
59. Mato Y, Isobe T, Takada H, Kanehiro H, Ohtake C, Kaminuma T. Plastic resin pellets as a transport medium for toxic chemicals in the marine environment. Environ Sci Technol. 2001;35(2):318–24.
60. Schönlau C, Larsson M, Lam MM, Engwall M, Giesy JP, Rochman C, et al. Aryl hydrocarbon receptor-mediated potencies in field-deployed plastics vary by type of polymer. Environ Sci Pollut Res. 2019;26(9):9079–88.
61. Ziccardi LM, Edgington A, Hentz K, Kulacki KJ, Kane Driscoll S. Microplastics as vectors for bioaccumulation of hydrophobic organic chemicals in the marine environment: A state-of-the-science review. Environ Toxicol Chem. 2016;35(7):1667–76.
62. Joo SH, Liang Y, Kim M, Byun J, Choi H. Microplastics with adsorbed contaminants: Mechanisms and Treatment. Environ Challenges. 2021;3:100042.
63. Lamichhane S, Bal Krishna KC, Sarukkalige R. Polycyclic aromatic hydrocarbons (PAHs) removal by sorption: A review. Chemosphere. 2016;148:336–53.
64. Lawal AT. Polycyclic aromatic hydrocarbons. A review. Fantke P, editor. Cogent Environ Sci. 2017;3:1.
65. Ravindra K, Sokhi R, Van Grieken R. Atmospheric polycyclic aromatic hydrocarbons: Source attribution, emission factors and regulation. Vol. 42, Atmospheric Environment. 2008.
66. Dat N-D, Chang MB. Review on characteristics of PAHs in atmosphere, anthropogenic sources and control technologies. Sci Total Environ. 2017;609:682–93.
67. Behera BK, Das A, Sarkar DJ, Weerathunge P, Parida PK, Das BK, et al. Polycyclic Aromatic Hydrocarbons (PAHs) in inland aquatic ecosystems: Perils and remedies through biosensors and bioremediation. Vol. 241, Environmental Pollution. 2018.
68. Chizhova T, Koudryashova Y, Prokuda N, Tishchenko P, Hayakawa K. Polycyclic aromatic hydrocarbons in the estuaries of two rivers of the sea of Japan. Int J Environ Res Public Health. 2020;17(17).
69. Wu H, Sun B, Li J. Polycyclic aromatic hydrocarbons in sediments/soils of the rapidly urbanized lower reaches of the river Chaohu, China. Int J Environ Res Public Health. 2019;16(13).
70. Zhang S, Yao H, Lu Y, Yu X, Wang J, Sun S, et al. Uptake and translocation of polycyclic aromatic hydrocarbons (PAHs) and heavy metals by maize from soil irrigated with wastewater. Sci Rep. 2017;7(1):1–11.
71. De Gelder S, Bakke MJ, Vos J, Rasinger JD, Ingebrigtsen K, Grung M, et al. The effect of dietary lipid composition on the intestinal uptake and tissue distribution of benzo[a]pyrene and phenanthrene in Atlantic salmon (*Salmo salar*). Comp Biochem Physiol Part - C Toxicol Pharmacol. 2016;185–186:65–76.
72. Collier TK, Anulacion BF, Arkoosh MR, Dietrich JP, Incardona JP, Johnson LL, et al. Effects on Fish of Polycyclic Aromatic HydrocarbonS (PAHS) and Naphthenic Acid Exposures. Vol. 33, Fish Physiology. 2013. 195–255 p.
73. Williams MA, Salice C, Reddy G. Wildlife Toxicity Assessment for Benzo[a]Pyrene. In: Wildlife Toxicity Assessments for Chemicals of Military Concern. Elsevier; 2015. p. 421–37.
74. Batel A, Linti F, Scherer M, Erdinger L, Braunbeck T. Transfer of benzo[a]pyrene from microplastics to Artemia nauplii and further to zebrafish via a trophic food web experiment: CYP1A induction and visual tracking of persistent organic pollutants. Environ Toxicol Chem. 2016;35(7):1656–66.
75. Batel A, Borchert F, Reinwald H, Erdinger L, Braunbeck T. Microplastic accumulation patterns and transfer of benzo[a]pyrene to adult zebrafish (*Danio rerio*) gills and zebrafish embryos. Environ Pollut. 2018;235:918–30.
76. Pittura L, Avio CG, Giuliani ME, D'Errico G, Keiter SH, Cormier B, et al. Microplastics as Vehicles of Environmental PAHs to Marine Organisms: Combined Chemical and Physical Hazards to the

Mediterranean Mussels, *Mytilus galloprovincialis*. Front Mar Sci. 2018;5:103.
77. O'Donovan S, Mestre NC, Abel S, Fonseca TG, Carteny CC, Cormier B, et al. Ecotoxicological Effects of Chemical Contaminants Adsorbed to Microplastics in the Clam *Scrobicularia plana*. Front Mar Sci. 2018;5:1–15.
78. Lusher AL, McHugh M, Thompson RC. Occurrence of microplastics in the gastrointestinal tract of pelagic and demersal fish from the English Channel. Mar Pollut Bull. 2013;67(1–2):94–9.
79. Wright SL, Thompson RC, Galloway TS. The physical impacts of microplastics on marine organisms: A review. Environ Pollut. 2013;178:483–92.
80. Koelmans AA, Besseling E, Foekema EM. Leaching of plastic additives to marine organisms. Environ Pollut. 2014;187:49–54.
81. Groh KJ, Backhaus T, Carney-Almroth B, Geueke B, Inostroza PA, Lennquist A, et al. Overview of known plastic packaging-associated chemicals and their hazards. Sci Total Environ. 2019;651:3253–68.
82. Galloway TS, Cole M, Lewis C. Interactions of microplastic debris throughout the marine ecosystem. Nat Ecol Evol. 2017;1(5):1–8.
83. Paffenhöfer GA, Köster M. The Effects of Microplastics on Dolioletta gegenbauri (Tunicata, Thaliacea). Arch Environ Contam Toxicol. 2020;78(1):94–105.
84. Messinetti S, Mercurio S, Parolini M, Sugni M, Pennati R. Effects of polystyrene microplastics on early stages of two marine invertebrates with different feeding strategies. Environ Pollut. 2018;237:1080–7.
85. Hariharan G, Purvaja R, Anandavelu I, Robin RS, Ramesh R. Accumulation and ecotoxicological risk of weathered polyethylene microplastics on green mussel (*Perna viridis*). Ecotoxicol Environ Saf. 2021;208:111765.
86. Islam N, Garcia da Fonseca T, Vilke J, Gonçalves JM, Pedro P, Keiter S, et al. Perfluorooctane sulfonic acid (PFOS) adsorbed to polyethylene microplastics: Accumulation and ecotoxicological effects in the clam Scrobicularia plana. Mar Environ Res. 2021;164.
87. Revel M, Lagarde F, Perrein-Ettajani H, Bruneau M, Akcha F, Sussarellu R, et al. Tissue-specific biomarker responses in the blue mussel Mytilus spp. exposed to a mixture of microplastics at environmentally relevant concentrations. Front Environ Sci. 2019;7:1–14.
88. Cappello T, De Marco G, Oliveri Conti G, Giannetto A, Ferrante M, Mauceri A, et al. Time-dependent metabolic disorders induced by short-term exposure to polystyrene microplastics in the Mediterranean mussel *Mytilus galloprovincialis*. Ecotoxicol Environ Saf. 2021;209:111780.
89. Ribeiro F, Garcia AR, Pereira BP, Fonseca M, Mestre NC, Fonseca TG, et al. Microplastics effects in Scrobicularia plana. Mar Pollut Bull. 2017;122(1–2):379–91.
90. Horn DA, Granek EF, Steele CL. Effects of environmentally relevant concentrations of microplastic fibers on Pacific mole crab (*Emerita analoga*) mortality and reproduction. Limnol Oceanogr Lett. 2020;5(1):74–83.
91. Wang T, Hu M, Xu G, Shi H, Leung JYS, Wang Y. Microplastic accumulation via trophic transfer: Can a predatory crab counter the adverse effects of microplastics by body defence? Sci Total Environ. 2021;754:142099.
92. He M, Yan M, Chen X, Wang X, Gong H, Wang W, et al. Bioavailability and toxicity of microplastics to zooplankton. Gondwana Res. 2021;
93. Botterell ZLR, Beaumont N, Dorrington T, Steinke M, Thompson RC, Lindeque PK. Bioavailability and effects of microplastics on marine zooplankton: A review. Environ Pollut. 2019;245(2019):98–110.
94. Barboza LGA, Lopes C, Oliveira P, Bessa F, Otero V, Henriques B, et al. Microplastics in wild fish from North East Atlantic Ocean and its potential for causing neurotoxic effects, lipid oxidative damage, and human health risks associated with ingestion exposure. Sci Total Environ. 2020;717:134625.
95. Reinold S, Herrera A, Saliu F, Hernández-González C, Martinez I, Lasagni M, et al. Evidence of microplastic ingestion by cultured European sea bass (*Dicentrarchus labrax*). Mar Pollut Bull. 2021;168(April).
96. Bayo J, Rojo D, Martínez-Baños P, López-Castellanos J, Olmos S. Commercial Gilthead Seabream (*Sparus aurata L.*) from the Mar Menor Coastal Lagoon as Hotspots of Microplastic Accumulation in the Digestive System. Int J Environ Res Public Health. 2021;18(13):6844.
97. Thiele CJ, Hudson MD, Russell AE, Saluveer M, Sidaoui-Haddad G. Microplastics in fish and fishmeal: an emerging environmental challenge? Sci Rep. 2021;11(1):1–12.
98. Savoca S, Capillo G, Mancuso M, Bottari T, Crupi R, Branca C, et al. Microplastics occurrence in the Tyrrhenian waters and in the gastrointestinal tract of two congener species of seabreams. Environ Toxicol Pharmacol. 2019;67:35–41.

99. Elizalde-Velázquez GA, Gómez-Oliván LM. Microplastics in aquatic environments: A review on occurrence, distribution, toxic effects, and implications for human health. Sci Total Environ. 2021;780:146551.
100. Wang W, Ge J, Yu X. Bioavailability and toxicity of microplastics to fish species: A review. Ecotoxicol Environ Saf. 2020;189:109913.
101. Boerger CM, Lattin GL, Moore SL, Moore CJ. Plastic ingestion by planktivorous fishes in the North Pacific Central Gyre. Mar Pollut Bull. 2010;60(12):2275–8.
102. Lusher AL, O'Donnell C, Officer R, O'Connor I. Microplastic interactions with North Atlantic mesopelagic fish. ICES J Mar Sci. 2016;73(4):1214–25.
103. Rummel CD, Löder MGJ, Fricke NF, Lang T, Griebeler E-M, Janke M, et al. Plastic ingestion by pelagic and demersal fish from the North Sea and Baltic Sea. Mar Pollut Bull. 2016;102(1):134–41.
104. Tanaka K, Takada H. Microplastic fragments and microbeads in digestive tracts of planktivorous fish from urban coastal waters. Sci Rep. 2016;6:34351.
105. Naidoo T, Smit A, Glassom D. Plastic ingestion by estuarine mullet *Mugil cephalus* (Mugilidae) in an urban harbour, KwaZulu-Natal, South Africa. African J Mar Sci. 2016;38(1):145–9.
106. Alomar C, Deudero S. Evidence of microplastic ingestion in the shark Galeus melastomus Rafinesque, 1810 in the continental shelf off the western Mediterranean Sea. Environ Pollut. 2017;223:223–9.
107. Kumar VE, Ravikumar G, Jeyasanta KI. Occurrence of microplastics in fishes from two landing sites in Tuticorin, South east coast of India. Mar Pollut Bull. 2018;135:889–94.
108. Abbasi S, Soltani N, Keshavarzi B, Moore F, Turner A, Hassanaghaei M. Microplastics in different tissues of fish and prawn from the Musa Estuary, Persian Gulf. Chemosphere. 2018;205:80–7.
109. Collicutt B, Juanes F, Dudas SE. Microplastics in juvenile Chinook salmon and their nearshore environments on the east coast of Vancouver Island. Environ Pollut. 2019;244:135–42.
110. Peters CA, Bratton SP. Urbanization is a major influence on microplastic ingestion by sunfish in the Brazos River Basin, Central Texas, USA. Environ Pollut. 2016;210:380–7.
111. McGoran AR, Clark PF, Morritt D. Presence of microplastic in the digestive tracts of European flounder, Platichthys flesus, and European smelt, Osmerus eperlanus, from the River Thames. Environ Pollut. 2017;220:744–51.
112. Sanchez W, Bender C, Porcher J-M. Wild gudgeons (*Gobio gobio*) from French rivers are contaminated by microplastics: Preliminary study and first evidence. Environ Res. 2014;128:98–100.
113. Zhang K, Xiong X, Hu H, Wu C, Bi Y, Wu Y, et al. Occurrence and Characteristics of Microplastic Pollution in Xiangxi Bay of Three Gorges Reservoir, China. Environ Sci Technol. 2017;51(7):3794–801.
114. Pazos RS, Maiztegui T, Colautti DC, Paracampo AH, Gómez N. Microplastics in gut contents of coastal freshwater fish from Río de la Plata estuary. Mar Pollut Bull. 2017;122(1–2):85–90.
115. Pegado T de S e S, Schmid K, Winemiller KO, Chelazzi D, Cincinelli A, Dei L, et al. First evidence of microplastic ingestion by fishes from the Amazon River estuary. Mar Pollut Bull. 2018;133:814–21.
116. Howe K, Clark M, Torroja C, Torrance J, Berthelot C, Muffato M, et al. The zebrafish reference genome sequence and its relationship to the human genome. Nature. 2013;496(7446):498–503.
117. MacRae CA, Peterson RT. Zebrafish as tools for drug discovery. Nat Rev Drug Discov. 2015;14(10):721–31.
118. Halpern ME, Rhee J, Goll MG, Akitake CM, Parsons M, Leach SD. Gal4/UAS Transgenic Tools and Their Application to Zebrafish. 2008.
119. Tonelli F, Bek JW, Besio R, Clercq A De. Zebrafish : A Resourceful Vertebrate Model to Investigate Skeletal Disorders. 2020;11.
120. Laizé V, Gavaia PJ, Cancela ML. Fish: A suitable system to model human bone disorders and discover drugs with osteogenic or osteotoxic activities. Drug Discov Today Dis Model. 2014;13:29–37.
121. Cormier B, Le Bihanic F, Cabar M, Crebassa J, Blanc M, Larsson M, et al. Chronic feeding exposure to virgin and spiked microplastics disrupts essential biological functions in teleost fish. J Hazard Mater. 2021;415:125626.
122. Bhagat J, Zang L, Nishimura N, Shimada Y. Zebrafish: An emerging model to study microplastic and nanoplastic toxicity. Sci Total Environ. 2020;728:138707.
123. Cormier B, Batel A, Cachot J, Bégout M, Braunbeck T, Cousin X, et al. Multi-Laboratory Hazard Assessment of Contaminated Microplastic Particles by Means of Enhanced Fish Embryo Test

With the Zebrafish (*Danio rerio*). Front Environ Sci. 2019;7:1–14.
124. Jemec Kokalj A, Kuehnel D, Puntar B, Žgajnar Gotvajn A, Kalčikova G. An exploratory ecotoxicity study of primary microplastics versus aged in natural waters and wastewaters. Environ Pollut. 2019;254.
125. Zhao Y, Qin Z, Huang Z, Bao Z, Luo T, Jin Y. Effects of polyethylene microplastics on the microbiome and metabolism in larval zebrafish. Environ Pollut. 2021;282:117039.
126. Qiang L, Cheng J. Exposure to microplastics decreases swimming competence in larval zebrafish (Danio rerio). Ecotoxicol Environ Saf. 2019;176:226–33.
127. Santos D, Félix L, Luzio A, Parra S, Bellas J, Monteiro SM. Single and combined acute and subchronic toxic effects of microplastics and copper in zebrafish (*Danio rerio*) early life stages. Chemosphere. 2021;277.
128. Malafaia G, de Souza AM, Pereira AC, Gonçalves S, da Costa Araújo AP, Ribeiro RX, et al. Developmental toxicity in zebrafish exposed to polyethylene microplastics under static and semi-static aquatic systems. Sci Total Environ. 2020;700:134867.
129. Zhao HJ, Xu JK, Yan ZH, Ren HQ, Zhang Y. Microplastics enhance the developmental toxicity of synthetic phenolic antioxidants by disturbing the thyroid function and metabolism in developing zebrafish. Environ Int. 2020;140:105750.
130. Wan Z, Wang C, Zhou J, Shen M, Wang X, Fu Z, et al. Effects of polystyrene microplastics on the composition of the microbiome and metabolism in larval zebrafish. Chemosphere. 2019;217:646–58.
131. LeMoine CMR, Kelleher BM, Lagarde R, Northam C, Elebute OO, Cassone BJ. Transcriptional effects of polyethylene microplastics ingestion in developing zebrafish (*Danio rerio*). Environ Pollut. 2018;243:591–600.
132. Karami A, Groman DB, Wilson SP, Ismail P, Neela VK. Biomarker responses in zebrafish (*Danio rerio*) larvae exposed to pristine low-density polyethylene fragments. Environ Pollut. 2017;223:466–75.
133. Gu W, Liu S, Chen L, Liu Y, Gu C, Ren HQ, et al. Single-Cell RNA Sequencing Reveals Size-Dependent Effects of Polystyrene Microplastics on Immune and Secretory Cell Populations from Zebrafish Intestines. Environ Sci Technol. 2020;54(6):3417–27.
134. Qiao R, Lu K, Deng Y, Ren H, Zhang Y. Combined effects of polystyrene microplastics and natural organic matter on the accumulation and toxicity of copper in zebrafish. Sci Total Environ. 2019;682:128–37.
135. Zhao Y, Bao Z, Wan Z, Fu Z, Jin Y. Polystyrene microplastic exposure disturbs hepatic glycolipid metabolism at the physiological, biochemical, and transcriptomic levels in adult zebrafish. Sci Total Environ. 2020;710:136279.
136. Lu K, Qiao R, An H, Zhang Y. Influence of microplastics on the accumulation and chronic toxic effects of cadmium in zebrafish (*Danio rerio*). Chemosphere. 2018;202:514–20.
137. Rainieri S, Conlledo N, Larsen BK, Granby K, Barranco A. Combined effects of microplastics and chemical contaminants on the organ toxicity of zebrafish (*Danio rerio*). Environ Res. 2018;162(December 2017):135–43.
138. Batel A, Baumann L, Carteny CC, Cormier B, Keiter SH, Braunbeck T. Histological, enzymatic and chemical analyses of the potential effects of differently sized microplastic particles upon long-term ingestion in zebrafish (*Danio rerio*). Mar Pollut Bull. 2020;153:111022.
139. Zhang J, Meng H, Kong X, Cheng X, Ma T, He H, et al. Combined effects of polyethylene and organic contaminant on zebrafish (*Danio rerio*): Accumulation of 9-Nitroanthracene, biomarkers and intestinal microbiota. Environ Pollut. 2021;277:116767.
140. Xu K, Zhang Y, Huang Y, Wang J. Toxicological effects of microplastics and phenanthrene to zebrafish (Danio rerio). Sci Total Environ. 2021;757:143730.
141. Pimentel MS, Faleiro F, Dionísio G, Repolho T, Pousão-Ferreira P, Machado J, et al. Defective skeletogenesis and oversized otoliths in fish early stages in a changing ocean. J Exp Biol. 2014;217(12):2062–70.
142. Boglione C, Gavaia P, Koumoundouros G, Gisbert E, Moren M, Fontagné S, et al. Skeletal anomalies in reared European fish larvae and juveniles. Part 1: normal and anomalous skeletogenic processes. Rev Aquac. 2013;5:99–120.
143. Boglione C, Gisbert E, Gavaia P, E. Witten P, Moren M, Fontagné S, et al. Skeletal anomalies in reared European fish larvae and juveniles. Part 2: main typologies, occurrences and causative factors. Rev Aquac. 2013;5:121–67.
144. Laizé V, Gavaia PJ, Tarasco M, Viegas MN, Caria J, Luis N, et al. Osteotoxicity of 3-methylcholanthrene in fish. Ecotoxicol Environ Saf. 2018;161:721–8.
145. Tarasco M, Cardeira J, Viegas MN, Caria J, Martins G, Gavaia PJ, et al. Anti-osteogenic activity

of cadmium in zebrafish. Fishes. 2019;4(1):11.
146. Darbre PD. Chemical components of plastics as endocrine disruptors: Overview and commentary. Birth Defects Res. 2020;112(17):1300–7.
147. Fernández I, Gavaia PJ, Laizé V, Cancela ML. Fish as a model to assess chemical toxicity in bone. Aquat Toxicol. 2018;194:208–26.
148. Huang W, Wang X, Zheng S, Wu R, Liu C, Wu K. Effect of bisphenol A on craniofacial cartilage development in zebrafish (Danio rerio) embryos: A morphological study. Ecotoxicol Environ Saf. 2021;212:111991.
149. Hall BK. Bones and Cartilage. Elsevier; 2015.
150. Watson CJ, Kwon RY. Skeletal System Morphophysiology. In: The Zebrafish in Biomedical Research. Elsevier; 2020. p. 109–14.
151. Bonjour JP. Calcium and phosphate: A duet of ions playing for bone health. J Am Coll Nutr. 2011;30.
152. Peacock M. Calcium metabolism in health and disease. Vol. 5, Clinical Journal of the American Society of Nephrology. 2010.
153. Hoffman CM, Calvi LM. Minireview: Complexity of hematopoietic stem cell regulation in the bone marrow microenvironment. Vol. 28, Molecular Endocrinology. 2014.
154. Apschner A, Schulte-Merker S, Witten PE. Not All Bones are Created Equal - Using Zebrafish and Other Teleost Species in Osteogenesis Research. Third Edit. Vol. 105, Methods in Cell Biology. Elsevier Inc.; 2011. 239–255 p.
155. Florencio-Silva R, Sasso GR da S, Sasso-Cerri E, Simões MJ, Cerri PS. Biology of Bone Tissue: Structure, Function, and Factors That Influence Bone Cells. Biomed Res Int. 2015;2015:1–17.
156. Manolagas SC. Osteocalcin promotes bone mineralization but is not a hormone. PLoS Genet. 2020;16(6):4–7.
157. Si J, Wang C, Zhang D, Wang B, Hou W, Zhou Y. Osteopontin in Bone Metabolism and Bone Diseases. Vol. 26, Medical Science Monitor. 2020.
158. Termine JD, Kleinman HK, Whitson SW, Conn KM, McGarvey ML, Martin GR. Osteonectin, a bone-specific protein linking mineral to collagen. Cell. 1981;26(1):99–105.
159. Golub EE, Boesze-Battaglia K. The role of alkaline phosphatase in mineralization. Curr Opin Orthop. 2007;18(5):444–8.
160. Bonewald LF, Johnson ML. Osteocytes, mechanosensing and Wnt signaling. Vol. 42, Bone. 2008.
161. Mohamed AMFS. An overview of bone cells and their regulating factors of differentiation. Vol. 15, Malaysian Journal of Medical Sciences. 2008.
162. Matic I, Matthews BG, Wang X, Dyment NA, Worthley DL, Rowe DW, et al. Quiescent Bone Lining Cells Are a Major Source of Osteoblasts During Adulthood. Stem Cells. 2016;34(12).
163. Karsenty G, Kronenberg HM, Settembre C. Genetic control of bone formation. Annu Rev Cell Dev Biol. 2009;25:629–48.
164. Sinha KM, Zhou X. Genetic and molecular control of osterix in skeletal formation. J Cell Biochem. 2013;114(5):975–84.
165. Knopf F, Hammond C, Chekuru A, Kurth T, Hans S, Weber CW, et al. Bone regenerates via dedifferentiation of osteoblasts in the zebrafish fin. Dev Cell. 2011;20(5):713–24.
166. Singh SP, Holdway JE, Poss KD. Regeneration of amputated zebrafish fin rays from de novo osteoblasts. Dev Cell. 2012;22(4):879–86.
167. Väänänen HK, Zhao H. Osteoclast Function. Biology and Mechanisms. In: Principles of Bone Biology, Two-Volume Set. 2008.
168. Ribet ABP, Ng PY, Pavlos NJ. Membrane Transport Proteins in Osteoclasts: The Ins and Outs. Front Cell Dev Biol. 2021;9:1–21.
169. Delaissé JM, Andersen TL, Engsig MT, Henriksen K, Troen T, Blavier L. Matrix metalloproteinases (MMP) and cathepsin K contribute differently to osteoclastic activities. Microsc Res Tech. 2003;61(6):504–13.
170. Dai R, Wu Z, Chu HY, Lu J, Lyu A, Liu J, et al. Cathepsin K: The Action in and Beyond Bone. Front Cell Dev Biol. 2020;8:1–13.
171. Hayman A. Tartrate-resistant acid phosphatase (TRAP) and the osteoclast/immune cell dichotomy. Autoimmunity. 2008;41(3):218–23.
172. Ma Q, Liang M, Wu Y, Luo F, Ma Z, Dong S, et al. Osteoclast-derived apoptotic bodies couple bone resorption and formation in bone remodeling. Bone Res. 2021;9(1).
173. Soysa NS, Alles N, Aoki K, Ohya K. Osteoclast formation and differentiation: An overview. J Med Dent Sci. 2012;59:65–74.
174. Walsh MC, Choi Y. Biology of the RANKL-RANK-OPG system in immunity, bone, and beyond.

Front Immunol. 2014;5:1–11.
175. Boyle WJ, Simonet WS, Lacey DL. Osteoclast differentiation and activiation. Nature. 2003;423(6937):337–42.
176. Al-Bari AA, Al Mamun A. Current advances in regulation of bone homeostasis. FASEB BioAdvances. 2020;2(11):668–79.
177. Kim JM, Lin C, Stavre Z, Greenblatt MB, Shim JH. Osteoblast-Osteoclast Communication and Bone Homeostasis. Cells. 2020;9(9):1–14.
178. Rutkovskiy A, Stensløkken K-O, Vaage IJ. Osteoblast Differentiation at a Glance. Med Sci Monit Basic Res. 2016;22:95–106.
179. Dallas SL, Prideaux M, Bonewald LF. The osteocyte: An endocrine cell . . . and more. Endocr Rev. 2013;34(5):658–90.
180. Walsh NC, Gravallese EM. Bone remodeling in rheumatic disease: a question of balance. Immunol Rev. 2010;233(1):301–12.
181. Boyce BF, Hughes DE, Wright KR, Xing L, Dai A. Recent advances in bone biology provide insight into the pathogenesis of bone diseases. Lab Invest. 1999;79(2):83–94.
182. Feng X, McDonald JM. Disorders of Bone Remodeling. Annu Rev Pathol Mech Dis. 2011;6(1):121–45.
183. Gonçalves R, Tarasco M, Schatzmayr D, Gavaia P. Preliminary evaluation of moniliformin as a potential threat for teleosts. Fishes. 2018;3(1):4.
184. Tarasco M, Laizé V, Cardeira J, Cancela ML, Gavaia PJ. The zebrafish operculum: A powerful system to assess osteogenic bioactivities of molecules with pharmacological and toxicological relevance. Comp Biochem Physiol Part C Toxicol Pharmacol. 2017;197:45–52.
185. Cardeira J, Gavaia PJ, Fernández I, Cengiz IF, Moreira-Silva J, Oliveira JM, et al. Quantitative assessment of the regenerative and mineralogenic performances of the zebrafish caudal fin. Sci Rep. 2016;6(July):39191.
186. Torvanger I, Metz JR, Olsvik PA, Søfteland L, Lie KK. Benzo(a)pyrene reduces osteoclast and osteoblast activity in ex-vivo scales of zebrafish (*Danio rerio* [Hamilton-Buchanan, 1822]) and goldfish (*Carassius auratus* [Linnaeus, 1758]). J Appl Ichthyol. 2018;34(2):431–9.
187. de Vrieze E, van Kessel MAHJ, Peters HM, Spanings FAT, Flik G, Metz JR. Prednisolone induces osteoporosis-like phenotype in regenerating zebrafish scales. Osteoporos Int. 2014;25(2):567–78.
188. Naidu R, Arias Espana VA, Liu Y, Jit J. Emerging contaminants in the environment: Risk-based analysis for better management. Chemosphere. 2016;154:350–7.
189. Crawford CB, Quinn B. Microplastic pollutants. Elsevier Science; 2017. 315 p.
190. Sousa JCG, Ribeiro AR, Barbosa MO, Pereira MFR, Silva AMT. A review on environmental monitoring of water organic pollutants identified by EU guidelines. J Hazard Mater. 2018;344:146–62.
191. Wang F, Wong CS, Chen D, Lu X, Wang F, Zeng EY. Interaction of toxic chemicals with microplastics: A critical review. Water Res. 2018;139:208–19.
192. de Sá LC, Oliveira M, Ribeiro F, Rocha TL, Futter MN. Studies of the effects of microplastics on aquatic organisms: What do we know and where should we focus our efforts in the future? Sci Total Environ. 2018;645:1029–39.
193. Foley CJ, Feiner ZS, Malinich TD, Höök TO. A meta-analysis of the effects of exposure to microplastics on fish and aquatic invertebrates. Sci Total Environ. 2018;631–632:550–9.
194. Chae Y, An Y-J. Effects of micro- and nanoplastics on aquatic ecosystems: Current research trends and perspectives. Mar Pollut Bull. 2017;124(2):624–32.
195. Gandara e Silva PP, Nobre CR, Resaffe P, Pereira CDS, Gusmão F. Leachate from microplastics impairs larval development in brown mussels. Water Res. 2016;106:364–70.
196. Laws EA. Aquatic pollution: an introductory text. 4th editio. Wiley; 2018. 759 p.
197. Panel E, Chain F. Presence of microplastics and nanoplastics in food, with particular focus on seafood. EFSA J. 2016;14(6).
198. GESAMP Joint Group of Experts on the Scientific Aspects of Marine Environmental Protection. Sources, fate and effects of microplastics in the marine environment: a global assessment" [Internet]. Vol. 90, Reports and Studies GESAMP. 2015.
199. Renzi M, Specchiulli A, Blašković A, Manzo C, Mancinelli G, Cilenti L. Marine litter in stomach content of small pelagic fishes from the Adriatic Sea: sardines (*Sardina pilchardus*) and anchovies (*Engraulis encrasicolus*). Environ Sci Pollut Res. 2019;26(3):2771–81.
200. Sobhanardakani S. Tuna fish and common kilka: health risk assessment of metal pollution through consumption of canned fish in Iran. J Consum Prot Food Saf. 2017;12(2):157–63.
201. Novakov NJ, Mihaljev ŽA, Kartalović BD, Blagojević BJ, Petrović JM, Ćirković MA, et al. Heavy

metals and PAHs in canned fish supplies on the Serbian market. Food Addit Contam Part B Surveill. 2017;10(3):208–15.
202. Singh L, Varshney JG, Agarwal T. Polycyclic aromatic hydrocarbons' formation and occurrence in processed food. Food Chem. 2016;199:768–81.
203. Habibullah-Al-Mamun M, Ahmed MK, Islam MS, Tokumura M, Masunaga S. Distribution of polycyclic aromatic hydrocarbons (PAHs) in commonly consumed seafood from coastal areas of Bangladesh and associated human health implications. Environ Geochem Health. 2018;
204. Kattaiyan S, Chinnaiah A. Assessment of heavy metals contamination in edible fish species and its entry in the human food chain. Int J Zool Stud. 2018;3:274–8.
205. Lin C-Y, Chiang C-Y, Tsai H-J. Zebrafish and Medaka: new model organisms for modern biomedical research. J Biomed Sci. 2016;23(1):19.
206. Wittbrodt J, Shima A, Schartl M. Medaka - A model organism from the far east. Nat Rev Genet. 2002;3(1):53–64.
207. Hill AJ, Teraoka H, Heideman W, Peterson RE. Zebrafish as a model vertebrate for investigating chemical toxicity. Toxicol Sci. 2005;86(1):6–19.
208. Vargas RA, Sarmiento K, Vásquez IC. Zebrafish (*Danio rerio*): A potential model for toxinological studies. Zebrafish. 2015;12(5):320–6.
209. Dai Y-J, Jia Y-F, Chen N, Bian W-P, Li Q-K, Ma Y-B, et al. Zebrafish as a model system to study toxicology. Environ Toxicol Chem. 2014;33(1):11–7.
210. Padilla S, Cowden J, Hinton DE, Yuen B, Law S, Kullman SW, et al. Use of medaka in Toxicity Testing. Curr Protoc Toxicol. 2009;39:1.10.1-1.10.36.
211. Carvan 3rd MJ, Sonntag DM, Cmar CB, Cook RS, Curran MA, Miller GL. Oxidative stress in zebrafish cells: Potential utility of transgenic zebrafish as a deployable sentinel for site hazard ranking. Sci Total Environ. 2001;274(1–3):183–96.
212. Carvan 3rd MJ, Dalton TP, Stuart GW, Nebert DW. Transgenic zebrafish as sentinels for aquatic pollution. Ann N Y Acad Sci. 2010;919(1):133–47.
213. Kim BM, Kim J, Choi IY, Raisuddin S, Au DWT, Leung KMY, et al. Omics of the marine medaka (*Oryzias melastigma*) and its relevance to marine environmental research. Mar Environ Res. 2016;113:141–52.
214. Zeng Z, Shan T, Tong Y, Lam SH, Gong Z. Development of estrogen-responsive transgenic medaka for environmental monitoring of endocrine disrupters. Environ Sci Technol. 2005;39(22):9001–8.
215. Rubin BS. Bisphenol A: An endocrine disruptor with widespread exposure and multiple effects. J Steroid Biochem Mol Biol. 2011;127(1–2):27–34.
216. Sajiki J, Yonekubo J. Leaching of bisphenol A (BPA) from polycarbonate plastic to water containing amino acids and its degradation by radical oxygen species. Chemosphere. 2004;55(6):861–7.
217. Howdeshell KL, Peterman PH, Judy BM, Taylor JA, Orazio CE, Ruhlen RL, et al. Bisphenol A is released from used polycarbonate animal cages into water at room temperature. Environ Health Perspect. 2003;111(9):1180–7.
218. Song YK, Hong SH, Jang M, Han GM, Jung SW, Shim WJ. Combined effects of UV exposure duration and mechanical abrasion on microplastic fragmentation by polymer type. Environ Sci Technol. 2017;51(8):4368–76.
219. Wagner M, Lambert S. Freshwater Microplastics [Internet]. Springer International Publishing; 2018. 302 p. (The Handbook of Environmental Chemistry; vol. 58).
220. Wright D. Failure of plastics and rubber products: causes, effects and case studies involving degradation. iSmithers Rapra Publishing; 2001. 400 p.
221. Lithner D, Damberg J, Dave G, Larsson Å. Leachates from plastic consumer products - Screening for toxicity with Daphnia magna. Chemosphere. 2009;74(9):1195–200.
222. Urbanek AK, Rymowicz W, Mirończuk AM. Degradation of plastics and plastic-degrading bacteria in cold marine habitats. Appl Microbiol Biotechnol. 2018;102(18):7669–78.
223. A. Glaser J. Biological Degradation of Polymers in the Environment. In: Plastics in the Environment. IntechOpen; 2019. p. 13.
224. Martins S, Monteiro JF, Vito M, Weintraub D, Almeida J, Certal AC. Toward an integrated zebrafish health management program supporting cancer and neuroscience research. Zebrafish. 2016;13:S47–55.
225. Best J, Adatto I, Cockington J, James A, Lawrence C. A novel method for rearing first-feeding larval zebrafish: polyculture with type L saltwater rotifers (*Brachionus plicatilis*). Zebrafish. 2010;7(3):289–95.
226. Khatak HS, Raj B. Corrosion of austenitic stainless steels: mechanism, mitigation and

monitoring. 1st editio. Woodhead Publishing; 2002.
227. Baddoo NR. Stainless steel in construction: A review of research, applications, challenges and opportunities. J Constr Steel Res. 2008;64(11):1199–206.
228. Lawrence C. The husbandry of zebrafish (*Danio rerio*): a review. Aquaculture. 2007;269(1–4):1–20.
229. Harper C, Lawrence C. The laboratory zebrafish. 1st editio. The Laboratory Zebrafish. CRC Press; 2016.
230. Ribas L, Piferrer F. The zebrafish (*Danio rerio*) as a model organism, with emphasis on applications for finfish aquaculture research. Rev Aquac. 2014;6(4):209–40.
231. Lawrence C, Mason T. Zebrafish housing systems: A review of basic operating principles and considerations for design and functionality. ILAR J. 2012;53(2):179–91.
232. Lawrence C, James A, Mobley S. Successful replacement of Artemia salina nauplii with marine rotifers (*Brachionus plicatilis*) in the diet of preadult zebrafish (*Danio rerio*). Zebrafish. 2015;12(5):366–71.
233. C. Certal A, Farias M, C. Certal A. Different feeds and feeding regimens have an impact on zebrafish larval rearing and breeding performance. Int J Mar Biol Res. 2016;1(1):1–8.
234. Martins G, Diogo P, Pinto W, Gavaia PJ. Early transition to microdiets improves Growth, reproductive performance and reduces skeletal anomalies in zebrafish (*Danio rerio*). Zebrafish. 2019;16(3):300–7.
235. Cauley JA. Public health impact of osteoporosis. J Gerontol - Ser A Biol Sci Med Sci. 2013;68(10):1243–51.
236. Compston J. Osteoporosis: Social and economic impact. Radiol Clin North Am. 2010;48(3):477–82.
237. Kim J, Lee E, Kim S, Lee TJ. Economic burden of osteoporotic fracture of the elderly in South Korea: A national survey. Value Heal Reg Issues. 2016;9:36–41.
238. Smith SS, Reyes JR, Arbon KS, Harvey WA, Hunt LM, Heggland SJ. Cadmium-induced decrease in RUNX2 mRNA expression and recovery by the antioxidant N-acetylcysteine (NAC) in the human osteoblast-like cell line, Saos-2. Toxicol Vitr. 2009;23(1):60–6.
239. Pisani P, Renna MD, Conversano F, Casciaro E, Muratore M, Quarta E, et al. Screening and early diagnosis of osteoporosis through X-ray and ultrasound based techniques. World J Radiol. 2013;5(11):398–410.
240. Bernabei R, Martone AM, Ortolani E, Landi F, Marzetti E. Screening , diagnosis and treatment of osteoporosis: A brief review. Clin Cases Miner Bone Metab. 2014;11(3):201–7.
241. Carson MA, Clarke SA. Bioactive compounds from marine organisms: Potential for bone growth and healing. Mar Drugs. 2018;16(9):340.
242. Carson MA, Nelson J, Cancela ML, Laizé V, Gavaia PJ, Rae M, et al. Red algal extracts from Plocamium lyngbyanum and Ceramium secundatum stimulate osteogenic activities in vitro and bone growth in zebrafish larvae. Sci Rep. 2018;8(1):7725.
243. Carson MA, Nelson J, Cancela ML, Laizé V, Gavaia PJ, Rae M, et al. Screening for osteogenic activity in extracts from Irish marine organisms: The potential of Ceramium pallidum. Cray JJ, editor. PLoS One. 2018;13(11):e0207303.
244. Lim Y-S, Ok Y-J, Hwang S-Y, Kwak J-Y, Yoon S. Marine collagen as a promising biomaterial for biomedical applications. Mar Drugs. 2019;17(8):467.
245. Surget G, Roberto VP, Le Lann K, Mira S, Guérard F, Laizé V, et al. Marine green macroalgae: A source of natural compounds with mineralogenic and antioxidant activities. J Appl Phycol. 2017;29(1):575–84.
246. Bergen DJM, Kague E, Hammond CL. Zebrafish as an emerging model for osteoporosis: A primary testing platform for screening new osteo-active compounds. Front Endocrinol. 2019;10:6.
247. Lieschke GJ, Currie PD. Animal models of human disease: Zebrafish swim into view. Nat Rev Genet. 2007;8(5):353–67.
248. Zampieri RM, Adessi A, Caldara F, Codato A, Furlan M, Rampazzo C, et al. Anti-inflammatory activity of Exopolysaccharides from Phormidium sp. ETS05, the most abundant cyanobacterium of the therapeutic Euganean thermal muds, using the zebrafish model. Biomolecules. 2020;10(4):582.
249. Doube M, Kłosowski MM, Arganda-Carreras I, Cordelières FP, Dougherty RP, Jackson JS, et al. BoneJ: Free and extensible bone image analysis in ImageJ. Bone. 2010;47(6):1076–9.
250. Bassett JHD, van der Spek A, Gogakos A, Williams GR. Quantitative X-ray imaging of rodent bone by Faxitron. In: Helfrich MH, Ralston SH, editors. Bone Research Protocols, Methods in Molecular Biology. Totowa, NJ: Humana Press; 2012. p. 499–506. (Methods in Molecular

Biology; vol. 816).
251. Rantalainen T, Nikander R, Heinonen A, Daly RM, Sievänen H. An open source approach for regional cortical bone mineral density analysis. J Musculoskelet Neuronal Interact. 2011;11(3):243–8.
252. Ding Y, Vanselow D, Yakovlev M, Katz S, Lin A, Clark D, et al. Three-dimensional histology of whole zebrafish by sub-micron synchrotron X-ray micro-tomography. bioRxiv. 2018;1:392381.
253. Charles JF, Sury M, Tsang K, Urso K, Henke K, Huang Y, et al. Utility of quantitative micro-computed tomographic analysis in zebrafish to define gene function during skeletogenesis. Bone. 2017;101:162–71.
254. Miura K, Paul-Gilloteaux P, Tosi S, Colombelli J. Workflows and Components of Bioimage Analysis. In: Miura K, Sladoje N, editors. Bioimage Data Analysis Workflows. Cham: Springer International Publishing; 2020. p. 1–7.
255. Kim Y Il, Lee S, Jung SH, Kim HT, Choi JH, Lee MS, et al. Establishment of a bone-specific col10a1:GFP transgenic zebrafish. Mol Cells. 2013;36(2):145–50.
256. Ridler TW, Calvard S. Picture Thresholding Using an Iterative Selection Method. IEEE Trans Syst Man Cybern. 1978;8(8):630–2.
257. Zack GW, Rogers WE, Latt SA. Automatic measurement of sister chromatid exchange frequency. J Histochem Cytochem. 1977;25(7):741–53.
258. Kapur JN, Sahoo PK, Wong AKC. A new method for gray-level picture thresholding using the entropy of the histogram. Comput Vision, Graph Image Process. 1985;29(3):273–85.
259. Li CH, Tam PKS. An iterative algorithm for minimum cross entropy thresholding. Pattern Recognit Lett. 1998;
260. Leymarie F, Levine MD. Fast raster scan distance propagation on the discrete rectangular lattice. CVGIP Image Underst. 1992;55(1):84–94.
261. Compston JE, McClung MR, Leslie WD. Osteoporosis. Lancet. 2019;393:364–76.
262. Sözen T, Özışık L, Başaran NÇ. An overview and management of osteoporosis. Eur J Rheumatol. 2017;4:46–56.
263. Cundy T. Paget's disease of bone. Metabolism. 2018;80:5–14.
264. Giacomotto J, Ségalat L. High-throughput screening and small animal models, where are we? Br J Pharmacol. 2010;160:204–16.
265. Lee KY, Jang GH, Byun CH, Jeun M, Searson PC, Lee KH. Zebrafish models for functional and toxicological screening of nanoscale drug delivery systems: promoting preclinical applications. Biosci Reports. 2017;37:BSR20170199.
266. Jang K, Sato K, Igawa K, Chung U, Kitamori T. Development of an osteoblast-based 3D continuous-perfusion microfluidic system for drug screening. Anal Bioanal Chem. 2008;390:825–32.
267. Rissanen JP, Halleen JM. Models and screening assays for drug discovery in osteoporosis. Expert Opin Drug Discov. 2010;5(12):1163–74.
268. Kolanthai E, Veerla SC, Khajuria DK, Mahapatra DR. Optical diagnostics of osteoblast cells and osteogenic drug screening. In: Choi B, editor. Photonic Therapeutics and Diagnostics XII. 2016. p. 96894I.
269. Czekanska EM, Stoddart MJ, Richards RG, Hayes JS. In search of an osteoblast cell model for in vitro research. Eur Cells Mater. 2012;24:1–17.
270. Yuan X-Y, Wang M, Lei S, Yang Q-X, Liu Y-Q. Rapid screening of active components with an osteoclastic inhibitory effect in Herba epimedii using quantitative pattern-activity relationships based on joint-action models. molecules. 2017;22:1767.
271. Fleming A, Sato M, Goldsmith P. High-Throughput In Vivo Screening for Bone Anabolic Compounds with Zebrafish. J Biomol Screen. 2005;10(8):823–31.
272. Chen J, Lai Y, Tsai J, Hsiao C. Live Fluorescent Staining Platform for Drug-Screening and Mechanism-Analysis in Zebrafish for Bone Mineralization. Molecules. 2017;22(12):2068.
273. Huang H, Lin H, Lan F, Wu Y, Yang Z, Zhang J. Application of bone transgenic zebrafish in anti-osteoporosis chemical screening. Anim Model Exp Med. 2018;1(1):53–61.
274. Rosa JT, Laizé V, Gavaia PJ, Cancela ML. Fish Models of Induced Osteoporosis. Front Cell Dev Biol. 2021;9.
275. Hwang WY, Fu Y, Reyon D, Maeder ML, Tsai SQ, Sander JD, et al. Efficient genome editing in zebrafish using a CRISPR-Cas system. Nat Biotechnol. 2013;31:227–9.
276. Cornet C, Di Donato V, Terriente J. Combining zebrafish and CRISPR/Cas9: Toward a more efficient drug discovery pipeline. Front Pharmacol. 2018;9:703.
277. Bairoch A. The Cellosaurus, a cell-line knowledge resource. J Biomol Tech. 2018;29:25–38.
278. Laizé V, Rosa JT, Tarasco M, Cancela ML. Status, challenges, and perspectives of fish cell

culture — Focus on cell lines capable of in vitro mineralization. In: Fernández I, Fernandes J, editors. Cellular and molecular approaches in fish biology. Academic Press; 2022. p. 381–404.
279. Vijayakumar P, Laizé V, Cardeira J, Trindade M, Cancela ML. Development of an In Vitro Cell System from Zebrafish Suitable to Study Bone Cell Differentiation and Extracellular Matrix Mineralization. Zebrafish. 2013;10(4):500–9.
280. Fernández I, Vijayakumar P, Marques C, Cancela ML, Gavaia PJ, Laizé V. Zebrafish vitamin K epoxide reductases: expression in vivo, along extracellular matrix mineralization and under phylloquinone and warfarin in vitro exposure. Fish Physiol Biochem. 2015;41(3):745–59.
281. Pombinho AR, Laizé V, Molha DM, Marques SMP, Cancela ML. Development of two bone-derived cell lines from the marine teleost Sparus aurata; evidence for extracellular matrix mineralization and cell-type-specific expression of matrix Gla protein and osteocalcin. Cell Tissue Res. 2004;315(3):393–406.
282. Roberto VP, Tarasco M, Le Diouron G, Stiger-Pouvreau V, Gavaia PJ, Guérard F, et al. Marine plants as valuable sources of antioxidant and anabolic bone compounds. Calcif Tissue Int. 2019;104(S1):91.
283. Tiago DM, Cancela ML, Aureliano M, Laizé V. Vanadate proliferative and anti-mineralogenic effects are mediated by MAPK and PI-3K/Ras/Erk pathways in a fish chondrocyte cell line. FEBS Lett. 2008;582(9):1381–5.
284. Marques CL, Rafael MS, Cancela ML, Laizé V. Establishment of primary cell cultures from fish calcified tissues. Cytotechnology. 2007;55(1):9–13.
285. Viegas MN, Dias J, Cancela ML, Laizé V. Polyunsaturated fatty acids regulate cell proliferation, extracellular matrix mineralization and gene expression in a gilthead seabream skeletal cell line. J Appl Ichthyol. 2012;28(3):427–32.
286. Tiago DM, Laizé V, Bargelloni L, Ferraresso S, Romualdi C, Cancela ML. Global analysis of gene expression in mineralizing fish vertebra-derived cell lines: new insights into anti-mineralogenic effect of vanadate. BMC Genomics. 2011;12(1):310.
287. Aleström P, D'Angelo L, Midtlyng PJ, Schorderet DF, Schulte-Merker S, Sohm F, et al. Zebrafish: Housing and husbandry recommendations. Lab Anim. 2019;Online first.
288. Tarasco M, Martins G, Gavaia PJ, Bebianno MJ, Cancela ML, Laizé V. ZEB316: A small stand-alone housing system to study microplastics in small teleosts. Zebrafish. 2019;00(00):1–9.
289. Tarasco M, Cordelières FP, Cancela ML, Laizé V. ZFBONE: An ImageJ toolset for semi-automatic analysis of zebrafish bone structures. Bone. 2020;138:115480.
290. Mork L, Crump G. Zebrafish Craniofacial Development: A Window into Early Patterning. In: Current Topics in Developmental Biology. 1st ed. Elsevier Inc.; 2015. p. 235–69.
291. Bensimon-Brito A, Cardeira J, Cancela ML, Huysseune A, Witten PE. Distinct patterns of notochord mineralization in zebrafish coincide with the localization of Osteocalcin isoform 1 during early vertebral centra formation. BMC Dev Biol. 2012;12(1):28.
292. Metz JR, de Vrieze E, Lock E-J, Schulten IE, Flik G. Elasmoid scales of fishes as model in biomedical bone research. J Appl Ichthyol. 2012;28(3):382–7.
293. Pasqualetti S, Banfi G, Mariotti M. The zebrafish scale as model to study the bone mineralization process. J Mol Histol. 2012;43(5):589–95.
294. Pasqualetti S, Banfi G, Mariotti M. Osteoblast and osteoclast behavior in zebrafish cultured scales. Cell Tissue Res. 2012;350(1):69–75.
295. de Vrieze E, Zethof J, Schulte-Merker S, Flik G, Metz JR. Identification of novel osteogenic compounds by an ex-vivo sp7:luciferase zebrafish scale assay. Bone. 2015;74:106–13.
296. Sire JY, Girondot M, Babiar O. Marking zebrafish, Danio rerio (*Cyprinidae*), using scale regeneration. J Exp Zool. 2000;286(3):297–304.
297. de Vrieze E, Sharif F, Metz JR, Flik G, Richardson MK. Matrix metalloproteinases in osteoclasts of ontogenetic and regenerating zebrafish scales. Bone. 2011;48(4):704–12.
298. Sehring IM, Weidinger G. Recent advancements in understanding fin regeneration in zebrafish. WIREs Dev Biol. 2020;9:e367.
299. Pfefferli C, Jaźwińska A. The art of fin regeneration in zebrafish. Regeneration. 2015;2(2):72–83.
300. Hou Y, Lee HJ, Chen Y, Ge J, Osman FOI, McAdow AR, et al. Cellular diversity of the regenerating caudal fin. Sci Adv. 2020;6:eaba2084.
301. Lebedeva L, Zhumabayeva B, Gebauer T, Kisselev I, Aitasheva Z. Zebrafish (*Danio rerio*) as a model for understanding the process of caudal fin regeneration. Zebrafish. 2020;17(6):359–72.
302. Iwasaki M, Kuroda J, Kawakami K, Wada H. Epidermal regulation of bone morphogenesis through the development and regeneration of osteoblasts in the zebrafish scale. Dev Biol. 2018;437(2):105–19.

303. Bergen DJM, Tong Q, Shukla A, Newham E, Zethof J, Lundberg M, et al. Regenerating zebrafish scales express a subset of evolutionary conserved genes involved in human skeletal disease. BMC Biol. 2022;20:21.
304. Akimenko MA, Marí-Beffa M, Becerra J, Géraudie J. Old questions, new tools, and some answers to the mystery of fin regeneration. Dev Dyn. 2003;226(2):190–201.
305. Poss KD, Keating MT, Nechiporuk A. Tales of regeneration in zebrafish. Dev Dyn. 2003;226(2):202–10.
306. Mortier GR, Cohn DH, Cormier-Daire V, Hall C, Krakow D, Mundlos S, et al. Nosology and classification of genetic skeletal disorders: 2019 revision. Am J Med Genet Part A. 2019;179(12):2393–419.
307. Kemp JP, Morris JA, Medina-Gomez C, Forgetta V, Warrington NM, Youlten SE, et al. Identification of 153 new loci associated with heel bone mineral density and functional involvement of GPC6 in osteoporosis. Nat Genet. 2017;49(10):1468–75.
308. Gregson CL, Newell F, Leo PJ, Clark GR, Paternoster L, Marshall M, et al. Genome-wide association study of extreme high bone mass: Contribution of common genetic variation to extreme BMD phenotypes and potential novel BMD-associated genes. Bone. 2018;114:62–71.
309. Kim SK. Identification of 613 new loci associated with heel bone mineral density and a polygenic risk score for bone mineral density, osteoporosis and fracture. PLoS One. 2018;13(7):e0200785.
310. Morris JA, Kemp JP, Youlten SE, Laurent L, Logan JG, Chai R, et al. An Atlas of Human and Murine Genetic Influences on Osteoporosis. bioRxiv. 2018.
311. Wheway G, Schmidts M, Mans D, Szymanska K, Nguyen T, Racher H, et al. An siRNA-based functional genomics screen for the identification of regulators of ciliogenesis and ciliopathy genes. Nat Cell Biol. 2015;17:1074–87.
312. Witten PE, Harris MP, Huysseune A, Winkler C, Outline C. Small teleost fish provide new insights into human skeletal diseases [Internet]. Biophysical Methods in Cell Biology Elsevier Ltd; 2017 p. 321–46.
313. Carnovali M, Banfi G, Mariotti M. Zebrafish Models of Human Skeletal Disorders: Embryo and Adult Swimming Together. Biomed Res Int. 2019;2019.
314. Tonelli F, Bek JW, Besio R, De Clercq A, Leoni L, Salmon P, et al. Zebrafish: A Resourceful Vertebrate Model to Investigate Skeletal Disorders. Front Endocrinol. 2020;11.
315. Valenti MT, Marchetto G, Mottes M, Dalle Carbonare L. Zebrafish: A Suitable Tool for the Study of Cell Signaling in Bone. Cells. 2020;9(8):1–14.
316. Howe K, Clark MD, Torroja CF, Torrance J, Berthelot C, Muffato M, et al. The zebrafish reference genome sequence and its relationship to the human genome. Nature. 2013;496(7446):498–503.
317. Mullins MC, Hammerschmidt M, Haffter P, Nüsslein-Volhard C. Large-scale mutagenesis in the zebrafish: in search of genes controlling development in a vertebrate. Curr Biol. 1994;4(3):189–202.
318. Nasevicius A, Ekker SC. Effective targeted gene 'knockdown' in zebrafish. Nat Genet. 2000;26:216–220.
319. Huang P, Xiao A, Zhou M, Zhu Z, Lin S, Zhang B. Heritable gene targeting in zebrafish using customized TALENs. Vol. 29, Nature Biotechnology. 2011. p. 699–700.
320. Wu N, Liu B, Du H, Zhao S, Li Y, Cheng X, et al. The progress of CRISPR/Cas9-mediated gene editing in generating mouse/zebrafish models of human skeletal diseases. Comput Struct Biotechnol J. 2019;17:954–62.
321. Meyer A, Van De Peer Y. From 2R to 3R: Evidence for a fish-specific genome duplication (FSGD). BioEssays. 2005;27(9):937–45.
322. Force A, Lynch M, Pickett FB, Amores A, Yan YL, Postlethwait J. Preservation of duplicate genes by complementary, degenerative mutations. Genetics. 1999;151(4):1531–45.
323. Luderman LN, Unlu G, Knapik EW. Zebrafish developmental models of skeletal diseases. In: Current Topics in Developmental Biology. 1st ed. Elsevier Inc.; 2017. p. 81–124.
324. Marí-Beffa M, Mesa-Román AB, Duran I. Zebrafish models for human skeletal disorders. Front Genet. 2021;12(August):675331.
325. Dietrich K, Fiedler IAK, Kurzyukova A, López-Delgado AC, McGowan LM, Geurtzen K, et al. Skeletal Biology and Disease Modeling in Zebrafish. J Bone Miner Res. 2021;36(3):436–58.
326. White RM, Sessa A, Burke C, Bowman T, LeBlanc J, Ceol C, et al. Transparent adult zebrafish as a tool for in vivo transplantation analysis. Cell Stem Cell. 2008;2:183–9.
327. Antinucci P, Hindges R. A crystal-clear zebrafish for in vivo imaging. Sci Rep. 2016;6:29490.
328. Guryev V, Koudijs MJ, Berezikov E, Johnson SL, Plasterk RHA, Eeden FJM Van, et al. Genetic variation in the zebrafish. Genome Res. 2006;16:491–7.

329. Lawrence C. The husbandry of zebrafish (*Danio rerio*): A review. Aquaculture. 2007;269:1–20.
330. Ribas L, Valdivieso A, Díaz N, Piferrer F. Appropriate rearing density in domesticated zebrafish to avoid masculinization: links with the stress response. J Exp Biol. 2017;220:1056–64.
331. Reed B, Jennings M. Guidance on the housing and care of zebrafish Danio rerio. Research Animals Department, RSPCA; 2011.
332. Barnard DE, Lewis SM, Teter BB, Thigpen JE. Open- and closed-formula laboratory animal diets and their importance to research. J Am Assoc Lab Anim Sci. 2009;48(6):709–13.
333. Lawrence C. New frontiers for zebrafish management. Methods Cell Biol. 2016;135(24):483–508.
334. Ulloa PE, Medrano JF, Feijoo CG. Zebrafish as animal model for aquaculture nutrition research. Front Genet. 2014;5:313.
335. Carvalho AP, Araújo L, Santos MM. Rearing zebrafish (*Danio rerio*) larvae without live food: evaluation of a commercial, a practical and a purified starter diet on larval performance. Aquac Res. 2006;37:1107–11.
336. Lawrence C, Best J, James A, Maloney K. The effects of feeding frequency on growth and reproduction in zebrafish (*Danio rerio*). Aquaculture. 2012;368–369:103–8.
337. Monteiro JF, Martins S, Farias M, Costa T, Certal AC. The impact of two different cold-extruded feeds and feeding regimens on zebrafish survival, growth and reproductive performance. J Dev Biol. 2018;6:15.
338. Westerfield M. The zebrafish book. A guide for the laboratory use of zebrafish (*Danio rerio*). 4th ed. University of Oregon Press, Eugene; 2000.
339. Diogo P, Martins G, Gavaia P, Pinto W, Dias J, Cancela L, et al. Assessment of nutritional supplementation in phospholipids on the reproductive performance of zebrafish, Danio rerio (Hamilton, 1822). J Appl Ichthyol. 2015;31(S1):3–9.
340. Graf SF, Hötzel S, Liebel U, Stemmer A, Knapp HF. Image-based fluidic sorting system for automated zebrafish egg sorting into multiwell plates. J Lab Autom. 2011;16(2):105–11.
341. White DT, Eroglu AU, Wang G, Zhang L, Sengupta S, Ding D, et al. ARQiv-HTS, a versatile whole-organism screening platform enabling in vivo drug discovery at high-throughput rates. Nat Protoc. 2016;11(12):2432–53.
342. Monstad-Rios AT, Watson CJ, Kwon RY. ScreenCube: A 3D Printed System for Rapid and Cost-Effective Chemical Screening in Adult Zebrafish. Zebrafish. 2018;15(1):1–8.
343. Reischl M, Bartschat A, Liebel U, Gehrig J, Müller F, Mikut R. ZebrafishMiner: An open source software for interactive evaluation of domain-specific fluorescence in zebrafish. Curr Dir Biomed Eng. 2017;3(2):199–202.
344. Liu T, Nie J, Li G, Guo L, Wong STC. ZFIQ: A software package for zebrafish biology. Bioinformatics. 2008;24(3):438–9.
345. Adatto I, Lawrence C, Thompson M, Zon LI. A new system for the rapid collection of large numbers of developmentally staged zebrafish embryos. PLoS One. 2011;6(6):e21715.
346. Mandrell D, Truong L, Jephson C, Sarker MR, Moore A, Lang C, et al. Automated zebrafish chorion removal and single embryo placement: Optimizing throughput of zebrafish developmental toxicity screens. J Lab Autom. 2012;17(1):66–74.
347. Spaink HP, Cui C, Wiweger MI, Jansen HJ, Veneman WJ, Marín-Juez R, et al. Robotic injection of zebrafish embryos for high-throughput screening in disease models. Methods. 2013;62:246–54.
348. Wang W, Liu X, Gelinas D, Ciruna B, Sun Y. A fully automated robotic system for microinjection of zebrafish embryos. PLoS One. 2007;2(9):e862.
349. Chi Z, Xu Q, Ai N, Ge W. Design and Development of an Automatic Microinjection System for High-Throughput Injection of Zebrafish Larvae. IEEE Robot Autom Lett. 2022;7:1848–55.
350. Mikut R, Dickmeis T, Driever W, Geurts P, Hamprecht FA, Kausler BX, et al. Automated processing of zebrafish imaging data: A survey. Zebrafish. 2013;10(3):401–21.
351. Wang J, Tan Z, Peng J, Qiu Q, Li M. The behaviors of microplastics in the marine environment. Mar Environ Res. 2016;113:7–17.
352. Tarasco M, Gavaia PJ, Bensimon-Brito A, Cardeira-da-Silva J, Ramkumar S, Cordelières FP, et al. New insights into benzo[α]pyrene osteotoxicity in zebrafish. Ecotoxicol Environ Saf. 2021;226:112838.
353. Lönnstedt OM, Eklöv P. Environmentally relevant concentrations of microplastic particles influence larval fish ecology. Science (80-). 2016;352(6290):1213–6.
354. Au SY, Bruce TF, Bridges WC, Klaine SJ. Responses of Hyalella azteca to acute and chronic microplastic exposures. Environ Toxicol Chem. 2015;34(11):2564–72.
355. Sjollema SB, Redondo-Hasselerharm P, Leslie HA, Kraak MHS, Vethaak AD. Do plastic

particles affect microalgal photosynthesis and growth? Aquat Toxicol. 2016;170:259–61.
356. Rehse S, Kloas W, Zarfl C. Short-term exposure with high concentrations of pristine microplastic particles leads to immobilisation of Daphnia magna. Chemosphere. 2016;153:91–9.
357. Sussarellu R, Suquet M, Thomas Y, Lambert C, Fabioux C, Pernet MEJ, et al. Oyster reproduction is affected by exposure to polystyrene microplastics. Proc Natl Acad Sci. 2016;113(9):201519019.
358. Lee K, Shim WJ, Kwon OY, Kang J. Size-Dependent E ff ects of Micro Polystyrene Particles in the Marine Copepod Tigriopus japonicus. Environ Sci Technol. 2013;47(August):11278–11283.
359. Wright SL, Rowe D, Thompson RC, Galloway TS. Microplastic ingestion decreases energy reserves in marine worms. Curr Biol. 2013;23(23):R1031–3.
360. Green DS, Boots B, Sigwart J, Jiang S, Rocha C. Effects of conventional and biodegradable microplastics on a marine ecosystem engineer (*Arenicola marina*) and sediment nutrient cycling. Environ Pollut. 2016;208:426–34.
361. Mak CW, Ching-Fong Yeung K, Chan KM. Acute toxic effects of polyethylene microplastic on adult zebrafish. Ecotoxicol Environ Saf. 2019;182:109442.
362. Sheng C, Zhang S, Zhang Y. The influence of different polymer types of microplastics on adsorption, accumulation, and toxicity of triclosan in zebrafish. J Hazard Mater. 2021;402:123733.
363. Qiang L, Cheng J. Exposure to microplastics decreases swimming competence in larval zebrafish (*Danio rerio*). Ecotoxicol Environ Saf. 2019;176:226–33.
364. Limonta G, Mancia A, Benkhalqui A, Bertolucci C, Abelli L, Fossi MC, et al. Microplastics induce transcriptional changes, immune response and behavioral alterations in adult zebrafish. Sci Rep. 2019;9(1):1–11.
365. Lei L, Wu S, Lu S, Liu M, Song Y, Fu Z, et al. Microplastic particles cause intestinal damage and other adverse effects in zebrafish Danio rerio and nematode Caenorhabditis elegans. Sci Total Environ. 2018;619–620:1–8.
366. Schneider CA, Rasband WS, Eliceiri KW. NIH Image to ImageJ: 25 years of image analysis. Nat Methods. 2012;9(7):671–5.
367. Tarasco M, Martins G, Gavaia PJ, Bebianno MJ, Cancela ML, Laizé V. ZEB316: A small stand-alone housing system to study microplastics in small teleosts. Zebrafish. 2020;17(1):18–26.
368. Diogo P, Martins G, Nogueira R, Marreiros A, Gavaia PJ, Cabrita E. Cryoprotectants synergy improve zebrafish sperm cryopreservation and offspring skeletogenesis. Cryobiology. 2019;91(October):115–27.
369. Bird NC, Mabee PM. Developmental morphology of the axial skeleton of the zebrafish,Danio rerio (Ostariophysi: Cyprinidae). Dev Dyn. 2003;228(3):337–57.
370. Bensimon-Brito A, Cardeira J, Dionísio G, Huysseune A, Cancela ML, Witten PE. Revisiting in vivo staining with alizarin red S - A valuable approach to analyse zebrafish skeletal mineralization during development and regeneration. BMC Dev Biol. 2016;16(1).
371. Pfaffl MW 2001. A new mathematical model for relative quantification in real-time RT-PCR. Nucleic Acids Res. 2001;29(9):e45.
372. TANG R, DODD A, LAI D, MCNABB WC, LOVE DR. Validation of Zebrafish (*Danio rerio*) Reference Genes for Quantitative Real-time RT-PCR Normalization. Acta Biochim Biophys Sin (Shanghai). 2007;39(5):384–90.
373. Espinosa C, Esteban MÁ, Cuesta A. Dietary administration of PVC and PE microplastics produces histological damage, oxidative stress and immunoregulation in European sea bass (*Dicentrarchus labrax L.*). Fish Shellfish Immunol. 2019;95:574–83.
374. Khosrovyan A, Gabrielyan B, Kahru A. Ingestion and effects of virgin polyamide microplastics on Chironomus riparius adult larvae and adult zebrafish Danio rerio. Chemosphere. 2020;259:127456.
375. Yang H, Lai H, Huang J, Sun L, Mennigen JA, Wang Q, et al. Polystyrene microplastics decrease F–53B bioaccumulation but induce inflammatory stress in larval zebrafish. Chemosphere. 2020;255.
376. Santos D, Félix L, Luzio A, Parra S, Cabecinha E, Bellas J, et al. Toxicological effects induced on early life stages of zebrafish (*Danio rerio*) after an acute exposure to microplastics alone or co-exposed with copper. Chemosphere. 2020;261.
377. Pannetier P, Morin B, Le Bihanic F, Dubreil L, Clérandeau C, Chouvellon F, et al. Environmental samples of microplastics induce significant toxic effects in fish larvae. Environ Int. 2020;134:105047.
378. Jovanović B, Gökdağ K, Güven O, Emre Y, Whitley EM, Kideys AE. Virgin microplastics are not causing imminent harm to fish after dietary exposure. Mar Pollut Bull. 2018;130:123–31.

379. Capó X, Company JJ, Alomar C, Compa M, Sureda A, Grau A, et al. Long-term exposure to virgin and seawater exposed microplastic enriched-diet causes liver oxidative stress and inflammation in gilthead seabream Sparus aurata, Linnaeus 1758. Sci Total Environ. 2021;767:144976.
380. Mazurais D, Ernande B, Quazuguel P, Severe A, Huelvan C, Madec L, et al. Evaluation of the impact of polyethylene microbeads ingestion in European sea bass (*Dicentrarchus labrax*) larvae. Mar Environ Res. 2015;112:78–85.
381. Jovanović B. Ingestion of microplastics by fish and its potential consequences from a physical perspective. Integr Environ Assess Manag. 2017;13(3):510–5.
382. Zhu M, Chernick M, Rittschof D, Hinton DE. Chronic dietary exposure to polystyrene microplastics in maturing Japanese medaka (*Oryzias latipes*). Aquat Toxicol. 2020;220:105396.
383. Assas M, Qiu X, Chen K, Ogawa H, Xu H, Shimasaki Y, et al. Bioaccumulation and reproductive effects of fluorescent microplastics in medaka fish. Mar Pollut Bull. 2020;158:4–9.
384. Wang J, Li Y, Lu L, Zheng M, Zhang X, Tian H, et al. Polystyrene microplastics cause tissue damages, sex-specific reproductive disruption and transgenerational effects in marine medaka (Oryzias melastigma). Environ Pollut. 2019;254:113024.
385. Sun D, Chen Q, Zhu B, Lan Y, Duan S. Long-term exposure to benzo[a]pyrene affects sexual differentiation and embryos toxicity in three generations of marine medaka (*Oryzias melastigma*). Int J Environ Res Public Health. 2020;17(3).
386. Corrales J, Fang X, Thornton C, Mei W, Barbazuk WB, Duke M, et al. Effects on specific promoter DNA methylation in zebrafish embryos and larvae following benzo[a]pyrene exposure. Comp Biochem Physiol Part - C Toxicol Pharmacol. 2014;163:37–46.
387. Gao D, Lin J, Ou K, Chen Y, Li H, Dai Q, et al. Embryonic exposure to benzo(a)pyrene inhibits reproductive capability in adult female zebrafish and correlation with DNA methylation. Environ Pollut. 2018;240:403–11.
388. Sant KE, Timme-Laragy AR. Zebrafish as a Model for Toxicological Perturbation of Yolk and Nutrition in the Early Embryo. Curr Environ Heal Reports. 2018;5(1):125–33.
389. Tarasco M, Gavaia PJ, Bensimon-Brito A, Cardeira-da-Silva J, Ramkumar S, Cordelières FP, et al. New insights into benzo[α]pyrene osteotoxicity in zebrafish. Ecotoxicol Environ Saf. 2021;226(July):112838.
390. Mo J, Au DW-T, Guo J, Winkler C, Kong RY-C, Seemann F. Benzo[a]pyrene osteotoxicity and the regulatory roles of genetic and epigenetic factors: A review. Crit Rev Environ Sci Technol. 2021;0(0):1–39.
391. Movahedinia A, Salamat N, Kheradmand P. Effects of the environmental endocrine disrupting compound benzo[a]pyrene on thyroidal status of abu mullet (*Liza abu*) during short-term exposure. Toxicol Reports. 2018;5:377–82.
392. Abe E, Marians RC, Yu W, Wu X, Ando T, Li Y, et al. TSH Is a Negative Regulator of Skeletal Remodeling. Cell. 2003;115(2):151–62.
393. Kim YS, Ho SB. Intestinal goblet cells and mucins in health and disease: Recent insights and progress. Curr Gastroenterol Rep. 2010;12(5):319–30.
394. Zhao X, Pack M. Modeling intestinal disorders using zebrafish. In: Methods in Cell Biology. Elsevier Ltd; 2017. p. 241–70.
395. Brugman S, Liu KY, Lindenbergh-Kortleve D, Samsom JN, Furuta GT, Renshaw SA, et al. Oxazolone-Induced Enterocolitis in Zebrafish Depends on the Composition of the Intestinal Microbiota. Gastroenterology. 2009;137(5):1757-1767.e1.
396. Farré R, Fiorani M, Rahiman SA, Matteoli G. Intestinal permeability, inflammation and the role of nutrients. Nutrients. 2020;12(4):1–18.
397. Hoseinifar SH, Yousefi S, Van Doan H, Ashouri G, Gioacchini G, Maradonna F, et al. Oxidative Stress and Antioxidant Defense in Fish: The Implications of Probiotic, Prebiotic, and Synbiotics. Rev Fish Sci Aquac. 2020;29(2):198–217.
398. Picardo M, Dell'Anna ML. Oxidative Stress. In: Vitiligo. Berlin, Heidelberg: Springer Berlin Heidelberg; 2010. p. 231–7.
399. Umamaheswari S, Priyadarshinee S, Bhattacharjee M, Kadirvelu K, Ramesh M. Exposure to polystyrene microplastics induced gene modulated biological responses in zebrafish (*Danio rerio*). Chemosphere. 2021;281:128592.
400. Umamaheswari S, Priyadarshinee S, Kadirvelu K, Ramesh M. Polystyrene microplastics induce apoptosis via ROS-mediated p53 signaling pathway in zebrafish. Chem Biol Interact. 2021;345(March):109550.
401. Rangasamy B, Malafaia G, Maheswaran R. Evaluation of antioxidant response and Na+-K+-ATPase activity in zebrafish exposed to polyethylene microplastics: Shedding light on a

physiological adaptation. J Hazard Mater. 2021;127789.
402. Wauquier F, Leotoing L, Coxam V, Guicheux J, Wittrant Y. Oxidative stress in bone remodelling and disease. Trends Mol Med. 2009;15(10):468–77.
403. Domazetovic V, Marcucci G, Iantomasi T, Brandi ML, Vincenzini MT. Oxidative stress in bone remodeling: Role of antioxidants. Clin Cases Miner Bone Metab. 2017;14(2):209–16.
404. Imhof HK, Rusek J, Thiel M, Wolinska J, Laforsch C. Do microplastic particles affect *Daphnia magna* at the morphological, life history and molecular level? PLoS One. 2017;12(11):1–20.
405. Mohanty BP, Mahanty A, Mitra T, Parija SC, Mohanty S. Heat Shock Proteins in Stress in Teleosts. In 2018. p. 71–94.
406. Xia X, Sun M, Zhou M, Chang Z, Li L. Polyvinyl chloride microplastics induce growth inhibition and oxidative stress in Cyprinus carpio var. larvae. Sci Total Environ. 2020;716.
407. Shin KH, Kim KW, Ahn Y. Use of biosurfactant to remediate phenanthrene-contaminated soil by the combined solubilization-biodegradation process. J Hazard Mater. 2006;137(3):1831–7.
408. Hadrup N, Mielzyńska-Švach D, Kozłowska A, Campisi M, Pavanello S, Vogel U. Association between a urinary biomarker for exposure to PAH and blood level of the acute phase protein serum amyloid A in coke oven workers. Environ Heal A Glob Access Sci Source. 2019;18(1):1–9.
409. Hilton DC, Trinidad DA, Hubbard K, Li Z, Sjödin A. Measurement of urinary Benzo[a]pyrene tetrols and their relationship to other polycyclic aromatic hydrocarbon metabolites and cotinine in humans. Chemosphere. 2017;189(1):365–72.
410. Oliveira M, Capelas S, Delerue-Matos C, Morais S. Grill workers exposure to polycyclic aromatic hydrocarbons: Levels and excretion profiles of the urinary biomarkers. Int J Environ Res Public Health. 2021;18(1):1–15.
411. Santonicola S, De Felice A, Cobellis L, Passariello N, Peluso A, Murru N, et al. Comparative study on the occurrence of polycyclic aromatic hydrocarbons in breast milk and infant formula and risk assessment. Chemosphere. 2017;175:383–90.
412. Suvarapu LN, Baek SO. Review on the Concentrations of Benzo[a]pyrene in the Indian Environment Since 1983. Polycycl Aromat Compd. 2017;37(4):235–56.
413. Moon H, Kang S, Kim H, Choi M, Yu J, Choi H, et al. Polycyclic Aromatic Hydrocarbons (PAHs) in Seawater and Marine Sediments from Mokpo Coast in Korea. J Korean Soc Environ Anal. 2007;10(2):83–90.
414. Manoli E, Samara C. Polycyclic aromatic hydrocarbons in natural waters: Sources, occurrence and analysis. TrAC - Trends Anal Chem. 1999;18(6):417–28.
415. Zhou J., Maskaoui K. Distribution of polycyclic aromatic hydrocarbons in water and surface sediments from Daya Bay, China. Environ Pollut. 2003;121(2):269–81.
416. Danion M, Deschamps MH, Thomas-Guyon H, Bado-Nilles A, Le Floch S, Quentel C, et al. Effect of an experimental oil spill on vertebral bone tissue quality in European sea bass (Dicentrarchus labrax L.). Ecotoxicol Environ Saf. 2011;74(7):1888–95.
417. Rondelli CM, Larsen MC, N'Jai A, Czuprynski CJ, Jefcoate CR. PAHs target hematopoietic linages in bone marrow through cyp1b1 primarily in mesenchymal stromal cells but not AhR: A reconstituted in vitro model. Stem Cells Int. 2016;2016.
418. Iqbal J, Sun L, Cao J, Yuen T, Lu P, Bab I, et al. Smoke carcinogens cause bone loss through the aryl hydrocarbon receptor and induction of Cyp1 enzymes. Proc Natl Acad Sci. 2013;110(27):11115–20.
419. Al-Bashaireh AM, Haddad LG, Weaver M, Chengguo X, Kelly DL, Yoon S. The Effect of Tobacco Smoking on Bone Mass: An Overview of Pathophysiologic Mechanisms. J Osteoporos. 2018;2018.
420. Chen YY, Kao TW, Wang CC, Wu CJ, Zhou YC, Chen WL. Association between polycyclic aromatic hydrocarbons exposure and bone turnover in adults. Eur J Endocrinol. 2020;182(3):333–41.
421. Guo J, Huang Y, Bian S, Zhao C, Jin Y, Yu D, et al. Associations of urinary polycyclic aromatic hydrocarbons with bone mass density and osteoporosis in U.S. adults, NHANES 2005–2010. Environ Pollut. 2018;240:209–18.
422. Seemann F, Peterson DR, Witten PE, Guo BS, Shanthanagouda AH, Ye RR, et al. Insight into the transgenerational effect of benzo[a]pyrene on bone formation in a teleost fish (*Oryzias latipes*). Comp Biochem Physiol Part - C Toxicol Pharmacol. 2015;178:60–7.
423. Olsvik PA, Hansen BH, Nordtug T, Moren M, Holen E, Lie KK. Transcriptional evidence for low contribution of oil droplets to acute toxicity from dispersed oil in first feeding Atlantic cod (*Gadus morhua*) larvae. Comp Biochem Physiol - C Toxicol Pharmacol. 2011;154(4):333–45.
424. Carls MG, Thedinga JF. Exposure of pink salmon embryos to dissolved polynuclear aromatic

hydrocarbons delays development, prolonging vulnerability to mechanical damage. Mar Environ Res. 2010;69(5):318–25.
425. Barron MG, Carls MG, Heintz R, Rice SD. Evaluation of fish early life-stage toxicity models of chronic embryonic exposures to complex polycyclic aromatic hydrocarbon mixtures. Toxicol Sci. 2004;78(1):60–7.
426. He C, Zuo Z, Shi X, Li R, Chen D, Huang X, et al. Effects of benzo(a)pyrene on the skeletal development of Sebastiscus marmoratus embryos and the molecular mechanism involved. Aquat Toxicol. 2011;101(2):335–41.
427. Seemann F, Jeong CB, Zhang G, Wan MT, Guo B, Peterson DR, et al. Ancestral benzo[a]pyrene exposure affects bone integrity in F3 adult fish (*Oryzias latipes*). Aquat Toxicol. 2017;183:127–34.
428. Corrales J, Thornton C, White M, Willett KL. Multigenerational effects of benzo[a]pyrene exposure on survival and developmental deformities in zebrafish larvae. Aquat Toxicol. 2014;148:16–26.
429. Allaeys I, Rusu D, Picard S, Pouliot M, Borgeat P, Poubelle PE. Osteoblast retraction induced by adherent neutrophils promotes osteoclast bone resorption: implication for altered bone remodeling in chronic gout. Lab Investig. 2011;91(6):905–20.
430. Bastian OW, Croes M, Alblas J, Koenderman L, Leenen LPH, Blokhuis TJ. Neutrophils inhibit synthesis of mineralized extracellular matrix by human bone marrow-derived stromal cells in vitro. Front Immunol. 2018;9:1–13.
431. Kim AR, Kim JH, Choi YH, Jeon YE, Cha JH, Bak EJ, et al. The presence of neutrophils causes RANKL expression in periodontal tissue, giving rise to osteoclast formation. J Periodontal Res. 2020;55(6):868–76.
432. Sugisaki R, Miyamoto Y, Yoshimura K, Sasa K, Kaneko K, Tanaka M, et al. Possible involvement of elastase in enhanced osteoclast differentiation by neutrophils through degradation of osteoprotegerin. Bone. 2020;132(October 2019):115216.
433. Renshaw SA, Loynes CA, Trushell DMI, Elworthy S, Ingham PW, Whyte MKB. Atransgenic zebrafish model of neutrophilic inflammation. Blood. 2006;108(13):3976–8.
434. Walker MB, Kimmel CB. A two-color acid-free cartilage and bone stain for zebrafish larvae. Biotech {&} Histochem Off Publ Biol Stain Comm. 2007;82(1):23–8.
435. Witten PE. Enzyme histochemical characteristics of osteoblasts and mononucleated osteoclasts in a teleost fish with acellular bone (*Oreochromis niloticus*, Cichlidae). Cell Tissue Res. 1997;287(3):591–9.
436. Andrews S. FastQC: a quality control tool for high throughput sequence data. 2010.
437. Bolger AM, Lohse M, Usadel B. Trimmomatic: a flexible trimmer for Illumina sequence data. Bioinformatics. 2014;30(15):2114–20.
438. Dobin A, Davis CA, Schlesinger F, Drenkow J, Zaleski C, Jha S, et al. STAR: Ultrafast universal RNA-seq aligner. Bioinformatics. 2013;
439. Liao Y, Smyth GK, Shi W. FeatureCounts: An efficient general purpose program for assigning sequence reads to genomic features. Bioinformatics. 2014;
440. Mo J, Au DWT, Wan MT, Shi J, Zhang G, Winkler C, et al. Multigenerational Impacts of Benzo[a]pyrene on Bone Modeling and Remodeling in Medaka (*Oryzias latipes*). Environ Sci Technol. 2020;54(19):12271–84.
441. da Silva Moreira S, de Lima Inocêncio LC, Jorge BC, Reis ACC, Hisano H, Arena AC. Effects of benzo(a)pyrene at environmentally relevant doses on embryo-fetal development in rats. Environ Toxicol. 2020;(November):1–9.
442. Monnouchi S, Maeda H, Yuda A, Serita S, Wada N, Tomokiyo A, et al. Benzo[a]pyrene/aryl hydrocarbon receptor signaling inhibits osteoblastic differentiation and collagen synthesis of human periodontal ligament cells. J Periodontal Res. 2016;51(6):779–88.
443. An L, Shi Q, Fan M, Huang G, Zhu M, Zhang M, et al. Benzo[a]pyrene injures BMP2-induced osteogenic differentiation of mesenchymal stem cells through AhR reducing BMPRII. Ecotoxicol Environ Saf. 2020;203:110930.
444. Zhou Y, Jiang R, An L, Wang H, Cheng S, Qiong S, et al. Benzo[a]pyrene impedes self-renewal and differentiation of mesenchymal stem cells and influences fracture healing. Sci Total Environ. 2017;587–588:305–15.
445. Capulli M, Paone R, Rucci N. Osteoblast and osteocyte: Games without frontiers. Arch Biochem Biophys. 2014;561(May):3–12.
446. Gavaia PJ, Simes DC, Ortiz-Delgado JB, Viegas CSB, Pinto JP, Kelsh RN, et al. Osteocalcin and matrix Gla protein in zebrafish (*Danio rerio*) and Senegal sole (*Solea senegalensis*): Comparative gene and protein expression during larval development through adulthood. Gene

Expr Patterns. 2006;6(6):637–52.
447. Roberto VP, Martins G, Pereira A, Rodrigues S, Grenha A, Pinto W, et al. Insights from dietary supplementation with zinc and strontium on the skeleton of zebrafish, *Danio rerio* (Hamilton, 1822) larvae: From morphological analysis to osteogenic markers. J Appl Ichthyol. 2018;34(2):512–23.
448. Fazenda C, Martins G, Gavaia PJ, Cancela ML, Conceição N. Generation of zebrafish Danio rerio (Hamilton, 1822) transgenic lines overexpressing a heat-shock mediated Gla-rich protein. J Appl Ichthyol. 2018;34(2):472–80.
449. Bagwell J, Norman J, Ellis K, Peskin B, Hwang J, Ge X, et al. Notochord vacuoles absorb compressive bone growth during zebrafish spine formation. Elife. 2020;9:1–28.
450. Martini A, Huysseune A, Witten PE, Boglione C. Plasticity of the skeleton and skeletal deformities in zebrafish (*Danio rerio*) linked to rearing density. J Fish Biol. 2020;14272.
451. Bensimon-Brito A, Cancela ML, Huysseune A, Witten PE. The zebrafish (*Danio rerio*) caudal complex - a model to study vertebral body fusion. J Appl Ichthyol. 2010;26(2):235–8.
452. Witten PE, Hall BK. Teleost Skeletal Plasticity: Modulation, Adaptation, and Remodelling. Copeia. 2015;103(4):727–39.
453. Boursiaki V, Theochari C, Zaoutsos SP, Mente E, Vafidis D, Apostologamvrou C, et al. Skeletal deformity of scoliosis in gilthead seabreams (*Sparus aurata*): Association with changes to calcium-phosphor hydroxyapatite salts and collagen fibers. Water. 2019;11(2).
454. Gray RS, Gonzalez R, Ackerman SD, Minowa R, Griest JF, Bayrak MN, et al. Postembryonic screen for mutations affecting spine development in zebrafish. Dev Biol. 2021;471:18–33.
455. Cox BD, De Simone A, Tornini VA, Singh SP, Di Talia S, Poss KD. In Toto Imaging of Dynamic Osteoblast Behaviors in Regenerating Skeletal Bone. Curr Biol. 2018;28(24):3937-3947.e4.
456. Suzuki N, Sato M, Nassar HF, Abdel-Gawad Fk, Bassem SM, Yachiguchi K, et al. Seawater Polluted with Highly Concentrated Polycyclic Aromatic Hydrocarbons Suppresses Osteoblastic Activity in the Scales of Goldfish, Carassius auratus. Zool Sci. 2016;33(4):407–13.
457. Mathew LK, Andreasen EA, Tanguay RL. Aryl hydrocarbon receptor activation inhibits regenerative growth. Mol Pharmacol. 2006;69(1):257–65.
458. Zodrow JM, Tanguay RL. 2,3,7,8-Tetrachlorodibenzo-P-Dioxin Inhibits Zebrafish Caudal Fin Regeneration. Toxicol Sci. 2003;76(1):151–61.
459. Braunstein JA, Robbins AE, Stewart S, Stankunas K. Basal epidermis collective migration and local Sonic hedgehog signaling promote skeletal branching morphogenesis in zebrafish fins. bioRxiv. 2021;55(2):312–7.
460. Hu Y, Harper M, Acosta B, Donahue J, Bui H, Lee H, et al. Thyroid hormone regulates proximodistal identity in the fin skeleton. bioRxiv. 2020;1–26.
461. Christou M, Iliopoulou M, Witten PE, Koumoundouros G. Segmentation pattern of zebrafish caudal fin is affected by developmental temperature and defined by multiple fusions between segments. J Exp Zool Part B Mol Dev Evol. 2018;(March):1–11.
462. Schraplau A, Schewe B, Neuschäfer-Rube F, Ringel S, Neuber C, Kleuser B, et al. Enhanced thyroid hormone breakdown in hepatocytes by mutual induction of the constitutive androstane receptor (CAR, NR1I3) and arylhydrocarbon receptor by benzo[a]pyrene and phenobarbital. Toxicology. 2015;328:21–8.
463. Peng F, Tsuji G, Zhang J, Chen Z, Furue M. Potential role of PM2.5 in melanogenesis. Environ Int. 2019;132(August):105063.
464. Stockinger B, Meglio P Di, Gialitakis M, Duarte JH. The Aryl Hydrocarbon Receptor: Multitasking in the Immune System. Annu Rev Immunol. 2014;32(1):403–32.
465. Larigot L, Juricek L, Dairou J, Coumoul X. AhR signaling pathways and regulatory functions. Biochim Open. 2018;7:1–9.
466. Roztocil E, Hammond CL, Gonzalez MO, Feldon SE, Woeller CF. The aryl hydrocarbon receptor pathway controls matrix metalloproteinase-1 and collagen levels in human orbital fibroblasts. Sci Rep. 2020;10(1):1–16.
467. Park R, Madhavaram S, Ji JD. The Role of Aryl-Hydrocarbon Receptor (AhR) in Osteoclast Differentiation and Function. Cells. 2020;9(10):2294.
468. Yu H, Jiang L, Wan B, Zhang W, Yao L, Che T, et al. The role of aryl hydrocarbon receptor in bone remodeling. Prog Biophys Mol Biol. 2018;134(1):44–9.
469. Zarei A, Morovat A, Javaid K, Brown CP. Vitamin D receptor expression in human bone tissue and dose-dependent activation in resorbing osteoclasts. Bone Res. 2016;4(1):1–10.
470. van de Peppel J, Franceschi RT, Li Y, van der Eerden BCJ. Vitamin D Regulation of Osteoblast Function. In: Vitamin D. Fourth Edi. Elsevier; 2018. p. 295–308.
471. Vimalraj S. Alkaline phosphatase: Structure, expression and its function in bone mineralization.

Gene. 2020;754(April):144855.
472. Mahapatra D, Franzosa JA, Roell K, Kuenemann MA, Houck KA, Reif DM, et al. Confirmation of high-throughput screening data and novel mechanistic insights into VDR-xenobiotic interactions by orthogonal assays. Sci Rep. 2018;8(1):1–16.
473. S. Baldwin W. Phase 0 of the Xenobiotic Response: Nuclear Receptors and Other Transcription Factors As a First Step in Protection from Xenobiotics. Nucl Recept Res. 2019;6.
474. Qin X, Wang X. Role of vitamin D receptor in the regulation of CYP3A gene expression. Acta Pharm Sin B. 2019;9(6):1087–98.
475. Matsunawa M, Amano Y, Endo K, Uno S, Sakaki T, Yamada S, et al. The aryl hydrocarbon receptor activator benzo[a]pyrene enhances vitamin D3 catabolism in macrophages. Toxicol Sci. 2009;109(1):50–8.
476. Matsunawa M, Akagi D, Uno S, Endo-Umeda K, Yamada S, Ikeda K, et al. Vitamin D receptor activation enhances benzo[a]pyrene metabolism via CYP1A1 expression in macrophages. Drug Metab Dispos. 2012;40(11):2059–66.
477. Haque S, Mondal S, Kundu D, Ghosh AR. Effect of Multiple Polycyclic Aromatic Hydrocarbons (Pahs) on Liver of Three Teleostean Fishes Labeobata, Labeorohita and Cirrhinusmrigala in Burdwan Loco Tank, Burdwan, West Bengal, India. Austin Environ Sci. 2017;2(1):1–8.
478. Izawa T, Arakaki R, Mori H, Tsunematsu T, Kudo Y, Tanaka E, et al. The Nuclear Receptor AhR Controls Bone Homeostasis by Regulating Osteoclast Differentiation via the RANK/c-Fos Signaling Axis. J Immunol. 2016;197(12):4639–50.
479. Izawa T, Arakaki R, Ishimaru N. Crosstalk between Cytokine RANKL and AhR Signalling in Osteoclasts Controls Bone Homeostasis. J Cytokine Biol. 2017;02(02).
480. Mollinedo F. Neutrophil Degranulation, Plasticity, and Cancer Metastasis. Trends Immunol. 2019;40(3):228–42.
481. Havixbeck JJ, Rieger AM, Wong ME, Hodgkinson JW, Barreda DR. Neutrophil contributions to the induction and regulation of the acute inflammatory response in teleost fish. J Leukoc Biol. 2016;99(2):241–52.
482. Havixbeck J, Barreda D. Neutrophil Development, Migration, and Function in Teleost Fish. Biology (Basel). 2015;4(4):715–34.
483. Yang SC, Tsai YF, Pan YL, Hwang TL. Understanding the role of neutrophils in acute respiratory distress syndrome. Biomed J. 2020;1–8.
484. Ray A, Kolls JK. Neutrophilic Inflammation in Asthma and Association with Disease Severity. Trends Immunol. 2017;38(12):942–54.
485. Wright HL, Moots RJ, Bucknall RC, Edwards SW. Neutrophil function in inflammation and inflammatory diseases. Rheumatology. 2010;49(9):1618–31.
486. Shi Q, Godschalk RWL, van Schooten FJ. Inflammation and the chemical carcinogen benzo[a]pyrene: Partners in crime. Mutat Res - Rev Mutat Res. 2017;774:12–24.
487. Barnwal P, Vafa A, Afzal S, Shahid A, Hasan S, Alpashree, et al. Benzo(a)pyrene induces lung toxicity and inflammation in mice: prevention by carvacrol. Hum Exp Toxicol. 2018;37(7):752–61.
488. Xie S, Zhou A, Xu N, Feng Y, Pan Z, Junaid M, et al. Benzo[a]pyrene induces microbiome dysbiosis and inflammation in the intestinal tracts of western mosquitofish (*Gambusia affinis*) and zebrafish (Danio rerio). Fish Shellfish Immunol. 2020;105(April):24–34.
489. Rehberger K, Escher BI, Scheidegger A, Werner I, Segner H. Evaluation of an in vitro assay to screen for the immunotoxic potential of chemicals to fish. Sci Rep. 2021;11(1):1–16.
490. Hao N, Whitelaw ML. The emerging roles of AhR in physiology and immunity. Biochem Pharmacol. 2013;86(5):561–70.
491. Hanieh H. Toward understanding the role of aryl hydrocarbon receptor in the immune system: Current progress and future trends. Biomed Res Int. 2014;2014.
492. Song JY, Casanova-Nakayama A, Möller AM, Kitamura SI, Nakayama K, Segner H. Aryl hydrocarbon receptor signaling is functional in immune cells of rainbow trout (*Oncorhynchus mykiss*). Int J Mol Sci. 2020;21(17):1–15.